# Structure and Dynamics of Mixed Microemulsions/Reverse Micellar Systems

*A thesis submitted for the award of the degree of*

**Doctor of Philosophy (Science)**

**in**

**Chemistry (Experimental)**

*By*

**Arindam Das**

Department of Chemistry

**University of Calcutta**

Kolkata, India

**2016**

*Dedicated to My Parents…*

# Abstract

This thesis is focused on the study of dynamics, hydrogen bonded structure and activity of water molecules present in restricted environments [e.g. micelles, reverse micelles (RMs) and microemulsion (ME)] with different surfactant mixtures. The dynamics of water molecules present in these systems are measured in the time scale ranging from nanosecond to sub-picosecond using time resolved fluorescence spectroscopy (TRFS). The hydrogen bonding states of water are obtained from Fourier transform infrared spectroscopy (FTIR). We have investigated the properties of water inside RMs by varying the size of the confinement, interfacial morphology and charge type of the interfaces. The results indicate that the physical properties of water in anionic (AOT)-nonionic (Ig-520) mixed RM is mostly governed by the interfacial stoichiometry and water content and merely displays any dependence on the mechanical properties of the interface. The physical features of nonionic surfactant(s) mixture (Ig-210/Ig-630/Cyclohexane) is different from that of the previous ionic-nonionic mixture and provides some unusual non-linear behaviour. Synergistic interactions are observed in both micellar as well as reverse micellar anionic (AOT)-nonionic (Tween-85) mixed system, moreover, the role of various biocompatible oils (EO, EP, EM) in solvation dynamics is detected. Formulation of a biocompatible mixed ME (Lecithin/TX-100/Butyl lactate/IPM) system in which the physical properties do not differ much from those of the lecithin based systems with the additional advantage of having higher solubilization capacity and low viscosity. In order to understand the effect of interfacial morphology on water activity we study the catalytic activity of a model enzyme α-chymotrypsin (CHT) on the substrate Ala–Ala–Phe–7-amido-4-methyl-coumarin (AMC) in anionic-nonionic mixed RM systems. We have modified the interfacial charge type of AOT RM with the incorporation of Brij surfactants of different Hydrophilic-lipophilic balances (HLBs) into it and studied the altered structure and dynamics of entrapped water in these mixed RMs. The enzymatic activity of the entrapped water is found to be dependent on the interface stoichiometry as well as HLB of the Brijs which provides a new route to regulate the reaction rate in RM systems according to the purpose. Thus, our study confirms that the presence of mixed surfactant systems at the interface improves the solubilization capacity as well as alters their properties from that of the individual ones which could be found advantageous in various biological and technological applications of these aggregated systems.

# List of publications

1. "Do the Physical Properties of Water in Mixed Reverse Micelles Follow a Synergistic Effect: A Spectroscopic Investigation", **Arindam Das**, Animesh Patra and Rajib Kumar Mitra, *The Journal of Physical Chemistry B*, **2013**, 117, 3593-3602.
2. "Formulation and Characterization of a Biocompatible Microemulsion Composed of Mixed Surfactants: Lecithin and Triton X-100", **Arindam Das** and Rajib Kumar Mitra, *Colloid and Polymer Science*, **2014,** 292:635–644.
3. "Does the Optimum Hydrophilic Lipophilic Balance Condition Affect the Physical Properties of Mixed Reverse Micelles: A Spectroscopic Investigation", **Arindam Das** and Rajib Kumar Mitra, *The Journal of Physical Chemistry B*, **2014**, 118, 5488-5498**.**
4. "Modulation of Anionic Reverse Micellar Interface with Non-ionic Surfactants can Regulate Enzyme Activity within the Micellar Waterpool", **Arindam Das**, Animesh Patra and Rajib Kumar Mitra, *Colloid and Polymer Science*, **2016,** 1:1–12.
5. "The Mixing Behavior of Anionic and Nonionic Surfactant Blends in Aqueous Environment Correlates in Fatty Acid Based Reverse Micelles", Kaushik Kundu, **Arindam Das,** Soumik Bardhan, Gulmi Chakraborty, Dibbendu Ghosh, Barnali Kar, Swapan K. Saha, Sanjib Senapati, Bidyut K. Paul, and Rajib Kumar Mitra**,** *Colloids and Surfaces A: Physicochem. Eng. Aspects*, 504, **2016**, 331–342.

# Acknowledgements

*It is a pleasant opportunity to express my thanks to all those who contributed in many ways to make this thesis possible and make it an unforgettable experience for me.*

*At the beginning, I would like to express my deepest gratitude to my supervisor, Dr. Rajib Kumar Mitra for his continuous supports, graceful helps, valuable discussions and modest guidance. I have greatly benefited from his in-depth knowledge, valuable inputs and continuous encouragement. He constantly motivated me to think and perform my plans independently.*

*I would like to thank all my lab mates: Animesh Patra, Debanjan Polley, Nirnay Samanta, Debasish Das Mahanta, Dr. Dipak Kumar Das, Kumar Neeraj and Amit Barh for providing a wonderful and friendly environment inside the lab.*

*I am obliged to my teacher and friends of Bengal Engineering and Science University (formerly BESU, now IIEST) Shibpur, Howrah for their continuous encouragement in research.*

*I would like to give my gratitude to some of graduate friends as well as childhood school friends for helping me in every possible ways and making my life more enjoyable with their presence.*

*I must address my special thanks to my special friends as well as brothers in the SNBNCBS for their support and the most enjoyable company made me able to easily cross the hurdles during my Ph.D. life. They always created a very cheerful atmosphere with delicious food and superb sense of humor which kept me going through this long journey.*

*Last but not the least, I would like to pay high regards to my mother, my two elder sisters, their family, and other family members for their sacrifices, sincere encouragement, support and inspiration throughout my life that have made me more courageous, dedicated and patient. I owe everything to them and they are the reasons for what I am today. Finally, I thank the S. N. Bose National Centre for Basic Sciences for giving me an opportunity to work with UGC fellowship.*

_____

***Arindam Das***

# Contents

# Chapter 1: Introduction

Surfactants are amphiphilic molecules that have both hydrophilic head groups and hydrophobic tail parts. The hydrophobic tail part may consist of a single chain or it may contain multiple number of chains. The head group can be either a charged or uncharged polar group. According to the nature of the head groups the surfactants are classified into anionic, cationic, non-ionic and zwitterionic (amphoteric). Surfactant molecules spontaneously accumulate in solvents to form a variety of self-organized assemblies such as micelle (M), reverse micelle (RM) or microemulsion (ME), which are homogenous, transparent, optically isotropic and thermodynamically stable dispersions of water and oil [1]. Surfactants are spontaneously aggregated in aqueous solutions to form micelles (M) while in organic solvents they aggregate to form reverse or inverted micelles. Normal micelles (M) are depicted as aggregates of surfactant molecules with the hydrophilic heads oriented towards the dispersing solvent (generally water), and the hydrophobic tails oriented towards the inner part of the assembly (the micellar core). Micelles appear as the dominant form at and above the so-called critical micelle concentration, CMC, but free surfactants are also present in the system as monomers. The aggregation number (the average number of surfactant molecules in a micelle) is dependent on the surfactant type and its concentration. The depiction of micelles is reversed when the solvent is changed from aqueous to a nonpolar medium. In order to minimize their contact with the bulk nonpolar solvents, the head groups of the surfactants associate themselves with the water molecules expanding their hydrophobic tails into the non-polar medium. RMs, a special type of ME systems[2] are self-assembled dispersions of surfactant aggregates which can solubilize considerable amount of water in a nonpolar solvent i.e. oil continuum. MEs [3] are stabilized by relatively large amounts of surfactant(s) frequently in combination with cosurfactant(s) in presence of oil and water [4, 5]. The structure of ME can be idealized as a set of interfaces dividing polar and nonpolar domains. Depending on the composition of the system, the microstructure of a ME may exist as water-in-oil (w/o) droplets, oil-in-water (o/w) droplets, or a bicontinuous structure. ME is heterogeneous at the nanometer scale, however, the coexistence of water and oil within a single phase is possible by the huge reduction of the interfacial tension by the surfactant(s). The three component systems consisting of water/surfactant/oil can adopt a variety of morphologies which are generally known as tertiary ME, while those based on four components (i.e., with cosurfactant) are known as pseudoternary

or quaternary ME [4]. MEs are graphically represented as stability areas in triangular phase diagrams where each triangular corner designates respective component [6]. RM can also be formed with cores including other non-aqueous polar solvents (such as ethyleneglycol, glycerol, formamide, dimethylacetamide, etc.) which have relatively high dielectric constants and are immiscible with hydrocarbons solvents [7]. Aggregation number of RMs increases with their water content, usually defined in terms of the hydration level of the RM $w_0$ = $[H_2O]$/[surfactant] [8]. From both the thermodynamic model and molecular simulations study it has been shown that a small number of polar solvent molecules activates the formation of large permanent aggregates of surfactants[9]. Generally, the amount of surfactant molecules influences the morphology of the self-assembled structures. At very low concentration the surfactants are dispersed randomly without any ordering due to the entropic driving force, while at the higher surfactant concentrations the self-assembled nano-structures can order themselves, since the enthalpic driving force overcomes the negative entropic one[10]. However, an overall positive entropy change accounts for the ultimate disorder during the self-assembling process of surfactant molecules in the oil medium. The removal of oil molecules to create room for the residence of the polar surfactant head groups in the form of micelles is considered to be associated with a positive entropy change. Thus the micelle and RM formation by surfactant is an entropy-directed process. The entropy-directed normal and reverse micellization processes are, therefore, universal[11, 12]. The free energy of ME formation can be considered to depend on the extent to which surfactant lowers the surface tension of the oil–water interface and the change in the entropy. The change in the interfacial area on microemulsification is very large due to the large number of very small droplets formation. The very large dispersion entropy is arising from the mixing of one phase in the other in the form of large numbers of small droplets. However, another favourable entropic contribution arises from the dynamic processes of surfactant exchange diffusion between the interfacial layer and monomer-surfactant. Thus a negative free energy of formation is attained due to large reductions in surface tension as well as significant favourable entropic change. In such cases, microemulsification is spontaneous and the resulting dispersion is thermodynamically stable[13].

RMs are of particular interest in many fields, ranging from the fundamental sciences to technological applications. They have numerous applications such as in the synthesis of inorganic nanoparticles, as models for biological systems, for the extraction and purification of biomolecules like food additives or medicinal substances in biologically compatible systems,

in drug delivery and as enzymatic reaction media [14-18]. In all cases, the efficient use of RMs requires a sound knowledge of the basic physicochemical properties of the specific system. For example, in order to model the distribution of various chemical species within the system, parameters such as droplet size, aggregation number, free surfactant concentration, structure and dynamics of water inside RM must be known. In general, a better understanding of RMs could lead to better performance or even extend the scope of possible applications.

These self-organized assemblies have been widely studied as carrier systems for active agents because of their unique properties of combining hydrophilic and hydrophobic domains within one homogeneous solution. Correspondingly, there has been extensive interest in studying the physicochemical properties of these systems for using them in a large variety of applications and formulations. In the last years MEs have received increasing interest in cosmetic [19] and pharmaceutical formulations, such as in food industries, for controlled as drug encapsulation, drug transport carrier and for solubility of high polar molecules[13]. As drug vehicle, MEs have the advantages of being stable and of easy preparation. Owing to the nanometric size, MEs improve transdermal diffusivity of drugs in cutaneous application for oral, topical and parenteral administration [20]. Due to the capability to solubilize a great amount of lipophilic or hydrophilic compounds, coupled with a large interfacial area, MEs also function as catalysts, increasing the efficacy of chemical reactions and synthesis of nano-products [13, 21-24]. However, the limitations on the use of such self-aggregated systems in pharmaceutical field arise mostly from the need for all the constituting components to be biologically and pharmaceutically acceptable, particularly the surfactants and the oils. This induces a huge drive to formulate such systems using biocompatible constituents. For this reason, different kinds of biocompatible oils like isoproyl myristate (IPM)[25], ethyl myristate (EM), ethyl palmitate (EP) and ethyl oleate (EO)[26] are used to formulate such systems. The double tailed anionic surfactant sodium bis(2-ethylhexyl)-sulfosuccinate (AOT) is one of the most extensively investigated surfactants for the study of such heterogeneous systems[27-29]. AOT based systems also find application in the field of drug delivery [30, 31]. Cationic surfactant didodecyldimethylammoniumbromide, DDAB based systems are also used as a safe and an efficient vehicle for sustained drug release[32]. Three major classes of nonionic surfactants, especially those based on poly(ethylene oxide) (PEO) have been used in this thesis for their several significant applications. For example, alkylpolyether surfactants ($C_iE_j$, Brij) are used as a detergent in high-performance liquid chromatrography (HPLC) applications[33]. Triton X-100 is used primarily for solubilizing membrane proteins during isolation of

membrane-protein complexes[34]. The class of Igepal i.e. nonylphenylpolyethylene oxide based surfactant, has shown broad application in industrial and biochemical processes[35]. Ethoxylated nonionic Tween-85 is also biodegradable[36, 37]. One of the most preferred biocompatible zwitterionic (phospholipids) surfactant is lecithin, which is also a nontoxic surfactant as recognized by safe (GRAS) status [38] used for many pharmaceutical applications.

Studies of reaction kinetics in restricted or confined systems are not only essential for a better understanding of (bio)chemical reactions in nanostructures, they also help to design new nanosystems to perform efficient catalytic processes[39]. Therefore, this area of research has attracted attention of many researchers for its several application in industrial biocatalytic processes. Over the past few decades RM has also been used as a common organic medium to perform biocatalysis as it provides with a useful microreactor[40] to protect the enzyme from solvent adverse effects and the catalytic reaction of water insoluble substrate can occur at the water-oil interface[41, 42]. It has been previously observed that enzyme kinetics rate in RM depends upon several factors like the microenvironment in the surroundings of the enzyme and the substrate, the partitioning of the substrate between the RM droplets and the external solvent, surfactant concentration, their charge type, salt concentration, temperature, the hydration level of the RM etc [43-49]. Rate of enzyme hydrolysis usually shows a bell shaped curve as a function of $w_0$ in RM i.e. it shows maximum activity at a certain $w_0$ [44].

It is a noticeable fact that the properties of water molecules in many self-organized assemblies show the features closely similar to the properties of water in biological systems, and in advantage these bio-mimicking systems are less complex and easy to prepare than the real biological systems. RM have been recognized as an ideal platform to study the properties of confined/restricted water for the past few decades [50-56]. The hydrodynamic diameter of the water pool of RM can be experimentally varied from 0.3 - 20 nm by adjusting the $w_0$[51, 57]. It has been inferred that upon confinement the hydrogen bonded water structure gets perturbed which is evident from the abundance of a noticeable fraction of water molecules with distorted hydrogen bonds relative to its bulk counter-part[58]. As a result of that, water present in RMs offers distinct differences in physical and chemical properties relative to its bulk counterpart [50, 51, 59-64]. Water exists as big polymer-like network rather than as an isolated individual in RM systems due to intermolecular hydrogen bonding. This network is being dynamic in nature owing to continuous hydrogen bond breaking and making occurring in ps and sub-ps time scale. Orientational relaxation dynamics of water molecules i.e. the

rearrangement of hydrogen bonds of water changes when water interacts with an interface, an ion or a large molecule [56, 61, 65-68]. The dynamics of bulk and confined water in restricted medium have been studied by several experimental techniques [50, 56, 59, 64, 65, 69-71]. Nuclear Magnetic Resonance (NMR) is a popular method to study the dynamics of water which reveals that the rotational motion of water slows down as a result of confinement [72]. Shape and size of RM have been measured by different techniques, such as small angle neutron scattering (SANS)[73], small-angle X-ray scattering (SAXS)[74, 75] and both dynamic and static light scattering[76]. Recently time-resolved vibrational spectroscopy has been used to study hydration dynamics in RM systems [61, 62, 67, 77] which measures the vibrational relaxation of isotopically labeled water, HOD through transient absorption experiments probing the OD stretch in $H_2O$ or the OH stretch in $D_2O$ and the transfer energy of $H_2O$ stretching vibrations for water in RM [78-80].

The interface inside RMs strongly interacts with the water molecules making them 'highly structured'; consequently the dynamics become relatively slow [51, 56, 81]. When water is sequestrated inside RM, there is a competition between water-water and water-surfactant interactions[82]. This retardation of dynamics of water inside RM can be defined by the most commonly used Core-Shell model [51, 83-85]. In this model the water molecules inside RM are divided into two types; firstly the water molecules which behave like bulk water are present in the core of the RM, and secondly the shell water, when all the water molecules are essentially interacting with the surfactant head groups i.e. water present at $w_0$=2 [83]. MD simulation result also shows that the core and shell water are not static in nature and there exists a slow inter conversion between them [86]. The vibrational relaxation time of 'shell water' (~5.2 ps) is significantly slower compared to that of 'core water' (1.7 ps)[51] and it is interesting that the shell water shows a strong dependency on the nature of the polar interface of RM. Hence, this altered retarded dynamics inside RM depends upon several factors like interface polarity, $w_0$, nonpolar solvent etc.[50, 55, 61, 79, 87-91] which can be modified by replacing single surfactant with mixture of different surfactants.

Mixtures of surfactants are often favored over the corresponding single surfactant(s) in industrial, pharmaceutical, and technological formulations for their superior performance and cost effectiveness in various aspects including solubilization, dispersion, suspension etc[92-98]. One of the most desired properties of RM is its high water solubilization capacity and mixture of surfactants can offer a many fold enhancement in it. Solubilization capacity of RM and physicochemical properties of the entrapped water have been found to be strongly

dependent on the chemical nature of the oil, surfactant charge type and $w_0$ [99]. There have been several reasons proposed for the observed synergistic solubilization behaviour, mostly based on either the interplay between the surfactant monolayer curvature and inter-droplet interaction or establishment of an optimum hydrophilic-lipophilic balance (HLB) or both [100-103]. HLB of a surfactant is a measure of the extent of its hydrophilicity or lipophilicity and can be calculated following the definition by Griffin [104]. HLB[105] of mixed surfactant systems can efficiently be tuned in order to provide with better solubilization behaviour [102, 103]. Modification of the interface by blending of surfactants brings about considerable changes in the elastic rigidity of the interfacial film[106]. Several studies of RM systems involving more than one surfactants using solubilization[102, 103, 107], conductivity[107, 108], interfacial composition[109], viscosity[110], spectroscopy[111-113], SANS[114, 115], FTIR and NMR measurement[58, 72] detect significant modification of the mechanical properties of the interface and consequently of the water structure in RM systems in comparison to the corresponding single surfactant systems. These findings summarize that the effects of surfactant blending on solubilization and other physical properties are direct consequences of mixing and physicochemical interactions in interfacial films.

In spite of numerous studies carried out in this direction, there still remains several unaddressed questions relating to the properties of such confined systems by using mixed surfactant systems replacing single surfactant. Some of them are: how an interface can be improved by using mixed surfactant system compared to that of single surfactant inside RM? Whether the mixing behaviour of several surfactants plays any role in the intermolecular hydrogen bond structure and dynamics of water in RM? Does the different mixed surfactant interface (anionic-nonionic, cationic-nonionic and nonionic-nonionic) influence the physical/chemical properties of water? How the mixed surfactant based interface modifies the activity of water molecules towards catalysis reactions inside RM? Moreover, the effect and advantages of surfactant blending interface in other than RM systems like ME and micellar system. The principal focus of this thesis is to study how interfacial property of various mixed surfactant system affect the structure, dynamics and activity of water inside restricted medium.

Ionic/nonionic mixed surfactants are frequently used in many biophysical applications as they deliver with more flexible physicochemical properties in terms of synergistic observations in RMs[116]. Doping of nonionic surfactant into the interface of ionic surfactant in RM brings about significant changes in the interfacial property as well as it modifies the structure of water inside the water pool. To illustrate this observation we have studied the

structure and dynamics of a mixed system (anionic AOT and non-ionic Igepal-520 in cyclohexane). It has been observed that the maximum solubilization capacity often displays synergistic effects whereas various physical and chemical properties of the mixed RM systems follow an overall linear trend with the surfactant mixing ratio. The many-fold increase in the solubilization capacity, however, does barely affect the physical properties of water. In order to appear at a more general conclusion it is important to perform the investigation with surfactant mixture of the same charge type. In accordance with that we have investigated the effect of mixing of two terminal HLB non-ionic surfactants Igepal-210 (HLB~4)/Igepal-630 (HLB~13)/cyclohexane system on the physicochemical properties of water encapsulated in the RM. Besides, in order to detect the effect of mixing property of various charge-type of surfactants on the interfacial property of RM we have related the results of (cationic) DDAB/ Ig-520/Cyclohexane mixed system with AOT/Ig-520/Cy system. Our next quest is to understand whether there exists any correlation between micellar and RM system by using the same surfactant mixture. To comprehend this we have investigated the effect of mixing of AOT and Tween-85 aqueous solutions as well as the corresponding mixed RM systems to realize whether the key features responsible for micellization reciprocate the physical properties of water inside the RM systems. Besides, we have formulated biocompatible ME based on a nontoxic highly lipophilic surfactant lecithin (L), pharmaceutical flavouring co-surfactant butyl lactate (BL), and hydrophilic biocompatible TX-100 (T) in biocompatible oil isopropyl myristate (IPM)[117] to establish the enrichment of solubilization behavior by tuning the optimum HLB of this mixed system. Finally, to observe the effect of interfacial morphology on the rate of enzyme kinetics we have measured the enzymatic activity of α-chymotrypsin (CHT) [44, 118] on the substrate Ala–Ala–Phe–7-amido-4-methyl-coumarin (AMC)[119] in mixed RM systems. To control the rate of catalytic activity of enzyme we have replaced AOT with three different Brij series and altered their HLB numbers at a constant mole fraction of Brij [ $X_{Brij} = \frac{n_{Brij}}{n_{AOT} + n_{Brij}}$ ] of 0.1 in IPM.

Investigations have been carried out on the structure, dynamics and activity of water present in bio-mimicking surfaces (e.g. RMs, MEs and micelle) with varying size, charge and geometry of the interface. Mainly three techniques have been utilized, namely, dynamic light scattering (DLS), Fourier transform infrared (FTIR) spectroscopy and time resolved fluorescence spectroscopy (TRFS) to measure the physical properties of water inside RM or ME system. DLS is used to measure the hydrodynamic diameter ($D_h$) and aggregation number

of the RM droplets. Fourier transform infrared (FTIR) spectroscopy is a very sensitive technique to study hydrogen bonding in water [65, 120-124]. Water produces characteristic symmetric and asymmetric O-H stretching bands in the frequency range of 3000-3800 $cm^{-1}$ in the mid infrared (MIR) region [125]. Such spectrum arises due to the presence of different types of hydrogen bonding states of water. To study the relative contribution of different types of water in this region, the total water spectra could be deconvoluted into three distinct types of hydrogen bonding environments, namely, multimer or isolated water (MW, water molecule which are not hydrogen bonded to any neighbouring molecule, peaking at ~ 3600 $cm^{-1}$), intermediate water (IW, unable to develop fully hydrogen bonded structure, peaking at 3460 $cm^{-1}$) and hydrogen-bonded water (HW, tetrahedrally hydrogen bonded water, peaking at 3330 $cm^{-1}$)[51, 58]. Instead of pure water the use of HOD molecule has been shown to be advantageous, as the O–D band is decoupled from the O–H band and appears in a region (2200–2800 $cm^{-1}$) which is comparatively free from other strong absorptions[126, 127]. As the intra-molecular interactions between the two OH (or OD) oscillators in $H_2O$ (or $D_2O$) molecules do not complicate the O–H (O–D) stretching band contour as observed for pure water[126] thus, the O–D stretching band reveals only the H-bonding interactions between water molecules. In this case, the total spectra could be deconvoluted similarly into three Gaussian sub-bands peaking at 2640±10 (MW), 2545±5 (IW) and 2450 $cm^{-1}$ (HW) respectively.

Fluorescence spectroscopy is a versatile technique to depict the polarity and microenvironment around a probe molecule [54, 128, 129]. It is also important to choose the correct probe so that it can provide with appropriate information and the geometry of the desired interface. To investigate hydration dynamics in biomolecules, supramolecular assemblies like protein [130-132], DNA [133-136], micelle [136-139], RM [139-142], cyclodextrin [143, 144] etc. time resolved fluorescence spectroscopy (TRFS) has been used for years. This spectroscopic technique, specially the slow relaxation process, which essentially represents the coupled rotational-translational orientation of water molecules, has recently been evolved as a potential tool to realize the interaction of confined water molecules with the interface. It is well-known that solvent relaxation for water is orders of magnitude slower at the vicinity of interface compared to that in pure water. TRFS study of bulk water yields two time scales: ~100 fs and ~1 ps [50, 145]. However, there coexist two types of water in restricted systems, firstly the water molecules having faster dynamics (~ few ps) and the other one is slower in dynamics with a timescale of hundreds of ps to several ns[137, 140, 146-148]. The origin of this bimodal distribution of water can be recognized as ‘bound’ water molecules

which is bound to the polar interface offering a dynamics significantly slower than that of pure and 'free-type' water molecules which are not hydrogen bonded with the interface but remain in the hydration layer[149]. Since the hydration layer is actively dynamic in nature, the inter conversion (hydrogen bond breaking and making) kinetics between these two species determines the amplitude and also the time scale of the hydration layer relaxation [132, 140, 150-152].

## 1.1 References


[1] B.K. Paul, S.P. Moulik, Microemulsions: an overview, Journal of Dispersion science and Technology, 18 (1997) 301-367.
[2] V. Uskoković, M. Drofenik, Synthesis of materials within reverse micelles, Surface Review and Letters, 12 (2005) 239-277.
[3] J.H. Schulman, W. Stoeckenius, L.M. Prince, Mechanism of formation and structure of micro emulsions by electron microscopy, The Journal of physical chemistry, 63 (1959) 1677-1680.
[4] S. Tenjarla, Microemulsions: an overview and pharmaceutical applications, Critical Reviews™ in Therapeutic Drug Carrier Systems, 16 (1999).
[5] S. Moulik, B. Paul, Structure, dynamics and transport properties of microemulsions, Advances in Colloid and Interface science, 78 (1998) 99-195.
[6] J. Kreuter, Colloidal drug delivery systems, CRC Press1994.
[7] J.J. Silber, R.D. Falcone, N.M. Correa, M.A. Biasutti, E. Abuin, E. Lissi, P. Campodonico, Exploratory study of the effect of polar solvents upon the partitioning of solutes in nonaqueous reverse micellar solutions, Langmuir, 19 (2003) 2067-2071.
[8] P.L. Luisi, B. Straub, Reverse Micelles: Biological and Technological Relevance of Amphiphilic Structures in Apolar Media, Plenum Pub Corp1984.
[9] A. Khoshnood, A. Firoozabadi, Polar solvents trigger formation of reverse micelles, Langmuir, 31 (2015) 5982-5991.
[10] P. Calandra, D. Caschera, V. Turco Liveri, D. Lombardo, How self-assembly of amphiphilic molecules can generate complexity in the nanoscale, Colloids and Surfaces A: Physicochemical and Engineering Aspects, 484 (2015) 164-183.
[11] P.R. Majhi, S.P. Moulik, Microcalorimetric investigation of AOT self-association in oil and the state of pool water in water/oil microemulsions, The Journal of Physical Chemistry B, 103 (1999) 5977-5983.
[12] J. Chen, J. Zhang, B. Han, X. Feng, M. Hou, W. Li, Z. Zhang, Effect of compressed CO2 on the critical micelle concentration and aggregation number of AOT reverse micelles in isooctane, Chemistry–A European Journal, 12 (2006) 8067-8074.
[13] M.J. Lawrence, G.D. Rees, Microemulsion-based media as novel drug delivery systems, Advanced drug delivery reviews, 45 (2000) 89-121.
[14] S. Furusaki, S. Ichikawa, M. Goto, Recent advances in reversed micellar techniques for bioseparation, Progress in Biotechnology, 16 (2000) 133-136.
[15] C.M. Carvalho, J.M. Cabral, Reverse micelles as reaction media for lipases, Biochimie, 82 (2000) 1063-1085.
[16] P. Luisi, M. Giomini, M. Pileni, B. Robinson, Reverse micelles as hosts for proteins and small molecules, Biochimica et Biophysica Acta (BBA)-Reviews on Biomembranes, 947 (1988) 209-246.
[17] E. Melo, M. Aires-Barros, J. Cabral, Reverse micelles and protein biotechnology, Biotechnology annual review, 7 (2001) 87-129.
[18] D.S. Mathew, R.-S. Juang, Role of alcohols in the formation of inverse microemulsions and back extraction of proteins/enzymes in a reverse micellar system, Separation and purification technology, 53 (2007) 199-215.

[19] S. Watnasirichaikul, N.M. Davies, T. Rades, I.G. Tucker, Preparation of biodegradable insulin nanocapsules from biocompatible microemulsions, Pharmaceutical research, 17 (2000) 684-689.
[20] M. Changez, M. Varshney, J. Chander, A.K. Dinda, Effect of the composition of lecithin/n-propanol/isopropyl myristate/water microemulsions on barrier properties of mice skin for transdermal permeation of tetracaine hydrochloride: in vitro, Colloids and Surfaces B: Biointerfaces, 50 (2006) 18-25.
[21] M.-P. Pileni, The role of soft colloidal templates in controlling the size and shape of inorganic nanocrystals, Nature materials, 2 (2003) 145-150.
[22] T. Hyeon, Chemical synthesis of magnetic nanoparticles, Chemical Communications, DOI 10.1039/B207789B(2003) 927-934.
[23] J. Eastoe, M.J. Hollamby, L. Hudson, Recent advances in nanoparticle synthesis with reversed micelles, Advances in colloid and interface science, 128 (2006) 5-15.
[24] A.K. Ganguli, A. Ganguly, S. Vaidya, Microemulsion-based synthesis of nanocrystalline materials, Chemical Society Reviews, 39 (2010) 474-485.
[25] R.C. Rowe, P.J. Sheskey, P.J. Weller, Handbook of pharmaceutical excipients, Pharmaceutical press London2006.
[26] Y.T. Mesaki, S. Masato Tanaka, Preparation of Capsules containing L-Cysteine with Melting Dispersion Cooling Method, Global Journal of Medical Research, 14 (2014).
[27] S. Moulik, K. Mukherjee, On the versatile surfactant aerosol-OT (AOT): its physicochemical and surface chemical behaviours and uses, Proceedings-indian national science academy part A, 62 (1996) 215-236.
[28] S. Nave, J. Eastoe, R.K. Heenan, D. Steytler, I. Grillo, What is so special about Aerosol-OT? 2. Microemulsion systems, Langmuir, 16 (2000) 8741-8748.
[29] S. Mukherjee, P. Chowdhury, W.F. DeGrado, F. Gai, Site-specific hydration status of an amphipathic peptide in AOT reverse micelles, Langmuir, 23 (2007) 11174-11179.
[30] R.R. Gupta, S.K. Jain, M. Varshney, AOT water-in-oil microemulsions as a penetration enhancer in transdermal drug delivery of 5-fluorouracil, Colloids and Surfaces B: Biointerfaces, 41 (2005) 25-32.
[31] M.D. Chavanpatil, A. Khdair, J. Panyam, Surfactant-polymer nanoparticles: a novel platform for sustained and enhanced cellular delivery of water-soluble molecules, Pharmaceutical research, 24 (2007) 803-810.
[32] L. Zhao, J. Liu, L. Zhang, Y. Gao, Z. Zhang, Y. Luan, Self-assembly properties, aggregation behavior and prospective application for sustained drug delivery of a drug-participating catanionic system, International Journal of Pharmaceutics, 452 (2013) 108-115.
[33] D.R.K. Richard J. Farn, J. Houston, Chemistry and Technology of Surfactants, Wiley-Blackwell, Oxford, DOI (2007) 1-23.
[34] S.A. Ostroumov, Biological effects of surfactants, CRC Press2005.
[35] M. Sedgwick, D. Crans, N. Levinger, What is inside a nonionic reverse micelle? Probing the interior of Igepal reverse micelles using decavanadate, Langmuir, 25 (2009) 5496-5503.
[36] R. Dong, J. Hao, Complex fluids of poly (oxyethylene) monoalkyl ether nonionic surfactants, Chemical reviews, 110 (2010) 4978-5022.
[37] H. Liu, S. Li, Y. Wang, F. Han, Y. Dong, Bicontinuous water-AOT/Tween85-isopropyl myristate microemulsion: A new vehicle for transdermal delivery of cyclosporin A, Drug development and industrial pharmacy, 32 (2006) 549-557.
[38] E.J. Acosta, T. Nguyen, A. Witthayapanyanon, J.H. Harwell, D.A. Sabatini, Linker-based bio-compatible microemulsions, Environmental science & technology, 39 (2005) 1275-1282.
[39] R.F. Khairutdinov, K.Y. Burshtein, N. Serpone, Photochemical reactions on the surface of a circular disk: a theoretical approach to kinetics in restricted two-dimensional space, Journal of Photochemistry and Photobiology A: Chemistry, 98 (1996) 1-14.
[40] M. Pileni, Reverse micelles as microreactors, The Journal of physical chemistry, 97 (1993) 6961-6973.

[41] P.L. Luisi, Enzymes hosted in reverse micelles in hydrocarbon solution, Angewandte Chemie International Edition in English, 24 (1985) 439-450.
[42] B. Orlich, R. Schomäcker, Enzyme catalysis in reverse micelles, History and Trends in Bioprocessing and Biotransformation, Springer2002, pp. 185-208.
[43] M.A. Biasutti, E.B. Abuin, J.J. Silber, N.M. Correa, E.A. Lissi, Kinetics of reactions catalyzed by enzymes in solutions of surfactants, Advances in colloid and interface science, 136 (2008) 1-24.
[44] S.K. Verma, K.K. Ghosh, Activity, stability and kinetic parameters for α-chymotrypsin catalysed reactions in AOT/isooctane reverse micelles with nonionic and zwitterionic mixed surfactants, Journal of Chemical Sciences, 125 (2013) 875-882.
[45] K. Tonova, Z. Lazarova, Reversed micelle solvents as tools of enzyme purification and enzyme-catalyzed conversion, Biotechnology advances, 26 (2008) 516-532.
[46] D. Goswami, J.K. Basu, S. De, Lipase applications in oil hydrolysis with a case study on castor oil: a review, Critical reviews in biotechnology, 33 (2013) 81-96.
[47] F. Lopez, G. Cinelli, L. Ambrosone, G. Colafemmina, A. Ceglie, G. Palazzo, Role of the cosurfactant in water-in-oil microemulsion: interfacial properties tune the enzymatic activity of lipase, Colloids and Surfaces A: Physicochemical and Engineering Aspects, 237 (2004) 49-59.
[48] M. Celej, M. D'andrea, P. Campana, G. Fidelio, M. Bianconi, Superactivity and conformational changes on alpha-chymotrypsin upon interfacial binding to cationic micelles, Biochem. J, 378 (2004) 1059-1066.
[49] F. Moyano, E. Setien, J.J. Silber, N.M. Correa, Enzymatic hydrolysis of N-benzoyl-L-tyrosine p-nitroanilide by α-chymotrypsin in DMSO-water/AOT/n-heptane reverse micelles. A unique interfacial effect on the enzymatic activity, Langmuir, 29 (2013) 8245-8254.
[50] M.D. Fayer, N.E. Levinger, Analysis of Water in Confined Geometries and at Interfaces, Annual Review of Analytical Chemistry, 3 (2010) 89-107.
[51] D.E. Moilanen, N.E. Levinger, D. Spry, M. Fayer, Confinement or the nature of the interface? Dynamics of nanoscopic water, Journal of the American Chemical Society, 129 (2007) 14311-14318.
[52] A.A. Bakulin, D. Cringus, P.A. Pieniazek, J.L. Skinner, T.L.C. Jansen, M.S. Pshenichnikov, Dynamics of Water Confined in Reversed Micelles: Multidimensional Vibrational Spectroscopy Study, The Journal of Physical Chemistry B, 117 (2013) 15545-15558.
[53] R. Costard, N.E. Levinger, E.T.J. Nibbering, T. Elsaesser, Ultrafast Vibrational Dynamics of Water Confined in Phospholipid Reverse Micelles, The Journal of Physical Chemistry B, 116 (2012) 5752-5759.
[54] K. Bhattacharyya, Solvation dynamics and proton transfer in supramolecular assemblies, Accounts of chemical research, 36 (2003) 95-101.
[55] K. Bhattacharyya, B. Bagchi, Slow dynamics of constrained water in complex geometries, The Journal of Physical Chemistry A, 104 (2000) 10603-10613.
[56] N. Nandi, K. Bhattacharyya, B. Bagchi, Dielectric relaxation and solvation dynamics of water in complex chemical and biological systems, Chemical Reviews, 100 (2000) 2013-2046.
[57] D.E. Rosenfeld, C.A. Schmuttenmaer, Dynamics of Water Confined Within Reverse Micelles, The Journal of Physical Chemistry B, 110 (2006) 14304-14312
[58] J.-B. Brubach, A. Mermet, A. Filabozzi, A. Gerschel, D. Lairez, M. Krafft, P. Roy, Dependence of water dynamics upon confinement size, The Journal of Physical Chemistry B, 105 (2001) 430-435.
[59] N.E. Levinger, L.A. Swafford, Ultrafast Dynamics in Reverse Micelles, Annual Review of Physical Chemistry 60 (2009) 385-406.
[60] N.E. Levinger, Water in confinement Science, 298 (2002) 1722-1723.
[61] A.M. Dokter, S. Woutersen, H.J. Bakker, Inhomogeneous dynamics in confined water nanodroplets, Proceedings of the National Academy of Sciences, 103 (2006) 15355-15358.
[62] D.E. Moilanen, E.E. Fenn, D. Wong, M.D. Fayer, Water dynamics in large and small reverse micelles: From two ensembles to collective behavior, The Journal of chemical physics, 131 (2009) 014704.
[63] M.D. Fayer, Water in a Crowd, Physiology, 26 (2011) 381-392.

[64] B. Bagchi, Water Dynamics in the Hydration Layer around Proteins and Micelles, Chemical Reviews, 105 (2005) 3197-3219.
[65] M.D. Fayer, Dynamics of Water Interacting with Interfaces, Molecules, and Ions, Accounts of Chemical Research, 45 (2012) 3-14.
[66] H.J. Bakker, M.F. Kropman, A.W. Omta, S. Woutersen, Hydrogen-Bond Dynamics of Water in Ionic Solutions, Physica Scripta, 69 (2004) C14.
[67] A.M. Dokter, S. Woutersen, H.J. Bakker, Anomalous slowing down of the vibrational relaxation of liquid water upon nanoscale confinement, Physical review letters, 94 (2005) 178301.
[68] A.W. Omta, M.F. Kropman, S. Woutersen, H.J. Bakker, Negligible Effect of Ions on the Hydrogen-Bond Structure in Liquid Water, Science, 301 (2003) 347-349.
[69] I.R. Piletic, D.E. Moilanen, N.E. Levinger, M.D. Fayer, What Nonlinear-IR Experiments Can Tell You about Water that the IR Spectrum Cannot, Journal of the American Chemical Society, 128 (2006) 10366-10367.
[70] H.-S. Tan, I.R. Piletic, M.D. Fayer, Orientational dynamics of water confined on a nanometer length scale in reverse micelles, The Journal of Chemical Physics, 122 (2005) 174501.
[71] N.E. Levinger, Ultrafast dynamics in reverse micelles, microemulsions, and vesicles, Current Opinion in Colloid & Interface Science, 5 (2000) 118-124.
[72] Q. Li, T. Li, J. Wu, Comparative study on the structure of reverse micelles. 2. FT-IR, 1H NMR, and electrical conductance of H2O/AOT/NaDEHP/n-heptane systems, The Journal of Physical Chemistry B, 104 (2000) 9011-9016.
[73] B. Svensson, U. Olsson, P. Alexandridis, K. Mortensen, A SANS investigation of reverse (water-in-oil) micelles of amphiphilic block copolymers, Macromolecules, 32 (1999) 6725-6733.
[74] L.K. Shrestha, T. Sato, K. Aramaki, Intrinsic parameters for structural variation of reverse micelles in nonionic surfactant (glycerol α-monolaurate)/oil systems: a SAXS study, Physical Chemistry Chemical Physics, 11 (2009) 4251-4259.
[75] B.A. Simmons, C.E. Taylor, F.A. Landis, V.T. John, G.L. McPherson, D.K. Schwartz, R. Moore, Microstructure determination of AOT+ phenol organogels utilizing small-angle X-ray scattering and atomic force microscopy, Journal of the American Chemical Society, 123 (2001) 2414-2421.
[76] V. Vasquez, B. Williams, O. Graeve, Stability and comparative analysis of AOT/water/isooctane reverse micelle system using dynamic light scattering and molecular dynamics, The Journal of Physical Chemistry B, 115 (2011) 2979-2987.
[77] E.E. Fenn, D.B. Wong, M.D. Fayer, Water dynamics at neutral and ionic interfaces, P Natl Acad Sci USA, 106 (2009) 15243-15248.
[78] D. Cringus, A. Bakulin, J. Lindner, P. Vöhringer, M.S. Pshenichnikov, D.A. Wiersma, Ultrafast energy transfer in water-AOT reverse micelles, The Journal of Physical Chemistry B, 111 (2007) 14193-14207.
[79] D. Cringus, J. Lindner, M.T. Milder, M.S. Pshenichnikov, P. Vöhringer, D.A. Wiersma, Femtosecond water dynamics in reverse-micellar nanodroplets, Chemical physics letters, 408 (2005) 162-168.
[80] I.R. Piletic, H.-S. Tan, M. Fayer, Dynamics of nanoscopic water: Vibrational echo and infrared pump-probe studies of reverse micelles, The Journal of Physical Chemistry B, 109 (2005) 21273-21284.
[81] O.A. El Seoud, Use of NMR to probe the structure of water at interfaces of organized assemblies, Journal of Molecular Liquids, 72 (1997) 85-103.
[82] N.M. Correa, J.J. Silber, R.E. Riter, N.E. Levinger, Nonaqueous polar solvents in reverse micelle systems, Chemical reviews, 112 (2012) 4569-4602.
[83] I.R. Piletic, D.E. Moilanen, D.B. Spry, N.E. Levinger, M.D. Fayer, Testing the Core/Shell Model of Nanoconfined Water in Reverse Micelles Using Linear and Nonlinear IR Spectroscopy, The Journal of Physical Chemistry A, 110 (2006) 4985-4999.
[84] A.M. Dokter, S. Woutersen, H.J. Bakker, Ultrafast dynamics of water in cationic micelles, The Journal of Chemical Physics, 126 (2007) 124507.
[85] R. Biswas, J. Furtado, B. Bagchi, Layerwise decomposition of water dynamics in reverse micelles: A simulation study of two-dimensional infrared spectrum, The Journal of Chemical Physics, 139 (2013) 144906.

[86] J. Faeder, B.M. Ladanyi, Molecular Dynamics Simulations of the Interior of Aqueous Reverse Micelles, The Journal of Physical Chemistry B, 104 (2000) 1033-1046.
[87] N. Sarkar, K. Das, A. Datta, S. Das, K. Bhattacharyya, Solvation dynamics of coumarin 480 in reverse micelles. Slow relaxation of water molecules, The Journal of Physical Chemistry, 100 (1996) 10523-10527.
[88] M.R. Harpham, B.M. Ladanyi, N.E. Levinger, K.W. Herwig, Water motion in reverse micelles studied by quasielastic neutron scattering and molecular dynamics simulations, The Journal of chemical physics, 121 (2004) 7855-7868.
[89] A. Chattopadhyay, S. Mukherjee, H. Raghuraman, Reverse micellar organization and dynamics: a wavelength-selective fluorescence approach, The Journal of Physical Chemistry B, 106 (2002) 13002-13009.
[90] P.A. Pieniazek, Y.-S. Lin, J. Chowdhary, B.M. Ladanyi, J. Skinner, Vibrational spectroscopy and dynamics of water confined inside reverse micelles, The Journal of Physical Chemistry B, 113 (2009) 15017-15028.
[91] J. Faeder, B. Ladanyi, Molecular dynamics simulations of the interior of aqueous reverse micelles, The Journal of Physical Chemistry B, 104 (2000) 1033-1046.
[92] S. Zhang, Fabrication of novel biomaterials through molecular self-assembly, Nature biotechnology, 21 (2003) 1171-1178.
[93] A. Bumajdad, J. Eastoe, S. Nave, D.C. Steytler, R.K. Heenan, I. Grillo, Compositions of mixed surfactant layers in microemulsions determined by small-angle neutron scattering, Langmuir, 19 (2003) 2560-2567.
[94] I. Lisiecki, M.P. Pileni, Synthesis of copper metallic clusters using reverse micelles as microreactors, Journal of the American Chemical Society, 115 (1993) 3887-3896.
[95] B.A. Simmons, S. Li, V.T. John, G.L. McPherson, A. Bose, W. Zhou, J. He, Morphology of CdS nanocrystals synthesized in a mixed surfactant system, Nano Letters, 2 (2002) 263-268.
[96] H. Shi, L. Qi, J. Ma, N. Wu, Architectural control of hierarchical nanobelt superstructures in catanionic reverse micelles, Advanced Functional Materials, 15 (2005) 442-450.
[97] P. Alexandridis, U. Olsson, B. Lindman, A record nine different phases (four cubic, two hexagonal, and one lamellar lyotropic liquid crystalline and two micellar solutions) in a ternary isothermal system of an amphiphilic block copolymer and selective solvents (water and oil), Langmuir, 14 (1998) 2627-2638.
[98] S.G. Pandalai, Recent Research Developments in Physical Chemistry, Research Signpost, 8 (2000) 337.
[99] B.K. Paul, R.K. Mitra, Water solubilization capacity of mixed reverse micelles: effect of surfactant component, the nature of the oil, and electrolyte concentration, Journal of colloid and interface science, 288 (2005) 261-279.
[100] H. Kunieda, M. Yamagata, Mixing of nonionic surfactants at water-oil interfaces in microemulsions, Langmuir, 9 (1993) 3345-3351.
[101] M.A. Pes, H. Kunieda, Surfactant distribution in mixed surfactant microemulsions, Trends Phys. Chem., 5 (1995) 75-89.
[102] M.J. Hou, D.O. Shah, Effects of the molecular structure of the interface and continuous phase on solubilization of water in water/oil microemulsions, Langmuir, 3 (1987) 1086-1096.
[103] P.D.T. Huibers, D.O. Shah, Evidence for Synergism in Nonionic Surfactant Mixtures: Enhancement of Solubilization in Water-in-Oil Microemulsions, Langmuir, 13 (1997) 5762 - 5765.
[104] P. Winsor, Hydrotropy, solubilisation and related emulsification processes, Transactions of the Faraday Society, 44 (1948) 376-398.
[105] H. Kunieda, K. Shinoda, Evaluation of the hydrophile-lipophile balance (HLB) of nonionic surfactants. I. Multisurfactant systems, J. Colloid Interface Sci., 107 (1985) 107-121.
[106] S. Chatterjee, R.K. Mitra, B.K. Paul, S.C. Bhattacharya, Interface of AOT/Brij mixed reverse micellar systems: Conductometric and spectrophotometric investigations, Journal of colloid and interface science, 298 (2006) 935-941.

[107] R.K. Mitra, B.K. Paul, Effect of NaCl and temperature on the water solubilization behavior of AOT/nonionics mixed reverse micellar systems stabilized in IPM oil, Colloids and Surfaces A, 255 (2005) 165-180.
[108] R.K. Mitra, B.K. Paul, Investigation on percolation in conductance of mixed reverse micelles, Colloids and Surfaces A: Physicochemical and Engineering Aspects, 252 (2005) 243-259.
[109] R.K. Mitra, B.K. Paul, S.P. Moulik, Phase behavior, interfacial composition and thermodynamic properties of mixed surfactant (CTAB and Brij-58) derived w/o microemulsions with 1-butanol and 1-pentanol as cosurfactants and n-heptane and n-decane as oils, J. Colloid Interface Sci., 300 (2006) 755-764.
[110] T. Kinugasa, A. Kondo, S. Nishimura, Y. Miyauchi, Y. Nishii, K. Watanabe, H. Takeuchi, Estimation for size of reverse micelles formed by AOT and SDEHP based on viscosity measurement, Colloids and Surfaces, A: Physicochemical and Engineering Aspects, 204 (2002) 193-199.
[111] D. Liu, J. Ma, H. Cheng, Z. Zhao, Fluorescence probing of mixed reverse micelles formed with AOT and nonionic surfactants in n-heptane, Colloids and Surfaces A: Physicochemical and Engineering Aspects, 139 (1998) 21-26.
[112] S. Chatterjee, R.K. Mitra, B.K. Paul, S.C. Bhattacharya, Interface of AOT/Brij mixed reverse micellar systems: Conductometric and spectrophotometric investigations, J. Colloid Interface Sci., 298 (2006) 935-941.
[113] S. Chatterjee, S. Nandi, S.C. Bhattacharya, Interface of AOT/Igepal CO720/cyclohexane/water mixed reverse micelle by spectroscopic approach, Colloids and Surfaces A: Physicochemical and Engineering Aspects, 279 (2006) 58-63.
[114] A. Bumajdad, J. Eastoe, R.K. Heenan, R.J. Lu, D.C.S. Steytler, S. Egelhaaf, E., Mixing in cationic surfactant films studied by small-angle neutron scattering, J. Chem. Soc., Faraday Trans., 94 (1998) 2143-2150.
[115] A. Bumajdad, J. Eastoe, P. Griffiths, D.C. Steytler, R.K. Heenan, J.R. Lu, P. Timmins, Interfacial Compositions and Phase Structures in Mixed Surfactant Microemulsions, Langmuir, 15 (1999) 5271-5278.
[116] R.K. Mitra, S.S. Sinha, P.K. Verma, S.K. Pal, Modulation of dynamics and reactivity of water in reverse micelles of mixed surfactants, The Journal of Physical Chemistry B, 112 (2008) 12946-12953.
[117] R. Saha, S. Rakshit, R.K. Mitra, S.K. Pal, Microstructure, morphology, and ultrafast dynamics of a novel edible microemulsion, Langmuir, 28 (2012) 8309-8317.
[118] R.D. Falcone, M.A. Biasutti, N.M. Correa, J.J. Silber, E. Lissi, E. Abuin, Effect of the addition of a nonaqueous polar solvent (glycerol) on enzymatic catalysis in reverse micelles. Hydrolysis of 2-naphthyl acetate by α-chymotrypsin, Langmuir, 20 (2004) 5732-5737.
[119] R. Biswas, S.K. Pal, Caging enzyme function: α-chymotrypsin in reverse micelle, Chemical physics letters, 387 (2004) 221-226.
[120] L. Cammarata, S.G. Kazarian, P.A. Salter, T. Welton, Molecular states of water in room temperature ionic liquids, Physical Chemistry Chemical Physics, 3 (2001) 5192-5200.
[121] T.K. Jain, M. Varshney, A. Maitra, Structural studies of aerosol OT reverse micellar aggregates by FT-IR spectroscopy, The Journal of Physical Chemistry, 93 (1989) 7409-7416.
[122] L.F. Scatena, M.G. Brown, G.L. Richmond, Water at Hydrophobic Surfaces: Weak Hydrogen Bonding and Strong Orientation Effects, Science, 292 ( 2001) 908-912.
[123] A.A. Bakulin, C. Liang, T. la Cour Jansen, D.A. Wiersma, H.J. Bakker, M.S. Pshenichnikov, Hydrophobic Solvation: A 2D IR Spectroscopic Inquest, Accounts of Chemical Research, 42 (2009) 1229-1238.
[124] Y. Maréchal, Horizons In Hydrogen Bond Research 1993 Proceedings of the Xth Workshop \ldHorizons in Hydrogen Bond Research\rd,IR spectroscopy of an exceptional H-bonded liquid: water, Journal of Molecular Structure, 322 (1994) 105-111.
[125] J.-B. Brubach, A. Mermet, A. Filabozzi, A. Gerschel, P. Roy, Signatures of the hydrogen bonding in the infrared bands of water, The Journal of Chemical Physics, 122 (2005) 184509.

[126] L.P. Novaki, N.M. Correa, J.J. Silber, O.A. El Seoud, FTIR and 1H NMR Studies of the Solubilization of Pure and Aqueous 1,2-Ethanediol in the Reverse Aggregates of Aerosol-OT, Langmuir, 16 (2000) 5573-5578.
[127] L.P. Novaki, P.A.R. Pires, O.A. El Seoud, Fourier transform-IR and 1H NMR studies on the structure of water solubilized by reverse aggregates of calcium bis(2-ethylhexyl) sulfosuccinate in organic solvents, Colloid Polym. Sci., 178 (2000) 143-149.
[128] K. Bhattacharyya, Nature of biological water: a femtosecond study, Chemical Communications, DOI 10.1039/B800278A(2008) 2848-2857.
[129] K. Bhattacharyya, Study of Organized Media Using Time-Resolved Fluorescence Spectroscopy, Journal of Fluorescence, 11 (2001) 167-176.
[130] S.K. Pal, J. Peon, A.H. Zewail, Biological water at the protein surface: Dynamical solvation probed directly with femtosecond resolution, Proceedings of the National Academy of Sciences, 99 (2002) 1763-1768.
[131] S.K. Pal, D. Mandal, D. Sukul, S. Sen, K. Bhattacharyya, Solvation Dynamics of DCM in Human Serum Albumin, The Journal of Physical Chemistry B, 105 (2001) 1438-1441.
[132] S.K. Pal, J. Peon, B. Bagchi, A.H. Zewail, Biological Water: Femtosecond Dynamics of Macromolecular Hydration, The Journal of Physical Chemistry B, 106 (2002) 12376-12395.
[133] S.K. Pal, L. Zhao, A.H. Zewail, Water at DNA surfaces: Ultrafast dynamics in minor groove recognition, Proceedings of the National Academy of Sciences, 100 (2003) 8113-8118.
[134] S.D. Verma, N. Pal, M.K. Singh, S. Sen, Sequence-Dependent Solvation Dynamics of Minor-Groove Bound Ligand Inside Duplex-DNA, The Journal of Physical Chemistry B, 119 (2015) 11019-11029.
[135] N. Pal, H. Shweta, M.K. Singh, S.D. Verma, S. Sen, Power-Law Solvation Dynamics in G-Quadruplex DNA: Role of Hydration Dynamics on Ligand Solvation inside DNA, The Journal of Physical Chemistry Letters, 6 (2015) 1754-1760.
[136] A. Patra, S. Hazra, G. Suresh Kumar, R.K. Mitra, Entropy contribution toward micelle-driven deintercalation of drug–DNA complex, The Journal of Physical Chemistry B, 118 (2014) 901-908.
[137] R. Mitra, S. Sinha, S. Pal, Interactions of Nile Blue with Micelles, Reverse Micelles and a Genomic DNA, Journal of Fluorescence, 18 (2008) 423-432.
[138] D. Mandal, S. Sen, K. Bhattacharyya, T. Tahara, Femtosecond study of solvation dynamics of DCM in micelles, Chemical Physics Letters, 359 (2002) 77-82.
[139] D. Banerjee, S.K. Pal, Solvation dynamics of LDS 750 in micelles, reverse micelles and proteins, Chemical Physics Letters, 451 (2008) 237-242.
[140] P.K. Verma, R. Saha, R.K. Mitra, S.K. Pal, Slow water dynamics at the surface of macromolecular assemblies of different morphologies, Soft Matter, 6 (2010) 5971-5979.
[141] P.K. Verma, A. Makhal, R.K. Mitra, S.K. Pal, Role of Solvation Dynamics in the Kinetics of Solvolysis Reactions in Microreactors, Physical Chemistry Chemical Physics, 11 (2009) 8467-8476.
[142] R.K. Mitra, S.S. Sinha, P.K. Verma, S.K. Pal, Modulation of Dynamics and Reactivity of Water in Reverse Micelles of Mixed Surfactants The Journal of Physical Chemistry B, 112 (2008) 12946-12953.
[143] S. Vajda, R. Jimenez, S.J. Rosenthal, V. Fidler, G.R. Fleming, E.W. Castner, Femtosecond to nanosecond solvation dynamics in pure water and inside the [gamma]-cyclodextrin cavity, Journal of the Chemical Society, Faraday Transactions, 91 (1995) 867-873.
[144] S. Sen, D. Sukul, P. Dutta, K. Bhattacharyya, Slow Solvation Dynamics of Dimethylformamide in a Nanocavity. 4-Aminophthalimide in β-Cyclodextrin, The Journal of Physical Chemistry A, 105 (2001) 10635-10639.
[145] R. Jimenez, G.R. Fleming, P. Kumar, M. Maroncelli, dynamics of water, Nature, 369 (1994) 471-473.
[146] S.S. Narayanan, S.S. Sinha, R. Sarkar, S.K. Pal, Picosecond to nanosecond reorganization of water in AOT/lecithin mixed reverse micelles of different morphology, Chemical Physics Letters, 452 (2008) 99-104.

[147] R. Sarkar, M. Ghosh, A.K. Shaw, S.K. Pal, Ultrafast surface solvation dynamics and functionality of an enzyme α-chymotrypsin upon interfacial binding to a cationic micelle, Journal of Photochemistry and Photobiology B: Biology, 79 (2005) 67-78.
[148] P.K. Verma, R.K. Mitra, S.K. Pal, A Molecular Picture of Diffusion Controlled Reaction: Role of Microviscosity and Hydration on Hydrolysis of Benzoyl Chloride at a Polymer Hydration Region, Langmuir, 25 (2009) 11336-11343.
[149] M. Cho, G.R. Fleming, S. Saito, I. Ohmine, R.M. Stratt, Instantaneous normal mode analysis of liquid water, The Journal of chemical physics, 100 (1994) 6672-6683.
[150] S.K. Pal, A.H. Zewail, Dynamics of water in biological recognition, Chemical Reviews, 104 (2004) 2099-2123.
[151] R.K. Mitra, S.S. Sinha, S.K. Pal, Temperature-Dependent Solvation Dynamics of Water in Sodium Bis(2-ethylhexyl)sulfosuccinate/Isooctane Reverse Micelles, Langmuir, 24 (2008) 49-56.
[152] R.K. Mitra, S.S. Sinha, S.K. Pal, Temperature Dependent Hydration at Micellar Surface: Activation Energy Barrier Crossing Model Revisited, The Journal of Physical Chemistry B, 111 (2007) 7577-7581.

# Chapter 2: Instrument Techniques and Systems

In order to explore the structure, dynamics and activity of water in restricted environments different steady-state and dynamical tools have been employed. These include solvation dynamics, fluorescence anisotropy, Fourier transform vibration stretching and enzyme kinetics. In this chapter, we have included a brief discussion about the above mentioned experimental tools. Overviews of the various systems and the fluorescent probes used in the studies have also been discussed.

## 2.1 Steady State and Dynamical Tool

### 2.1.1 Solvation Dynamics

**Theory:** Solvation dynamics relates to the way of reorganization of polar solvent molecules around a dipole created instantaneously or an electron/proton injected suddenly in a polar liquid. A change in the probe (solute) is made at time t = 0 by an ultra-short excitation pulse which leads to the creation of a dipole. This dipole gives rise to an instantaneous electric field on the solvent molecules. The interaction of permanent dipoles of the solvent with the instantaneously created electric field shifts the free energy minimum of the solvent to a non-zero value of the polarization. Since the electronic excitation is much faster than the nuclear motion of atoms in molecules (according to the Frank-Condon principle), the instantaneously excited probe in the vicinity of the solvent molecules find themselves in a relatively high-energy configuration at t=0. Consequently, the solvent molecules around the probe begin to move and relax back to reach their new equilibrium positions (Figure 2.1). The nuclear motion involved in the rearrangement or relaxation process can be broadly classified into rotational and translational motions [1, 2].

Owing to its extensive hydrogen bonding, the rotational motion of water would also include hindered rotation and libration, while translation would include the intermolecular vibration. There are two specific types of high frequency motions: libration and intermolecular vibration, and those are anticipated to play a leading role in the faster part of solvent relaxation. The molecular motions involved are shown schematically in Figure 2.1. In Figure 2.2a we show a typical solvation time correlation function. For clarity, we approximate the motions responsible for the decay in different regions.

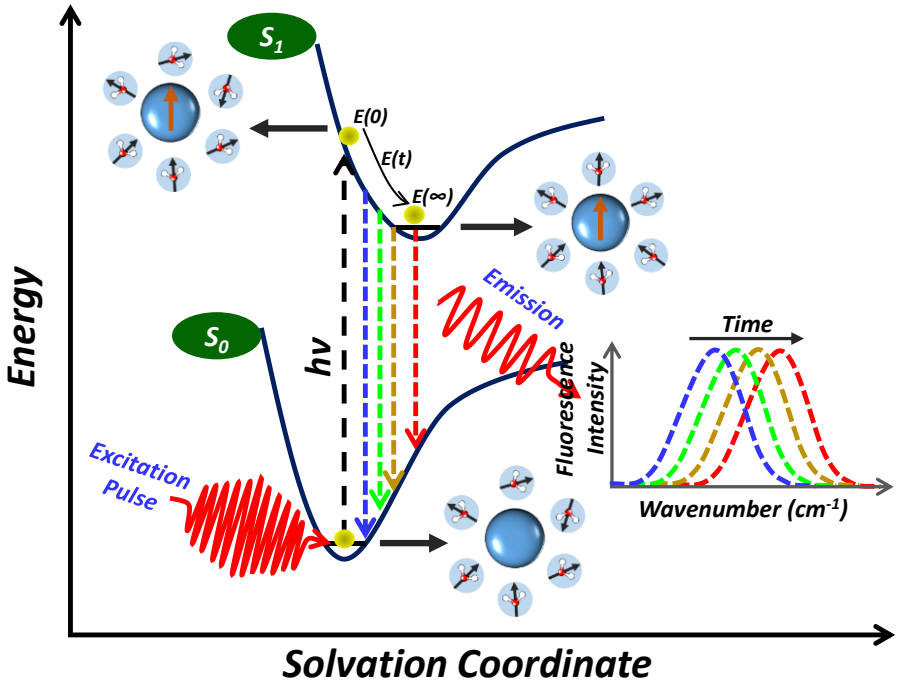


**Figure 2.1**: Schematic representation of the potential energy surfaces involved in solvation relaxation process showing the water orientational motions along the solvation coordinate together with instantaneous excitation. As solvation proceeds the energy of the solute comes down giving rise to a red shift in the fluorescence spectrum.

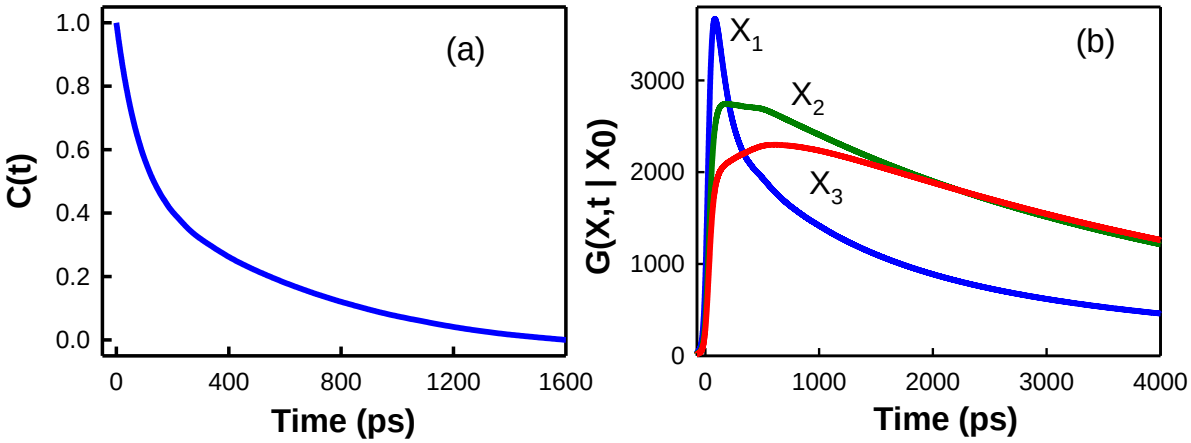


**Figure 2.2:** (a) A typical solvation time correlation function for water in restricted environment. (b) Green's function $G(X,t \mid X_0)$ for population relaxation along the solvation coordinate (X) is plotted against time in picosecond. In G, $X_0$ is the initial position at t = 0. This Figure shows the position and time dependence of the population fluorescence intensity. At early times (when the population is at $X_1$) there is ultrafast rise followed by an ultrafast decay. At intermediate times (when the population is at $X_2$) there is a rise followed by a slow decay as shown by the green line. At long times when the population is nearly relaxed (position $X_3$, red line) only a rise is observed.

The calculated solvation correlation function is always bi-exponential in nature. Within linear response theory, the solvation correlation function is related to the solvation energy as,

$$C(t) = \frac{\langle E(t)\rangle - \langle E(\infty)\rangle}{\langle E(0)\rangle - \langle E(\infty)\rangle} \qquad (2.1)$$

where, $\langle E(0)\rangle$, $\langle E(t)\rangle$ and $\langle E(\infty)\rangle$ are energy along the solvation coordinate of the probe at time t=0, t and ∞ respectively.

Figure 2.1 demonstrates a graphical representation of the solvation potential and the motions involved in the relaxation process for the water molecules around the instantaneously created dipole. From the shape of the potential it can be understood that the transient behaviour of the population during solvation should be a decay function on the blue edge of the spectrum and a rise function on the red edge, as depicted in Figure 2.2.

**Experimental Methods:** In order to experimentally determine the solvation correlation function of a probe in an environment, a number of fluorescence transients are taken at different wavelengths across the emission spectral range of the probe. All the collected fluorescence transients are fitted by using a nonlinear least square fitting procedure to a function,

$$\left( X(t) = \int_0^t E(t')R(t-t')dt' \right) \tag{2.2}$$

including of convolution of the instrument response function (IRF) (*E(t)*) with a sum of exponentials,

$$\left( R(t) = A + \sum_{i=1}^{N} B_i \exp\left(-t/\tau_i\right) \right) \tag{2.3}$$

where, $B_i$ is the pre-exponential factor, $\tau_i$ is the characteristic lifetime of the i$^{th}$ process and a background (*A*). Relative concentration in a multi-exponential decay is finally expressed as:

$$\alpha_n = \frac{B_n}{\sum_{i=1}^{N} B_i}. \tag{2.4}$$

The relative contribution of a particular decay component ($f_n$) in the total fluorescence is defined as,

$$f_n = \frac{\tau_n B_n}{\sum_{i=1}^{N} B_i \tau_i} \times 100. \tag{2.5}$$

The quality of the curve fitting is controlled by reduced chi-square (0.9-1.1) and residual data. The motivation of the fitting is to resolve the decays in an analytical form appropriate for advanced data analysis.

In order to construct time resolved emission spectra (TRES) we follow the technique described in references [3, 4]. As described above, the emission intensity decays are analyzed in terms of the multi-exponential model,

$$I(\lambda,t)=\sum_{i=1}^{N}\alpha_i(\lambda)\exp\left(-t/\tau_i(\lambda)\right) \tag{2.6}$$

where $\alpha_i(\lambda)$ are the pre-exponential factors, with $\Sigma\alpha_i(\lambda)$ = 1.0. In this analysis we compute a new set of intensity decays, which are normalized so that the time-integrated intensity at each wavelength is equal to the steady-state intensity at that wavelength. Considering $F(\lambda)$ to be the steady-state emission spectrum, we calculate a set of $H(\lambda)$ values using,

$$H(\lambda)=\frac{F(\lambda)}{\int_0^\infty I(\lambda,t)dt} \tag{2.7}$$

which for multi-exponential analysis becomes,

$$\mathrm{H}(\lambda)=\frac{\mathrm{F}(\lambda)}{\sum_i \alpha_i(\lambda)\tau_i(\lambda)} \tag{2.8}$$

Then, the appropriately normalized intensity decay functions are given by,

$$I'(\lambda,t)=H(\lambda)I(\lambda,t)=\sum_{i=1}^{N}\alpha_i'(\lambda)\exp\left(-t/\tau_i(\lambda)\right) \tag{2.9}$$

where $\alpha'_i(\lambda) = H(\lambda)\alpha_i(\lambda)$. The values of $I'(\lambda,t)$ are used to calculate the intensity at any wavelength and time, and thus the TRES. The values of the emission maxima and spectral width are determined by nonlinear least-square fitting of the spectral shape of the TRES. The spectral shape is assumed to follow a lognormal line shape,

$$I(\bar{\nu})=I_0\exp\left\{-\left[\ln 2\left(\frac{\ln(\alpha+1)}{b}\right)^2\right]\right\} \tag{2.10}$$

with $\alpha=\frac{2b(\bar{\nu}-\overline{\nu_{\max}})}{\Delta}-1$ where $I_0$ is amplitude, $\bar{\nu}_{max}$ is the wavenumber of the emission maximum and spectral width is given by, $\Gamma=\Delta\left[\frac{\sinh(b)}{b}\right]$. The terms $b$ and $\Delta$ are asymmetry and width parameters, respectively and equation (2.10) reduces to a Gaussian function for $b$ = 0. The time-dependent fluorescence Stokes shifts, as estimated from TRES are used to

construct the normalized spectral shift correlation function or the solvent correlation function *C(t)* and is defined as,

$$C(t) = \frac{\bar{\nu}(t) - \bar{\nu}(\infty)}{\bar{\nu}(0) - \bar{\nu}(\infty)} \tag{2.11}$$

where, $\bar{\nu}(0)$, $\bar{\nu}(t)$ and $\bar{\nu}(\infty)$ are the emission maxima (in $cm^{-1}$) of the TRES at time zero, *t* and infinity, respectively. The $\bar{\nu}(\infty)$ value is considered to be the emission frequency beyond which insignificant or no spectral shift is observed. The *C(t)* function represents the temporal response of the solvent relaxation process, as occurs around the probe following its photoexcitation and the associated change in the dipole moment.

In order to understand distribution of probe or any excited state phenomenon occurring during the excitation we have constructed time-resolved area normalized emission spectroscopy (TRANES), which is a well-established technique [5, 6] and is a modified version of TRES. TRANES were constructed by normalizing the area of each spectrum in TRES such that the area of the spectrum at time t is equal to the area of the spectrum at $t = 0$. A useful feature of this method is that presence of an iso-emissive point in the spectra identifies emission from two species, which are kinetically coupled either irreversibly or reversibly or not coupled at all.

### 2.1.2 Fluorescence Anisotropy

Anisotropy is defined as the extent of polarization of the emission from a fluorophore. These measurements are based on the principle of photo-selective excitation of those fluorophore molecules whose absorption transition dipoles are parallel to the electric vector of the polarized excitation light. In an isotropic solution, fluorophores are oriented randomly. However, upon selective excitation, partially oriented population of fluorophores with polarized fluorescence emission results. The relative angle between the absorption and emission transition dipole moments determines the maximum measured anisotropy ($r_0$). The fluorescence anisotropy ($r$) and polarization ($P$) are defined by,

$$r = \frac{I_{II} - I_{\perp}}{I_{II} + 2I_{\perp}} \tag{2.12}$$

$$P = \frac{I_{II} - I_{\perp}}{I_{II} + I_{\perp}} \tag{2.13}$$

where $I_{\parallel}$ and $I_{\perp}$ are the fluorescence intensities of vertically and horizontally polarized emission when the fluorophore is excited with vertically polarized light. Polarization and anisotropy are interrelated as,

$$r = \frac{2P}{3-P} \tag{2.14}$$

$$P = \frac{3r}{2+r} \tag{2.15}$$

Although polarization and anisotropy provides the same information, anisotropy is preferred since the latter is normalized by the total fluorescence intensity ($I_T = I_{II} + 2I_{\perp}$) and in case of multiple emissive species anisotropy is additive while polarization is not. Several phenomena, including rotational diffusion and energy transfer, can decrease the measured anisotropy to values lower than the maximum theoretical values. Following a pulsed excitation the time resolved fluorescence anisotropy, *r(t)* of a sphere is given by,

$$r(t) = r_0 \exp(-t/\tau_{rot}) \tag{2.16}$$

where $r_0$ is the anisotropy at time $t = 0$ and $\tau_{rot}$ is the rotational correlation time of the sphere.

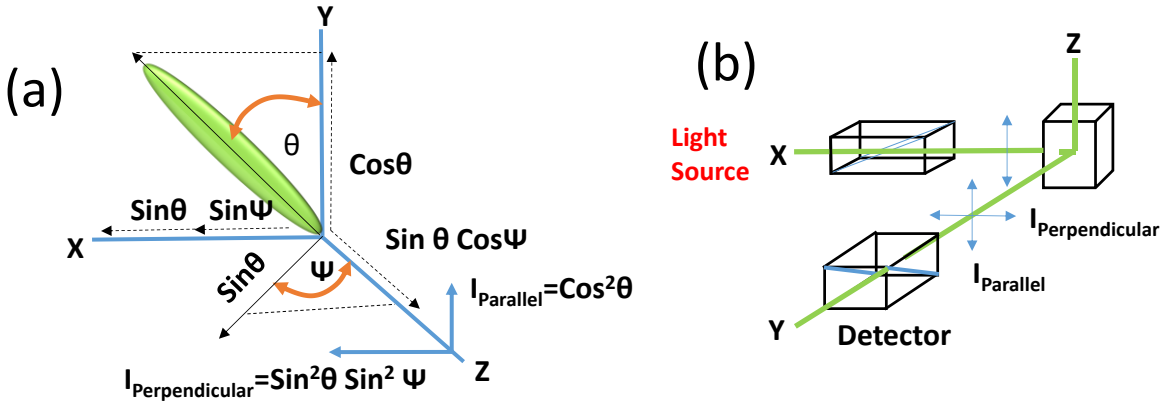


**Figure 2.3:** (a) Emission intensity of a single fluorophore (green ellipsoid) in a coordinate system. (b) Schematic representation of the measurement of fluorescence anisotropy.

**Experimental methods:** For time resolved anisotropy (*r(t)*) measurements (Figure 2.3b), emission polarization is adjusted to be parallel and perpendicular to that of the excitation polarization. Spencer and Weber have derived the relevant equations for the time dependence of $I_{II}(t)$ (equation (2.17)) and $I_{\perp}(t)$ (equation (2.18)) for single rotational and fluorescence relaxation times, $\tau_{rot}$ and $\tau_f$, respectively,

$$I_{II}(t) = \exp(-t/\tau_f)\left(1 + 2r_0 \exp(-t/\tau_{rot})\right) \tag{2.17}$$

$$I_{\perp}(t) = \exp\left(-t/\tau_f\right)\left(1 - r_0 \exp\left(-t/\tau_{rot}\right)\right) \tag{2.18}$$

The total fluorescence is given by,

$$F(t) = I_{II}(t) + 2I_{\perp}(t) = 3\exp\left(-t/\tau_f\right) = F_0 \exp\left(-t/\tau_f\right) \tag{2.19}$$

The time dependent anisotropy, *r(t)* is given by,

$$r(t) = \frac{I_{II}(t) - I_{\perp}(t)}{I_{II}(t) + 2I_{\perp}(t)} = r_0 \exp\left(-t/\tau_{rot}\right) \tag{2.20}$$

*F(t)* depends upon $\tau_f$ while *r(t)* depends upon $\tau_{rot}$, thus these two lifetimes can be separated. This separation is not possible in steady-state measurements. It should be noted that the degree of polarization (*P*) is not independent of $\tau_f$ and is therefore not a useful quantity as *r*. For reliable measurement of *r(t)*, three limiting cases can be considered.

(a) If $\tau_f < \tau_{rot}$, the fluorescence decays before the anisotropy decays, and hence only $r_0$ can be measured.

(b) If $\tau_{rot} < \tau_f$, in contrast to steady-state measurements, $\tau_{rot}$ can be measured in principle. The equations (2.17) and (2.18) show that the decay of the parallel and perpendicular components depends only upon $\tau_{rot}$. The only experimental drawback of this case is that those photons are emitted after few times period of the $\tau_{rot,}$ cannot contribute to the determination of $\tau_{rot}$.

(c) If $\tau_{rot} \approx \tau_f$, then it becomes the ideal situation since almost all photons are counted within the time (equal to several rotational relaxation times) in which *r(t)* shows measurable changes.

For systems with multiple rotational correlation times, *r(t)* is given by,

$$r(t) = r_0 \sum_i \beta_i e^{-t/\tau_i} \tag{2.21}$$

where $\sum_i \beta_i = 1$. It should be noted that the instrument monitoring the fluorescence, particularly the spectral dispersion element, responds differently to different polarizations of light, thus emerging the need for a correction factor. For example, the use of diffraction gratings can yield intensities of emission, which depends strongly upon the orientation with respect to the plane of the grating. It is inevitably necessary when using such instruments to correct for the anisotropy in response. This instrumental anisotropy is usually termed as G-factor (grating factor) and is defined as the ratio of the transmission efficiency for vertically polarized light to

that for horizontally polarized light ($G = I_{II} + I_{\perp}$). Hence, values of fluorescence anisotropy, *r(t)* corrected for instrumental response, would be given by, [7]

$$r(t) = \frac{I_{II}(t) - GI_{\perp}(t)}{I_{II}(t) + 2GI_{\perp}(t)} \tag{2.22}$$

The G-factor at a given wavelength can be determined by exciting the sample with horizontally polarized excitation beam and collecting the two polarized fluorescence decays, one parallel and other perpendicular to the horizontally polarized excitation beam. G-factor can also be determined following long time tail matching technique. If $\tau_{rot} < \tau_f$, it is expected that the curves for $I_{II}(t)$ and $I_{\perp}(t)$ would become identical. If in any experiment they are not, it can usually be assumed that this is due to a non-unitary G-factor. Hence normalizing the two decay curves on the tail of the decay eliminates the G-factor in the anisotropy measurement.

Since the origin of the slower solvation time constants is diffusive in nature we analyze the anisotropy data with a wobbling-in-cone model [8-10]. According to this model, the rotational anisotropy decay function is defined as,

$$r(t) = r_0[\beta e^{-\frac{t}{\tau_{slow}}} + (1-\beta)e^{-t/\tau_{fast}}] \tag{2.23}$$

where $\beta = S^2$, and S is the generalized order parameter that describes the degree of restriction on the wobbling-in-cone orientational motion. Its magnitude is considered as a measure of the spatial restriction of the probe and can have value from zero (for unrestricted rotation of the probe) to one (for completely restricted motion). The semicone angle $\theta_W$ is related to the ordered parameter as,

$$S = \frac{1}{2}\cos\theta_W(1+\cos\theta_W) \tag{2.24}$$

The diffusion coefficient for wobbling motion $D_W$ can be obtained from the following relation,

$$D_W = \frac{1}{(1-S^2)\tau_W}\left[\frac{x^2(1+x)^2}{2(1-x)}\left\{\ln\left(\frac{1+x}{2}\right) + \frac{1-x}{2}\right\} + \frac{1-x}{24}(6+8x-x^2-12x^3-7x^4)\right] \tag{2.25}$$

where x = $\cos\theta_w$ and $\tau_w$ is defined as, $\frac{1}{\tau_w} = \frac{1}{\tau_{fast}} - \frac{1}{\tau_{slow}}$.

## 2.2 Instrumental Setup

### 2.2.1 Steady State Absorption and Emission Technique

Steady-state UV-Vis absorption and emission spectra of the probe molecules were measured with Shimadzu UV-2450 spectrophotometer and Jobin Yvon Fluoromax-3 fluorimeter, respectively. Schematic ray diagrams of these two instruments are shown in Figures 2.4 and 2.5.

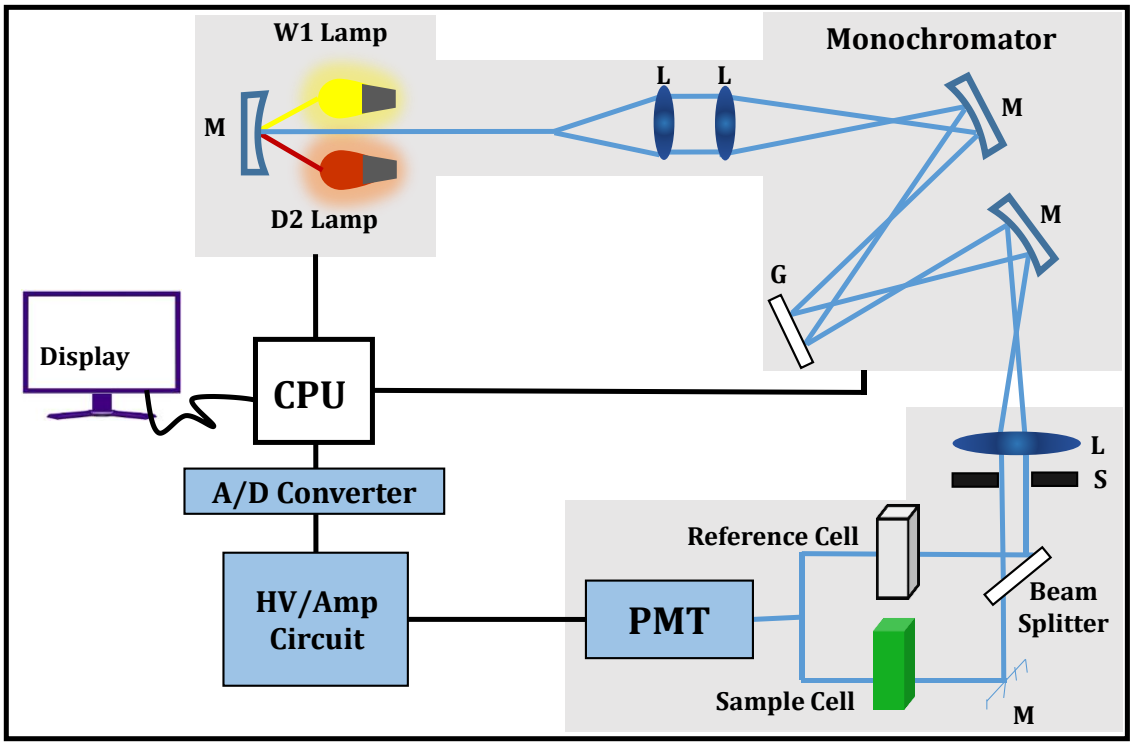


**Figure 2.4.** Schematic ray diagram of an absorption spectrophotometer. Tungsten halogen (W1) and Deuterium lamps (D2) are used as light sources in the visible and UV regions, respectively. M, G, L, S, PMT designate mirror, grating, lens, shutter and photomultiplier tube, respectively. CPU, A/D converter and HV/Amp indicate central processing unit, analog to digital converter and High-voltage/Amplifier circuit, respectively.

Shimadzu UV-2450 gives the facility to measure absorption spectrum in the range of 190-900 nm with a spectral resolution of 0.1 nm, however, experiments are carried out at 1 nm wavelength interval in a cuvette of 1 cm path length. A Deuterium light is used as ultraviolet light source and tungsten light is used as visible light source with a lamp interchange wavelength of 282-293 nm. The only monochromator used in this instrument consists of high performance blazed holographic grating and photomultiplier tube (PMT) is used as the detector. All the absorption spectra are baseline corrected using reference sample. Working principle of UV-Vis spectroscopy follows Beer's Lambert law according to which if $I_0$ is the

intensity of light incident on the cell, and I is that of the emergent light, then absorbance is given by,

$$A = \log_{10}\left(\frac{I_0}{I}\right) = \varepsilon c l \qquad (2.26)$$

where, A is proportional to the concentration (c) of the optically active substance and optical path length (l). If 'c' is in mole $l^{-1}$ and 'l' is in cm, then ε is called the molar absorptivity or molar extinction coefficient.

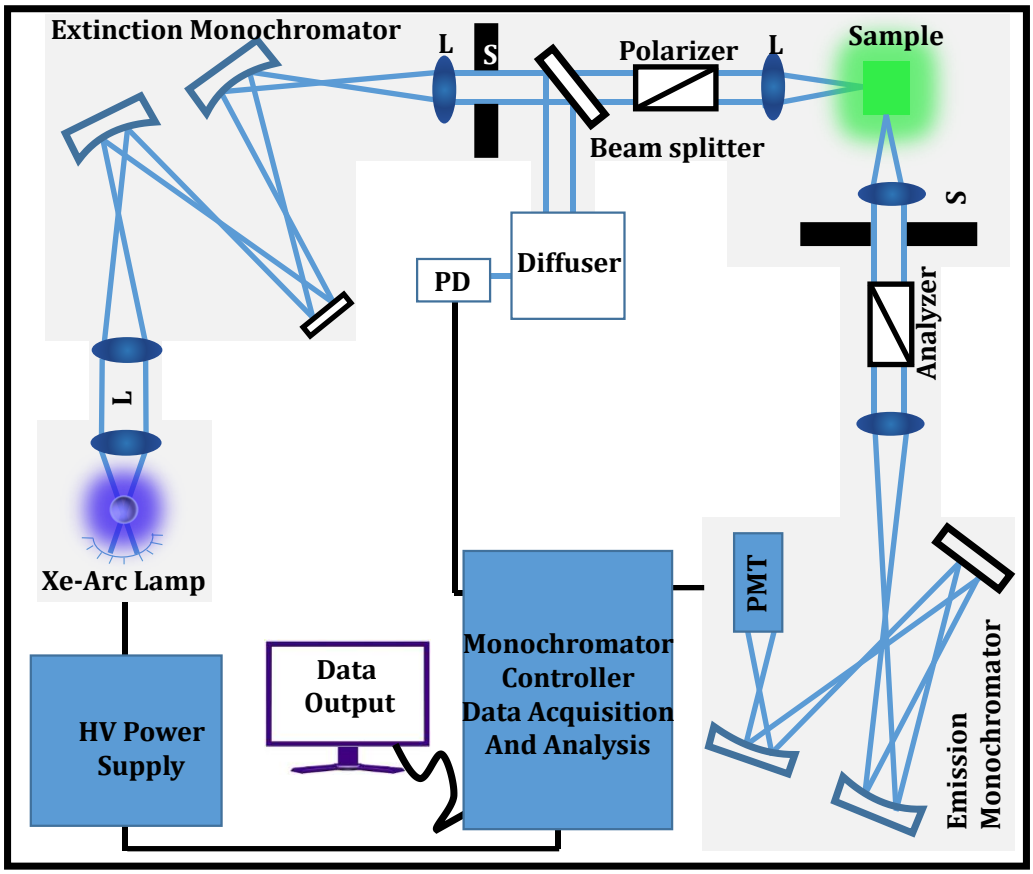


**Figure 2.5.** Schematic ray diagram of an emission spectrofluorimeter. M, G, L, S, PMT and PD represent mirror, grating, lens, shutter, photomultiplier tube and reference photodiode, respectively.

In Fluoromax-3 an ozone free Xe-Arc lamp has been used as a source of continuous wave light. A Fluromax-3 consists of two monochromators[11] which are excitation and emission monochromators. The essential part of these monochromators is reflection grating, the gratings of Fluoromax contains 1200 grooves/mm and are blazed at 330 nm (excitation) and 500 nm (emission). These gratings give an excitation wavelength coverage of 220-600 nm and emission

wavelength coverage of 290-850 nm. All the excitation and emission spectrum are collected in quartz cuvette of 1 cm path length and at 1 nm wavelength interval.

### 2.2.2 Time Correlated Single Photon Counting (TCSPC) Technique

All the picosecond-resolved fluorescence[12] transients were recorded using TCSPC technique[11]. The schematic block diagram of a TCSPC system is shown in Figure 2.6. TCSPC setup from Edinburgh instruments, U.K., was used during fluorescence decay acquisitions. The instrument response functions (IRFs) of the laser sources at different excitation wavelengths varied between 60 ps to 80 ps. Fluorescence signal from the samples was detected by a photomultiplier after dispersion through a grating monochromator. For all the transients, the polarizer in the emission side was adjusted to be at 54.7° (magic angle) with respect to the polarization axis of the excitation beam.

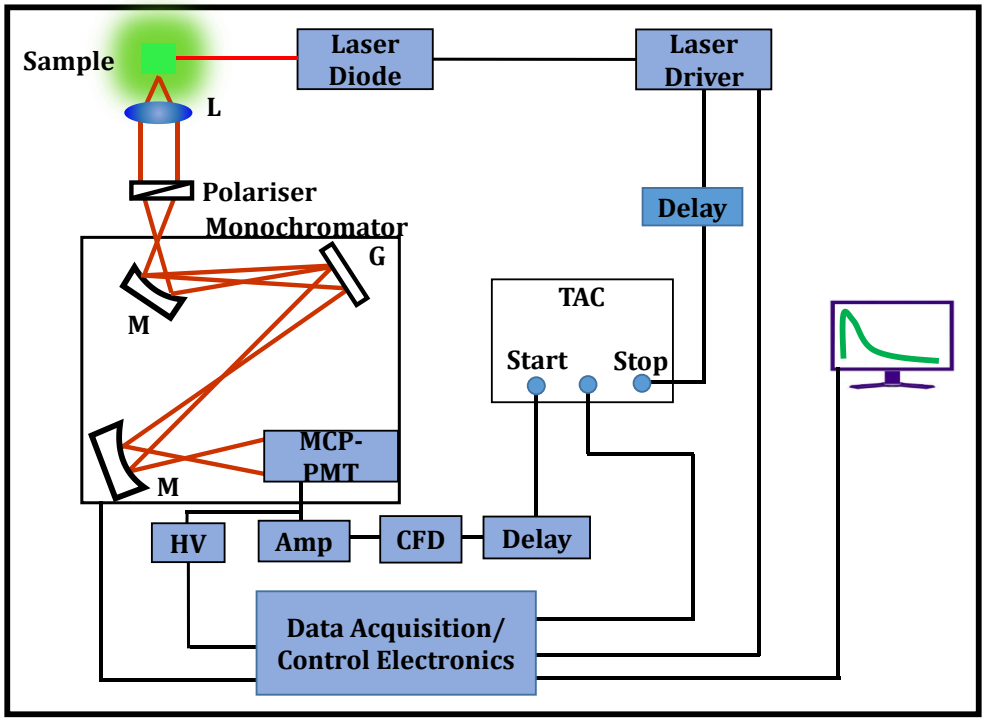


**Figure 2.6**. Schematic ray diagram of a time correlated single photon counting (TCSPC) spectrophotometer. A signal from microchannel plate photomultiplier tube (MCP-PMT) is amplified (Amp) and connected to start channel of time to amplitude converter (TAC) via constant fraction discriminator (CFD) and delay. The stop channel of the TAC is connected to the laser driver via a delay line. L, M, G and HV represent lens, mirror, grating and high voltage source, respectively.

### 2.2.3 Fourier Transform Infra-Red (FTIR) Measurement

FTIR measurements were performed on a JASCO FTIR-6300 spectrometer (transmission mode). Michelson interferometer[13] is the heart of FTIR spectrometer. It consists of a fixed mirror (M4), a moving mirror (M5) and a beam-splitter (BS1), as illustrated in Figure 2.7. The collimated IR beam from the source is partially transmitted to the moving mirror and partially reflected to the fixed mirror by the beam-splitter. The two IR beams are then reflected back to the beam-splitter by the mirrors. The detector then sees the transmitted beam from the fixed mirror and reflected beam from the moving mirror, simultaneously. The two combined beams interfere constructively or destructively depending on the wavelength of the light (or frequency in wavenumbers) and the optical path difference introduced by the moving mirror. The resulting signal is called an interferogram which has the unique property that every data point (a function of the moving mirror position) which makes up the signal has information about every infrared frequency which comes from the source. The measured interferogram signal is then processed through a Fourier transform to obtain the final spectrum. Each spectrum consists of 100 scans (1500−4000 $cm^{-1}$) acquired at 0.5 $cm^{-1}$ resolution.

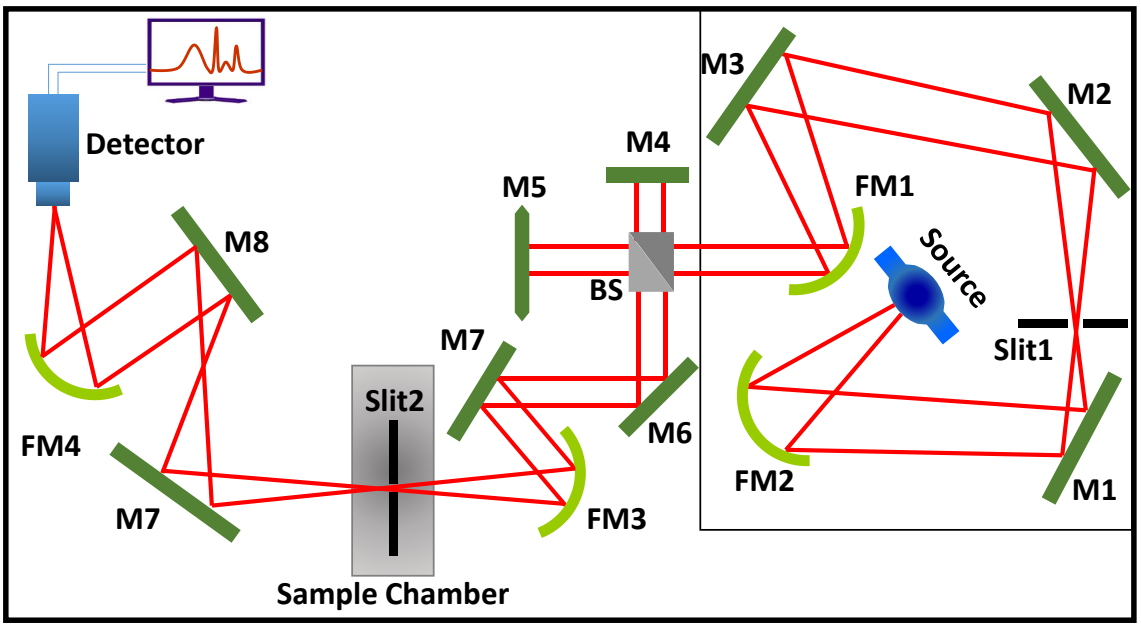


**Figure 2.7.** Schematic of Fourier Transform Infrared (FTIR) spectrometer. It is basically a Michelson interferometer in which one of the two fully-reflecting mirrors is movable, allowing a variable delay (in the travel-time of the light) to be included in one of the beams. M, FM and BS1 represent the mirror, focussing mirror and beam splitter, respectively. M5 is a moving mirror.

## 2.3 Other Measurements

### 2.3.1 Phase Study of ME System

**Construction of phase diagrams:** At constant temperature, the phase diagram of a ternary system comprising of surfactant, oil and polar solvent can be best represented by a Gibbs triangle with the three components as the apexes [14, 15]. In case of a quaternary system comprising of surfactant, cosurfactant, oil and polar solvent, a phase tetrahedral is the best representation of the phase diagram with (surfactant and cosurfactants), oil and polar solvent as the four apexes. Such representation can be simplified by keeping the surfactant: cosurfactant molar ratio constant and cutting the phase tetrahedral at a constant mixture of surfactant molar ratio, which results in a simplified Gibbs triangle. The phase diagram in the present thesis has been constructed using these modified Gibbs triangles. To construct the phase diagrams, oil and surfactants were mixed in different proportions in sealed test tubes, equilibrated at room temperature and then titrated with polar solvents using a microsyringe followed by vigorous shaking in a vortex shaker. The appearance of different phases has been identified with naked eyes and the triangular phase diagrams are constructed accordingly. To carry out the phase volume measurements, calculated amount of surfactant(s), oil and polar solvents were taken in graduated sealed test tubes, shaken vigorously for at least 10–15 min in a vortex shaker, and then kept at room temperature. The samples were kept for long enough time to ensure complete phase separation and then the phase volumes were noted after inspection through naked eyes.

Construction of fish-tail phase diagrams[16] of ME have also been carried out at room temperature. Triangular phase diagram ascertains the limit of single-phase ME domain, whereas fish-tail diagrams were constructed to determine the minimum amount of amphiphile required to form single phase ME[17]. Different phases or Winsors[18] were identified with visual inspection[19]. The appearance of three phase region could clearly be identified as the phases are distinct as shown in figure 2.8.

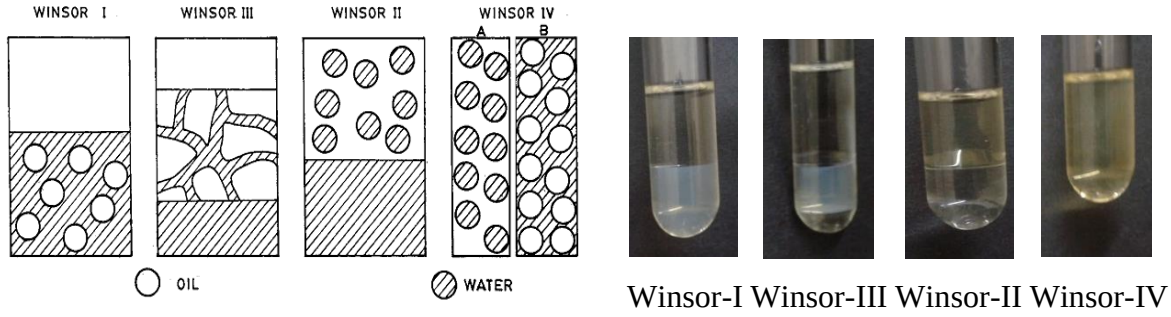


**Fig 2.8:** A representation of different phases or Winsors in ME

### 2.3.2 Study of Various Physical Properties of Water in ME and RM

***(a) Measurement of Solubilization Capacity:*** Water was gradually injected using micro-syringe of varying capacity into 2 ml of surfactant(s) solution in organic solvent (oil) maintained at fixed room temperature with constant stirring in a vortex shaker. The beginning of permanent turbidity at each composition of surfactant blend in oil denotes maximum solubilization of water.

***(b) Dynamic Light Scattering (DLS) Measurement:*** For the estimation of size and size distribution of reverse micellar droplets, DLS measurement was performed with Malvern Nano S instrument employing a 4 mW He-Ne laser ($\lambda$ = 632.8 nm) equipped with a thermostated sample chamber. During the process of data collection, scattering photons were collected at a scattering angle of $173^0$. The instrument measures the time-dependent fluctuation in the intensity of light scattered from the particles in solution at a fixed scattering angle. Measurements were performed at 303 K. Hydrodynamic diameter ($D_h$) of the RM droplets was estimated from the intensity autocorrelation function of the time-dependent fluctuation in intensity. According to Stokes-Einstein equation, $D_h$ is defined as;

$$D_h = \frac{k_B T}{3\pi\eta D} \tag{2.27}$$

where, $k_B$ T, η and D indicate the Boltzmann constant, temperature, viscosity and diffusion coefficient of the solution, respectively. In a typical size distribution graph from the DLS measurement, the *x*-axis shows a distribution of size classes in nanometers, while the *y*-axis shows the relative intensity of the scattered light [20].

***(c) Aggregation number calculation:*** To calculate the aggregation number ($N_{agg}$), i.e., the number of surfactant molecules per RM the following equation was applied [21]

$$r_{DLS} = \sqrt[3]{\frac{3N_{agg}}{4\pi}\left(\frac{V_{H_2O,total}}{n_{surf,micelle}} + V_{surf,hphile}\right)} + l_{hphobe} \tag{2.28}$$

where $r_{DLS}$ is the hydrodynamic radius of the RM $= \frac{d_{hydrodynamic}}{2}$; $d_{hydrodynamic}$ is measured from DLS experiment., $V_{H_2O,total}$ is total volume of water in the system, $n_{surf,micelle}$ is the number of surfactant molecules in all RM, $N_{av}$ is Avogadro number, $V_{surf,hphile}$ is volume of the hydrophilic part of the surfactant which is calculated from [22]. For $X_{Brij}$ = 0.1system, $V_{surf,hphile}$ is calculated from this equation

$$V_{surf,hphile} = x_1 V_{AOT} + x_2 V_{Brij} \quad (2.29)$$

Where $x_1$ is 0.9 and $x_2$ is 0.1. $V_{AOT}$ is head group volume of AOT (0.65 $nm^3$, obtained from [23] $V_{Brij,hphile}$ is calculated from [24], where molar volume of single PEO group i.e. $CH_2CH_2O$ is given and we multiply it by the number of PEO group of different Brij molecules and then the molar volume of OH is added. $l_{hphobe}$ is the length of hydrophobic tail of the surfactant. In the present case AOT concentration is much higher at $X_{Brij} = 0.1$, we use only the hydrophobic tail length of AOT which is 1.257 nm [23].

***(d) Surface Tension Measurement:*** Tensiometric measurements were performed with a K9 tenisometer (Kruss, Germany) by the platinum ring detachment method. A concentrated surfactant solution was added to a known amount of water, and the surface tension values were measured after thorough mixing and temperature equilibration. A microsyringe was used to add surfactant solution gradually to water in the measuring vessel maintained at the fixed room temperature.

***(e) Viscosity, Conductivity and Adiabatic Compressibility Measurement:*** Viscosity of the ME systems at different temperatures were measured by an automated micro viscometer (AVMn) from Anton Paar (Austria). Electrical conductivity of the ME systems measured using a Sension378 conductivity meter (Hach Company, Loveland, CO) at room temperature. For the measurement of conductivity of ME, a solution of 0.9% NaCl was used as the aqueous phase. High precision density (ρ) and sound velocity (u) were measured by a density meter; model DSA-5000 from Anton Paar (Austria).

Adiabatic compressibility (β) of the mixture can be determined by measuring the solution density (ρ) and the sound velocity (u) and applying the Laplace's equation,

$$\beta = \frac{1}{\rho u^2} \quad (2.30)$$

The apparent specific volume of the solute (water) $\phi_v$ is given by[25],

$$\phi_v = \frac{1}{\rho_0} + \frac{\rho_0 - \rho}{c\rho_0} \quad (2.31)$$

where c is the concentration of water in the solution, $\rho_0$ and ρ are the densities of the dry RM ($w_0$=0) and wet RM, respectively. The partial apparent adiabatic compressibility ($\phi_k$) of water is obtained from the relation[26],

$$\phi_k = \beta_0(2\phi_v - 2[u] - \frac{1}{\rho_0}) \quad (2.32)$$

where, [u] is the relative specific sound velocity increment given by,

$$[u] = \frac{u-u_0}{u_0 c} \quad (2.33)$$

where $u_0$ and u are the sound velocities in dry RM and wet RM, respectively.

***(f) FTIR Measurement:*** Relative populations of different types of water and H-bonded structure of water inside RM or ME were measured by mid-infrared Fourier Transform Infrared spectrometer. FTIR spectra in the 3000-3800 $cm^{-1}$ window and 10% $D_2O$ in $H_2O$ in the 2200-2800 $cm^{-1}$ window were recorded on a JASCO FTIR-6300 spectrometer (transmission mode) using $CaF_2$ window. In order to discard the absorbance of the surfactant(s), we take the measured absorbance of the wet RM after ensuring baseline corrections with the stock solutions (i.e. dry RM, $w_0$=0).

## 2.4 Systems

### 2.4.1 Micelle

Micelles can be represented as aggregates of surfactant molecules having hydrophilic heads oriented towards the dissolving solvent (here water) and the hydrophobic tails ordering towards the inside part of the assembly (the micellar core) (Figure 2.4). Micelles appear as the dominant form above the so-called 'critical micelle concentration', CMC, however, free surfactants are also present in the system as monomers.

### 2.4.2 Reverse micelle (RM)

RMs are isotopic mixtures of water, surfactant, and organic solvent in which small aqueous droplets coated with a layer of surfactant molecules are dispersed in a nonpolar solvent. In this thesis various types of surfactants have been used with differently head groups like anionic AOT [Sodium 1,4-bis(2-ethylhexoxy)-1,4-dioxobutane-2-sulfonate], cationic DDAB (didodecyldimethylammonium bromide) and two types of nonionic surfactant like Igepal series (Igepal CO-520, Igepal CA-210 & Igepal CA-630), Brij series (Brij-30, Brij-35, Brij-52, Brij-58, Brij-92, Brij-97) etc. (molecular structures of these surfactants are given in the Figure 2.9). Cyclohexane (Cy) and IPM have been used as the oil to prepare RM [27]. AOT is the most common surfactant that forms stable RM and the properties of its aggregate have been examined in detail[28, 29]. Igepal is also capable to form well defined slightly bigger RMs compared to that of AOT[30]. It is interesting to note that Brij surfactants are too hydrophilic to form RM in oil [31].

### 2.4.3 Microemulsion (ME)

MEs are isotropic, fluid, transparent, thermodynamically stable dispersion of oil and water, stabilized by surfactant(s)[32]. The structure of ME can be idealized as a set of interfaces dividing polar and nonpolar domains. Depending on the composition of the system, the microstructure of an ME may exist as water-in-oil (w/o) droplets, oil-in-water (o/w) droplets, or a bicontinuous structure.

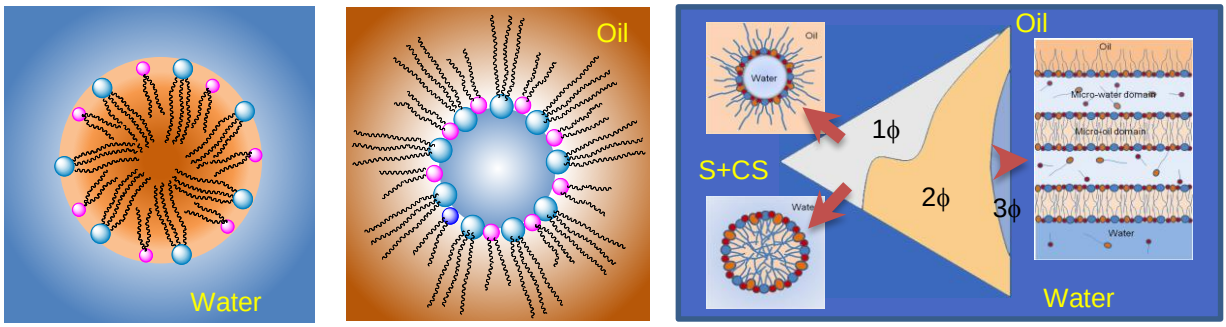


**Fig 2.10:** A representation of different mixed organized assembles; left panel is mixed micelle, middle panel is mixed RM and right panel is ME with mixture of surfactant (S) and cosurfactant (CS).

### 2.4.4 Surfactants

The following surfactants are used: anionic: sodium bis(2-ethylhexyl)sulfosuccinate (AOT), non-ionic: polyoxyethylene(5)nonylphenylether (Igepal CO-520), Lecithin, butyl lactate, TritonX-100, Igepal®CA-210, Igepal®CA-630, polyoxyethylene(4)laurylether **(**Brij-30**),** polyoxyethylene (23)laurylether (Brij-35**),** polyoxyethylene(2)oleylether (Brij-92), polyoxyethylene(2)cetylether (Brij-52), polyoxyethylene(10)oleylether (Brij-97), polyoxyethylene(20)cetylether (Brij-58), polyoxyethylene(20)sorbitantrioleate (Tween-85) and cationic: didodecyldimethylammonium bromide (DDAB).

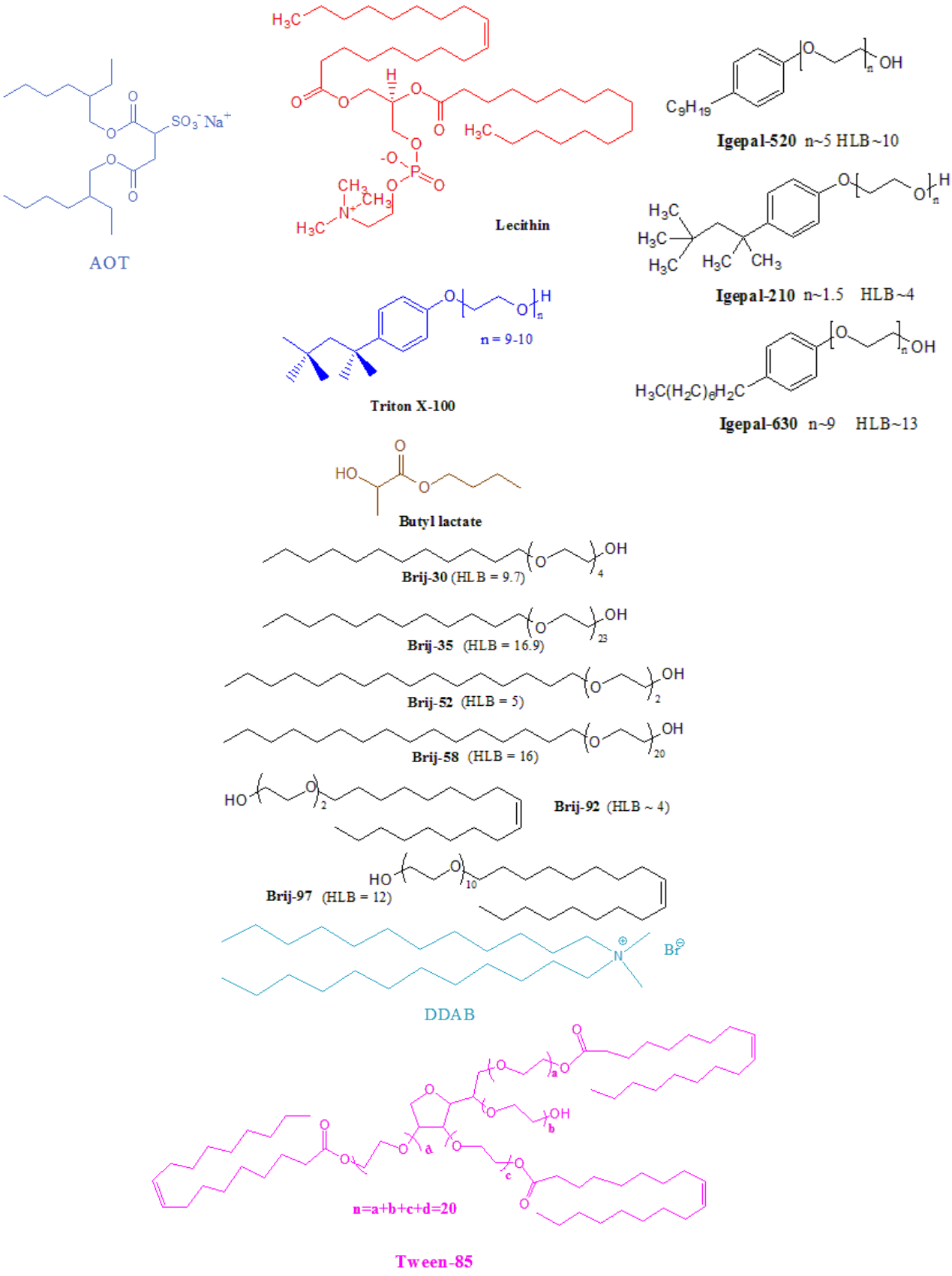


**Figure 2.9:** Molecular structure of different surfactants

### 2.4.5 Solvents

Biocompatible oils like isoproyl myristate (IPM), ethyl myristate (EM), ethyl palmitate (EP) and ethyl oleate (EO) as well as a hydrocarbon oil cyclohexane (Cy) are used.

### 2.4.6 α-Chymotrypsin (CHT)

α-chymotrypsin (Figure 2.11), isolated from bovine pancreas, is a member of the family serine endopeptidase (molecular weight of 25,191 Da) catalysing the hydrolysis of peptides in the small intestine. The three dimensional structure of CHT was solved by David Blow [33]. The molecule is a three-dimensional ellipsoid of dimensions 51 × 40 × 40 Å and comprises of 245 amino acid residues. CHT contains several antiparallel β-pleated sheet regions and little α-helix content. All charged groups are on the surface of the molecule except the catalytic triad of histidine57 (His57), aspartate102 (Asp102) and serine195 (Ser195), which are essential for catalysis. The Ser195 residue is hydrogen bonded to His57 residue, which in turn is hydrogen bonded to β-carboxyl group of Asp102. An oxyanion hole is formed by amide nitrogen of glycine193 and Ser195. It is selective for hydrolysing peptide bonds on the carboxyl side of the aromatic side chains of tyrosine, tryptophan and phenylalanine and of large hydrophobic residues such as methionine. It also catalyses the hydrolysis of ester bonds. CHT enhances the rate of peptide hydrolysis by a factor of $10^9$. The reaction has two distinct phases, acylation and deacylation of the enzyme. Upon binding of the substrate, the hydroxyl group of the Ser195 attacks the carbonyl group of peptide bond to generate a tetrahedral intermediate. In this transient structure, the oxygen atom of the substrate now occupies the oxyanion hole. The acyl-enzyme intermediate forms, assisted by the proton donation of His57. The N-terminal portion is then released and replaced by water. The acyl-enzyme intermediate subsequently undergoes hydrolysis and the enzyme is regenerated.

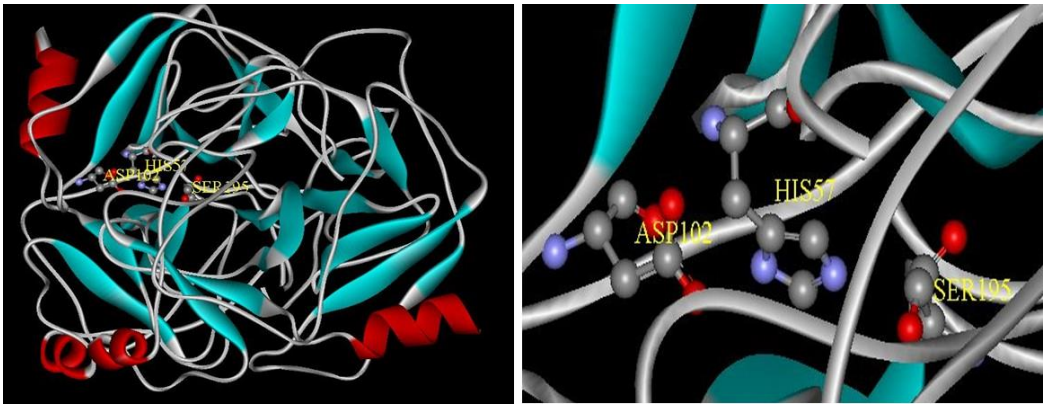


**Figure 2.11***:* X-ray crystallographic structure (PDB code: 1YPH) of α-chymotrypsin depicting the catalytic triad (His57, Asp102 and Ser195).

### 2.4.7 Protease Substrates: Ala-Ala-Phe-7-amido-4-methylcoumarin

AMC is a fluorescent aromatic tripeptide substrate (Figure 2.12) suitable for the cleavage by serine protease. Its concentration is determined using the extinction coefficient, ε= 16 $mM^{-1}cm^{-1}$ at 325 nm. The rate of catalytic activity is determined by monitoring absorbance of cleaved product (7-amido-4-methylcoumarin) having ε = 7.6 $mM^{-1}cm^{-1}$ at 370 nm in aqueous buffer solution. The extinction co-efficient of the product in AOT RM $w_0$=10 is 11.19 $mM^{-1}cm^{-1}$ [34].

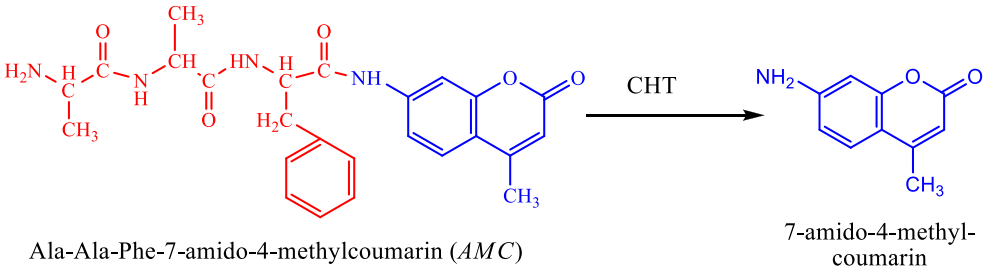


**Figure 2.12.** Molecular structure of substrates and chymotrypsin catalysed hydrolysis product formed from the substrates (Only spectroscopy monitored product is given, other products are not shown in the figure).

### 2.4.8 Molecular Probes

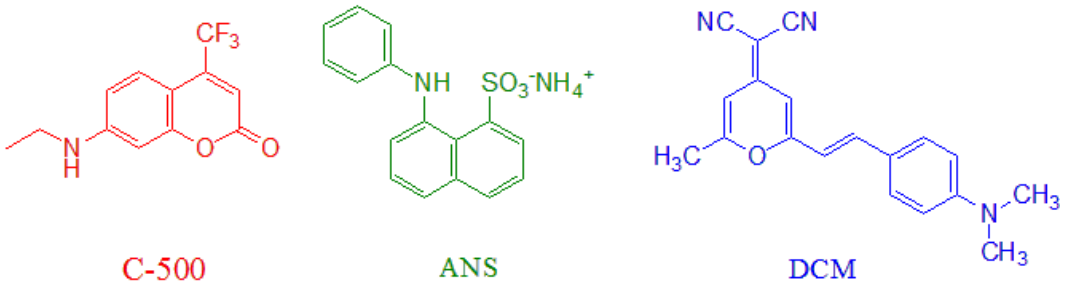


**Figure 2.13:** Molecular structure of C-500, ANS and DCM

**A. Coumarin 500 (C500):** The solvation probe C500 (Figure 2.13) is sparingly soluble in water and shows reasonably good solubility in isooctane. In bulk water the absorption peak (400 nm) is significantly red shifted compared to that in isooctane (360 nm). The emission peak of C500 in bulk water (500 nm) also shows a 90 nm red shift compared to that in isooctane (excitation at 350 nm). The significantly large solvochromic effect in the absorption and emission spectra of C500 makes the dye an attractive solvation probe for micro-heterogeneous environments. The choice of the probe is based on the fact that the probe molecule resides at the interface when it gets excited[20]. The photophysics of the probe have previously been studied in details [35].

**B. 1-anilino-8-naphthalenesulfonic acid, ammonium salt (ANS):** ANS is a well-known solvation probe[36] in aqueous solution, the emission peak of ANS is observed at ~520 nm with a lifetime of ~0.25 ns. The steady-state emission is quenched dramatically in polar solvents. Because of its bi-chromophoric structure, ANS is known to undergo charge transfer (CT) from one aromatic moiety to the other ring. In nonpolar solvents, the emission is strong and mostly form the locally excited state i.e., before charge separation. In polar solvents, the fluorescence decreases which is dominated by the emission from the CT state. As ANS can undergo twisted intramolecular charge transfer (TICT) upon photoexcitation[37], its internal photophysics is not straightforward. However, water inside RM is less polar and highly viscous compared to bulk water which minimizes the rate of non-radiative electron transfer process and thus the TICT process, if any, does not significantly affect the conclusions drawn from the fluorescence measurements[38].

**C. 4-di-(cyanomethylene)-2-methyl-6-(*p*-dimethylaminostyryl)-4H-pyran (DCM)**: DCM (Figure 2.13) is insoluble in water, however soluble in polar organic solvent like ethanol and hydrocarbon solvents like n-heptane. DCM possess a considerable high dipole moment in the excited state (26.3 D) compared to its ground state (5.6 D)[39]. Femtosecond studies reviled various intramolecular processes in the excited state of DCM e.g. electron transfer process and twisted intramolecular charge-transfer[40].

### 2.4.9 Sample Preparation

In this section we will discuss the detail of different sample preparation to study water in restricted environments.

**Preparation of Micellar Solution:** The stock solutions of aqueous micellar solutions were prepared by dissolving surfactants in water. Desired concentration of micelle was ensured by the addition of quantitative amount of stock solution in water with simultaneous stirring of the mixture for an hour. Anionic AOT and nonionic Tween-85 are used to form micelle in water.

**Preparation of Reverse Micellar Solution:** In order to prepare reverse micellar solutions with specific degree of hydration ($w_0$ = [$H_2O$]/[Surfactant]) calculated volume of water was added to a known volume of 0.1 M surfactant solution in cyclohexane or IPM. In case of dissolving a probe inside the water of RM a little amount of aqueous solution of the probe was added during the preparation of the specific RM. All the FTIR, steady state fluorescence and absorption spectra were collected after baseline correction by $w_0$=0 of that RM.

**Preparation of Microemulsion:** To prepare ME, a calculated amount of surfactant (Lecithin and TX-100), cosurfactant (butyl lactate), and oil (IPM) were taken in a sealed tube, shaken vigorously in a vortex mixture, and equilibrated at fixed room temperature. Then water was added into it with the help of a microsyringe, and the mixture was shaken vigorously and then kept at fixed temperature. Reading of different phases was taken by visual observation, after conformation of attainment of complete equilibrium.

### 2.4.10 Measurement of BzCl hydrolysis rate

The kinetics of BzCl solvolysis reaction was determined by measuring the temporal change in the absorbance of BzCl monitored at 313 nm using UV spectrophotometer [41]. The initial BzCl concentration was kept constant at ~10 μM. The reaction follows simple first order kinetics [42, 43]. BzCl is first solubilized in solvent (Cy) and then added into the RM, wherein it gets compartmentalized into the organic phase and the interphase; the interfacial water molecules act as nucleophile to cleave the C-Cl bond. Another partition could also be considered in which BzCl is distributed between the interface and the aqueous phase. The overall reaction rate is accumulation of the rates at these two different phases, however, the very fast reaction in water does not eventually affect the overall slow kinetics.

### 2.4.11 Measurement of Enzyme kinetics

For the enzyme kinetics measurements aqueous stock solutions of CHT were prepared in phosphate buffer (10 mM) at pH 7.0 using double distilled water. Concentration of the enzyme samples in aqueous solution was determined using the extinction coefficient ($\varepsilon = 51\ mM^{-1}cm^{-1}$) value at 280 nm. The enzyme concentration was kept fixed at 0.65 μM. Initial catalytic rates were measured in the time window where the absorbance varies almost linearly with time. To measure the reaction rate in the RM systems, the stock substrate was first injected into the RM solution and stirred until the solution became clear. Then the stock enzyme solution was added to it to initiate the reaction.

## 2.5 References

[1] S.K. Pal, J. Peon, B. Bagchi, A.H. Zewail, Biological Water: Femtosecond Dynamics of Macromolecular Hydration, The Journal of Physical Chemistry B, 106 (2002) 12376-12395.
[2] G.R. Fleming, M. Cho, Chromophore-Solvent Dynamics, Annual review of physical chemistry, 47 (1996) 109-134.
[3] M.L. Horng, J.A. Gardecki, A. Papazyan, M. Maroncelli, Subpicosecond measurements of polar solvation dynamics: coumarin 153 revisited, The Journal of Physical Chemistry, 99 (1995) 17311-17337.
[4] J.R. Lakowicz, Principles of fluorescence spectroscopy, Kluwer Academic/Plenum, New York, 1999.
[5] N. Periasamy, A.S.R. Koti, Time resolved fluorescence spectroscopy: TRES and TRANES, Proceedings of Indian Academy of Sciences, 69A (2003) 41-48.
[6] A.S.R. Koti, M.M.G. Krishna, N. Periasamy, Time-resolved area-normalized emission spectroscopy (TRANES): A novel method for confirming emission from two excited states, The Journal of Physical Chemistry A, 105 (2001) 1767-1771.
[7] J.R. Lakowicz, Principles of Fluorescence Spectroscopy, 2nd ed., Kluwer Academic/Plenum, New York, 2006.
[8] G. Lipari, A. Szabo, Effect of librational motion on fluorescence depolarization and nuclear magnetic resonance relaxation in macromolecules and membranes, Biophysical Journal, 30 (1980) 489.
[9] C.C. Wang, R. Pecora, Time-correlation functions for restricted rotational diffusion, The Journal of Chemical Physics, 72 (1980) 5333-5340.
[10] H.-S. Tan, I.R. Piletic, M.D. Fayer, Orientational dynamics of water confined on a nanometer length scale in reverse micelles, The Journal of Chemical Physics, 122 (2005) 174501.
[11] J.R. Lakowicz, Principles of fluorescence spectroscopy, Springer Science & Business Media2013.
[12] D.V. O'Conner, D. Philips, Time correlated single photon counting, Academic Press, London, 1984.
[13] V. Saptari, Fourier transform spectroscopy instrumentation engineering, SPIE Optical Engineering Press2004.
[14] R.K. Mitra, B.K. Paul, Physicochemical investigations of microemulsification of eucalyptus oil and water using mixed surfactants (AOT+ Brij-35) and butanol, Journal of colloid and interface science, 283 (2005) 565-577.
[15] R.K. Mitra, B.K. Paul, Physicochemical investigations of anionic–nonionic mixed surfactant microemulsions in nonaqueous polar solvents: I. Phase behavior, Colloid and Polymer Science, 284 (2006) 733-744.
[16] R.K. Mitra, B.K. Paul, Effect of temperature and salt on the phase behavior of nonionic and mixed nonionic–ionic microemulsions with fish-tail diagrams, Journal of colloid and interface science, 291 (2005) 550-559.
[17] H. Kunieda, A. Nakano, M.A. Pes, Effect of oil on the solubilization in microemulsion systems including nonionic surfactant mixtures, Langmuir, 11 (1995) 3302-3306.
[18] P. Winsor, Hydrotropy, solubilisation and related emulsification processes, Transactions of the Faraday Society, 44 (1948) 376-398.
[19] S. Moulik, B. Paul, Structure, dynamics and transport properties of microemulsions, Advances in Colloid and Interface science, 78 (1998) 99-195.
[20] R.K. Mitra, S.S. Sinha, S.K. Pal, Temperature-dependent solvation dynamics of water in sodium bis (2-ethylhexyl) sulfosuccinate/isooctane reverse micelles, Langmuir, 24 (2008) 49-56.
[21] J.-L. Lemyre, S. Lamarre, A. Beaupré, A.M. Ritcey, A new approach for the characterization of reverse micellar systems by dynamic light scattering, Langmuir, 26 (2010) 10524-10531.
[22] N. Funasaki, S. Hada, S. Neya, Volumetric study of solubilization of hydrophobic liquids in nonionic micelles, The Journal of Physical Chemistry, 88 (1984) 1243-1248.
[23] K.M. S. P. Moulik, On the Versatile Surfactant Aerosol-OT (AOT): Its Physicochemical and Surface Chemical Behaviours and Uses, Proc. Ind. National Sci. Acad. Rev., Article No. 3 (1996) 215-232.

[24] H. Preu, A. Zradba, S. Rast, W. Kunz, E.H. Hardy, M.D. Zeidler, Small angle neutron scattering of D 2 O–Brij 35 and D 2 O–alcohol–Brij 35 solutions and their modelling using the Percus–Yevick integral equation, Physical Chemistry Chemical Physics, 1 (1999) 3321-3329.
[25] A.A. Zamyatnin, Amino Acid, Peptide, and Protein Volume in Solution, Ann. Rev. Biophys. Bioeng., 13 (1984) 145-165.
[26] A.P. Sarvazyan, Ultrasonic Velocimetry of Biological Compounds, Ann. Rev. Biophys. Biophys. Chem., 20 (1991) 321-342.
[27] B.K. Paul, R.K. Mitra, Water solubilization capacity of mixed reverse micelles: Effect of surfactant component, the nature of the oil, and electrolyte concentration, Journal of Colloid and Interface Science, 288 (2005) 261-279.
[28] R.E. Riter, E.P. Undiks, N.E. Levinger, Impact of counterion on water motion in aerosol OT reverse micelles, Journal of the American Chemical Society, 120 (1998) 6062-6067.
[29] S. Nave, J. Eastoe, R.K. Heenan, D. Steytler, I. Grillo, What is so special about Aerosol-OT? 2. Microemulsion systems, Langmuir, 16 (2000) 8741-8748.
[30] A. Das, A. Patra, R.K. Mitra, Do the physical properties of water in mixed reverse micelles follow a synergistic effect: a spectroscopic investigation, The Journal of Physical Chemistry B, 117 (2013) 3593-3602.
[31] R.K. Mitra, S.S. Sinha, P.K. Verma, S.K. Pal, Modulation of dynamics and reactivity of water in reverse micelles of mixed surfactants, The Journal of Physical Chemistry B, 112 (2008) 12946-12953.
[32] B.K. Paul, S.P. Moulik, Microemulsions: an overview, Journal of Dispersion science and Technology, 18 (1997) 301-367.
[33] J.J. Birktoft, D.M. Blow, The Structure of Crystalline Alpha-Chymotrypsin, V.The Atomic Structure of Tosyl-Alpha-Chymotrypsin at 2 Angstroms Resolution, Journal of Molecular Biology, 68 (1972) 187-240.
[34] R. Biswas, S.K. Pal, Caging enzyme function: a-chymotrypsin in reverse micelle, Chemical Physics Letters, 387 (2004) 221-226.
[35] S. Nad, H. Pal, Photophysical Properties of coumarin-500 (C500): unusual behavior in nonpolar solvents, J. Phys. Chem. A, 107 (2003) 501-507.
[36] R.P. DeToma, J.H. Easter, L. Brand, Dynamic interactions of fluorescence probes with the solvent environment, Journal of the American Chemical Society, 98 (1976) 5001-5007.
[37] E.M. Kosower, Intramolecular donor-acceptor systems. 9. Photophysics of (phenylamino) naphthalenesulfonates: a paradigm for excited-state intramolecular charge transfer, Acc. Chem. Res., 15 (1982) 259-266.
[38] J. Zhang, F.V. Bright, Nanosecond reorganization of water within the interior of reversed micelles revealed by frequency-domain fluorescence spectroscopy, J. Phys. Chem., 95 (1991) 7900-7907.
[39] S.K. Pal, D. Mandal, D. Sukul, K. Bhattacharyya, Solvation dynamics of 4-(dicyanomethylene)-2-methyl-6-(p-dimethylaminostyryl)-4H-pyran (DCM) in a microemulsion, Chemical physics letters, 312 (1999) 178-184.
[40] T. Gustavsson, G. Baldacchino, J.-C. Mialocq, S. Pommeret, A femtosecond fluorescence up-conversion study of the dynamic Stokes shift of the DCM dye molecule in polar and non-polar solvents, Chemical physics letters, 236 (1995) 587-594.
[41] P.K. Verma, A. Makhal, R.K. Mitra, S.K. Pal, Role of Solvation Dynamics in the Kinetics of Solvolysis Reactions in Microreactors, Phys. Chem. Chem. Phys., 11 (2009) 8467-8476.
[42] M.A. Lopez-Quintela, C. Tojo, M.C. Blanco, L. Garcıa Rio, J.R. Leis, Microemulsion dynamics and reactions in microemulsions, Curr. Opin. Colloid Interface Sci. , 9 (2004) 264-278.
[43] L. Garcia-Rio, J.R. Leis, E. Iglesias, Influence of Water Structure on Solvolysis in Water-in-Oil Microemulsions, J. Phys. Chem., 99 (1995) 12318-12326.

# Chapter 3: Structure, Dynamics and Activity of Anionic-nonionic Mixed Surfactant Reverse Micellar System

## 3.1 Introduction

Aggregates of surfactants in oil continuum exhibit the remarkable ability to solubilize large amount of water to form RM, which offers an unique platform to realize several constrained environment like living cell[1]. The physical and chemical properties of water molecules localized in the interior of the RMs are different from those of pure water, the difference becoming progressively smaller as the water content in the micellar system increases. When the RM size is small, the interface strongly interacts with most of the water molecules making them 'highly structured'. Since hydrogen bond dynamics is a concerted process requiring the rearrangement of the hydrogen bonds of many water molecules, the dynamics become relatively slow. This constrain is partially relaxed at higher hydration and the system approaches a pure water like behaviour. Solubilization capacity of RM and physicochemical properties of the entrapped water has been found to be strongly dependent on the chemical nature of the dispersant phase (oil), surfactant and also on the hydration level of the RM ($w_0$= [water]/[surfactant])[2, 3]. Surfactant mixtures often give rise to enhanced performance over the individual components, and such mixtures could potentially be employed in a wide range of practical applications. It has recently been reported that addition of non-ionic surfactant into the interface of ionic surfactants produces significant modification of enzyme activity[4-6], polymer synthesis[7], nanoparticle synthesis[8], chemical activity[9] in RM. A proper rationale of such modified behaviour is strongly demanding specially in many biophysical applications that depend upon the extent of electrostatic and hydrophobic interactions of the RM interface with specific moiety or segments of solubilized biological macromolecules[10-12].

Modification of the interface by blending of surfactants brings about considerable changes in the elastic rigidity of the interfacial film. Earlier studies with RM systems involving more than one surfactant using solubilization[13-16], conductivity[15, 17], interfacial composition[18], viscosity[19], spectroscopic[20-22], SANS[23-25], FTIR and NMR measurements[26, 27] identify significant modification of the mechanical properties of the interface and consequently of the water structure in RM systems in comparison to the corresponding single surfactant systems. These findings summarize that the effects of

surfactant blending on solubilization and other physical properties are a direct consequence of mixing, and physicochemical interactions in interfacial films.

It is well-known that water inside RMs is highly structured and its dynamics is highly restricted[28, 29]. A recent study[30] has concluded that confinement of water in the RM interior is responsible for the observed slow relaxation dynamics, irrespective of the charge of the interface. On the other hand, Levinger et al.[31-33] compared the ultrafast solvation dynamics of ionic (AOT) and non-ionic (Brij-30) RM systems and find that solvation dynamics of the former is slower than that of the latter. A possible source for the observed difference might be the difference in the interaction of water with the charged and uncharged interfaces. However, the effect of mixing of surfactants on the relaxation dynamics of water has only rarely been explored[34, 35].

In a previous study[36], we attempted to correlate the structure, dynamics and reactivity of entrapped water in RM consisting of a mixture of ionic (AOT) and non-ionic (Brij-30) surfactant in isooctane, which has a high molecular volume and less penetrability in the surfactant interface. This leads the solubilization capacity of AOT/isooctane RM systems to be limited by the inter-droplet interaction effect[13]. AOT/Brij-30 mixed system in isooctane does not offer any synergistic effect in terms of water solubilization capacity. The physical properties of water also showed a linear trend with mixing and it was found that the entrapped water reaches a pure water like behaviour as $X_{\text{Brij-30}}$ (mole fraction of Brij-30 in the surfactant mixture) increases, which is due to the weaker interaction of Brij-30 head group with water compared to that of the charged head group of AOT. To complement this study, we study the structure and dynamics of a mixed system in which synergistic modification of the surfactant monolayer in terms of solubilization capacity could be realized. The mixture of ionic surfactant AOT and non-ionic surfactant Igepal-520 in cyclohexane (Cy) offers such a platform[16]. Both AOT[37] and Igepal CO-520[38] are well-studied surfactants that can form RM without the addition of any cosurfactant. In the present contribution we have studied the structure and slow (sub-ns) relaxation dynamics of water in RMs constituted of AOT and Igepal CO-520 in Cy at different mixing ratios with the key objective to reveal whether the synergistic geometric modification of the interface affects the physical nature of entrapped water. The micellar sizes at different mixing ratios have been measured by dynamic light scattering (DLS) technique. The physical properties of the entrapped water have been determined using Fourier transform infrared spectroscopy (FTIR), densimetric measurements and solubility study. Relaxation dynamics of water inside RM has been probed by time-resolved fluorescence spectroscopy using coumarin 500 (C500) as the fluorophore. This spectroscopic technique, specially the slow

relaxation process, which essentially represents the coupled rotational-translational orientation of water molecules, has recently been evolved as a potential tool to understand the interaction of confined water molecules with the interface[36, 39-44]. Using a fluorophore that essentially resides at the water-surfactant interface, the extent of modification of water dynamics in response to any change in interfacial morphology could be rationalized by probing such relaxation processes. The choice of the probe is based on the fact that when excited at 409 nm, only the probe molecules residing at the interface and/or facing the polar core get excited[40]. Thus the spectroscopic information obtained is essentially the responses from the interfacial region only, which is a prerequisite for our study. To understand the geometrical restriction of the probe at the interface, rotational relaxation dynamics of the dye in different RM systems have also been determined. All the measurements have been done at six different mixing ratios of AOT and Igepal with the mole fraction of Igepal in the mixture ($X_{Igepal}$ = [Igepal]/([AOT] + [Igepal])), varying as 0, 0.2, 0.4, 0.6, 0.8 and 1 at three hydration levels, namely, $w_0$ = 5, 10 and 15.

## 3.2 Results and Discussions

***Solubilization capacity measurements:*** Figure 3.1 depicts the maximum water solubilization capacity of mixed AOT/Igepal/Cy RM systems. Both AOT and Igepal are fairly soluble in Cy and both these systems solubilize water in the $w_{0,max}$ range of 20-25, which is in good agreement with the reported literature[16]. The mixed surfactant systems exhibit a considerable synergism in the water solubilization capacity wherein $w_{0,max}$ (maximum solubilization capacity) initially increases with increasing $X_{Igepal}$ to pass through a maximum at $X_{Igepal}$=0.4 beyond which it decreases. Such synergistic solubilization behaviour has earlier been reported in a few mixed surfactant systems[14-16, 24, 25, 45]. The extent of water solubilization in general can be explained in the light of a theoretical model developed by Hou and Shah[13]. Solubilization capacity of water in RM is geometrically related to the radius of curvature of the surfactant film separating the water droplets from the oil continuum. This in turn is thermodynamically related to the stability of the RM. The stability of a RM is primarily decided by the entropic contribution of droplet dispersion, curvature effect and the interaction between the droplets[46, 47]. The radius of curvature and hence water solubilization capacity decreases as the chain length of oil decreases, chain length of cosurfactant increases or size of the polar head group of the surfactant increases.

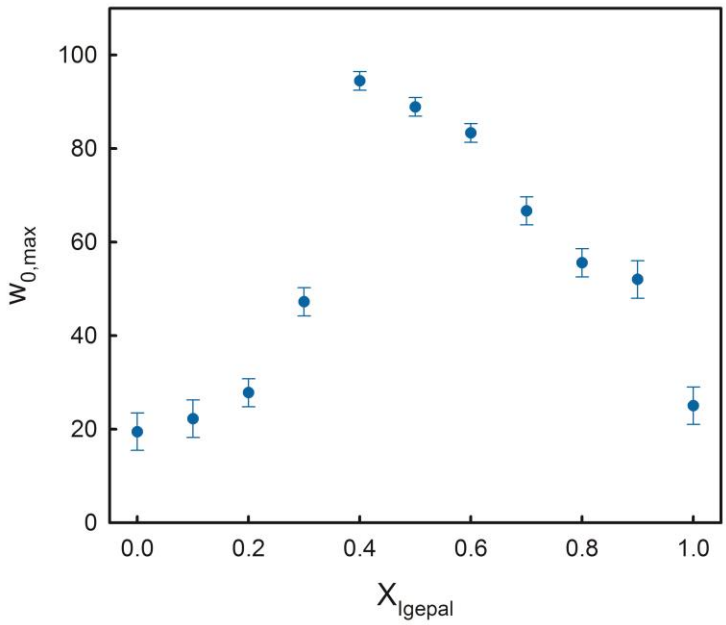


**Figure 3.1.** Maximum solubilization capacity ($w_{0,max}$) of AOT/Igepal/Cy mixed reverse micellar systems as a function of $X_{Igepal}$.

AOT/Cy is a system consisting of a rather rigid interface (owing to the low molecular weight of Cy (~180 $Å^3$) and high penetration of Cy in the interfacial region making the attractive strength small and favouring greater spontaneous curvature) with very low values of $\Delta\rho$ (difference between densities in the continuous phase and in the penetrable length of the interfacial layer) and $\xi$ (penetrable length of the interfacial layer during interpenetration of droplets). In such a case the interaction among the droplets is very weak compared to the curvature effect, and solubilization capacity is essentially limited by the radius of curvature. Solubilization capacity can be improved if the interface is doped with a second surfactant (herein Igepal 520) which decreases the spontaneous curvature of the interfacial film making the interface more fluid. However, in doing so both $\Delta\rho$ and $\xi$ increases, which in turn increases the interaction between the droplets. The increase in $w_{0,max}$ is limited as the spontaneous radius of curvature approaches the critical radius $R_c$. Beyond this point the increase in $\Delta\rho$ and $\xi$ decreases $w_{0,max}$. The observed synergism is thus a consequence of systematic alteration of the mechanical properties of the interfacial monolayer which is optimized at $X_{Igepal}$=0.4. It is now interesting to investigate whether such a modification imprints the physical properties of the encapsulated water molecules inside the RMs.

***DLS, aggregation number and compressibility Measurements:*** We measure the size of the RM droplets using DLS technique and the results are depicted in figure 3.2a and table 3.1. The data analysis essentially assumes the droplets to be spherical in nature and for small $w_0$ ($\leq$15)

values, such an assumption holds well. As observed from the figure droplet size increases with increase in $w_0$ as well as $X_{Igepal}$. The $w_0$ dependency is a clear consequence of the increasing water load[40, 48]. Igepal forms larger droplets compared to AOT[19, 38] and this accounts for the increased droplet size of mixed RM systems with increasing $X_{Igepal}$. No anticipated deviation from linearity in the $X_{Igepal}$=0.4 region is unambiguously noticed. This increase in droplet radius with $X_{Igepal}$ is consistent with the hard sphere model of AOT/Cy system as has been discussed earlier. We also measure the droplet size at $X_{Igepal}$=0.4 with increasing $w_0$ values (data not shown). The size increases linearly with $w_0$ clearly indicating that addition of water increases droplet size rather than forming multiple droplets.

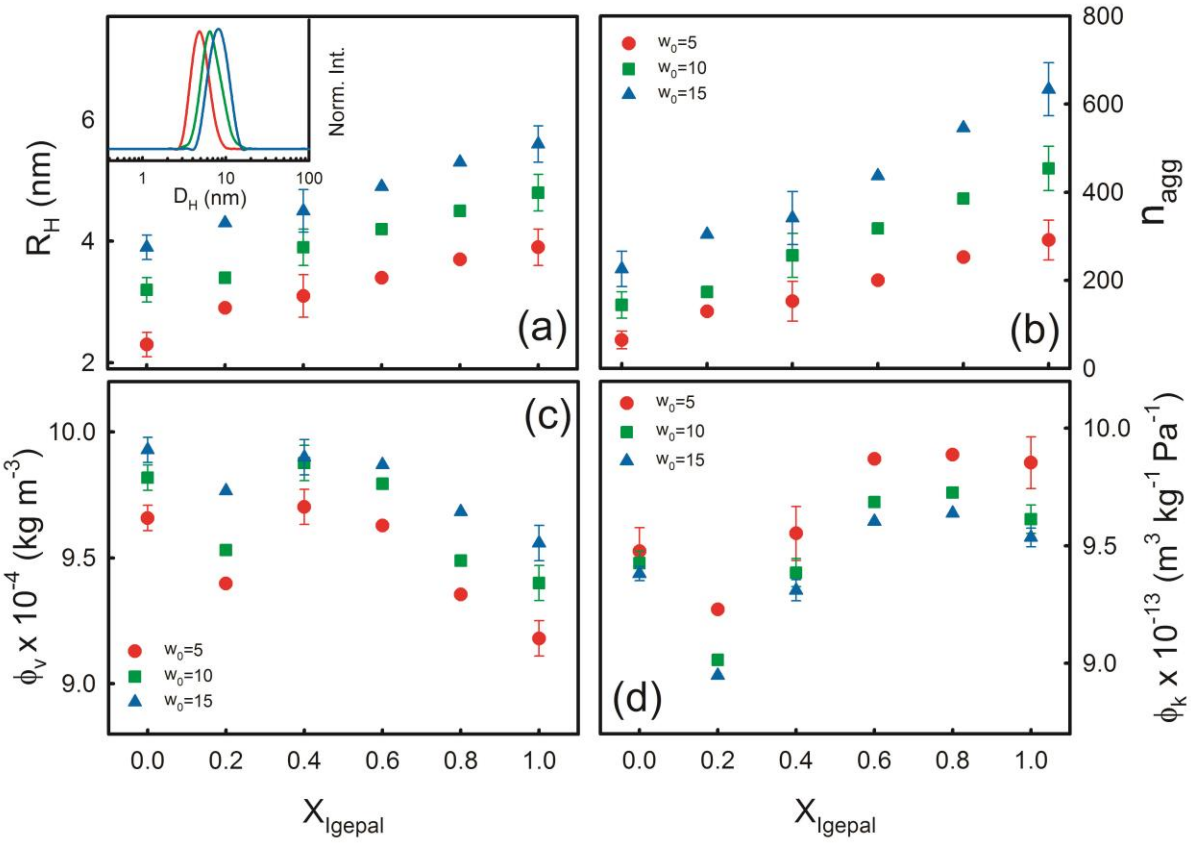


**Figure 3.2.** (a) Hydrodynamic radius ($R_H$) of AOT/Igepal/Cy mixed reverse micellar systems as a function of $X_{Igepal}$. The inset shows a typical normalized scattering intensity profile of $X_{Igepal}$=0 (red), 0.4 (green) and 1.0 (blue) RM systems. (b) The aggregation number ($n_{agg}$) of the mixed RMs as a function of $X_{Igepal}$. (c) Specific volume, $\phi_v$ and (d) partial apparent adiabatic compressibility, $\phi_k$ of water in these mixed RMs at different $w_0$ values as a function of $X_{Igepal}$.

**Table 3.1.** DLS, volumetric and densimetric measurement parameters for AOT/Igepal/Cy/water mixed RM systems at different $w_0$ and mixing ratios.

| $w_0$ | $R_H$ (nm) | ρ (kg $m^{-3}$) | u (m $s^{-1}$) | $n_{agg}$ | $\varphi_v \times 10^{-4}$ ($m^3$ $kg^{-1}$) | $\varphi_k \times 10^{-13}$ ($m^3$ $kg^{-1}$ $Pa^{-1}$) |
|---|---|---|---|---|---|---|
| | | | **$X_{Igepal}$=0** | | | |
| 5 | 2.3 | 785.759 | 1222.35 | 64 | 9.66 | 9.48 |
| 10 | 3.2 | 787.722 | 1220.26 | 144 | 9.81 | 9.43 |
| 15 | 3.9 | 789.564 | 1218.42 | 226 | 9.93 | 9.38 |
| | | | **$X_{Igepal}$=0.2** | | | |
| 5 | 2.9 | 785.313 | 1223.22 | 129 | 9.40 | 9.23 |
| 10 | 3.4 | 787.503 | 1221.14 | 175 | 9.53 | 9.01 |
| 15 | 4.3 | 789.290 | 1219.68 | 304 | 9.77 | 8.95 |
| | | | **$X_{Igepal}$=0.4** | | | |
| 5 | 3.1 | 784.657 | 1224.72 | 152 | 9.70 | 9.55 |
| 10 | 3.9 | 786.579 | 1222.78 | 257 | 9.88 | 9.39 |
| 15 | 4.5 | 788.576 | 1220.77 | 341 | 9.90 | 9.31 |
| | | | **$X_{Igepal}$=0.6** | | | |
| 5 | 3.4 | 784.155 | 1226.32 | 200 | 9.63 | 9.87 |
| 10 | 4.2 | 786.146 | 1224.08 | 318 | 9.79 | 9.69 |
| 15 | 4.9 | 788.094 | 1221.96 | 437 | 9.87 | 9.60 |
| | | | **$X_{Igepal}$=0.8** | | | |
| 5 | 3.7 | 783.197 | 1227.91 | 252 | 9.35 | 9.89 |
| 10 | 4.5 | 785.434 | 1225.24 | 386 | 9.49 | 9.73 |
| 15 | 5.3 | 787.358 | 1223.14 | 546 | 9.68 | 9.64 |
| | | | **$X_{Igepal}$=1.0** | | | |
| 5 | 3.9 | 781.923 | 1229.18 | 337 | 9.18 | 9.85 |
| 10 | 4.8 | 784.175 | 1226.61 | 425 | 9.40 | 9.61 |
| 15 | 5.6 | 786.248 | 1224.33 | 599 | 9.56 | 9.54 |

We calculate the aggregation number ($n_{agg}$) of RM systems and the results are depicted in of figure 3.2b and table 3.1. It is found that Igepal RM systems have higher aggregation number compared to the AOT RM systems. The $n_{agg}$ values obtained for AOT are in good agreement with those reported by Maitra et al. using NMR technique[49]. It is interesting to note that as Igepal is mixed with AOT $n_{agg}$ increases, which is a consequence of the reduced electrostatic repulsion between the charged head groups of AOT, thereby accommodating more surfactant molecules at the interface. Since surfactant concentration is fixed at 0.1 M, increase in aggregation number at a fixed $w_0$ value is indicative of a decrease in the number of water droplets which provides additional support to the increased droplet size as evidenced from DLS

measurements (figure 3.2a). No considerable change in the aggregation behaviour is realized at $X_{Igepal}$=0.4. We also calculate the apparent specific volume ($\phi_v$) and partial apparent adiabatic compressibility ($\phi_k$) of water in these RM systems (figure 3.2c, 3.2d and table 3.1). The obtained $\phi_v$ values are in the same order of magnitude as obtained for other RM systems[36, 50, 51] and is smaller than that of pure water ($1.003\times10^{-3}$ $m^3kg^{-1}$). On the other hand all the calculated compressibility values are higher than that of pure water ($4.5\times10^{-10}$ $Pa^{-1}$), which essentially indicates the highly structured nature of water inside RM. In all these systems $\phi_v$ increases with increasing $w_0$ which is in accordance with previous observations[51] and accounts for the fact that the abundance of high density interfacial water at lower hydration is responsible for the reduced $\phi_v$. The $\phi_v$ values do not exhibit any distinct feature with the mixing ratio, it only reduces marginally as Igepal concentration is increased (figure 3.2c). AOT RM systems offer higher $\phi_v$ values compared to nonionic RM systems[51] which corroborates the present observation of decreasing $\phi_v$ with increasing nonionic content. The $\phi_k$ values also exhibit good agreement with previous reports[36, 50, 51] and offer an overall increasing trend with increasing Igepal concentration. The compressibility data thus provides evidence that water structure is essentially perturbed inside RM due to its interaction with the charged/polar interface, however, the overall linear behavior of the compressibility values indicate that the interfacial stochiometric optimization at $X_{Igepal}$=0.4 in regard to water solubilization capacity is not reflected in the physical properties of water.

***FTIR Measurements:*** To obtain a deeper insight into the water structure we measure the MIR FTIR spectra of all the mixed RM systems. In all these measurements we subtract the data of $w_0$=0 (dry RM) systems from the hydrated systems and thus the signals essentially provide information from water molecules embodied in the RM water pool. We focus our attention in the 3000-3800 $cm^{-1}$ frequency window as this is a fingerprint region for the symmetric and asymmetric vibrational stretch of O-H bonds in water[52, 53]. The overall spectrum of water in this frequency window could be deconvoluted into three Gaussian sub-bands peaking at ~3600, 3460 and 3330 $cm^{-1}$ regions with relative weightage of ~5, 30 and 65%, respectively (data not shown). The peak at ~3600 $cm^{-1}$ i.e. the high frequency component enjoys the major contributions from the 'multimer'[26] water molecules which do not produce strong hydrogen bonds with neighbouring water molecules[54] and have generally been realized in extreme hydrophobic environments [55].

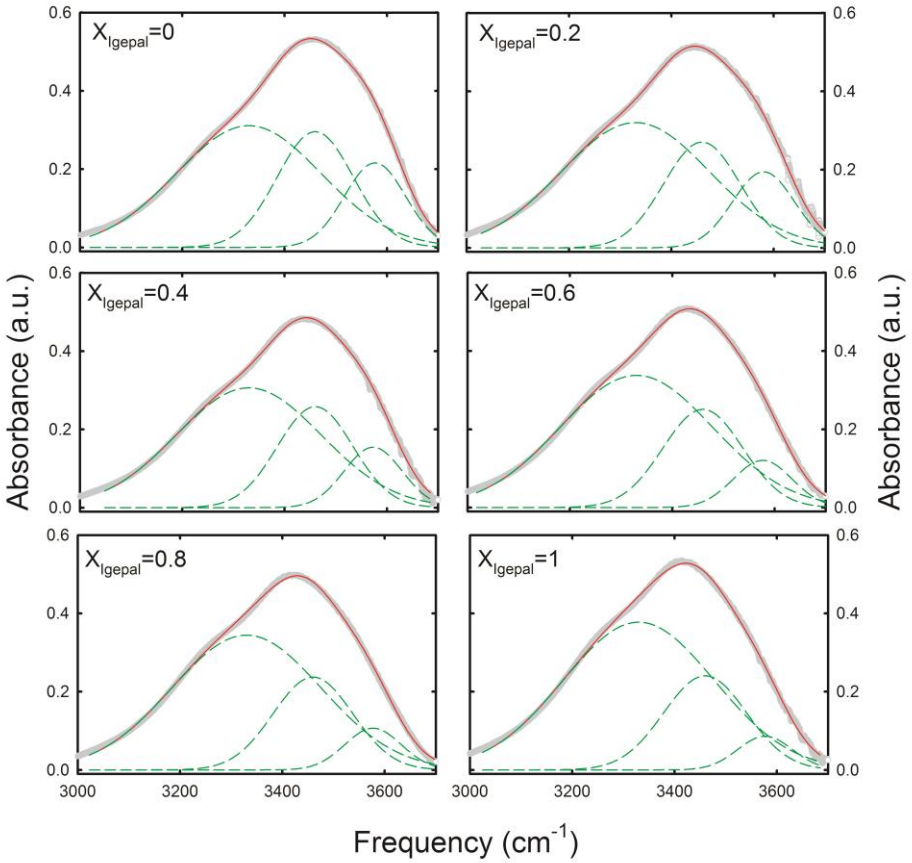


**Figure 3.3:** FTIR spectra of AOT/Igepal/Cy mixed reverse micellar systems at various $X_{Igepal}$ values at $w_0$=10 measured in the 3000-3800 $cm^{-1}$ window. The total curve (grey colour) has been deconvoluted into three different Gaussian curves (green dotted lines) peaking at 3600, 3460 and 3330 $cm^{-1}$. The red lines represent overall fits.

The second component peaking at 3460 $cm^{-1}$ involves the so-called 'intermediate' water molecules which are unable to develop fully hydrogen bonds and somewhat connected to other water molecules with distorted H-bonds[26]. Finally, the third kind of water molecule i.e. the lower frequency component (peaking at 3330 $cm^{-1}$) emanates from the 'network' (sometimes called as 'bulk type') water molecules which are fully hydrogen bonded with the neighbouring water molecules and contributes its majority of share in pure water.

We deconvolute the MIR spectra of all the RM systems into three Gaussian components keeping the peak positions fixed as those of pure water (figure 3.3). A free fitting often produces more accurate contributions; however, fixing the peak positions allows comparing the change in the relative weightage of each component at variable interfacial compositions. We plot the relative contribution of each curve towards the total spectra and plot it as a function of $X_{Igepal}$ (figure 3.4). This relative contribution is proportional to the fraction of water molecules belonging to that particular stretching mode. As evidenced from the figure the relative abundance of the fully hydrogen bonded water molecules are fewer in RM systems

compared to that in pure water; this observation is rather intuitive taking into consideration the interaction of water molecules with the both ionic and non-ionic RM interface[26, 56, 57].

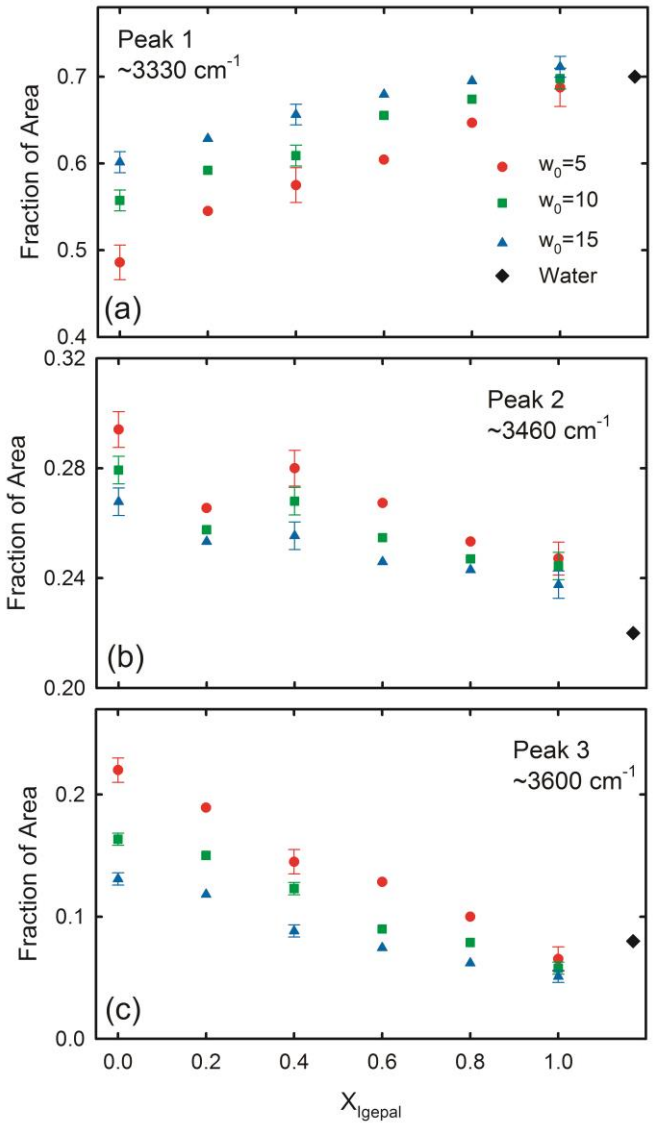


**Figure 3.4.** Relative area under curves peaking at 3330 $cm^{-1}$ (a), 3460 $cm^{-1}$ (b) and ~3600 $cm^{-1}$ (c) for AOT/Igepal/Cy mixed reverse micellar systems at $w_0$=5, 10 and 15.

The 'multimer' water molecules, often identified as the 'bound type' water molecules, shows characteristic slow dynamics compared to the 'network' or 'bulk-type' water owing to their strong interaction with the RM interface[58, 59]. It can be observed from figure 3.4c that the relative abundance of the 'multimer' water molecules in AOT RM systems is twice as large as compared to that in network water. With progressive inclusion of Igepal in the interface, abundance of the 'multimer' water decreases. This leads to conclude that the interaction of

water molecules with the polar uncharged head group of Igepal is weaker in comparison to that of ionic AOT. With increasing $w_0$, the content of 'multimer' water molecules decreases and at high $X_{Igepal}$ it eventually reaches a value comparable to that in pure water. The population corresponding to the 'intermediate' water (peaking at 3460 $cm^{-1}$) shows a marginal variation with both interfacial stoichiometry as well as water content. However, an overall weak decreasing trend is observed with increasing $X_{Igepal}$.

Let us now consider the population of 'network' water (peaking at 3330 $cm^{-1}$); it is observed that in AOT RM systems the population of such type of water molecules is considerably lower than that in pure water (figure 3.4a). This lower population is compensated by the abundance of 'multimer' water in RM. It can also be observed that the relative content of 'network' water increases considerably with increasing $w_0$. On the other hand, Igepal systems show behaviour more comparable to that of pure water and increase in $w_0$ offers only marginal effect on the relative abundance of 'network' water content. It can be argued that the interaction of the water molecules with the hydroxyl head group of Igepal[60] is comparable to that of water-water hydrogen bonded network which eventually results in the elevated population of 'network' water. It can also be observed that with increasing content of Igepal, the relative abundance gradually moves towards that of pure water clearly indicating a linear effect of mixing of surfactants at the interface. The present FTIR measurements strongly corroborate the finding of Brubach et al.[26] who reported that for nonionic fluorocarbon RMs with increasing $w_0$ and at high surfactant content the fraction of 'multimer water' (3600 $cm^{-1}$ region) molecules decreases which is compensated by increasing 'network water' (3330 $cm^{-1}$ region). It is worth mentioning here that such a trend observed which is observed in RM systems is strikingly opposite to that of water confined in 'hard' medium. Le Caër et al.[61] has recently studied the infrared spectra of water confined in pore glasses as a function of the pore size ranging from 8 to 320 nm in the 30–4000 $cm^{-1}$ spectral range using the attenuated total reflection (ATR) technique. When the pore size of silica decreases the intensity of the 'network' water (~3310 $cm^{-1}$) component increases and that of the 'intermediate' water component (3450 $cm^{-1}$) decreases while the contribution of 'multimer' water (~3590 $cm^{-1}$) remains practically unchanged. But in RM the variations are opposite; i.e. the 'intermediate' water contribution decreases with the micelle hydrodynamic radius, whereas the 'network' water contribution increases and the 'multimer' water component (~3600 $cm^{-1}$) also decreases. The observed deference may arise due to the more rigid silica walls, as compared to the smoother RM surface. It can be concluded from the IR spectroscopic studies that the synergistic

modification of the mechanical properties of the interface does not significantly influence the hydrogen bonded structure of water.

***Fluorescence Measurements:*** A comprehensive understanding of the dynamics of encapsulated water is obtained from steady state and time resolved fluorescence studies using C-500 as the fluoroprobe. It has been shown that in RM systems, selective excitation at 409 nm excites the C-500 molecules at the interface only[40] which justifies the choice of the probe. Figure 3.5 depicts the emission spectra of the mixed RM systems at $w_0$=10. The corresponding emission maxima ($\lambda_{max}$) are presented in table 3.2. C-500 in water produces an emission maximum at ~505 nm, and in AOT/isooctane RM systems it has been reported to suffer a progressive blue shift with decreasing $w_0$[40]. AOT/Cy RM system at $w_0$=5 produces an emission peak at 495 nm which suffers a red shift of ~4 nm at $w_0$=15 (table 3.2). The observed red shift with increasing $w_0$ is quite intuitive keeping in mind that once the surfactant head group is solvated, the rest of the water molecules only populate the well-structured water pool, thereby increasing the polarity in the vicinity of the surfactant imposing the observed red shift. The emission peak suffers a progressive blue shift with increasing Igepal content along with a broadening of the emission profile. The broadening of the spectral shape could be due to multiple locations of the probe molecules, namely in 'bulk type' water, interfacial water and deep into the interfacial layer. It should be remembered that C-500 is only sparingly soluble in water and selective excitation of the probe at 409 nm excludes the contribution from the 'network' water molecules. We deconvolute the observed spectra of $X_{Igepal}$=1 into two Gaussian components with fixing one peak to appear at 500 nm (in accordance with the peak position of the probe residing at the waterpool) and found that the other peak is centered at ~478 nm (figure 3.5). The area under the later curve is half of that obtained for the former. This relative weightage is found to be invariant of $w_0$ indicating that the distribution of probe molecules at the Igepal/Cy interface is independent of the water content in the RM. C-500 has extensively been used as a fluorophore to study the relaxation dynamics of water in confined medium [40, 41, 43]. In the present study the decay transients of the probe in the blue end of the spectrum could be fitted with multiple decay components whereas those in the red end could be fitted only by considering an added rise component (figure 3.6). Such an observation is indicative of the solvation of the probe[62] and we construct the solvent correlation function, C(t) following equation (2.11 in chapter 2). Some representative C(t) plots for different $X_{Igepal}$ values at $w_0$=10 are shown in figure 3.7a. All the C(t) curves are fitted bi-exponentially and the time constants are presented in table 3.2.

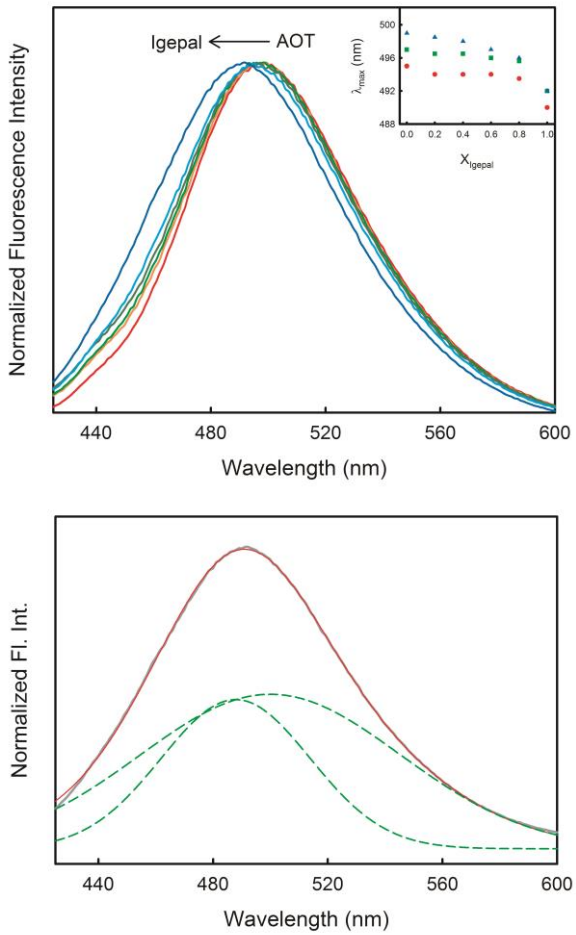


**Figure 3.5:** *Upper panel:* Emission spectra of C-500 in AOT/Igepal/Cy RM systems at different $X_{Igepal}$ with $w_0$=10. The emission maximum at different $w_0$ values as a function of $X_{Igepal}$ has been shown in the inset (circle, square and triangle corresponds to $w_0$=5, 10 and 15 respectively. *Lower panel:* Deconvolution of the emission spectrum of $w_0$=10 system for Igepal/Cy RM system.

At a first step, we check that the observed time resolved spectral shift is not associated with any internal photophysics of the probe itself. In order to do so we construct the time-resolved area normalized emission spectra (TRANES)[63] for all these systems. A representative illustration is shown in figure 3.6. No apparent iso-emissive point is recognized in the TRANES profile, which confirms that the probe contains only a single 'species'. Therefore, the observed time dependent spectral shift can be attributed solely to the inhomoginity of the microenvironment experienced by the probe. As can be observed from table 3.2, the time constants are in the order of hundreds of ps and a few ns, which are orders of magnitude slower than that observed in pure water[64]. It should be taken into consideration that the sub-ps orientational dynamics of water is considerably restricted in the confined systems like RMs. Selective photo-excitation of interfacial probe molecules coupled with the limitation of our

instrumental resolution (IRF~80 ps) refrained us from detecting the signals responsible for the ultrafast dynamics of water molecules. The reported timescales thus have the sole contribution of water molecules residing at the RM interface only, which is in accord with the essence of this study.

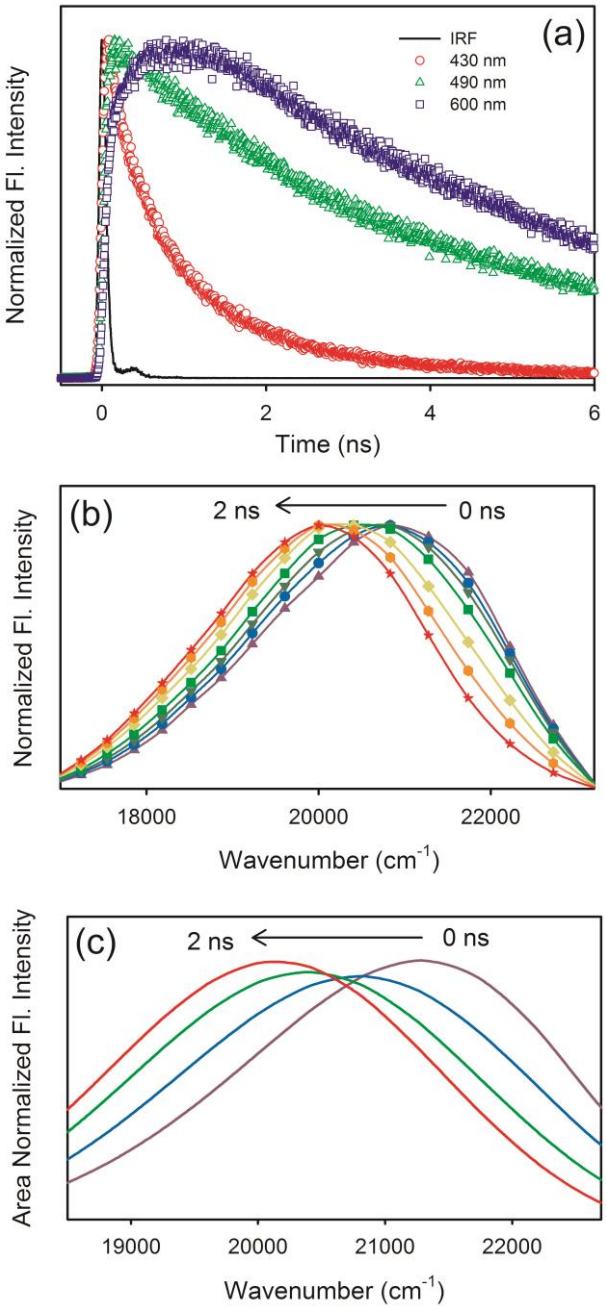


**Figure 3.6:** (a) Representative fluorescence decay transients of C-500 in AOT/CY/water RM system at $w_0$=10 at three different wavelengths. (b) The corresponding time-resolved emission spectra (TRES). (c) The corresponding time resolved area normalised emission spectra (TRANES).

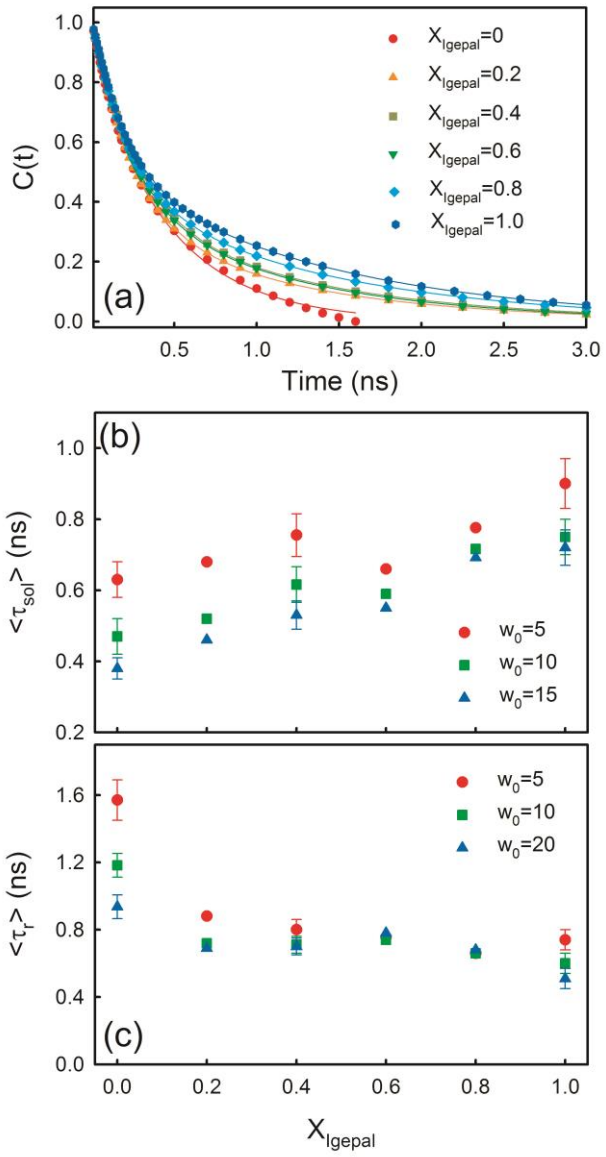


**Figure 3.7.** (a) Representative solvent correlation function, C(t) curves of C-500 for AOT/Igepal/Cy reverse micellar systems at $w_0$=10 for different $X_{Igepal}$ values. The solid lines are bi-exponential fittings. (b) Average solvation time constant $<\tau_{sol}>$ as a function of $X_{Igepal}$. (c) Average rotational time constant, $<\tau_r>$ as a function of $X_{Igepal}$.

We obtain an average Stokes shift of 1000±100 $cm^{-1}$, which is only ~25% of the Stokes shift calculated from the steady state measurements as intuited from the loss of ultrafast fluorescence signals. We plot the average time constant, $< \tau_{solv} >= \sum_i a_i \tau_i$ as a function of $X_{Igepal}$ at three different $w_0$ values (figure 3.7b). It is observed that with increasing $w_0$, solvation dynamics gets faster for all these systems. For pure AOT systems the $<\tau_{solv}>$ values are in comparable agreement with those obtained in AOT/isooctane RM systems using the same fluorophore[40]. At $w_0$=5, a considerable fraction of water molecules solvate the RM interface and thus exhibits restricted dynamics as evidenced from high $<\tau_{solv}>$ values. At $w_0 \geq 10$, a well defined RM water-

pool is built up [65-67] and the relative fraction of the slow moving water molecules gets reduced resulting in an overall faster solvation. It has been observed that $<\tau_{solv}>$ is faster in pure AOT systems compared to that in pure Igepal systems. This retardation is attributed to the possible contribution of the terminal hydroxyl groups of Igepal towards the measured relaxation dynamics. $<\tau_{solv}>$ does not offer any remarkable pattern around $X_{Igepal}$=0.4, instead an overall increasing trend with $X_{Igepal}$ is registered.

**Table 3.2.** Emission maximum ($\lambda_{max}$), bi-exponential fitting parameters of the C(t) and rotational anisotropy decay curves of C-500 in AOT/Igepal/Cy/water mixed RM systems at different $w_0$ and mixing ratios.

| $w_0$ | $\lambda_{max}$ | Solvation dynamics | | | Anisotropy | | |
|---|---|---|---|---|---|---|---|
| | (nm) | $\tau_1$ ($a_1$) (ns) | $\tau_2$ ($a_2$) (ns) | $<\tau_{sol}>$ (ns) | $\tau_{r1}$($a_1$) (ns) | $\tau_{r2}$ ($a_2$) (ns) | $<\tau_r>$ (ns) |
| | | | | $X_{Igepal}$=0 | | | |
| 5 | 495 | 0.12 (0.22) | 0.78 (0.78) | 0.63 | 0.46 (0.29) | 2.04 (0.71) | 1.57 |
| 10 | 497 | 0.11 (0.23) | 0.51 (0.77) | 0.42 | 0.43 (0.37) | 1.63 (0.63) | 1.18 |
| 15 | 499 | 0.10 (0.23) | 0.48 (0.77) | 0.39 | 0.42 (0.37) | 1.24 (0.63) | 0.94 |
| | | | | $X_{Igepal}$=0.2 | | | |
| 5 | 494 | 0.20 (0.48) | 1.14 (0.52) | 0.69 | 0.27 (0.46) | 1.41 (0.54) | 0.88 |
| 10 | 496 | 0.20 (0.58) | 1.05 (0.42) | 0.56 | 0.25 (0.50) | 1.20 (0.50) | 0.72 |
| 15 | 498 | 0.21 (0.65) | 0.96 (0.35) | 0.47 | 0.23 (0.48) | 1.13 (0.52) | 0.70 |
| | | | | $X_{Igepal}$=0.4 | | | |
| 5 | 494 | 0.22 (0.52) | 1.35 (0.48) | 0.76 | 0.29 (0.52) | 1.35 (0.48) | 0.80 |
| 10 | 496 | 0.22 (0.58) | 1.18 (0.42) | 0.62 | 0.24 (0.49) | 1.16 (0.51) | 0.71 |
| 15 | 498 | 0.21 (0.64) | 1.11 (0.36) | 0.53 | 0.24 (0.50) | 1.18 (0.50) | 0.71 |
| | | | | $X_{Igepal}$=0.6 | | | |
| 5 | 494 | 0.22 (0.57) | 1.28 (0.43) | 0.67 | 0.27 (0.53) | 1.31 (0.47) | 0.76 |
| 10 | 496 | 0.21 (0.58) | 1.10 (0.42) | 0.58 | 0.24 (0.50) | 1.25 (0.50) | 0.74 |
| 15 | 497 | 0.20 (0.60) | 1.08 (0.40) | 0.55 | 0.30 (0.62) | 1.57 (0.38) | 0.78 |
| | | | | $X_{Igepal}$=0.8 | | | |
| 5 | 493 | 0.23 (0.57) | 1.52 (0.43) | 0.78 | 0.18 (0.55) | 1.24 (0.45) | 0.66 |
| 10 | 495 | 0.22 (0.54) | 1.31 (0.46) | 0.72 | 0.18 (0.50) | 1.13 (0.50) | 0.66 |
| 15 | 496 | 0.21 (0.57) | 1.29 (0.43) | 0.67 | 0.23 (0.51) | 1.16 (0.49) | 0.68 |
| | | | | $X_{Igepal}$=1 | | | |
| 5 | 490 | 0.20 (0.46) | 1.49 (0.54) | 0.89 | 0.21 (0.52) | 1.31 (0.48) | 0.74 |
| 10 | 492 | 0.19 (0.49) | 1.32 (0.51) | 0.77 | 0.20 (0.55) | 1.08 (0.45) | 0.60 |
| 15 | 492 | 0.20 (0.50) | 1.24 (0.50) | 0.72 | 0.18 (0.57) | 0.95 (0.43) | 0.51 |

In order to understand the nature of geometrical restriction imposed on the probe molecule by the interfacial layer, we determine the rotational anisotropy of all these systems. All the rotational decay transients can be fitted bi-exponentially and the time constants ($\tau_r$) are presented in table 3.2. The observed $\tau_r$ values are in comparable agreement with AOT/isooctane systems using the same fluorophore[40]. C-500 in water produces a rotational anisotropy decay time constant of ~70 ps[68]. The observed slow rotational relaxation implies a considerable hindrance inside the RM waterpool as experienced by the probe molecules which reaffirms the solvation dynamics results. It can be observed that the rotation of the probe is eased as $w_0$ is increased. The restriction is more prominent in the AOT systems, and decreases as Igepal is doped into the interface. The imposed restriction in the AOT system might arise out of the strong interaction of the probe with the surfactant charged interface. As also evidenced from figure 3.7c, the change in the average rotational time constant, $< \tau_r >= \sum_i a_i \tau_{r_i}$ follows a fairly linear trend, with a weak dependence on $w_0$.

***General discussion:*** In the present contribution we have made a systematic spectroscopic investigation to underline any possible correlation between the mechanical properties of a RM interface and physical properties of its adjacent water molecules. Optimization of solubilization capacity of RM is a much anticipated field of research in surface science as high water uptake of RMs is often beneficial for many biophysical applications of RM. It has now been established that increased solubilization capacity involves suitable modification of the mechanical properties of the surfactant monolayer and also of the interaction between the RM droplets[13]. Several previous studies have shown that such an improvement could easily be achieved by blending of surfactants. Mixture of surfactants also brings about desired modification in many applications [4-9]. However, a proper rationale of the process involved is still not vividly understood. In this regard it was pertinent to investigate whether such a modification in the surfactant interface is reflected in the physical properties as well as dynamics of the entrapped water molecules. In our previous study[36] using mixed surfactant system AOT/Brij-30 in isooctane we concluded that the physical properties and dynamics of water follow a linear trend with mixing. However, in such a system solubilization capacity was limited by the droplet interaction effect as isooctane is a less penetrating hydrocarbon into the interface. Also the solubilization behaviour did not show any synergistic effect and hence a linear trend in water properties was much intuited. It remains to answer whether physical properties of water follow a non-linear trend of interface curvature with mixing.

AOT/Igepal/Cy mixed RM system exhibits synergistic water solubilization behaviour with maximum solubilization occurring at a $X_{Igepal}$=0.4 mixing ratio (figure 3.1). Since the interface of AOT/Cy RM is rigid and non-interacting, the solubilization capacity is primarily governed by the curvature effect. Addition of Igepal induces fluidity in it, which increases its solubilization power. However, in doing so it in turn increases the inter droplet interaction which eventually limits the extent of solubilization. Thus the interface undergoes a systematic geometric modification with $X_{Igepal}$. Such a nonlinear behaviour offers the system to be a perfect platform to investigate the water structure and dynamics.

DLS studies show linear increase in droplet size with increasing Igepal doping into the RM interface. Such a linear trend is also noticed in the aggregation number and partial molar volume calculations (figure 3.2). O-H stretching vibration as obtained from FTIR measurements in the 3000-3800 $cm^{-1}$ region show three different types of water molecule inside the RMs compared with pure water and progressively follows the linear mixing behaviour of the surfactants (figure 3.4). FTIR study identifies that the relative population of multimer water component i.e. water molecules residing in totally hydrophobic environment is larger in AOT RM compared to that in Igepal RM, and it follows an overall linear trend with $X_{Igepal}$ and eventually resembles the values of pure water. No marked deviation from the linear trend is observed in the maximum solubilization region. Sub-ns relaxation dynamics of the entrapped water as revealed by the time resolved fluorescence spectroscopy using C-500 as the probe identifies the confined nature of the entrapped water in all the studied systems, a behaviour markedly different from that in pure water. The dynamics, however, shows a gradual change with the change in interface stoichiometry and any characteristic feature around the solubilization inflation point is not unambiguously noticed. It therefore emerges that changes in the mechanical properties of surfactant film merely affects the structure and relaxation dynamics of the entrapped water molecules, which is believed to essentially be governed by the water content and the surface charge type only.

## 3.3 Conclusion

In AOT/Igepal/Cy mixed surfactant systems a five-fold increase in solubilization capacity is obtained compared to the constituent surfactants at $X_{Igepal}$=0.4. DLS studies show a linear increase in the droplet size with $X_{Igepal}$. Densimetric and acoustic measurements also do not

reveal any characteristic feature around the maximum solubilization point. FTIR study in the 3000-3800 $cm^{-1}$ region identifies that the relative population of 'multimer' water component i.e. water molecules residing mostly in hydrophobic environment is larger in AOT RM compared to that in Igepal RM, and it follows a linear trend with $X_{Igepal}$. Sub-ns relaxation dynamics of the entrapped water as revealed by C-500 does also exhibit a more or less linear trend with no characteristic feature around the solubilization inflation point. These results conclude that the changes in the mechanical properties of RM interface barely affect the slow relaxation dynamics of the entrapped water molecules.

## 3.4 References


[1] S. Moulik, B. Paul, Structure, dynamics and transport properties of microemulsions, Advances in Colloid and Interface science, 78 (1998) 99-195.

[2] K.A. Johnson, D.O. Shah, Effect of oil chain length and electrolytes on water solubilization in alcohol-free pharmaceutical microemulsions J. Colloid Interface Sci., 107 (1985) 269-271.

[3] G. Lundsten, S. Backlund, G. Kiwilsza, Solubility limits of water in systems of aromatic oils and non-ionic surfactants, Progress in Colloid and Polymer Science, 97 (1994) 194-198.

[4] A. Shome, S. Roy, P. Das, Nonionic Surfactants: A Key to Enhance the Enzyme Activity at Cationic Reverse Micellar Interface, Langmuir, 23 (2007) 4130-4136.

[5] D.-H. Chen, M.-H. Liao, Effects of mixed reverse micellar structure on stability and activity of yeast alcohol dehydrogenase, J. Mol. Cat. B: Enzymatic, 18 (2002) 155-162.

[6] J. Lan, Y. Zhang, X. Huang, M. Hu, W. Liu, Y. Li, Y. Qu, P. Gao, Improvement of the catalytic performance of lignin peroxidase in reversed micelles, J. Chem. Tech. Biotech., 83 (2008) 64 - 70.

[7] A.K. Poulsen, L. Arleth, K. Almdal, A.M. Scharff-Poulsen, Unusually large acrylamide induced effect on the droplet size in AOT/Brij30 water-in-oil microemulsions, J. Colloid Interface Sci., 306 (2007) 143-153.

[8] J. Zhang, B. Han, J. Liu, X. Zhang, J. He, Z. Liu, T. Jiang, G. Yang, Recovery of Silver Nanoparticles Synthesized in AOT/C12E4 Mixed Reverse Micelles by Antisolvent CO2, Chemistry - A European Journal, 8 (2002) 3879-3883.

[9] P.K. Singh, A.K. Satpati, M. Kumbhakar, H. Pal, S. Nath, A Nanoreactor for Tuning the Chemical Reactivity of a Solute, J. Phys Chem. B, 112 (2008) 11447-11450.

[10] E.P. Melo, M.R. Aires-Barros, J.M.S. Cabral, Reverse micelles and protein biotechnology Original Research Article, Biotechnol. Ann. Rev., 7 (2001) 87-129.

[11] N. Streitner, C. Voss, E. Flaschel, Reverse micellar extraction systems for the purification of pharmaceutical grade plasmid DNA, J. Biotech., 131 (2007) 188-196.

[12] S. Furusaki, S. Ichikawa, M. Goto, Recent advances in reversed micellar techniques for bioseparation, Prog. Biotech., 16 (2000) 133-136.

[13] M.J. Hou, D.O. Shah, Effects of the molecular structure of the interface and continuous phase on solubilization of water in water/oil microemulsions, Langmuir, 3 (1987) 1086-1096.

[14] P.D.T. Huibers, D.O. Shah, Evidence for Synergism in Nonionic Surfactant Mixtures: Enhancement of Solubilization in Water-in-Oil Microemulsions, Langmuir, 13 (1997) 5762 - 5765.

[15] R.K. Mitra, B.K. Paul, Effect of NaCl and temperature on the water solubilization behavior of AOT/nonionics mixed reverse micellar systems stabilized in IPM oil, Colloids and Surfaces A, 255 (2005) 165-180.

[16] B.K. Paul, R.K. Mitra, Water solubilization capacity of mixed reverse micelles: Effect of surfactant component, the nature of the oil, and electrolyte concentration, J. Colloid Interface Sci., 288 (2005) 261-279.
[17] R.K. Mitra, B.K. Paul, Investigation on percolation in conductance of mixed reverse micelles, Colloids and Surfaces A: Physicochemical and Engineering Aspects, 252 (2005) 243-259.
[18] R.K. Mitra, B.K. Paul, S.P. Moulik, Phase behavior, interfacial composition and thermodynamic properties of mixed surfactant (CTAB and Brij-58) derived w/o microemulsions with 1-butanol and 1-pentanol as cosurfactants and n-heptane and n-decane as oils, J. Colloid Interface Sci., 300 (2006) 755-764.
[19] T. Kinugasa, A. Kondo, S. Nishimura, Y. Miyauchi, Y. Nishii, K. Watanabe, H. Takeuchi, Estimation for size of reverse micelles formed by AOT and SDEHP based on viscosity measurement, Colloids and Surfaces, A: Physicochemical and Engineering Aspects, 204 (2002) 193-199.
[20] D. Liu, J. Ma, H. Cheng, Z. Zhao, Fluorescence probing of mixed reverse micelles formed with AOT and nonionic surfactants in n-heptane, Colloids and Surfaces A: Physicochemical and Engineering Aspects, 139 (1998) 21-26.
[21] S. Chatterjee, R.K. Mitra, B.K. Paul, S.C. Bhattacharya, Interface of AOT/Brij mixed reverse micellar systems: Conductometric and spectrophotometric investigations, J. Colloid Interface Sci., 298 (2006) 935-941.
[22] S. Chatterjee, S. Nandi, S.C. Bhattacharya, Interface of AOT/Igepal CO720/cyclohexane/water mixed reverse micelle by spectroscopic approach, Colloids and Surfaces A: Physicochemical and Engineering Aspects, 279 (2006) 58-63.
[23] A. Bumajdad, J. Eastoe, R.K. Heenan, R.J. Lu, D.C.S. Steytler, S. Egelhaaf, E., Mixing in cationic surfactant films studied by small-angle neutron scattering, J. Chem. Soc., Faraday Trans., 94 (1998) 2143-2150.
[24] A. Bumajdad, J. Eastoe, P. Griffiths, D.C. Steytler, R.K. Heenan, J.R. Lu, P. Timmins, Interfacial Compositions and Phase Structures in Mixed Surfactant Microemulsions, Langmuir, 15 (1999) 5271-5278.
[25] A. Bumajdad, J. Eastoe, S. Nave, D.C. Steytler, R.K. Heenan, I. Grillo, Compositions of Mixed Surfactant Layers in Microemulsions Determined by Small-Angle Neutron Scattering, Langmuir, 19 (2003) 2560-2567.
[26] J.-B. Brubach, A. Mermet, A. Filabozzi, A. Gerschel, D. Lairez, M.P. Krafft, P. Roy, Dependence of Water Dynamics upon Confinement Size, J. Phys. Chem. B, 105 (2001) 430-435.
[27] Q. Li, T. Li, J. Wu, Comparative Study on the Structure of Reverse Micelles. 2. FT-IR, 1H NMR, and Electrical Conductance of H2O/AOT/NaDEHP/n-Heptane Systems, J. Phys. Chem. B, 104 (2000) 9011-9016.
[28] K. Bhattacharyya, Solvation Dynamics and Proton Transfer in Supramolecular Assemblies, Acc. Chem. Res., 36 (2003) 95-101.
[29] M.D. Fayer, Water in a Crowd, Physiology, 26 (2011) 381-392.
[30] D.E. Moilanen, N.E. Levinger, D.B. Spry, M.D. Fayer, Confinement or the Nature of the Interface? Dynamics of Nanoscopic Water, J. Am. Chem. Soc., 129 (2007) 14311-14318.
[31] D. Pant, N.E. Levinger, Polar Solvation Dynamics in Nonionic Reverse Micelles and Model Polymer Solutions, Langmuir, 16 (2000) 10123-10130.
[32] D. Pant, R.E. Riter, N.E. Levinger, Influence of restricted environment and ionic interactions on water solvation dynamics, J. Chem. Phys., 109 (1998) 9995-10003.
[33] R.E. Riter, E.P. Undiks, N.E. Levinger, Impact of Counterion on Water Motion in Aerosol OT Reverse Micelles, J. Am. Chem. Soc., 120 (1998) 6062-6067.
[34] S.S. Narayanan, S.S. Sinha, R. Sarkar, S.K. Pal, Validation and divergence of the activation energy barrier crossing transition at AOT/lecithin reverse micellar interface, J. Phys. Chem. B, 112 (2008) 2859.
[35] S.S. Narayanan, S.S. Sinha, R. Sarkar, S.K. Pal, Picosecond to nanosecond reorganization of water in AOT/lecithin mixed reverse micelles of different morphology, Chem. Phys. Lett., 452 (2008) 99-104.

[36] R.K. Mitra, S.S. Sinha, P.K. Verma, S.K. Pal, Modulation of Dynamics and Reactivity of Water in Reverse Micelles of Mixed Surfactants J. Phys. Chem. B, 112 (2008) 12946-12953.
[37] S. Nave, J. Eastoe, R.K. Heenan, D. Steytler, I. Grillo, What Is So Special about Aerosol-OT? 2. Microemulsion Systems, Langmuir, 16 (2000) 8741-8748.
[38] S. Lipgens, D. Schuebel, L. Schlicht, J.-H. Spilgies, G. Ilgenfritz, J. Eastoe, R.K. Heenan, Percolation in Nonionic Water (w/o)-Microemulsion Systems: A Small Angle Neutron Scattering Study, Langmuir, 14 (1998) 1041-1049.
[39] R.K. Mitra, S.S. Sinha, S.K. Pal, Temperature Dependent Hydration at Micellar Surface: Activation Energy Barrier Crossing Model Revisited, J.Phys.Chem.B, 111 (2007) 7577-7581.
[40] R.K. Mitra, S.S. Sinha, S.K. Pal, Temperature-Dependent Solvation Dynamics of Water in Sodium Bis(2-ethylhexyl)sulfosuccinate/Isooctane Reverse Micelles, Langmuir, 24 (2008) 49-56.
[41] A. Patra, P.K. Verma, R.K. Mitra, Slow Relaxation Dynamics of Water in Hydroxypropyl Cellulose-Water Mixture Traces Its Phase Transition Pathway: A Spectroscopic Investigation, J. Phys. Chem. B, 116 (2012) 1508-1516.
[42] P.K. Verma, A. Makhal, R.K. Mitra, S.K. Pal, Role of Solvation Dynamics in the Kinetics of Solvolysis Reactions in Microreactors, Phys. Chem. Chem. Phys., 11 (2009) 8467-8476.
[43] P.K. Verma, R. Saha, R.K. Mitra, S.K. Pal, Slow water dynamics at the surface of macromolecular assemblies of different morphologies, Soft Matter, 6 (2010) 5971-5979.
[44] P.K. Verma, R.K. Mitra, S.K. Pal, A Molecular Picture of Diffusion Controlled Reaction: Role of Microviscosity and Hydration on Hydrolysis of Benzoyl Chloride at a Polymer Hydration Region, Langmuir, 25 (2009) 11336-11343.
[45] N. Seedher, M. Manik, Solubilization in mixed surfactant reverse micellar systems, J. Surface Sci. Technol., 9 (1993) 81-86.
[46] E. Ruckenstein, J.C. Chi, Stability of microemulsions J. Chem. Soc., Faraday Trans. 2, 71 (1975) 1690-1707.
[47] E. Ruckenstein, R. Krishnan, Swollen micellar models for solubilization, J. Colloid Interface Sci., 71 (1979) 321-335.
[48] S.P. Moulik, G.C. De, B.B. Bhowmik, A.K. Panda, Physicochemical Studies on Microemulsions. 6. Phase Behavior, Dynamics of Percolation, and Energetics of Droplet Clustering in Water/AOT/n-Heptane System Influenced by Additives (Sodium Cholate and Sodium Salicylate), J. Phys. Chem. B, 103 (1999) 7122-7129.
[49] A. Maitra, Determination of size parameters of water-Aerosol OT-oil reverse micelles from their nuclear magnetic resonance data, J. Phys. Chem., 88 (1984) 5122–5125.
[50] D. Banerjee, S.S. Sinha, S.K. Pal, Interplay between Hydration and Electrostatic Attraction in Ligand Binding: Direct Observation of Hydration Barrier at Reverse Micellar Interface J. Phys. Chem. B, 111 (2007) 14239.
[51] A. Amararene, M. Gindre, J.-Y. Le Huerou, C. Nicot, W. Urbach, M. Waks, Water Confined in Reverse Micelles: Acoustic and Densimetric Studies, J. Phys. Chem. B, 101 (1997) 10751-10756.
[52] A.J. Lock, H.J. Bakker, Temperature dependence of vibrational relaxation in liquid H2O, J. Chem. Phys., 117 (2002) 1708-1713.
[53] S.A. Corcelli, J.L. Skinner, Infrared and Raman Line Shapes of Dilute HOD in Liquid H2O and D2O from 10 to 90 °C, J. Phys. Chem. A, 109 (2005) 6154-6165.
[54] H. Graener, G. Seifert, Vibrational and orientational relaxation of monomeric water molecules in liquids, J. Chem. Phys. , 98 (1993) 36-45.
[55] L.F. Scatena, M.G. Brown, G.L. Richmond, Water at Hydrophobic Surfaces: Weak Hydrogen Bonding and Strong Orientation Effects, Science, 292 ( 2001) 908-912.
[56] N. Zhou, Q. Li, J. Wu, J. Chen, S. Weng, G. Xu, Spectroscopic Characterization of Solubilized Water in Reversed Micelles and Microemulsions: Sodium Bis(2-ethylhexyl) Sulfosuccinate and Sodium Bis(2-ethylhexyl) Phosphate in n-Heptane, Langmuir, 17 (2001) 4505-4509.
[57] Q. Zhong, D.A. Steinhurst, E.E. Carpenter, J.C. Owrutsky, Fourier Transform Infrared Spectroscopy of Azide Ion in Reverse Micelles, Langmuir, 18 (2002) 7401-7408.

[58] K.B. Bhattacharyya, B., Slow Dynamics of Constrained Water in Complex Geometries J. Phys. Chem. A, 104 (2000) 10603-10613.
[59] S.K. Pal, J. Peon, B. Bagchi, A.H. Zewail, Biological water: Femtosecond dynamics of macromolecular hydration, J. Phys. Chem. B, 106 (2002) 12376-12395.
[60] E.E. Fenn, D.B. Wong, M.D. Fayer, Water dynamics at neutral and ionic interfaces, Proc. Natl. Acad. Sci. USA, 106 (2009) 15243-15248.
[61] S.L. Caer, S. Pin, S. Esnouf, Q. Raffy, J.P. Renault, J.-B. Brubach, G. Creff, P. Roy, A trapped water network in nanoporous material: the role of interfaces, Phys. Chem. Chem. Phys., 13 (2011) 17658-17666.
[62] M. Maroncelli, G.R. Fleming, Picosecond solvation dynamics of coumarin 153: the importance of molecular aspects of solvation, J. Chem. Phys., 86 (1987) 6221-6238.
[63] A.S.R. Koti, M.M.G. Krishna, N. Periasamy, Time-resolved area-normalized emission spectroscopy (TRANES): A novel method for confirming emission from two excited states, J. Phys. Chem. A, 105 (2001) 1767-1771.
[64] R. Jimenez, G.R. Fleming, P.V. Kumar, M. Maroncelli, Femtosecond Solvation Dynamics of Water, Nature, 369 (1994) 471-473.
[65] A. Amararene, M. Gindre, J.-Y. Le Huérou, W. Urbach, D. Valdez, M. Waks, Adiabatic compressibility of AOT [sodium bis(2-ethylhexyl)sulfosuccinate] reverse micelles: Analysis of a simple model based on micellar size and volumetric measurements, Phys. Rev. E, 61 (2000) 682 - 689.
[66] M. D'Angelo, D. Fioretto, G. Onori, L. Palmieri, A. Santucci, Dynamics of water-containing sodium bis(2-ethylhexyl)sulfosuccinate (AOT) reverse micelles: A high-frequency dielectric study, Phys. Rev. E, 54 (1996) 993-996.
[67] G. Carlstroem, B. Halle, Water dynamics in microemulsion droplets. A nuclear spin relaxation study, Langmuir, 4 (1988) 1346-1352.
[68] D. Banerjee, P.K. Verma, S.K. Pal, A Temperature Dependent Femtosecond-Resolved Hydration Dynamics of Water in Aqueous Guanidinium Hydrochloride Solution, Photochem. Photobiol. Sci., 8 (2009) 1441-1447.

# Chapter 4: Structure, Dynamics and Activity of Nonionic-nonionic Mixed Surfactant Reverse Micellar System

## 4.1 Introduction

Reverse micelles are stable dispersions of otherwise immiscible water droplets in oil continuum, the stability been rendered by surfactant(s) monolayer at the droplet interface[1]. RMs have witnessed the ever spreading application in various fields of science and technology. Often RMs composed of mixture of surfactants are found to be advantageous over the use of single surfactants, and can display properties superior than the individual ones [2-5]. One of the most desired property of RM is its high water solubilization capacity and mixture of surfactants can offer a many fold enhancement in it. The hydrophilic-lipophilic balance (HLB)[6] of mixed surfactant systems can efficiently be tuned in order to provide with better solubilization behavior [7, 8]. However, a proper rationale of such modified mixing behaviour is still demanded, and needs a more generalized approach to optimize the mixing stoichiometry in order to yield the maximum effect. There have been several explanation offered for the observed synergistic solubilization behaviour, mostly based on either the interplay between the surfactant monolayer curvature and inter-droplet interaction or establishment of an optimum HLB or both [7-10]. Most of the earlier studies on mixed RMs have been carried out using anionic surfactant (mostly 1,4-bis(2-ethylhexoxy)-1,4-dioxobutane-2-sulfonate, AOT) and non-ionic (mostly polyoxyethylene ethers) surfactants and these mixed RM systems have offered substantial modification in enzyme kinetics[3, 11, 12], polymer synthesis[13], nanoparticle synthesis[14] and chemical activity [5, 15]. Our group has also put forward a systematic study to underline the effect of mixing of surfactants of different charge types on solubilization behavior[16], conductivity[17], interfacial property[18, 19] etc. It has been observed that the maximum solubilization capacity often shows synergistic effects whereas various physical and chemical properties of the mixed RM systems follow an overall linear relationship with the mixing ratio [7, 8, 16, 20]. This makes dynamics and activity easily tunable by tuning the surfactant mixing ratio only. The many-fold increase in the solubilization capacity certainly associates considerable perturbation on the mechanical properties of the surfactant monolayer and one can envisage a consequent impact on the physical properties of the entrapped water in the waterpool. Our previous study has unambiguously revealed that the

modulation of the interface does hardly affect the physical properties of water, which rather is governed by the polarity of the interface and the content of different types of water molecules present in the waterpool [20]. However, this conclusion has been drawn on the basis of the mixture of surfactants having two different charge types, viz. anionic AOT and non-ionic Igepal-520 and thus the interaction of water with the interface could not have been generalized as such interaction is mostly assisted by the charge type of the interface. In order to appear at a more general and comprehensive understanding, it is therefore important to carry out the investigation with surfactant mixture of the same charge type as it could eliminate the possible effect of the charge type on the observed behaviour. In accordance with that we have investigated the effect of mixing two non-ionic surfactants of different HLB numbers on the physicochemical properties of water encapsulated in the RM.

Igepal (nonylphenylpolyethylene oxide based surfactants) series of surfactant provides with a wide range of amphiphilicity that can easily be tuned by changing the ethylene oxide (EO) chain length and systematically vary the HLB from a very small value of ~4 to as high as ~13. Most importantly many of the Igepal series surfactants are capable of forming RM in hydrocarbon oils. The Igepal based RM systems has previously been investigated using percolation phenomenon[21], droplet clustering[22], small angle neutron scattering technique[23], ultrafast relaxation dynamics[24-26] and preparation of nanomaterials [27-29]. Owing to a wide distribution of polar EO chain length in Igepal surfactants (from ~1.5 to 10), the RM interface can substantially be modified by blending them for specific applications, and this justifies the choice of these set of surfactants in the present study. In the present contribution, we have used the blend of two terminal surfactants, namely Igepal-210 (HLB ~ 4) and Igepal-630 (HLB ~ 13) in cyclohexane (Cy). The interfacial polarity as well as the HLB of this system has systematically been varied by changing the mixing ratio. As this particular blend is expected to offer synergism in the solubilization behaviour[8] the essence of the present investigation is to identify whether such non-linear behaviour is also been reflected in the structure, dynamics and activity of the water molecules in the RM waterpool. The micellar sizes at different mixing ratios ($X_{Ig}$) and hydration level ($w_0$, defined as the ratio of the molar concentration of water and that of surfactant(s)) have been measured using dynamic light scattering (DLS) technique. The physical properties of the entrapped water have been determined using high precision densimetry measurements. Hydrogen bonded structure of water inside RM has been investigated using mid-infrared FTIR spectroscopy. The slow (sub-ns) sub-diffusive relaxation dynamics of water inside RM has been probed by ps-resolved fluorescence spectroscopy technique using coumarin 500 (C500) as the fluorophore with an

excitation wavelength of 409 nm in order to extract specific information on the water molecules residing at the interface. To understand the geometrical restriction of the probe at the interface, rotational anisotropy of the probe in different RM systems have also been determined. Finally, to correlate the dynamics with activity, we measure the kinetics of solvolysis of benzoyl chloride (BzCl) in the RMs at different surfactant compositions.

## 4.2 Results and Discussions

***Solubilization Measurements:*** Figure 4.1 depicts the solubilization profile of the mixed RM systems as a function of the surfactant mixing ratio ($X_{Ig630}$). Both the surfactants are fairly soluble in Cy and can solubilize only a small volume of water in the $w_{0,max}$ (maximum solubilization capacity) range of 2-3. The mixed surfactant systems, however, display a considerable synergism in the water solubilization capacity wherein $w_{0,max}$ increases sharply with increasing $X_{Ig630}$ to pass through a maximum at $X_{Ig630}$=0.3. Such synergism is generally expected for ionic-nonionic surfactant mixtures [7, 16, 20] wherein Columbic, ion-dipole or hydrogen bonding interaction among polar head-groups dominate the solubilization phenomenon. In case of nonionic surfactants the intermolecular interactions are minimal and only a subtle synergistic effect can be envisaged. The observed synergism in the present system can thus be explained on the basis of the H-L balance of the mixed surfactant system [8]. Ig-210 is a low HLB surfactant and tends to solubilize in oil continuum, whereas Ig-630 is hydrophilic. Unlike the widely used AOT RM in which nearly all surfactant molecules reside in the RM shells[30], the high individual monomeric solubility makes Igepal surfactants less available at the oil/water interface and thus making the RM inefficient to solubilize large volume of water. An ideal surfactant system is required to have an HLB in the range of 8-10 to offer the maximum solubilization capacity; for the present system we calculate the HLB of the mixture by following a model proposed by Huibers et al.[8] assuming that the surfactants distribute at the interface in proportion to their relative mole fractions. As can be observed from figure 4.1, the maximum in solubilization capacity is observed at $X_{Ig630}$=0.3 wherein the HLB passes through the specified range of 8-10. The observed non-linearity in the solubilization capacity thus shows strong correlation with the partition of the surfactant at the interface, however, other effects like the interplay between the optimum radius of curvature of the surfactant films and inter-droplet interaction[7] could not a-priori be ruled out. It now stands interesting to investigate whether the remarkable synergistic effect as observed in solubilization capacity be reciprocate in the physical behaviour of the mixed RMs.

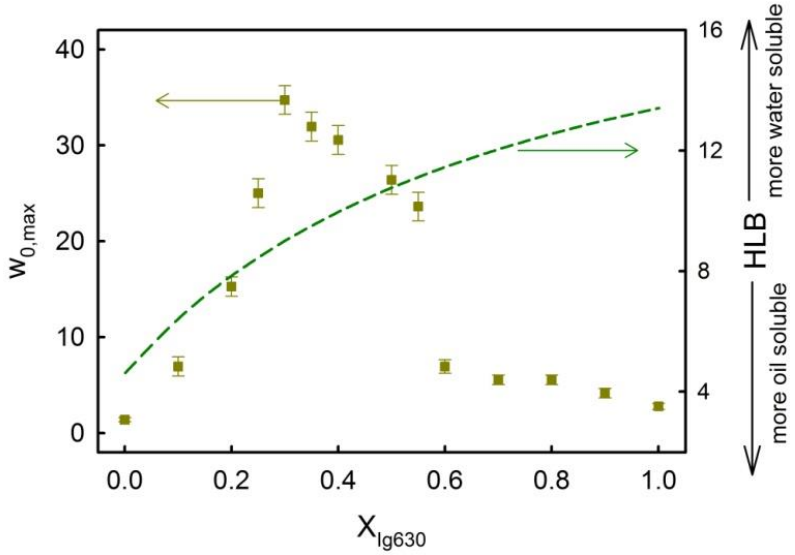


**Figure 4.1.** Maximum solubilization capacity ($w_{0,max}$) and HLB number of Igepal-210 + Igepal-630 mixed RMs in cyclohexane as a function of the surfactant mixing ratio.

***DLS Measurements:*** The results of the DLS measurements are depicted in figure 4.2. It is interesting to note that the droplet size of the Igepal based system does not always hold a linear relationship with $w_0$ since a significant portion of the surfactant molecules are in a free state, i.e. dissolved in the oil phase and does not associate with the RM [23, 31]. Also there can be possibility of the formation of non-spherical aggregates depending upon the composition of the RM [32]. However, for a simpler understanding of the effect of mixing of surfactants on the droplet size we estimate the size of the RM droplets assuming the droplets to be spherical in nature [33]. Figure 4.2a depicts a representative scattering intensity distribution for the mixed systems at a fixed $w_0$=5. The choice of this particular $w_0$ value lies on the fact that at $w_0$=5, all the mixed systems form stable RMs. It is found that in the range of $X_{Ig630}$=0.2 to 0.6, the size distribution is distinctly bi-modal with an intense peak appearing at ~10 nm and the other weak distribution is observed at ~200 nm. For the terminal compositions, the distribution is essentially mono-modal with a single peak appearing at ~10 nm. The observed droplet size of ~10 nm is in good agreement with those obtained with other Igepal RM systems [20, 32, 33], however, the appearance of the second peak at a bigger size distribution is quite intriguing. We plot the droplet size (of the smaller RMs) as a function of $X_{Ig630}$ for different $w_0$ values (up to $w_0$=10) in figure 4.2b. It is evident that within the experimental $w_0$ range, the droplet size increases linearly with increasing $w_0$, a feature rather common in conventional dilute RM solutions[20, 32-34] revealing that the RMs are special and non-interacting [32]. However, a distinct feature in the droplet profile is observed in which the size passes through a minimum

at $X_{Ig630}$~0.4. This result is in sharp contradiction with our previous studies involving ionic-nonionic mixtures wherein a linear change in the droplet size was observed as a function of the surfactant mixing ratio [5, 20]. It is interesting to note that the minimum in the droplet size distribution is realized in a mixing ratio where exactly the maximum in solubilization capacity (optimization of HLB) is observed (figure 4.1) and DLS shows a distinct bi-modal distribution

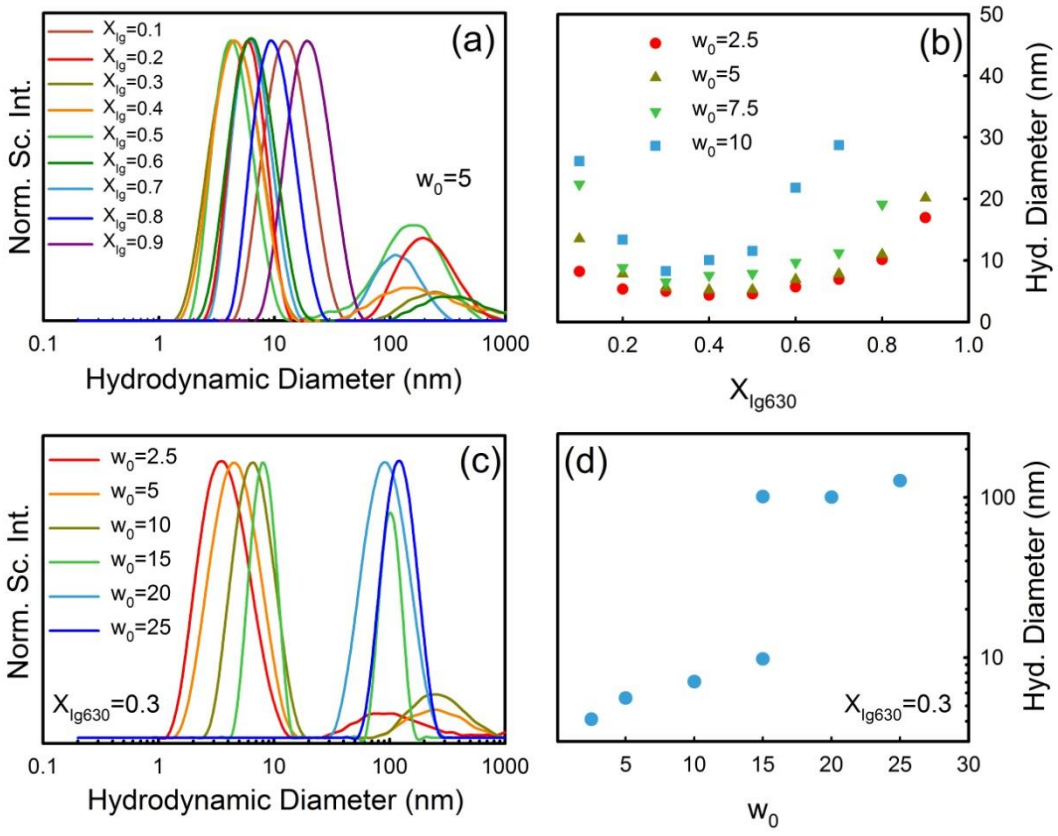


**Figure 4.2.** (a) Scattering profiles of mixed RMs with different mixing ratios at a fixed $w_0$=5. (b) Average hydrodynamic diameter of mixed RM at different mixing ratios and different water content ($w_0$). (c) Scattering profiles of mixed RMs with different $w_0$ values at $X_{Ig630}$=0.3. (d) Average hydrodynamic diameter of mixed RM at different water content ($w_0$) with $X_{Ig630}$=0.3.

(figure 4.2a) with the appearance of a second peak at ~100 nm (figure 4.2a). Since the formation of cylinder like aggregates[35] can be discarded in Igepal RM due to the high solubility of the surfactants in the continuous phases[33], the ~100 nm size distribution indicates the possible formation of larger sized RM droplets in addition to the smaller ones. Owing to the high oil solubility a relatively large fraction of the surfactant molecules remain in the monomeric form and do not essentially participate in RM formation at lower $w_0$ values. In case of the terminal mixtures the high monomeric solubility restricts the formation of larger RMs, however, for the intermediate mixing fractions the surfactants are more partitioned at the

interface (optimum HLB) resulting in the observed high water solubilization capacity. In order to obtain a better insight we carry out DLS measurements for a fixed $X_{Ig630}$=0.3 at different $w_0$ values. The results are depicted in figure 4.2c,d. It is found that the size distribution remains bimodal up to $w_0$=15, with the peak intensity being dominant for the smaller droplets. For $w_0$=15, the peak intensities are comparable indicating an even distribution of the droplets and at higher hydration only the peak at ~100 nm persists. The hydrodynamic diameter increases linearly in the low hydration region, and then increases sharply to ~100 nm at $w_0 \geq 15$ (figure 4.2d). This result indicates that at low hydration, there occurs a distribution of surfactants between the smaller and larger droplets, and a linear increase in droplet size corroborates with the fact that more surfactant partition into the interface to accommodate more water in individual droplets. At $w_0$=15, the distribution is optimum, and with further increase in hydration, larger sized droplets prevail over the smaller ones.

***Viscosity and Densimetry Measurements:*** We measure the bulk viscosity of the RM systems in order to realize any possible intermediate structural modification other than the droplet type. Figure 4.3a shows the viscosity profile of the mixed RM systems as a function of $X_{Ig630}$ at a constant $w_0$=5 and 3b shows the viscosity profile of the mixed RM systems as a function of $w_0$ at a constant $X_{Ig630}$=0.3. The viscosity profile as a function of $w_0$ reveals a sudden ~2 fold increase at $w_0$=15, wherein the much intuited droplet size transition has been realized in the DLS measurements (figure 4.2d). The profile depicted in figure 4.3a shows a continuous increase in viscosity with Ig-630 content, with no characteristic feature in the $X_{Ig630}$=0.3 region, indicating no major structural transition to occur in this region, a behaviour much consistent with AOT/Igepal mixed RM systems [20]. We also calculate the apparent specific volume ($\phi_v$) of water in these RM systems using equation 2 (figure 4.3c,d). The obtained $\phi_v$ values are found to be of the same order of magnitude as those obtained for ionic-nonionic mixed RM systems[20, 36] and is smaller than that of pure water (~$10\times10^{-4}$ $m^3kg^{-1}$), which essentially indicates the highly structured nature of water inside RM. For $X_{Ig630}$=0.3 systems, $\phi_v$ shows a linear increase with $w_0$, and at $w_0$=25, it approaches a value comparable to that of bulk water. On the other hand, when Ig-630 concentration is increased at fixed $w_0$=5, $\phi_v$ decreases linearly up to $X_{Ig630}$=0.5 (figure 4.3c), beyond which the change is only marginal. It is thus evident

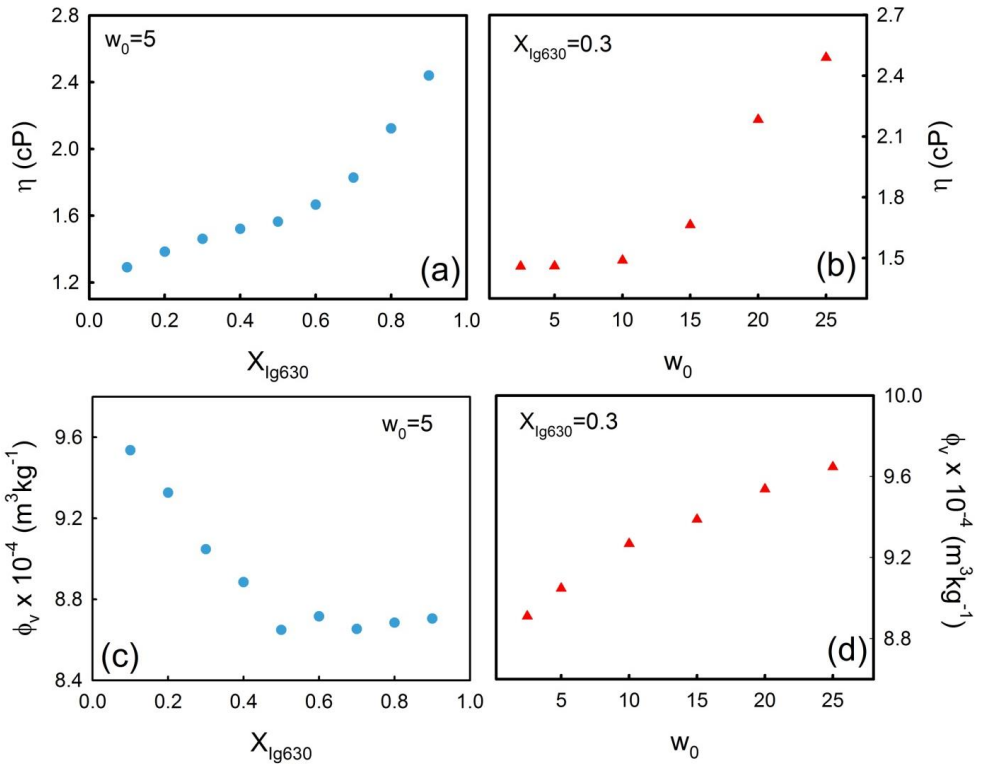


**Figure 4.3.** (a) Viscosity of mixed RMs as a function of $X_{Ig630}$ at a fixed $w_0$=5. (b) Viscosity of mixed RMs as a function of $w_0$ at a fixed $X_{Ig630}$ =0.3. (c) Adiabatic compressibility of mixed RMs as a function of $X_{Ig630}$ at a fixed $w_0$=5. (d) Adiabatic compressibility of mixed RMs as a function of $w_0$ at a fixed $X_{Ig630}$ =0.3.

that Ig-210 rich mixed RM system ($X_{Ig630}$=0.1) offers higher $\phi_v$ values compared to the Ig-630 rich mixed RM system ($X_{Ig630}$=0.9) possibly indicating that Ig-210 forms less intermolecular hydrogen bonds with the RM waterpool than Ig-630, which seems quite intuitive keeping in mind the longer EO chain of the later compared to that in the former one. The densimetry measurements thus confirm that water structure is considerably perturbed inside RM due to its interaction with the interface, however, no distinct feature correlating the synergistic behavior of water solubilization capacity. More direct information on the water structure is therefore extracted from FTIR measurements.

***FTIR Measurements:*** For in depth understanding of the water structure inside the mixed RM systems we measure the MIR FTIR spectra of these systems. In all these measurements we subtract the data of $w_0$=0 (dry RM) systems from the corresponding hydrated systems and thus the signals essentially provide information from water molecules embodied in the RM water pool. We focus our attention in the 3000-3800 $cm^{-1}$ frequency window as this is a fingerprint region for the symmetric and asymmetric vibrational stretch of O-H bonds in water [20]. The overall spectrum of pure water in this frequency window could be deconvoluted into three Gaussian sub-bands peaking at ~3600, 3460 and 3330 $cm^{-1}$. The peak at ~3600 $cm^{-1}$ ($\nu_3$) is due

to the ‘bound type’ water molecules which make bonds with the interface and thus do not produce stable hydrogen bonds with the neighbouring water molecules [37, 38]. The second component peaking at 3460 $cm^{-1}$ ($\nu_2$) involves the so-called ‘intermediate’ water molecules which are somewhat connected to neighbouring water molecules with distorted hydrogen bonds [37]. The third kind of water molecule [peaking at 3330 $cm^{-1}$ ($\nu_1$)] originates from the ‘network’ or ‘bulk type’ water molecules which are fully hydrogen bonded with the neighbouring water molecules and contributes its majority of share in pure water. We deconvolute the MIR spectra of all the RM systems into three Gaussian components keeping the peak positions fixed as those of pure water for a better comparison purpose (a representative figure is shown in figure 4.4a and 4.4b)[20]. We plot the relative contribution of each curve towards the total spectra as a function of $X_{Ig630}$ (figure 4.4c) at a fixed $w_0$=5, and as a function of water content ($w_0$) at $X_{Ig630}$=0.3 (figure 4.3d). This relative contribution is essentially

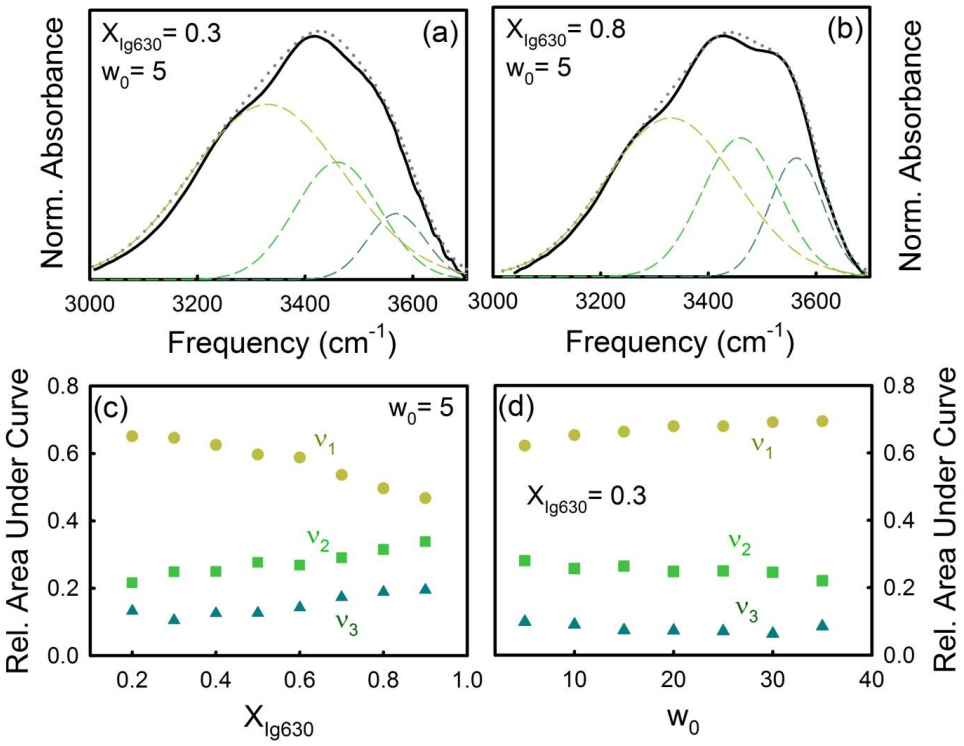


**Figure 4.4.** FTIR spectra of Igepal 630 + Igepal 210 mixed RM systems at two different mixing ratios, $X_{Ig630}$=0.3 (a) and $X_{Ig630}$=0.8 (b). The broken lines are the deconvoluted curves. The grey dotted lines represent the overall fits. (c) Relative area under each deconvoluted curves as a function of $X_{Ig630}$ at a fixed $w_0$=5. (d) Relative area under each deconvoluted curves as a function of $w_0$ at a fixed $X_{Ig630}$=0.3 with $\nu_1$, $\nu_2$ and $\nu_3$ correspond to network, intermediate and bound water, respectively.

proportional to the fraction of water molecules belonging to that particular stretching mode and in pure water their relative abundance is: 5% (bound water), 29% (intermediate water) and 66% (network water).

It can be observed from figure 4.4c that the relative abundance of the 'network' water molecules decreases at the expense of an increase in the content of 'intermediate' and 'bound' water molecules as the content of the hydrophilic surfactant Ig-630 increases in the mixture. The relative abundance of 'network' water decreases from 65% ($X_{Ig630}$=0.2) to 47% ($X_{Ig630}$=0.9) with a concomitant increase in 'bound' water from 13% to 19% and 'intermediate' water from 22% to 34%. It can be argued that the interaction between water and the EO chains of Igepal, which is eventually responsible for the appearance of $\nu_2$ and $\nu_3$, increases with increasing Ig-630 content and thereby decreasing the extent of hydrogen bond formation between the neighbouring water molecules ($\nu_1$ contribution). The interaction of water molecules with the polar head group of Ig-630 is stronger in comparison to that of Ig-210 as the former has a bigger EO chain which increases the abundance of 'network' water contribution in the Ig-210 rich system. At the same hydration level ($w_0$=5), anionic AOT/Cy offers 49% 'network' water, 29% 'intermediate' water and 22% 'bound' water[20]; these values are quite comparable to those obtained in Ig-630 rich RM systems indicating that the water molecules are highly structured in these RM systems. On the other hand, for $X_{Ig630}$=0.3 system (figure 4.4d), with increasing $w_0$, the content of 'network' water molecules increases only marginally compensated with a slight decrease in the content of 'intermediate' water molecules while the contribution from the 'bound' water molecules being almost unaltered. As has been noted earlier, a huge change in the droplet conformation is observed in the $w_0$ profile (figure 4.2d), however, the water structure does not suffer any considerable modification. Therefore, synergistic modification of the mechanical properties of the interface does not significantly influence the hydrogen bonded structure of water inside RM.

***Fluorescence Measurements:*** We estimate the dynamics of the encapsulated water molecules from steady state and time resolved fluorescence studies using C-500 as the fluoroprobe. It has previously been shown that in AOT RM systems, selective excitation at 409 nm excites the C-500 molecules at the interface only [39]. To ensure whether the same observation validates in the Igepal based systems also, we measure the difference absorption spectrum of C-500 in which the absorption spectrum of the dry RM $w_0$=0 system is subtracted from that of the $w_0$=5 system (figure 4.5a). The difference spectrum thus provides with specific information of the

interfacial water molecules only. As observed from the figure, the difference absorption spectrum produces a peak at ~420 nm, with a positive value at ~409 nm. Thus the choice of the excitation wavelength is justified and provides specific information on the dynamics of the interfacial water molecules. Figure 4.5b depicts the emission spectra of C-500 as a function of the surfactant mixing ratio while figure 4.5c represents that as a function of $w_0$. C-500 produces an emission peak at 480 nm with $X_{Ig630}$=0.1, which then suffers a 4-5 nm red shift as the content of Ig-630 increases in the mixture. The peak position is considerably blue shifted in comparison to that in ionic surfactant AOT/Cy RM[20] and in bulk water [40]. This observation strongly validates the fact that water inside Igepal RMs is highly structured compared to the other conventional RMs, and mixing of two surfactants of different HLB values has minimal effect on it. In order to probe the dynamics of the encapsulated water, we study the time resolved emission spectroscopy.

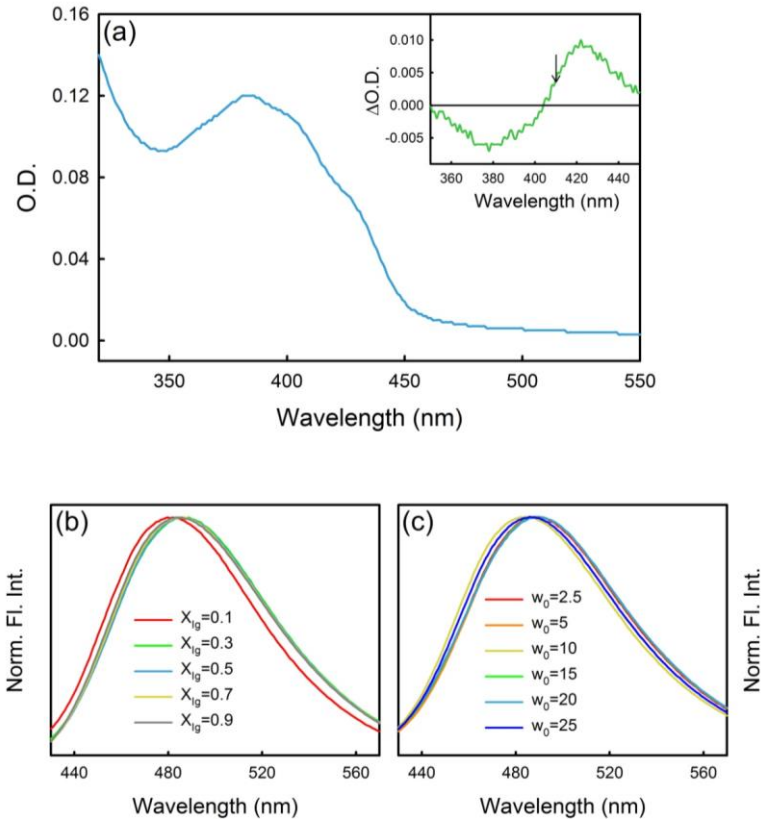


**Figure 4.5.** (a) Absorption spectrum of C-500 in mixed RM with $X_{Ig630}$=0.3 with $w_0$=5. The inset shows differential spectrum in which the spectrum of dry RM ($w_0$=0) has been substracted from that of the $w_0$=5 system. (b) Emission spectrum of C-500 in mixed RM with different $X_{Ig630}$ at a fixed $w_0$=5. (c) Emission spectrum of C-500 in mixed RM with different $w_0$ at a fixed $X_{Ig630}$=0.3.

A representative emission decay transient of C-500 at three different wavelengths in mixed RM is shown in figure 4.6a. The decay transients of the probe in the blue end of the spectrum (430 nm) could be fitted with multiple decay components having time constants of 150 ps (46%), 850 ps (43%) and 4000 ps (11%), whereas that in the red end (600 nm) could be fitted only after considering an additional rise component of 270 ps along with two decay components. Such an observation is suggestive of the solvation of the probe[41] and we construct the corresponding time resolved emission spectra (a representative plot is shown in figure 4.6b). From the TRES, we construct the solvent correlation function, C(t) following equation in chapter 2. Some representative C(t) for different $X_{Ig630}$ values at $w_0$=5 and different $w_0$ at $X_{Ig630}$=0.3 are shown in figure 4.4a and 4b, respectively. All the C(t) curves are fitted with multi-exponential decay model and the corresponding time constants are summarized in table 4.1. In this context it is important to check whether the observed time resolved spectral shift is associated with any internal photo-physics of the probe itself. In order to do so we construct the time-resolved area normalized emission spectra (TRANES)[42]; a representative plot is shown in figure 4.6c. Appearance of any iso-emissive point in the TRANES profile indicates the presence of multiple species of the probe and in the present system the absence of any such iso-emissive point strongly affirms the probe to remain only as a single 'species'. Therefore, the observed time dependent spectral shift can be attributed solely to the inhomogeneity of the microenvironment experienced by the probe. The multiple time constants are due to the multiple location of the probe and solvation by the different types of water molecules as evidenced from FTIR measurements. As can be observed from table 4.1, the time constants are in the order of hundreds of ps and a few ns, which in turn are orders of magnitude slower than that observed in pure water [43]. The measured dynamic Stokes shift (~1200 $cm^{-1}$) is also much smaller compared to the steady state Stokes' shift (~3000 $cm^{-1}$). It is important to note here that the sub-ps rotational dynamics of pure water is considerably restrained in confined environments like in RMs [44, 45]. Moreover, selective photo-excitation of the interfacial probe molecules allows the detection of signals from slow relaxation (sub-diffusive in nature) at the interface only. The ultrafast relaxation (of sub-ps timescale) is beyond the resolution of our present set up, we thus restrict our discussion based on the sub-diffusive translational relaxation of water at the RM interface which occurs in sub-ns time scale. The essence of the present investigation is to underline the effect of the interface perturbation on the water relaxation dynamics, and thus the discussion made on the slow relaxation dynamics stands valid enough.

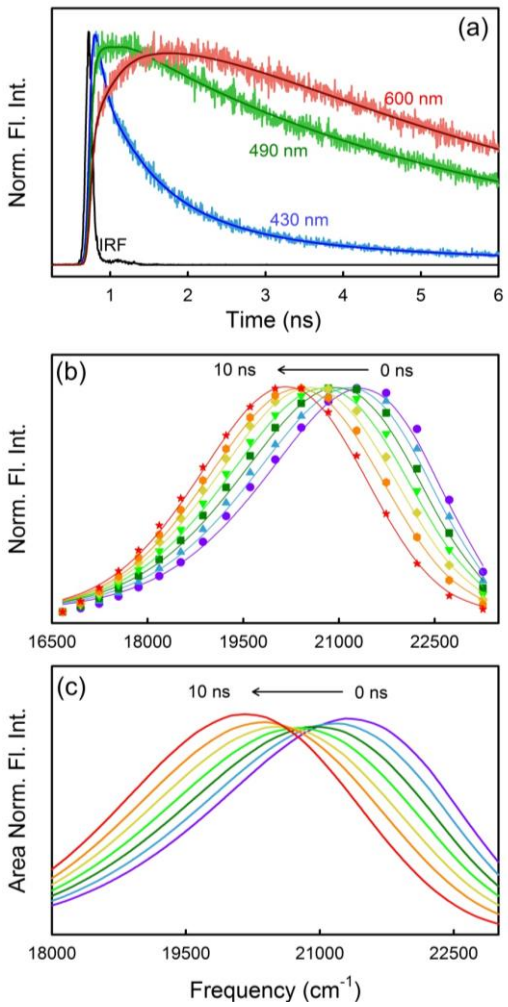


**Figure 4.6.** (a) Emission transients of C-500 in mixed RM with $X_{Ig630}$=0.3 with $w_0$=5 at three different wavelengths. The solid lines are multi-exponential fits. (b) Time resolved emission spectra of C-500 in mixed RM with $X_{Ig630}$=0.3 with $w_0$=5. (c) Area normalized time resolved emission spectra of C-500 in mixed RM with $X_{Ig630}$=0.3 with $w_0$=5.

We plot the average time constant, $< \tau >= \sum_i a_i \tau_i$ as a function of $X_{Ig630}$ at $w_0$=5 (inset of figure 4.7a) and as a function of $w_0$ at $X_{Ig630}$=0.3 (inset of figure 4.7b). The obtained values are found to be of comparable magnitude, however marginally slower to those obtained with conventional ionic AOT RM systems [39]. It is observed that at a fixed composition of $X_{Ig630}$=0.3, solvation dynamics gets faster with increasing $w_0$ up to $w_0$=15, beyond which the change is marginal. Such a hydration dependent acceleration of solvation time scale in RM has previously been observed for both single[39] as well as mixed[5, 20] surfactant systems and can be interpreted on the basis of increasing fraction of the fast solvating 'bulk' water molecules in the RM waterpool. As has been observed from the DLS measurements, there occurs a huge increase in the droplet size at $w_0 \geq 15$ and further addition of water does not change the size considerably (figure 4.2d). The <τ> values also do not exhibit much change beyond this threshold, confirming that the added water does only form newer RMs without

significantly perturbing the structure of individual RM droplets. The solvation dynamics thus follows a trend corroborating the droplet size distribution. It is interesting to note here that the $<\tau>$ value for $w_0$=15 is much slower compared that of ionic AOT RM at identical condition[20] in spite of the fact that AOT RM offers a higher abundance of 'bound' water (13%) compared to the mixed Igepal RM systems (7%). This perhaps invokes the fact that the EO polar head group does participate in the solvation process in the Igepal systems making the overall dynamics slower. On the other hand, it is observed that $<\tau>$ increases gradually with progressive increase in Ig-630 content in the surfactant mixture (figure 4.4b). The DLS profile has shown distinct bimodal distribution of droplet size in the intermediate mixing region, whereas it is mono-dispersed in the

**Table 4.1.** Solvation dynamics parameters for C-500 in Igepal 210 and Igepal 630 mixed surfactant systems

| System | $\tau_1$ (ns) | $\tau_2$ (ns) | $\tau_3$ (ns) | $<\tau>$ (ns) | $\tau_{r1}$ (ns) | $\tau_{r2}$ (ns) | $<\tau_r>$ (ns) | $D_w \times 10^8$ ($s^{-1}$) |
|---|---|---|---|---|---|---|---|---|
| **X=0.1, $w_0$=5** | 0.18 (38%) | 0.75 (32%) | 2.34 (30%) | 1.01 | 0.22 (57%) | 1.61 (43%) | 0.82 | 5.02 |
| **X=0.3, $w_0$=2.5** | 0.26 (36%) | 1.07 (34%) | 2.49 (30%) | 1.20 | 0.25 (44%) | 1.81 (56%) | 1.12 | 3.28 |
| **X=0.3, $w_0$=5** | 0.29 (36%) | 0.86 (31%) | 2.30 (33%) | 1.13 | 0.27 (55%) | 1.89 (45%) | 1.0 | 3.89 |
| **X=0.3, $w_0$=10** | 0.23 (40%) | 1.03 (37%) | 2.24 (23%) | 0.99 | 0.24 (49%) | 1.70 (51%) | 0.98 | 3.84 |
| **X=0.3, $w_0$=15** | 0.22 (33%) | 0.61 (32%) | 1.89 (34%) | 0.92 | 0.25 (52%) | 1.63 (48%) | 0.91 | 3.89 |
| **X=0.3, $w_0$=20** | 0.18 (35%) | 0.87 (46%) | 2.25 (19%) | 0.89 | 0.24 (52%) | 1.58 (48%) | 0.88 | 4.06 |
| **X=0.3, $w_0$=25** | 0.33 (58%) | 1.66 (42%) | - | 0.90 | 0.24 (54%) | 1.62 (46%) | 0.87 | 4.26 |
| **X=0.5, $w_0$=5** | 0.23 (36%) | 1.09 (36%) | 2.26 (28%) | 1.10 | 0.21 (42%) | 1.59 (58%) | 1.05 | 3.34 |
| **X=0.7, $w_0$=5** | 0.18 (33%) | 0.88 (30%) | 2.54 (37%) | 1.26 | 0.31 (44%) | 1.98 (56%) | 1.25 | 2.58 |
| **X=0.9, $w_0$=5** | 0.20 (35%) | 0.82 (18%) | 2.48 (47%) | 1.39 | 0.33 (40%) | 1.96 (60%) | 1.30 | 2.15 |

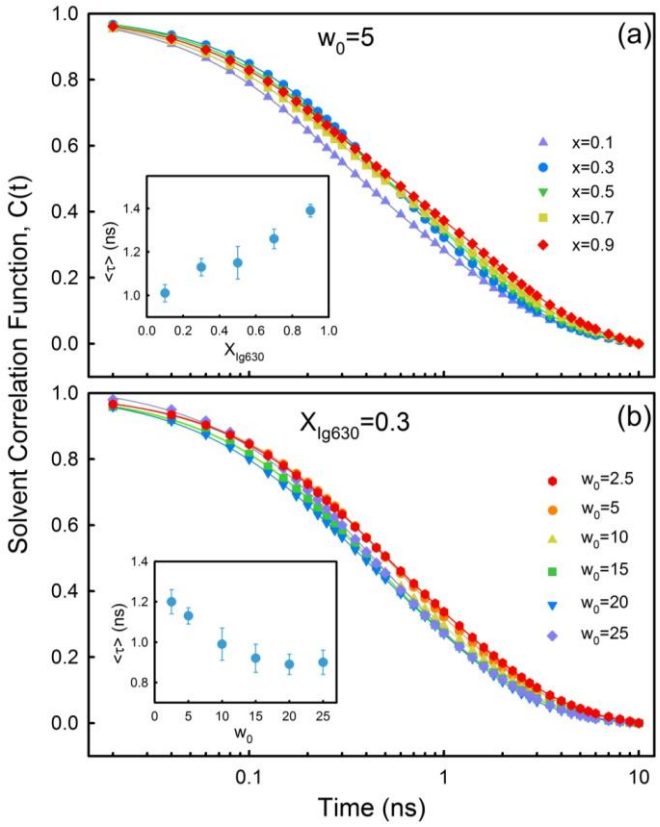


**Figure 4.7.** (a) Solvent correlation function of C-500 in mixed RMs as a function of $X_{Ig630}$ at a fixed $w_0$=5. The inset shows the average solvation time constant. (b) Solvent correlation function of C-500 in mixed RMs as a function of $w_0$ at a fixed $X_{Ig630}$=0.3. The inset shows the average solvation time constant.

terminal mixtures. Moreover, the droplet size also passes through a minimum when plotted against $X_{Ig630}$. The non-linearity in the droplet size as observed from DLS is thus unable to explain the observed linearity in the <τ> profile and can rather be rationalized in the view of the FTIR measurements. FTIR measurements have revealed that the extent of the 'network' water decreases at the expense of 'bound' water with increasing hydrophilic contribution in the mixture as more water molecules participate in the bond formation with the polar head group of the surfactant. Thus the interaction of water with the head groups outplays the effect of size.

In order to understand the geometrical restriction imposed on the probe molecule by the interface, we fit the rotational anisotropy decay transients bi-exponentially (figure 4.8) and the time constants ($\tau_r$) are presented in table 4.1. The observed rotational timescale of the probe in RM is order of magnitude slower compared to that in pure water (~70 ps)[40] affirming the restriction imposed on the probe inside the RM. The average rotational time constant, $< \tau_r > = \sum_i a_i \tau_{r_i}$ follows a trend similar to that obtained in the solvation dynamics measurements (figure 4.9a). It can be observed that the rotation of the probe is eased as $w_0$ is increased, while

the restriction increases as Ig-630 is doped into the interface. The imposed restriction in the Ig-630 rich mixtures might arise out of the strong interaction of the probe with the long EO chain of the surfactant. A rough estimate of the local microviscosity ($\eta_m$) as experienced by the probe can be obtained assuming a Stokes-Debye-Einstein relation in which the rotational time constant can be expressed in the form [46, 47], $\tau_r = \frac{\eta_m V}{k_b T}$ where V is the hydrodynamic volume of the probe and $\tau_r$ is the slow rotational time constant. Assuming a molecular volume of ~198 $Å^3$ for C-500[40], we estimate a microviscosity of ~35 cp experienced by the probe, which is considerably higher than the bulk viscosity, and increases slightly with increase in the Ig-630 content in the mixture.

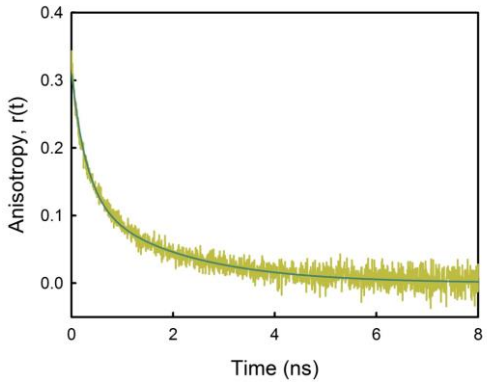


**Figure 4.8.** Anisotropy decay transient of C-500 in mixed RM with $X_{Ig630}$=0.3 with $w_0$=5. The solid line represents a double exponential fit.

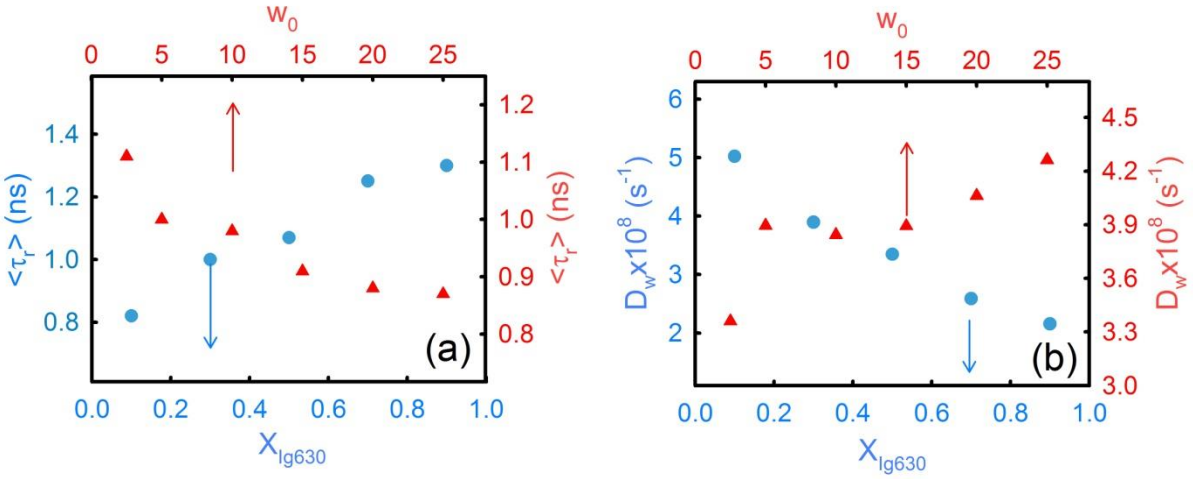


**Figure 4.9.** (a) Average anisotropy rotational time constant C-500 in mixed RMs as a function of $X_{Ig630}$ (blue symbols) and $w_0$ (red symbols). (b) Diffusion coefficient of water (as obtained from equation 7) in mixed RMs as a function of $X_{Ig630}$ (blue symbols) and $w_0$ (red symbols).

To understand the effect of surfactant mixing on the rotational relaxation process of the probe inside the RM water core in a more quantitative manner, the bi-exponential anisotropy decay has been analyzed using a two-step wobbling-in-cone model [48, 49]. According to this model, the rotational anisotropy decay function is defined as,

$$r(t) = r_0[\beta e^{-t/\tau_{slow}} + (1-\beta)e^{-t/\tau_{fast}}] \quad (4.1)$$

where $\beta=S^2$, and S is the generalized order parameter that describes the degree of restriction on the wobbling-in-cone orientational motion. Its magnitude is considered as a measure of the spatial restriction of the probe and can have value from zero (for unrestricted rotation of the probe) to one (for completely restricted motion). The semicone angle $\theta_W$ is related to the ordered parameter as,

$$S = \frac{1}{2}\cos\theta_W(1+\cos\theta_W) \quad (4.2)$$

The diffusion coefficient for wobbling motion $D_W$ can be obtained from the following relation,

$$D_W = \frac{1}{(1-S^2)\tau_W}\left[\frac{x^2(1+x)^2}{2(1-x)}\left\{\ln\left(\frac{1+x}{2}\right)+\frac{1-x}{2}\right\}+\frac{1-x}{24}(6+8x-x^2-12x^3-7x^4)\right] \quad (4.3)$$

where $x = \cos\theta_w$ and $\tau_w$ is defined as, $\frac{1}{\tau_w} = \frac{1}{\tau_{fast}} - \frac{1}{\tau_{slow}}$. The obtained $D_w$ values are presented in table 4.1 and figure 4.9b. The $D_w$ values are found to be of the same order of magnitude as has been reported earlier for AOT/Brij-30 mixed RM systems [5]. $D_w$ gradually decreases with increasing $X_{Ig630}$ corroborating the fact that the probe experiences progressively more restricted rotation in the RM. The smaller $D_w$ value at higher $X_{Ig630}$ also indicates that diffusion gets slower at higher Ig-630 content which eventually results in a slower solvation dynamics (figure 4.7b) which, in turn, is a manifestation of the higher abundance of 'bound' water as revealed from FTIR measurements (figure 4.4c).

***Kinetics Measurements:*** We study the kinetics of solvolysis of benzoyl chloride (BzCl) to underline the activity of water in the mixed systems. The reaction is a well-studied one in the restricted medium and is reported to follow simple first order kinetics [50, 51]. BzCl is first solubilized in Cy and then added into the RM, wherein it gets compartmentalized into the organic phase and the interphase; the interfacial water molecules act as nucleophile to cleave the C-Cl bond. The reaction is monitored as the rate of decay of the absorbance of BzCl at 313

nm. The normalized absorbance transients of BzCl of the mixed RM systems is shown in Figure 4.10a as a

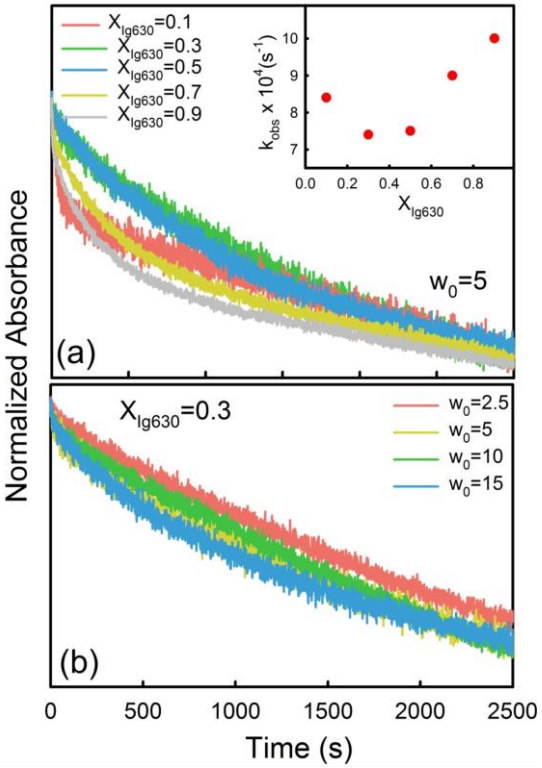


**Figure 4.10.** (a) Normalized absorbance transient of BzCl in mixed RM as a function of $X_{Ig630}$ at a fixed $w_0$=5. The inset shows the observed rate constant as a function of the mixing ratio. (b) Normalized absorbance transient of BzCl in mixed RMs as a function of $w_0$ at a fixed $X_{Ig630}$ =0.3.

function of $X_{Ig630}$ at a fixed $w_0$=5. It is observed that the rate vs. $X_{Ig630}$ profile offers an inverted bell shaped pattern in which reaction gets slower in the $X_{Ig630}$=0.3-0.5 region compared to the terminal mixing ratios. The reaction gets marginally faster with increasing the hydration level from $w_0$=2 to 15 (figure 4.10b). It is interesting to note that the rate of the reaction is orders of magnitude slower compared to that in pure water (1.1 $s^{-1}$)[52] and comparable to that obtained in earlier studies in RM systems including non-ionic surfactants [5]. The considerably retarded reaction kinetics in RM compared to that in pure water clearly suggests that nucleophilicity of water molecules gets reduced as it forms bonds with the polar head groups at the interface. In this context, it is important also to consider the partition of the substrate into the different phases. BzCl is preferentially partitioned into the oil phase and the interface, with a distribution constant of $K_{oi}$. Another partition could also be considered in which BzCl is distributed between the interface and the aqueous phase ($K_{iw}$). The overall reaction rate is accumulation of the rates at the two different phases. Since the reaction is very fast in water, $K_{iw}$ eventually does not affect the overall slow kinetics. Also, the solvation dynamics of water, which eventually

manifests the nucleophilic behaviour of water[53] does exhibit a regular retarded dynamics at higher Ig-630 content owing to the higher polarity of the surfactant head-group compared to that of Ig-210 (figure 4.7a) and progressive acceleration with increase in the hydration level from $w_0$=2 to 15 (figure 4.7b). Both these results are unable to explain the observed non-linearity in the reaction kinetics trend, which is much in contradiction with AOT/Brij-30 mixed RM systems in which reaction kinetics did follow a trend predictable from the solvation dynamics studies [5]. The present study unambiguously indicates that it is the $K_{oi}$ that governs the overall kinetics with $K_{iw}$ imposing only minimal effects. As intuited from the DLS measurements as well as HLB calculations, in the $X_{Ig630}$=0.3-0.5 region the surfactants are more partitioned at the interface compared to the corresponding terminal mixing ratios, which eventually affects $K_{oi}$ and hence the reaction rate.

## 4.3 Conclusion

Ig-210/Ig-630/Cy mixed surfactant RM system provides a ten-fold increase in the water solubilization capacity at $X_{Ig630}$=0.3 compared to the constituent individual surfactants (figure 4.1). The individual surfactants are either very lipophilic or hydrophilic and can solubilize only limited volume of water owing to their high monomeric partitioning in the dispersed phases. The HLB could be tuned by mixing these two surfactants and at $X_{Ig630}$~0.3, it offers an optimum HLB value as a large fraction of surfactants is eventually partitioned at the oil-water interface. DLS measurements show a distinct bimodal distribution of droplet size in this optimum HLB region, whereas in the terminal HLB regions the droplets are essentially mono-dispersed (figure 4.2). At a fixed $X_{Ig630}$~0.3 the smaller droplets prevails at low $w_0$ with a gradual increase in the size with $w_0$, however, at $w_0 \geq 15$, addition of water preferentially produces the bigger droplets. Such a feature is considerably different from the ionic-nonionic mixed surfactant systems in which the droplet size grossly follows a linear trend with the mixing ratio [5, 20]. Bulk viscosity of the mixed RM system shows a $X_{Ig630}$ dependency and expectedly shows a considerable increase at $w_0 \geq 15$ corroborating the bigger droplet formation. It thus stands interesting to identify whether the physical properties of water inside the RMs reciprocate a similar trend. FTIR measurements provide an insight of the structure of the encapsulated water, and it is observed that it follows an overall linear trend as the content of 'bound' water increases at the expense of the 'network' water with increasing the content of the hydrophilic surfactant Ig-630 in the mixture. The increase in $w_0$ at a fixed composition marginally increases the share of 'network' water (figure 4.4). The change in the water dynamics also traces the FTIR trends as

the slow (sub-diffusive) relaxation dynamics of water gets linearly retarded with progressive increase in the content of hydrophilic Ig-630 in the mixture corroborating the increase in the content of 'bound' water as evidenced from the FTIR studies. Unlike the solubilization and DLS results, the water structure and the slow relaxation dynamics follows a linear trend. Since the choice of the probe provides us with selective information on the interface only, the present observation clarifies that the slow relaxation dynamics of water is solely governed by its interaction with the interface and is almost indifferent to the geometry of the interface [20]. On the other hand, the reaction kinetics of a simple nucleophilic reaction does not offer any linear trend and the rate gets slower in the optimum HLB region. This observation is striking compared to the ionic-nonionic mixed system, wherein a linear trend had been realized [5]. As the solvolysis reaction largely depends on the distribution of the substrate between the oil phase and the interface, and a highly concentrated interface perhaps disturbs the distribution resulting in a retarded kinetics. The physical features of nonionic surfactant(s) mixture is thus appeared to be different from ionic-nonionic mixture and provides some unusual non-linear behaviour that can be explained only considering the monomeric solubility of the individual surfactants in the bulk phases. The observed linear trend in most of the ionic-nonionic mixed RM systems provides with the privilege to predict its physical properties as well as the flexibility to tune it in accordance with the desired applications, however, for nonionic-nonionic mixed RM systems one has to be more careful in doing so.

## 4.4 References

[1] B.K. Paul, S.P. Moulik, Microemulsions: an overview, Journal of Dispersion science and Technology, 18 (1997) 301-367.
[2] B.A. Simmons, S. Li, V.T. John, G.L. McPherson, A. Bose, W. Zhou, J. He, Morphology of CdS Nanocrystals Synthesized in a Mixed Surfactant System, NanoLetters, 2 (2002) 263-268.
[3] A. Shome, S. Roy, P. Das, Nonionic Surfactants: A Key to Enhance the Enzyme Activity at Cationic Reverse Micellar Interface, Langmuir, 23 (2007) 4130-4136.
[4] H. Shi, L. Qi, J. Ma, N. Wu, Architectural control of hierarchical nanobelt superstructures in catanionic reverse micelles Adv. Functional Materials, 15 (2005) 442-450.
[5] R.K. Mitra, S.S. Sinha, P.K. Verma, S.K. Pal, Modulation of Dynamics and Reactivity of Water in Reverse Micelles of Mixed Surfactants J. Phys. Chem. B, 112 (2008) 12946-12953.
[6] H. Kunieda, K. Shinoda, Evaluation of the hydrophile-lipophile balance (HLB) of nonionic surfactants. I. Multisurfactant systems, J. Colloid Interface Sci., 107 (1985) 107-121.
[7] M.J. Hou, D.O. Shah, Effects of the molecular structure of the interface and continuous phase on solubilization of water in water/oil microemulsions, Langmuir, 3 (1987) 1086-1096.
[8] P.D.T. Huibers, D.O. Shah, Evidence for Synergism in Nonionic Surfactant Mixtures: Enhancement of Solubilization in Water-in-Oil Microemulsions, Langmuir, 13 (1997) 5762 - 5765.

[9] H. Kunieda, M. Yamagata, Mixing of nonionic surfactants at water-oil interfaces in microemulsions, Langmuir, 9 (1993) 3345-3351.
[10] M.A. Pes, H. Kunieda, Surfactant distribution in mixed surfactant microemulsions, Trends Phys. Chem., 5 (1995) 75-89.
[11] D.-H. Chen, M.-H. Liao, Effects of mixed reverse micellar structure on stability and activity of yeast alcohol dehydrogenase, J. Mol. Cat. B: Enzymatic, 18 (2002) 155-162.
[12] J. Lan, Y. Zhang, X. Huang, M. Hu, W. Liu, Y. Li, Y. Qu, P. Gao, Improvement of the catalytic performance of lignin peroxidase in reversed micelles, J. Chem. Tech. Biotech., 83 (2008) 64 - 70.
[13] A.K. Poulsen, L. Arleth, K. Almdal, A.M. Scharff-Poulsen, Unusually large acrylamide induced effect on the droplet size in AOT/Brij30 water-in-oil microemulsions, J. Colloid Interface Sci., 306 (2007) 143-153.
[14] J. Zhang, B. Han, J. Liu, X. Zhang, J. He, Z. Liu, T. Jiang, G. Yang, Recovery of Silver Nanoparticles Synthesized in AOT/C12E4 Mixed Reverse Micelles by Antisolvent CO2, Chemistry - A European Journal, 8 (2002) 3879-3883.
[15] P.K. Singh, A.K. Satpati, M. Kumbhakar, H. Pal, S. Nath, A Nanoreactor for Tuning the Chemical Reactivity of a Solute, J. Phys Chem. B, 112 (2008) 11447-11450.
[16] B.K. Paul, R.K. Mitra, Water solubilization capacity of mixed reverse micelles: Effect of surfactant component, the nature of the oil, and electrolyte concentration, J. Colloid Interface Sci., 288 (2005) 261-279.
[17] R.K. Mitra, B.K. Paul, Investigation on percolation in conductance of mixed reverse micelles, Colloids and Surfaces A: Physicochemical and Engineering Aspects, 252 (2005) 243-259.
[18] R.K. Mitra, B.K. Paul, S.P. Moulik, Phase behavior, interfacial composition and thermodynamic properties of mixed surfactant (CTAB and Brij-58) derived w/o microemulsions with 1-butanol and 1-pentanol as cosurfactants and n-heptane and n-decane as oils, J. Colloid Interface Sci., 300 (2006) 755-764.
[19] S. Chatterjee, R.K. Mitra, B.K. Paul, S.C. Bhattacharya, Interface of AOT/Brij mixed reverse micellar systems: Conductometric and spectrophotometric investigations, J. Colloid Interface Sci., 298 (2006) 935-941.
[20] A. Das, A. Patra, R.K. Mitra, Do the Physical Properties of Water in Mixed Reverse Micelles Follow a Synergistic Effect: A Spectroscopic Investigation, J. Phys. Chem. B, 117 (2013) 3593-3602.
[21] L. Schlicht, J.-H. Spilgies, F. Runge, S. Lipgens, S. Boye, D. Schübel, G. Ilgenfritz, Temperature-, electric field- and solute-induced percolation in water-in-oil microemulsions, Biophys. Chem., 58 (1996) 39-52.
[22] H. Mays, J. Pochert, G. Ilgenfritz, Droplet Clustering in Ionic and Nonionic Water in Oil Microemulsions: Rate of Exchange between Clusters Studied by Phosphorescence Quenching, Langmuir, 11 (1995) 4347-4354.
[23] S. Lipgens, D. Schuebel, L. Schlicht, J.-H. Spilgies, G. Ilgenfritz, J. Eastoe, R.K. Heenan, Percolation in Nonionic Water (w/o)-Microemulsion Systems: A Small Angle Neutron Scattering Study, Langmuir, 14 (1998) 1041-1049.
[24] D.E. Moilanen, N.E. Levinger, D.B. Spry, M.D. Fayer, Confinement or the Nature of the Interface? Dynamics of Nanoscopic Water, J. Am. Chem. Soc., 129 (2007) 14311-14318.
[25] S. Park, D.E. Moilanen, M.D. Fayer, Water Dynamics - The Effects of Ions and Nanoconfinement J. Phys. Chem. B, 112 (2008) 5279-5290.
[26] G.M. Sando, K. Dahl, J.C. Owrutsky, Surfactant Charge Effects on the Location, Vibrational Spectra, and Relaxation Dynamics of Cyanoferrates in Reverse Micelles, J. Phys. Chem. B, 109 ( 2005) 4084-4095.
[27] E.E. Carpenter, S. Calvin, R.M. Stroud, V.G. Harris, Passivated Iron as Core−Shell Nanoparticles, Chem. Mater., 15 (2003) 3245-3246.
[28] C.R. Vestal, Z.J. Zhang, Synthesis and Magnetic Characterization of Mn and Co Spinel Ferrite-Silica Nanoparticles with Tunable Magnetic Core, Nano Lett., 3 (2003) 1739-1743.

[29] D.-S. Bae, K.-S. Han, J.H. Adair, Synthesis and microstructure of Pd/SiO2 nanosized particles by reverse micelle and sol-gel processing, J. Mater. Chem., 12 (2002) 3117-3120.
[30] T.K. De, A. Maitra, Solution behavior of aerosol OT in non-polar solvents, Adv. Colloid Interface Sci., 59 (1995) 95-193.
[31] F.J. Arriagada, K. Osseo-Asare, Synthesis of Nanosize Silica in a Nonionic Water-in-Oil Microemulsion: Effects of the Water/Surfactant Molar Ratio and Ammonia Concentration, J. Colloid Interface Sci., 211 (1999) 210-220.
[32] A.V. Ivanchikhina, S.A. Tovstun, V.F. Razumov, Influence of surfactant polydispersity on the structure of polyoxyethylene (5) nonylphenyl ether/cyclohexane/water reverse microemulsions, J. Colloid Interface Sci., 395 (2013) 127-134.
[33] J.-L. Lemyre, S. Lamarre, A. Beaupre, A.M. Ritcey, A New Approach for the Characterization of Reverse Micellar Systems by Dynamic Light Scattering., Langmuir, 26 (2010) 10524-10531.
[34] M.P. Pileni, Reverse micelles as microreactors J. Phys Chem., 97 (1993) 6961-6973.
[35] R. Strey, O. Glatter, K.V. Schubert, E.W. Kaler, Small-angle neutron scattering of D2O-C12E5 mixtures and microemulsions with n-octane: Direct analysis by Fourier transformation J. Chem. Phys., 105 (1996) 1175-1188.
[36] A. Amararene, M. Gindre, J.-Y. Le Huerou, C. Nicot, W. Urbach, M. Waks, Water Confined in Reverse Micelles: Acoustic and Densimetric Studies, J. Phys. Chem. B, 101 (1997) 10751-10756.
[37] J.-B. Brubach, A. Mermet, A. Filabozzi, A. Gerschel, D. Lairez, M.P. Krafft, P. Roy, Dependence of Water Dynamics upon Confinement Size, J. Phys. Chem. B, 105 (2001) 430-435.
[38] H. Graener, G. Seifert, Vibrational and orientational relaxation of monomeric water molecules in liquids, J. Chem. Phys. , 98 (1993) 36-45.
[39] R.K. Mitra, S.S. Sinha, S.K. Pal, Temperature-Dependent Solvation Dynamics of Water in Sodium Bis(2-ethylhexyl)sulfosuccinate/Isooctane Reverse Micelles, Langmuir, 24 (2008) 49-56.
[40] D. Banerjee, P.K. Verma, S.K. Pal, A Temperature Dependent Femtosecond-Resolved Hydration Dynamics of Water in Aqueous Guanidinium Hydrochloride Solution, Photochem. Photobiol. Sci., 8 (2009) 1441-1447.
[41] M. Maroncelli, The dynamics of solvation in polar liquids, J. Mol. Liq., 57 (1993) 1-37.
[42] A.S.R. Koti, M.M.G. Krishna, N. Periasamy, Time-resolved area-normalized emission spectroscopy (TRANES): A novel method for confirming emission from two excited states, J. Phys. Chem. A, 105 (2001) 1767-1771.
[43] R. Jimenez, G.R. Fleming, P.V. Kumar, M. Maroncelli, Femtosecond Solvation Dynamics of Water, Nature, 369 (1994) 471-473.
[44] N.E. Levinger, Ultrafast dynamics in reverse micelles, microemulsions, and vesicles, Current Opinion in Colloid & Interface Science, 5 (2000) 118-124.
[45] M.D. Fayer, N.E. Levinger, Analysis of Water in Confined Geometries and at Interfaces, Annu. Rev. Anal. Chem. , 3 (2010) 89-107.
[46] L.A. Philips, S.P. Webb, J.H. Clark, High pressure studies of rotational reorientation dynamics: The role of dielectric friction J. Chem. Phys., 83 (1985) 5810-5821.
[47] B. Kalman, N. Clarke, L.B.A. Johansson, Dynamics of a new fluorescent probe, 2,5,8,11-tetra-tert-butylperylene in solution, cubic lyotropic liquid crystals, and model membranes, J. Phys. Chem., 93 (1989) 4608-4615.
[48] G. Lipari, A. Szabo, Effect of librational motion on fluorescence depolarization and nuclear magnetic resonance relaxation in macromolecules and membranes, Biophys. J., 30 (1980) 489.
[49] G. Lipari, A. Szabo, Padé approximants to correlation functions for restricted rotational diffusion, J. Chem. Phys., 75 (1981) 2971-2976.
[50] M.A. Lopez-Quintela, C. Tojo, M.C. Blanco, L. Garcıa Rio, J.R. Leis, Microemulsion dynamics and reactions in microemulsions, Curr. Opin. Colloid Interface Sci. , 9 (2004) 264-278.
[51] L. Garcia-Rio, J.R. Leis, E. Iglesias, Influence of Water Structure on Solvolysis in Water-in-Oil Microemulsions, J. Phys. Chem., 99 (1995) 12318-12326.

[52] C. Cabaleiro-Lago, L. Garcia-Rio, P. Herves, J. Perez-Juste, Reactivity of Benzoyl Chlorides in Nonionic Microemulsions: Potential Application as Indicators of System Properties, J. Phys. Chem. B., 109 (2005) 22614-22622.
[53] P.K. Verma, A. Makhal, R.K. Mitra, S.K. Pal, Role of Solvation Dynamics in the Kinetics of Solvolysis Reactions in Microreactors, Phys. Chem. Chem. Phys., 11 (2009) 8467-8476.

# Chapter 5: Correlation of Mixing Behaviour of Surfactants between Aqueous and Reverse Micellar Systems

## 5.1 Introduction

Surfactant molecules spontaneously accumulate in solvents to form a variety of organized assemblies such as micelle, reverse micelle or microemulsion, different lamellar phases and vesicles etc [1]. The importance of such systems has increased substantially over years because of their various applications in many areas including drug delivery, media for membrane mimetic photochemistry and chemical reactions [2, 3]. Mixtures of surfactants are often favored over the corresponding single surfactant(s) in industrial, pharmaceutical, and technological formulations for their superior performance and cost effectiveness due to their flexible physicochemical properties in terms of synergistic interaction. The quest for new and improved ionic/nonionic surfactant mixtures has now been an important topic in surface science [4-6]. As mixed micellar systems often improve therapeutic efficiency of various drugs, they find application in pharmaceutical technology [7-9]. On the other hand, aggregates of surfactants in oil continuum can solubilize substantial amount of water to form RM, which has emerged as a potential nano-sized system to mimic biological environment [10, 11]. Doping of nonionic surfactant into the interface of ionic surfactant in RM brings about significant changes in the interfacial property as well as it modifies the structure of water inside the nanopool [12-14]. Mixtures of anionic/nonionic surfactants in RM offer advantageous applications in various fields including enzyme activity, nanoparticle synthesis etc.[15, 16]. In spite of extensive studies of micelles and RMs using similar set of surfactant(s) [17-20], a proper understanding at a molecular level is still in demand. In the presence study, we have investigated the effect of mixing of two surfactants (anionic and nonionic) on the physicochemical characterization of the mixed micellar solutions as well as the corresponding RMs in order to optimize and design their properties. Such investigation stands useful from both academic as well as application point of view.

We explore the micellization behavior of an anionic, sodium di-2-ethylhexylsulfosuccinate (AOT) and nonionic, polyoxyethylene (20) sorbitan trioleate (Tween-85) surfactant and their mixtures in water. Micelle formation has been investigated using extensive surface tension measurements and analysis. AOT is a well-known biocompatible

double-tailed surfactant [21] which shows unique micellization behavior compared to the single-chain conventional surfactants and has been used in lubricants and also, as emulsifiers. AOT based ME finds application in the field of drug delivery [22-24], also AOT influences to increase the intestinal absorption of many drugs [25, 26]. Ethoxylated nonionic Tween-85 is also biodegradable [27], making the overall formulation based on AOT and Tween-85 blends acceptable for pharmaceutical research. Here we report the micellization behavior of AOT and Tween-85 mixed systems from the viewpoint of their interfacial adsorption, nature of interaction and process energetics in detail; such study is rather sparse in the literature [28, 29].

Effort has also been made to form RMs using the combination of AOT and Tween-85 surfactants at different mixing ratios in fatty acid ethyl ester continuum, namely ethyl myristate (EM), ethyl palmitate (EP) and ethyl oleate (EO). It is important to note that apart from the difference in molar volume (Table 5.3), these oils contain similar ethyl chain on either side of the hydrophilic ester moiety and long fatty acid chain of different lengths, viz., myristate, palmitate and oleate. Of these oils, EO contains a cis-double bond in the hydrocarbon chain of fatty acid (Table 5.3). Tween-85 RM is reported to solubilize considerable amount of water and protein [30], and possesses certain unique features for RM enzymology [31]. It was also proposed that enzymatic activities in AOT RMs are improved by the addition of nonionic surfactants into it [32, 33]. Moreover, long chain fatty acid esters are environment friendly [34], low toxic and highly biodegradable [35], and most interestingly they show structural resemblance with the lipids in living systems. Also, their physicochemical behavior in surfactant/water system is much less studied than the conventional *n*-alkanes. Earlier, AOT/Tween-85 mixed RMs was successfully utilized for transdermal delivery of 5-fluorouracil, extraction of amoxicillin and topical delivery of Cyclosporin A [36-38]. But these formulated systems were mostly based on isopropyl myristate (IPM) or hydrocarbon oil. Thus, formulation and characterization of RMs stabilized by EM, EP and EO have been investigated for the first time in this report. We carry out conductivity measurement to investigate any characteristic change that occurs in the RM structure with increasing content of Tween-85 ($X_{Tween\text{-}85}$) and also, to underline the mechanism of the solubilization process. RM droplet size has been measured using dynamic light scattering (DLS) technique. The structure of the entrapped water has been determined using Fourier transform infrared spectroscopy (FTIR) measurements. The retarded dynamics of water entrapped in the mixed RMs has been studied by the solvation probe 4-(dicyanomethylene)-2-methyl-6-(p-dimethylamino-styryl)-4H-pyran (DCM) using picosecond resolved fluorescence spectroscopy technique. The fluorescence spectra of DCM strongly depend on the polarity of the medium [39], and hence, it can act as a

good probe to contemplate the microenvironment of RMs [40, 41]. The probe DCM has previously been used to report the solvation dynamics of various organized nano-assemblies [42, 43]. To ascertain the geometrical restriction of the probe at the interface, rotational relaxation dynamics of DCM in these systems have also been determined. The present study thus reports micellar and reverse micellar interfacial properties of mixed surfactant systems to understand whether the key features responsible for micellization reciprocate the physical properties of water inside the RMs. The findings of this study are expected to improve the basic understanding of the formation and characterization of both mixed micellar and RM systems useful in drug delivery and as nontoxic nano-templates for future applications.

## 5.2 Results and Discussions

### 5.2.1 Formation and Characterization Single and Mixed Micelles

***Determination of critical micelle concentration (CMC) of solutions containing surfactant mixtures:*** We measure surface tension of the mixed surfactants to examine the micellization behavior at different mole fractions of Tween-85 in the mixture (*i.e.*, $X_{Tween-85} = \frac{[Tween-85]}{[AOT]+[Tween-85]}$). We obtain the $CMC_{expt}$ from the break point of the surface tension ($\gamma$) versus surfactant concentration (c in mmol $lit^{-1}$) plot (Fig. 5.1A) and the values are summarized in Table 5.1. It is found that $CMC_{expt}$ for pure Tween-85 is expectedly less than that of pure AOT. The $CMC_{expt}$ data obtained from the surface tension measurement for pure AOT and Tween-85 is in good agreement with the literature values reported earlier [44-46]. With an increase in $X_{Tween-85}$, $CMC_{expt}$ decreases (Table 5.1) due to the partitioning and preferential adsorption of the neutral head group of Tween-85 into the palisade layer of the charged AOT micelles. The introduction of Tween-85 into the AOT micelles causes several features, such as, (1) a reduction in the head group repulsion between the anionic head groups of AOT and (2) simultaneous increase in the hydrophobic interactions between the tails of the surfactants, both these factors favoring early micellization. Surface tension at CMC ($\gamma_{CMC}$) obtained for all the single and binary compositions are provided in Table 5.1. The higher $\gamma_{CMC}$ values of all the mixed compositions compared to AOT micelle indicates a loosely packed arrangement of AOT and Tween-85 molecules at the air-water interface.

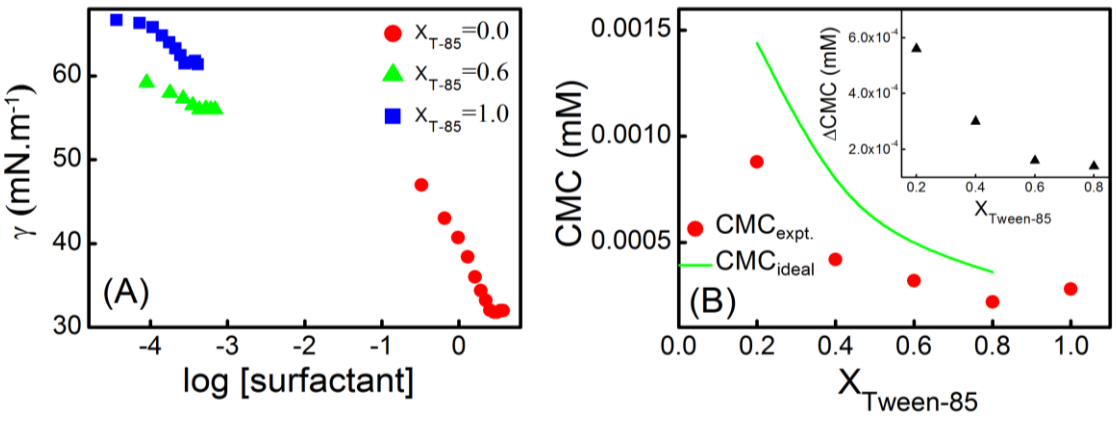


**Fig. 5.1 (A)** Tensiometric determination of CMC of aqueous AOT and Tween-85 surfactant systems by varying the mixing compositions ($X_{Tween-85}$). **(B)** Variation of CMC; the inset shows the deviation of CMC as a function of $X_{Tween-85}$.

Mixed micelles comprising of two or more surfactants often involve mutual interaction between the constituents and thus deviate from the ideal behavior. Mixed micelle formation may be represented as;

$$\frac{1}{CMC_{ideal}} = \sum_i \frac{\alpha_i}{f_i CMC_i} \tag{5.1}$$

Where, $CMC_i$ and $CMC_{ideal}$ stand for the CMC of the $i^{th}$ species and the ideal mixture respectively; $\alpha_i$ and $f_i$ are the mole fraction and activity coefficient of the $i^{th}$ component, respectively in the mixed micelle. For ideal conditions, $f_i = 1$ and equation (1) leads to the Clint's equation [47],

$$\frac{1}{CMC_{ideal}} = \sum_i \frac{\alpha_i}{CMC_i} \tag{5.2}$$

For the binary mixtures of AOT and Tween-85, equation (9) can be written as,

$$\frac{1}{CMC_{ideal}} = \frac{X_{Tween-85}}{CMC_1} + \frac{(1-X_{Tween-85})}{CMC_2} \tag{5.3}$$

This is an idealization which neglects the interaction among different surfactants in the aggregated state and considers the CMCs of the individual components reflecting their relative tendency toward micellization in the mixed state. The theory is, therefore, an oversimplification and can be applied only in fairly dilute solutions. The theory is, however, a tool, divergence from which in the positive and negative side signifies antagonistic and synergistic behavior, respectively. A comparison of $CMC_{expt}$ and those obtained from Clint's equation ($CMC_{ideal}$) has been illustrated in Fig. 5.1B and Table 5.1. For the mixed AOT/Tween-85 systems, $CMC_{expt}$ values are found to be lower than those calculated from Clint's equation (see the

deviation of CMC i.e. ΔCMC versus $X_{Tween\text{-}85}$ plot in Fig. 5.1B inset), which indicates non-ideal mixing behavior and demonstrates favorable synergism between the constituent surfactants in the mixed micelles.

***Mixed micellar composition and interaction parameter:*** Non-ideal behavior micellar solutions can be rationalized by using the Regular Solution Theory (RST), proposed by Rubingh based on the phase separation model of micellization [48];

$$\frac{\left[\left(X_1^m\right)^2 \ln\left(CMC_{12}\, X_{Tween-85} / CMC_1 X_1^m\right)\right]}{\left(1-X_1^m\right)^2 \ln[CMC_{12}(1-X_{Tween-85}) / CMC_2(1-X_1^m)]} = 1 \qquad (5.4)$$

where, $X_1^m$ and $X_{Tween\text{-}85}$ are the micellar mole fraction and mole fraction of Tween-85 in the mixed micelle, respectively and $CMC_1$, $CMC_2$ and $CMC_{12}$ represent the experimental CMC values of the individual surfactant and their binary mixtures, respectively. The basic assumption in RST is that the excess entropy and mixing volume are zero and hence the excess enthalpy of mixing is equal to the excess free energy, which can be expressed using the results applied to "regular solution" mixtures. Even though the regular solution treatment is simple, it is to be noted that the basic assumption in this treatment, i.e. mixing entropy is zero, is not thermodynamically valid for describing non-ideal mixed micelles. Therefore, this model should be viewed only as a useful empirical model. Furthermore, regular solution treatment is successful mainly with respect to the correlation of mixed critical micelle concentrations with one interaction parameter [48]. $X_1^m$ can be calculated solving the above mentioned equation iteratively. $X_1^m$ in the mixed micelle has been found to be higher than the stoichiometric mole fraction of Tween-85 for all of the studied compositions (Table 5.2) [49]. The degree of interaction between Tween-85 and AOT in mixed micelles is manifested by micellar interaction parameter ($\beta^m$) given by the relation developed by Rubingh [48], and Rosen [50];

$$\beta^m = \frac{\left[\ln\left(CMC_{12} X_{Tween-85} / CMC_1 X_1^m\right)\right]}{\left(1-X_1^m\right)^2} \qquad (5.5)$$

The interaction parameter $\beta^m$ can be evaluated from the estimated $X_1^m$ value and experimentally determined $CMC_{12}$ (i.e., CMC of the mixed system) value using equation (5.5). Herein, $\beta^m$ accounts for the deviation from ideality; a negative $\beta^m$ value indicates an attractive synergistic interaction while a positive value indicates a repulsive interaction or antagonism. It is evident that the $\beta^m$ values are negative for all the binary compositions and increases with increasing $X_{Tween\text{-}85}$ (Table 5.2) which indicates the interactions to be attractive in nature.

**Table 5.1.** Interfacial and thermodynamic parameters of aqueous binary mixtures of AOT and Tween-85 at 303K.

| | $\gamma_{CMC}$ ($mN.m^{-1}$) | $CMC_{expt.}$ (mM) | $CMC_{ideal}$ (mM) | $10^3\pi_{CMC}$ ($N.m^{-1}$) | $10^6\Gamma_{max}$( $mol.m^{-2}$) | $A_{min}$ ($nm^2$) | $-\Delta G^0_{ads}$ ($kJ.mol^{-1}$) | $-\Delta G^0_{mic}$ ($kJ.mol^{-1}$) | $\Delta G^S_{min}$ ($kJ.mol^{-1}$) |
|---|---|---|---|---|---|---|---|---|---|
| 0 | 31.60 | 2.63 | - | 42.620 | 1.945 | 0.085 | 27.28 | 25.09 | 1.62 |
| 0.2 | 55.30 | 0.00088 | 0.00144 | 15.470 | 0.285 | 5.823 | 99.52 | 45.25 | 193.95 |
| 0.4 | 56.01 | 0.00042 | 0.00072 | 15.196 | 0.256 | 6.495 | 106.56 | 47.11 | 219.11 |
| 0.6 | 55.27 | 0.00032 | 0.00048 | 16.706 | 0.262 | 6.316 | 111.56 | 47.79 | 339.05 |
| 0.8 | 60.42 | 0.00022 | 0.00036 | 10.677 | 0.163 | 10.185 | 114.24 | 48.74 | 370.64 |
| 1.0 | 61.50 | 0.00028 | - | 12.042 | 0.564 | 2.942 | 69.39 | 48.04 | 108.98 |

**Table 5.2.** Interaction parameter and activity coefficients of aqueous binary mixtures of AOT and Tween-85 at 303K.

| $X_{Tween-85}$ | $CMC_{expt.}$ (mM) | $X_1^m$ | $-\beta^m$ | $f_1^m$ | $f_2^m$ |
|---|---|---|---|---|---|
| 0.2 | 0.00088 | 0.8197 | 9.274 | 0.0478 | 0.00196 |
| 0.4 | 0.00042 | 0.8199 | 10.709 | 0.0299 | 0.00075 |
| 0.6 | 0.00032 | 0.8499 | 11.085 | 0.0405 | 0.00033 |
| 0.8 | 0.00022 | 0.8399 | 12.676 | 0.0238 | 0.00031 |

This observation combined with the negative deviation of $CMC_{expt}$ from $CMC_{ideal}$ (Fig. 5.1B) rationales the synergism owing to a greater interaction between the surfactants in the mixed micelles. The $\beta^m$ values obtained for the present mixed system (Table 5.2) are comparable with those reported for dodecyldiethoxylamine oxide/sodium dodecylsulfate (DDEAO/SDS) mixed micelles [51], however, are higher than mixed AOT and Brij-35/TritonX-100/Tween-20/Myrj-45 [28] and AOT and $C_{10}E_8/C_{10}E_{10}/C_{13}E_{10}$ systems [29]. AOT/Tween-85 mixed system thus produces a relatively better synergistic interaction. Knowing the interaction parameter for the mixed micelles, it is possible to determine the activity coefficient of the surfactants in the mixtures, which can be estimated as [45],

$$f_1^m = exp\left[\beta^m \left(1 - X_1^m\right)^2\right] \tag{5.6}$$

$$f_2^m = exp\left[\beta^m \left(X_1^m\right)^2\right] \tag{5.7}$$

Where, $f_1^m$ and $f_2^m$ are the activity coefficients of Tween-85 and AOT, respectively [52]. The $f_1^m$ and $f_2^m$ are found to be less than unity (Table 5.2) which signifies non-ideal mixing behavior favored by attractive interactions between Tween-85 and AOT.

***Adsorption behavior at the air-water interface:*** In order to understand the solute-solute, solute-solvent interactions within micellar solution and the effectiveness of the surface-active molecule, we analyze the interfacial properties of the surfactants in solution in terms of adsorption behavior. The maximum surface excess concentration at the air-water interface ($\Gamma_{max}$) is an effective measure of the extent of adsorption of various components while the minimum area per surfactant head group adsorbed at the interface ($A_{min}$) is indicative of the tight or loose packing of the surfactant molecule. In the sub-micellar region, $\Gamma_{max}$ and $A_{min}$ can be obtained from the surface tension data on the basis of the adsorption isotherms using the Gibbs equation [53, 54];

$$\Gamma_{max} = -\frac{1}{nRT}\left(\frac{d\gamma}{dlnc}\right) \quad (5.8)$$

$$A_{min} = \frac{10^{18}}{\Gamma_{max} N_A} \quad (5.9)$$

Where, c is the concentration of the amphiphile in mmol $l^{-1}$. Here, n corresponds to the number of species, whose concentrations at the interface vary with surfactant concentration in solution. For pure surfactants, the values of n are 1 and 2 for nonionic and anionic surfactants, respectively. For anionic + nonionic mixed micelles the n values are 3 [55]. For surfactant mixtures in water, the Gibbs surface excess of surfactants per unit area of surface is related to the surface pressure ($\Pi_{CMC}$), which is defined as,

$$\Pi_{CMC} = \gamma_{sol} - \gamma_{CMC} \quad (5.10)$$

Where, $\gamma_{sol}$ and $\gamma_{CMC}$ are surface tensions of pure water and surfactant solution at the CMC, respectively. The values of $\Pi_{CMC}$, $\Gamma_{max}$ and $A_{min}$ for single and binary mixture are presented in Table 5.1. Both $\Gamma_{max}$ and $A_{min}$ values for AOT are in good agreement with the literature values [44, 56]. The smaller $A_{min}$ value of pure AOT (0.085 $nm^2$) compared to that of pure Tween-85 (2.942 $nm^2$) suggests that the former has a higher packing density at the air-water interface than the latter. The longer and higher number of hydrophobic chains of Tween-85 as compared to that in AOT makes the former one more prone to bend producing larger $A_{min}$ [57]. A lower value of $\Gamma_{max}$ and a higher value of $A_{min}$ at all the mixed compositions compared to the pure systems were also reported earlier for mixed Gemini-conventional surfactant solutions [55]. The steric hindrance exerted by the long polyoxyethylene (POE) chains of Tween-85 manifests a higher $A_{min}$ value for mixed combinations [55].

***Thermodynamic analysis on the mixed micelle formation and interfacial adsorption:***

The standard free energy of mixed micelle formation per mole of the monomer unit ($\Delta G^0_{mic}$) for binary surfactant mixture can be obtained from the following equation assuming the

concentration of the free surfactants in presence of the micelle to be equal to the corresponding CMC [29, 58, 59].

$$\Delta G_{mic}^{0} = RT \ln X_{cmc} \quad (5.11)$$

Where, $X_{cmc}$ is the CMC expressed in terms of mole fraction. The standard free energy of interfacial adsorption ($\Delta G^0_{ads}$) at the air/saturated monolayer interface of micelle is obtained from the relation [51, 59];

$$\Delta G_{ads}^{0} = \Delta G_{mic}^{0} - (\frac{\Pi_{cmc}}{\Gamma_{max}}) \quad (5.12)$$

The values of $\Delta G^0_{mic}$ and $\Delta G^0_{ads}$ for the pure and mixed systems at different compositions are found to be negative (Table 5.1), which implies the micellization process to be spontaneous in nature. However, $\Delta G^0_{ads}$ is found to be more negative than $\Delta G^0_{mic}$, suggesting the adsorption process to be dominantly spontaneous than micelle formation [60]. Interestingly, AOT and Tween-85 mixture shows more spontaneous micelle formation compared to $C_{10}E_8$ or $C_{10}E_{10}$ or $C_{13}E_{10}$ [29]. The observed synergism in the mixed adsorbed monolayer can also be quantified in terms of another thermodynamic parameter, free energy of a surface at equilibrium ($G^s_{min}$) given by [57];

$$G_{min}^{s} = A_{min}\gamma_{CMC}N_A \quad (5.13)$$

The $G^S_{min}$ (Table 5.1) essentially measures synergism, and is defined as the free energy change associated during its transition from the bulk phase to the surface. $G^S_{min}$ values are found to be higher for the mixtures implying the formation of thermodynamically more stable surfaces with enhanced surface activity for the mixed systems [61].

Our study thus have established that mixed micelles based on AOT and Tween-85 provide with better surface activity in terms of CMC than the single ones, synergistic interaction between the components and also favorable micellization behavior in terms of thermodynamic parameters. It now stands interesting to further study the behavior of these surfactants in non-polar solvents.

### 5.2.2 Formation and Characterization Single and Mixed RMs

***Solubilization of Water in Mixed RMs:***

Solubilization capacity of water in mixed AOT/Tween-85 RMs [at mole fraction of Tween-85 in mixture of AOT/Tween-85 ($X_{Tween\text{-}85}$) = 0 to 1.0 by keeping fixed total surfactant concentration] in ethyl ester of fatty acids (viz. EM, EP and EO) are presented in Fig. 5.2A and Table 5.4. AOT RMs in EM, EP and EO solubilize a substantial amount of water, $w_0$ (=

[water]/[surfactant]) ~ 30, 24 and 17, respectively). Tween-85 is also fairly soluble in these oils and all these Tween-85 based RMs solubilize water in the range of $w_0$ = 10-20. Addition of Tween-85 in AOT RMs exhibits a considerable synergism in the water solubilization capacity wherein $w_0$ initially increases with increasing $X_{Tween\text{-}85}$ to pass through a maximum at $X_{Tween\text{-}85}$ = 0.05, beyond which it decreases. The results are depicted in Fig. 5.2A and Table 5.4. Solubilization of water in RMs depends upon several factors, for example, type of surfactant (and co-surfactant or a second surfactant), oil, temperature, additives etc.[62]. In the present study, we vary $X_{Tween\text{-}85}$ and the oil independently. The driving force of such solubilization process is the spontaneous curvature and the elasticity (or rigidity) of the interfacial film formed by the surfactants [63]. If the interfacial curvature and the bending elasticity are fixed, solubilization can be maximized by minimizing the interfacial bending stress of the rigid interface and the attractive interdroplet interaction [64]. The extent of water solubilization, in general, can be explained in light of a theoretical model developed by Hou and Shah [65]. Such synergistic solubilization behavior has previously been reported only in a few hydrocarbons and aromatic solvent based mixed surfactant systems [66-70]. From comparative results of previous report of Paul and Mitra [68], it can be concluded that AOT/EM or EP or EO based RMs shows larger increment in water solubilization capacity in presence of Tween-85 compared to AOT/Tween-20 or Tween-40 or Brij-35 or Brij-58/IPM MEs at similar $X_{non\text{-}ionic}$ (= 0.05). However, mixed RMs stabilized in hydrocarbon oils such as cyclohexane or *n*-heptane showed higher solubilization capacity compared to our present RM systems [65-67, 69]. It can be observed that the maximum solubilization capacity of water ($w_{0,max}$) in AOT or mixed AOT/Tween-85 RMs follows the order; EO < EP < EM (Table 5.4). In the present study, the carbon number in the acid chain is varied (i.e., myristate, $C_{14}$; palmitate, $C_{16}$ and oleate, $C_{18:1}$) whereas the carbon number in the alcohol chain remains fixed (Table 5.3). The order for the solubilization capacity thus corroborates the model proposed by Leung and Shah which states that smaller the molar volume or shorter the linear hydrocarbon chain of the oil, larger is the effect of increasing radius of curvature, and hence higher is the solubilization capacity [63].

**Table 5.3.** Physicochemical properties of ethyl ester of fatty acid oils.

| Oil | Molecular structure | Carbon number in the acid chain | Carbon number in the alcohol chain | Total carbon number | Molar volume ($cm^3/mol$) | Equivalent Alkane Carbon Number (EACN) |
|---|---|---|---|---|---|---|
| EM | 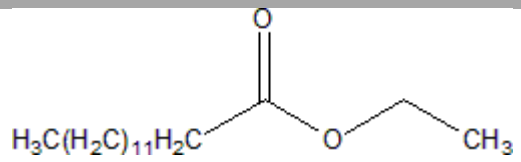 | 14 | 2 | 16 | 297.83 | 5.3[a] |
| EP | 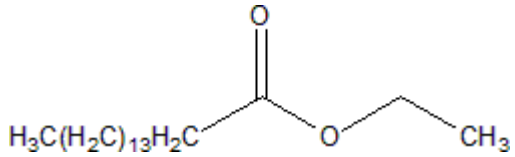 | 16 | 2 | 18 | 331.19 | 6.8[a] |
| EO | 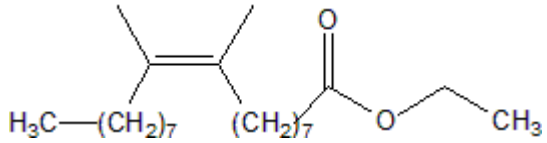 | 18:1 | 2 | 20 | 356.92 | 7.3[a] |

**Table 5.4.** Solubilization of water ($w_{0,max}$) in mixed surfactant reverse micellar systems stabilized in ethyl ester of fatty acid oils with total surfactant concentration, $S_T$ = 0.1mol $dm^{-3}$. [a]$w_0$ = [water]/[AOT] in different oil at [$S_T$] = 0.1 mol $l^{-1}$. [b]$w_{0,max}$ represents the maximum solubilization of water at a particular $X_{Tween-85}$ given in the parenthesis.

| Surfactant | Oil | $w_0$[a] | $w_{0,max}$[b] |
|---|---|---|---|
| AOT/Tween-85 | EM | 29.6 | 37.0 (0.05) |
| | EP | 24.1 | 36.1 (0.05) |
| | EO | 16.7 | 32.4 (0.05) |

***Conductometric Studies:*** The maximum solubilization of water is often correlated with the percolation of conductance, which extracts information about the nature of interaction among the droplets in RMs [10]. We carry out conductance study for mixed RMs wherein solubilization maxima ($w_{0,max}$) are observed. In addition, samples from both sides of the corresponding maxima, i.e., ascending or descending branches of solubilization capacity vs. $X_{Tween-85}$ profile (Fig. 5.2A) are also chosen. Fig. 5.2B and the corresponding inset depict the conductivity of these systems wherein a sudden increase in the conductance (i.e., percolation in conductance) has been observed beyond a certain $w_0$. The corresponding volume-induced percolation threshold ($w_p$) are presented in Fig. 5.3. The $w_p$ is shifted towards lower $w_0$ value with increase in $X_{Tween-85}$. It is interesting to note that all these systems show solubilization maxima at $X_{Tween-85,max}$= 0.05. "Transient fusion-mass transfer-fission" is the mechanism,

which was proposed and widely explained in the literature to describe the occurrence of conductance percolation in various w/o ME systems [10]. The rigidity of the oil/water interface and the interdroplet interactions among the aggregates are probably the most important factors that determine the exchange rate of the ions and water molecules during the fusion processes [71]. The RM systems can be assumed to be so rigid due to their smaller droplet size that it cannot form any such fused droplet network to facilitate percolation at $X_{Tween\text{-}85} < X_{Tween\text{-}85,max}$. But progressive incorporation of Tween-85 at $X_{Tween\text{-}85} \geq X_{Tween\text{-}85,max}$ modifies the interface in such a way that it becomes more flexible and facilitates droplet fusion and hence the percolation process. It may be due to the presence of the head group of non-ionic surfactant at the interface shields the head group repulsion of AOT molecules, and make the interface more flexible. A similar trend has also been observed for EP and EO stabilized systems (not exemplified). It can also be noted that EM, EP and EO oils possess both high molar volume (Table 5.3) and high viscosity (> 4.0 mPa s at 303 K) [72] than conventional linear hydrocarbon oils which makes the droplets difficult to collide and aggregate into clusters and eventually leads to non-percolating AOT/oil(s) systems [71]. Any factor that decreases the rigidity of the interface and/or the interdroplet interaction would also increase the ease of conductance percolation. The droplet size of RMs depends upon the flexibility of the interface, which in turn is related to the changes in the critical packing parameter (CPP), which is given by P = v/al, where 'v' and 'l' are the volume and the length of hydrophobic chain, respectively, and 'a' is the cross-section area of the polar head group of the surfactant [73]. Lower the value of P leads to higher interfacial flexibility and consequently, facilitates percolation as described in previous reports [58, 71]. For mixed AOT/Tween-85 systems, the $P_{eff}$ (effective packing parameter) can be calculated using the relationship proposed by Evans and Ninham [74];

$$P_{eff} = \frac{(\frac{xv}{al})_A + (\frac{xv}{al})_B}{x_A + x_B} \qquad (5.14)$$

Where, $x_A$ and $x_B$ are the mole fractions of AOT and Tween-85 present at the oil/water interface, respectively. The increase in content of Tween-85 ($X_{Tween\text{-}85}$) decreases the value of $P_{eff}$ and increases the droplet size and subsequently increases the solubilization capacity of AOT/oil(s) RMs which is in accordance with the results reported by Liu et al. [62]. These observations have also been supported by DLS measurement (see later) (Fig. 5.2C).

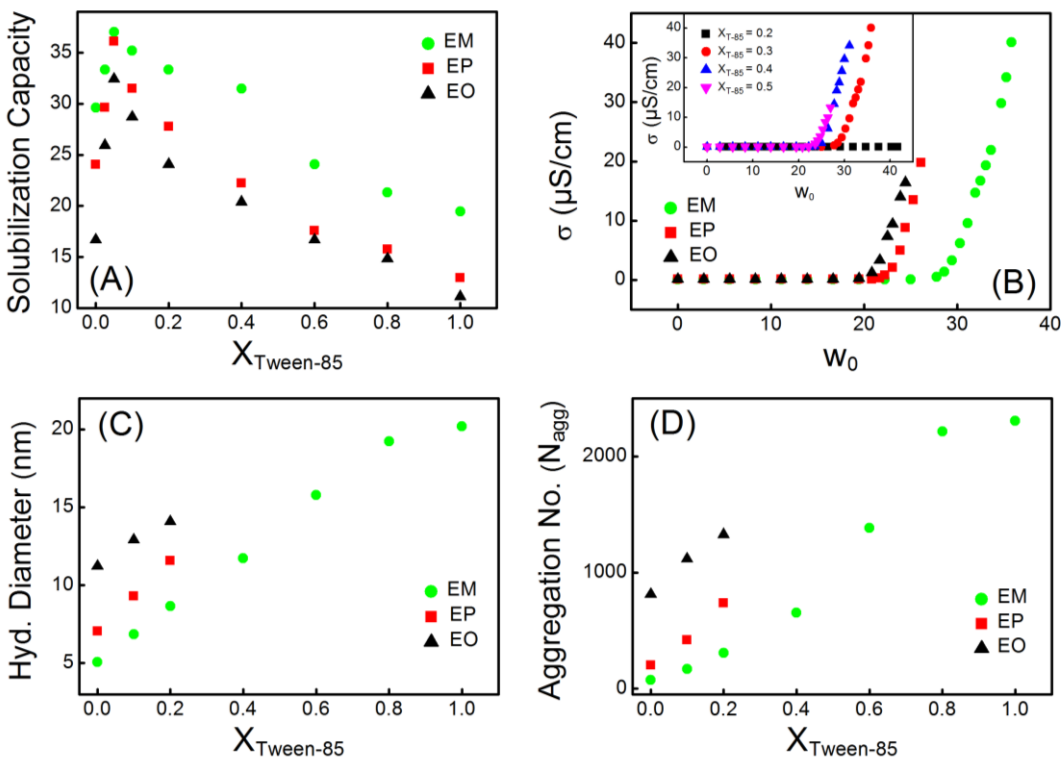


**Fig. 5.2. (A)** Solubilization capacity of mixed AOT/Tween-85/oil RMs as a function of $X_{Tween-85}$. **(B)** Variation of conductivity as a function of $w_0$ in three oils at $X_{Tween-85}$ = 0.3; the inset shows the variation of conductivity as a function of $w_0$with at a content of Tween-85 in the mixed system ($X_{Tween-85}$ = 0.2). **(C)** Hydrodynamic diameter ($D_h$) and **(D)** The aggregation number ($N_{agg}$) of mixed RMs at a fixed $w_0$ (= 10) as a function of $X_{Tween-85}$.

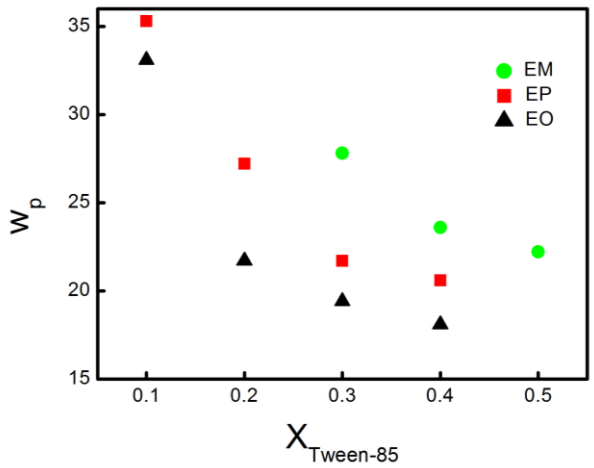


**Fig. 5.3.** Volume induced percolation threshold ($w_p$) in mixed RM of the three oils as a function of $X_{Tween-85}$ at fixed surfactant concentration of 0.1 mol $l^{-1}$.

We also study the effect of the oil type on the percolation phenomenon in these RMs at fixed compositions of $X_{Tween-85}$ = 0.2 and 0.3. It is observed (Fig. 5.2B and Fig. 5.3) that $w_p$

follows the order: EM < EP < EO, which is consistent with the order of molar volume or hydrocarbon chain length of oils and supports the model proposed by Leung and Shah for linear hydrocarbons [63]. It is also important to consider the variation in penetrating ability of these oils with the varying fatty acid chain length. All these factors play collective roles in tuning the interfacial flexibility, attractive interdroplet interaction as well as droplet dimensions and subsequently, $w_p$.

***DLS and Aggregation Number Measurements:*** Hydrodynamic diameter ($D_h$) of these RMs have been measured using DLS technique and the results are presented in Fig. 5.2C. The data analysis essentially assumes the droplets to be spherical in nature and for $w_0 = 10$, such an assumption holds reasonable. As observed from Fig. 5.2C, droplet size increases with increase in $X_{Tween\text{-}85}$. The result indicates that flexibility of the oil/water interface increases with increase in the droplet size, which in turn increases the inter-droplet interaction and facilitates the conductance percolation process (see Fig. 5.2B) [75]. Further, $D_h$ depends on the oil type and follows the order: EM < EP < EO at comparable composition for both AOT and mixed AOT/Tween-85 RMs, which expectedly shows a reverse order with $w_p$, corroborating the proposed mechanism of conductance percolation and microstructures of these systems.

We calculate the aggregation number ($N_{agg}$) of RM systems as a function of $X_{Tween\text{-}85}$ at a fixed $w_0 = 10$, by using the following expression [76];

$$\left(D_h/2\right) = \sqrt[3]{\frac{3N_{agg}}{4\pi}\left[V_{H_2O,total}/n_{surf.in\ RMs} + V_s\right]} \tag{5.15}$$

where, $V_{H_2O,total}$, $n_{surf.in\ RMs}$, and $V_s$ are the total volume of water, number of surfactant molecules in RMs and molecular volumes of surfactant(s), respectively. Molecular volume of AOT ($V_{AOT}$) was reported to be 0.611 $nm^3$ [77], whereas molecular volume of Tween-85 ($V_{Tween\text{-}85}$) has been calculated using following equation [16];

$$V_{Tween-85} = v_{CH_3} + 11v_{CH_2} + v_O + (n-1)v_{CH_2CH_2O} + v_{CH_2CH_2OH} \tag{5.16}$$

Where, n is the number of polyoxyethylene groups, $v_i$ indicates volume contribution for each group. Group molar volumes (i.e., $v_{CH_3}$, $v_{CH_2}$, $v_{CH_2CH_2O}$ and $v_{CH_2CH_2OH}$) used for the estimation of molecular volume of Tween-85 have been taken form Preu et al. [78]; Molecular volume of mixed surfactant systems ($V_s$) have been calculated using following equation;

$$V_s = X_{AOT}V_{AOT} + X_{Tween-85}V_{Tween-85} \tag{5.17}$$

Where, $X_{AOT}$ and $X_{Tween\text{-}85}$ are the mole fraction of AOT and Tween-85 in binary mixture. The model assumes RMs to be compact spheres and neglects the presence of solvent molecules between the surfactant hydrophobic tails [76]. A representative plot of $N_{agg}$ as a function of $X_{Tween\text{-}85}$ for these systems is depicted in Fig. 5.2D. It is found that Tween-85 RMs have higher aggregation number compared to the AOT RMs. It is also interesting to note that $N_{agg}$ increases as Tween-85 is mixed with AOT, which is a consequence of the reduced electrostatic repulsion between the charged head groups of AOT, thereby accommodating more surfactant molecules at the interface, which also corroborates the observed increase in the $D_h$ (Fig. 5.2C). The $N_{agg}$ obtained for fatty acid ester stabilized mixed RMs at different mixing compositions is in good agreement with previous report [79], however higher than hydrocarbon oil stabilized mixed RMs [70].

***FTIR Measurements:*** For comprehensive understanding of the water structure inside the mixed RMs we measure the MIR (mid-infrared) FTIR spectra of these systems. In all these measurements we subtract the data of $w_0 = 0$ (dry RM) solutions from the corresponding hydrated solutions, and thus, the signals essentially provide information of the water molecules embodied in the RM water pool only. According to the 'three states' model, water is present in 'layers' of different structures within RM confinement. The 'bulk-like' water molecules are fully hydrogen bonded with the neighboring water molecules and have physical properties in close resemblance with those in bulk water, producing an O-H stretching peak at ~ 3280 $cm^{-1}$. The surfactant head group bound water molecules are termed as 'bound' water peaking at ~ 3460 $cm^{-1}$. Other than these two types, a third type, 'trapped' water molecules (peaking at ~ 3570 $cm^{-1}$), resides within the hydrophobic tails of surfactants [80-82]. In view of this, we have deconvoluted the MIR spectra of these RM systems into three Gaussian sub-bands. For a quantitative estimation of their relative abundance, the fraction of each species has been determined from the area of each Gaussian curve with respect to the total area [70]. This relative contribution is proportional to the fraction of water molecules belonging to that particular stretching mode. As evidenced from the figure the relative abundance of the fully hydrogen bonded water molecules are fewer in RMs compared to that in pure water; this observation is rather intuitive taking into consideration the interaction of water molecules with RM interfaces [82, 83]. For the AOT/EM or EP or EO RMs, the fraction of bound water molecules is higher than that of the bulk-like water molecules (Fig. 5.4). Further, it is observed that the relative abundance of the "bound" water molecules decreases at the expense of an increase in the content of "bulk-type" water molecules as the content of the nonionic surfactant,

Tween-85 ($X_{Tween-85}$) increases in the RMs (Fig. 5.4). This leads to conclude that the interaction of water molecules with the polar uncharged head group (POE chains) of Tween-85 is weaker than that with ionic AOT, which is in accordance with previous report [70]. The population corresponding to the "trapped" water (peaking at ~3570 $cm^{-1}$) shows a marginal variation with $X_{Tween-85}$ (Fig. 5.4), however, an overall increasing trend is observed. The "bulk-type" and the "trapped" water molecules follow the trend, EM < EP < EO, whereas, a reverse order is found for the "bound" water molecules (Figs. 5.4A-C). The distinct variation in "trapped" water molecules with the oil type might be due to the different degree of penetration of the oils into the surfactant aggregate, which affects intermolecular spacing as well as the arrangement of surfactant molecules at the interface. Similar effect was reported earlier for R-(+)-limonene (LIM) and isobutyl benzene (IBB) derived MEs stabilized by anionic surfactant [84]. Due to the shorter fatty acid chain length of EM, it can penetrate easily into the interface

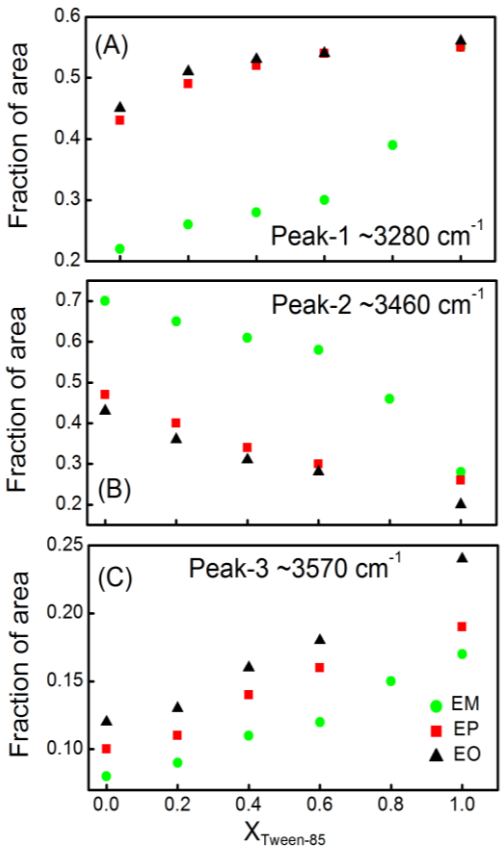


**Fig. 5.4.** Relative area under curves peaking at ~3280 $cm^{-1}$ (A), ~3460 $cm^{-1}$ (B), and ~3570 $cm^{-1}$ (C) for AOT/Tween-85/EM or EP or EO mixed RMs at a fixed $w_0$ = 10 as a function of $X_{Tween-85}$.

and as a consequence, push the water molecules out of the extreme hydrophobic environments [85]. The observed sequence can be explained in the light of a competition between the polar ester moiety of these oils and the trapped water molecules for the surfactant palisade layer.

***Steady-State Fluorescence Measurements:*** Steady-state emission profile of DCM in different RMs has been monitored as a function of $X_{Tween\text{-}85}$ for particular oil and also at a fixed $X_{Tween\text{-}85}$ in various oils (Fig. 5.5) and the corresponding emission peaks ($\lambda_{max}$) are presented in Table 5.5. The emission peaks in RMs get significantly red-shifted (560-580 nm) compared to DCM in the oils ($\lambda_{max}$ ~ 550 nm) (Table 5.5). We deconvoluted the observed spectra into two Gaussian components with one peak fixed to 550 nm and found that the other peak at 580 nm contributes ten times larger than the 550 nm contribution, strongly suggesting the presence of a considerable fraction of DCM molecules at the surfactant-water interface of the RM where the microenvironment is more polar than the oil itself [40, 43].

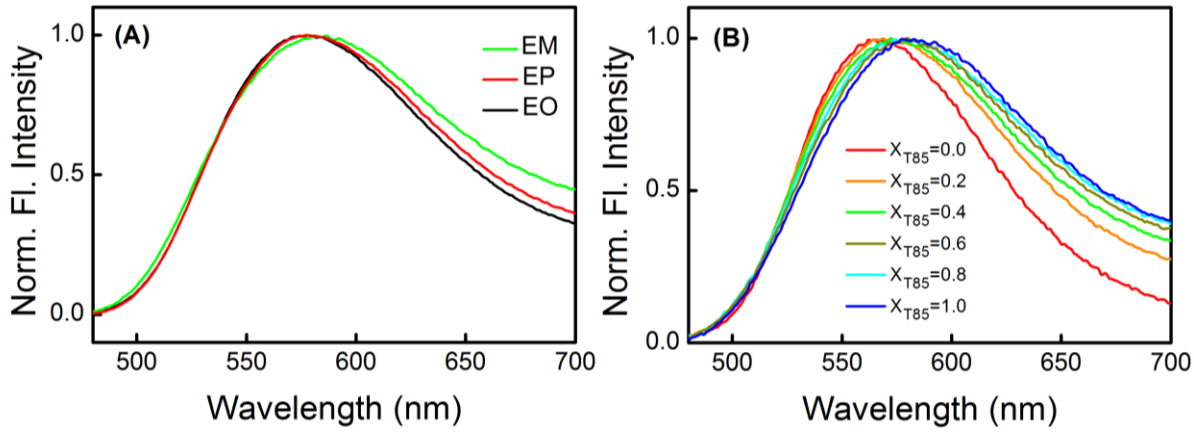


**Fig. 5.5(A)** Normalized Emission spectra of AOT/Tween-85/EM or EP or EO mixed RMs at a fixed composition ($w_0$ = 5 and $X_{Tween\text{-}85}$ = 0.6). **(B)** Normalized Emission spectra of DCM in AOT/Tween-85/EM mixed reverse micellar systems at a fixed $w_0$ = 5 as a function of $X_{Tween\text{-}85}$.

***Time-resolved Emission Spectral Studies:*** We study sub-ns resolved solvation dynamics of DCM in the RM systems and investigate the effect of confinement on water relaxation dynamics with the change in the composition of the surfactant mixture ratio as well as oil. Fig. 5.6A (inset) shows the decay transients of DCM at three selected wavelengths of 520 (at the blue end of the spectrum), 580 (around the peak position), and 670 (at the red end of the spectrum) nm in AOT/Tween-85/EM mixed RMs at $w_0$ = 5 and at $X_{Tween\text{-}85}$ = 0.6. It is evidenced from the figure that all decay patterns are strongly wavelength dependent. At 520 nm the transient is fast with decay components of 140 ps (44%), 580 ps (53%) and 2600 ps (3%). At the extreme red end (670 nm) a decay component of 3440 ps along with a rise component of 600 ps are obtained. Using the decay transients at different wavelengths we construct the TRES for different $X_{Tween\text{-}85}$ values in these oils. A representative TRES of DCM in AOT/Tween-85/EM mixed RMs at a fixed $w_0$ = 5 and at fixed $X_{Tween\text{-}85}$ = 0.6 is presented in

Fig. 5.6A, wherein a significant dynamic fluorescence Stokes shift is observed (Table 5.5). We construct the solvent correlation function, C(t), following equation (chapter 2). Some representative C(t) plots for different $X_{Tween\text{-}85}$ values at $w_0$ = 5 are shown in Fig. 5.7A. All the C(t) curves are fitted bi-exponentially and the time constants are presented in Table 5.5. For all the systems two distinct time-scales are obtained, one in the order of hundreds of ps and the other is of the order of several ns. It is important to check whether the observed time resolved spectral shift is associated with any internal photo-physics of the probe itself. In order to do so we construct the corresponding time-resolved area normalized emission spectra (TRANES) [86], a representative diagram is shown in Fig. 5.6B. No apparent iso-emissive point is recognized in the TRANES profile, which confirms that the probe contains only a single 'species'. Therefore, the observed time dependent spectral shift can be attributed solely to the inhomogeneity of the microenvironment experienced by the probe. It is also important to note here that the sub-picosecond rotational dynamics of pure water is considerably restrained in confined environments of RMs [87]. The limitation of instrumental resolution (IRF ~ 80 ps) refrained us from detecting the signals responsible for the ultrafast dynamics of water molecules. Thus the obtained slow timescales have the only contribution of water molecules residing at the RM interface, which is in fact the essence of our study.

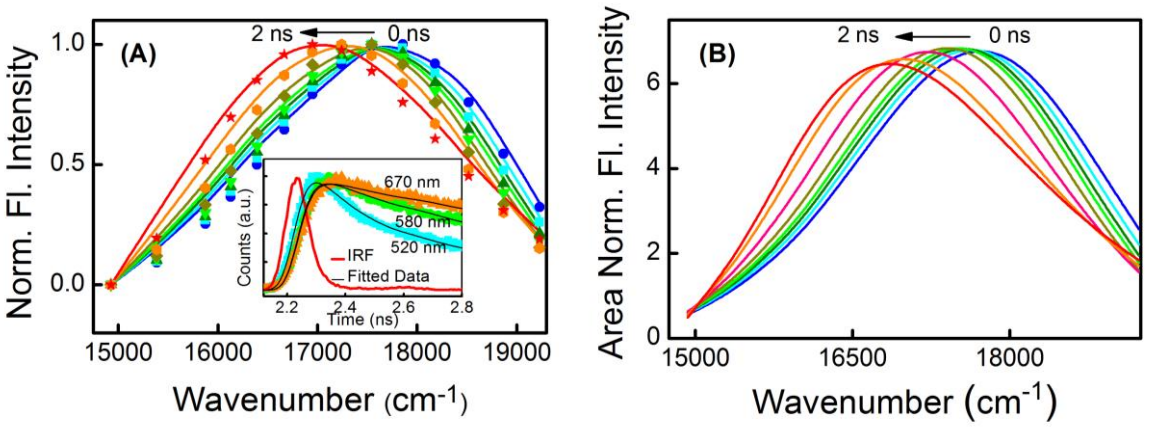


**Fig. 5.6(A)** Time resolved emission spectra (TRES) and fluorescence decay transients (inset) of DCM in AOT/Tween-85/EM mixed RM at a fixed composition ($w_0$ = 5 and $X_{Tween\text{-}85}$ = 0.6). **(B)** Area normalized time resolved emission spectra (TRANES) of DCM in AOT/Tween-85/EM mixed RM at a fixed composition ($w_0$ = 5 and $X_{Tween\text{-}85}$ = 0.6).

We plot the average time constant, $< \tau_{solv} > = \sum_i a_i \tau_i$ as a function of $X_{Tween\text{-}85}$ at $w_0$ = 5 for three different oils (Fig. 5.7B) and it is observed that the average solvation time decreases with increase in $X_{Tween\text{-}85}$. Water present in the vicinity of the surfactant head group, i.e., at the interfacial regions, experiences restricted environment compared to the water in the

core of the RMs, which results in the relative slow solvation. The water molecules present in the RM core contribute to the faster component of hundreds of ps [70]. Solvation dynamics gets faster as $X_{Tween-85}$ increases. It can be noted that the $\lambda_{max}$ value for DCM in Tween-85/oil RM is red-shifted

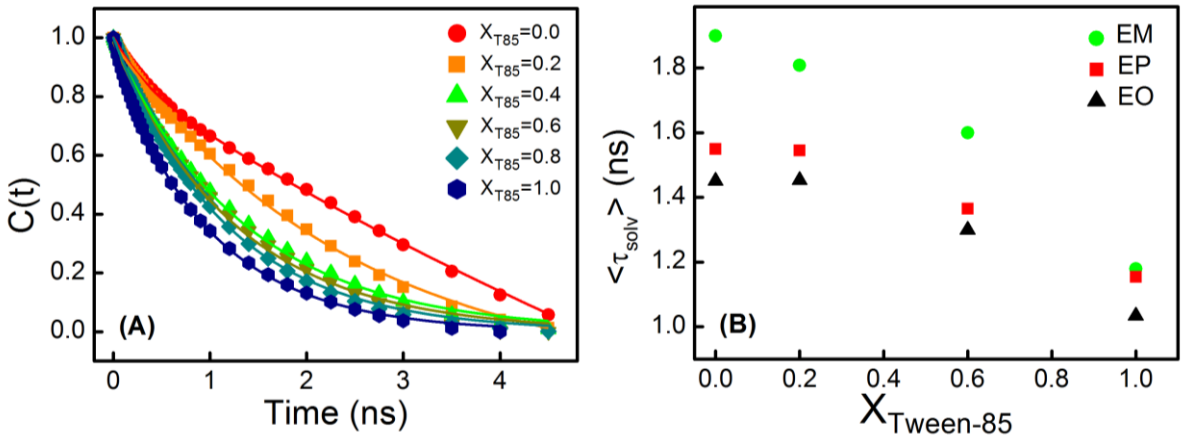


**Fig. 5.7(A)** Solvent correlation function, C(t) in AOT/Tween-85/EM mixed reverse micellar systems at a fixed $w_0 = 5$ as a function of $X_{Tween-85}$. **(B)** Average solvation time constant of DCM in AOT/Tween-85/EM or EP or EO mixed reverse micellar systems at a fixed $w_0 = 5$ and as a function of $X_{Tween-85}$.

compared to that of AOT/oil RM (Table 5.5), suggesting the location of the probe to be shifted toward the bulk water with the increase in $X_{Tween-85}$, and this difference in location is manifested with significantly higher contribution of bulk water with the observed overall faster dynamics [88]. From FTIR and DLS study it is evident that with the increase in $X_{Tween-85}$ the size of RM as well as the relative abundance of 'bulk-type' water content increases which supports the accelerated $\langle \tau_{solv} \rangle$ values at higher Tween-85 content. Further, Fig. 5.7B shows that the average solvation time at a particular $X_{Tween-85}$ follows the order, EM > EP > EO. The faster solvation of EO stabilized systems compared to EP and EM is very similar to the trend of their droplet size (vide. Fig. 5.2C). The larger droplet size of EO stabilized systems leads to the increase in the free motion of ions in the core of RMs, and subsequently, faster solvation time.

From the steady-state and time-resolved fluorescence decay measurements we have obtained an information about the location of the probe molecules. However, for better understanding time-resolved fluorescence anisotropy measurements of DCM in these reverse micellar systems are performed using picoseconds TCSPC set up. It provides important information about the rotational motion of the chromophore in this confined medium.

**Table 5.5.** Solvation dynamics parameter of DCM probe in mixed AOT/Tween-85 reverse micellar systems in different oils with varying content of Tween-85 in the mixed system ($X_{Tween-85}$) at $w_0$ =5 at 303K.

| Composition | $\lambda_{max}$/nm | $\tau_1$/ns ($a_1$) | $\tau_2$/ns ($a_2$) | $<\tau_{sol}>$/ns |
|---|---|---|---|---|
| | | **EM Oil** | | |
| $X_{T85}$ = 0.0 | 563 | 0.67 (0.45) | 2.89 (0.55) | 1.89 |
| $X_{T85}$ = 0.2 | 570 | 0.65 (0.37) | 2.49 (0.63) | 1.81 |
| $X_{T85}$ = 0.6 | 577 | 0.41 (0.22) | 1.94 (0.78) | 1.60 |
| $X_{T85}$ = 1.0 | 586 | 0.22 (0.15) | 1.35 (0.85) | 1.18 |
| | | **EP Oil** | | |
| $X_{T85}$ = 0.0 | 562 | 0.88 (0.46) | 2.12 (0.54) | 1.55 |
| $X_{T85}$ = 0.2 | 568 | 0.76 (0.33) | 1.93 (0.67) | 1.54 |
| $X_{T85}$ = 0.6 | 575 | 0.37 (0.21) | 1.62 (0.79) | 1.36 |
| $X_{T85}$ = 1.0 | 582 | 0.17 (0.11) | 1.27 (0.89) | 1.15 |
| | | **EO Oil** | | |
| $X_{T85}$ = 0.0 | 560 | 0.91 (0.44) | 1.88 (0.56) | 1.45 |
| $X_{T85}$ = 0.2 | 567 | 0.89 (0.26) | 1.65 (0.74) | 1.45 |
| $X_{T85}$ = 0.6 | 572 | 0.32 (0.19) | 1.53 (0.81) | 1.30 |
| $X_{T85}$ = 1.0 | 580 | 0.15 (0.07) | 1.10 (0.93) | 1.03 |

***Time-resolved Anisotropy Studies:*** In order to understand the nature of geometrical restriction imposed on the probe molecule by the interfacial layer, we determine the rotational anisotropy decay transients which can be fitted multi-exponentially and the time constants ($\tau_r$) are presented in Table 5.4, Supplementary material. Representative anisotropy decay is shown in Fig. 5.8A. The average rotational time constant, $< \tau_{rot} > = \sum_i a_i \tau_{r_i}$ follows somewhat increasing trend as a function of $X_{Tween-85}$ at $w_0$ = 5 for those three different oil systems (Fig. 5.8B) using fluorophore DCM. The anisotropy decays in RMs are found to be tri-exponential in nature. This suggests that within the AOT/Tween-85 containing RMs, DCM probes are distributed in three broadly different regions: a very fast region near the bulk EM or EP or EO of rotational relaxation time around 0.06 ns, a fast region near head group of surfactants of rotational relaxation time ~0.60 ns, and a slow region of rotational relaxation time ~10 ns at the water pool, which is comparable to earlier report [89]. At $w_0$ = 5, the rotation of a considerable fraction of water molecules in the RM interface exhibits more restricted dynamics as evidenced from high $<\tau_{solv}>$ values. The increased $< \tau_r >$ with increasing $X_{Tween-85}$

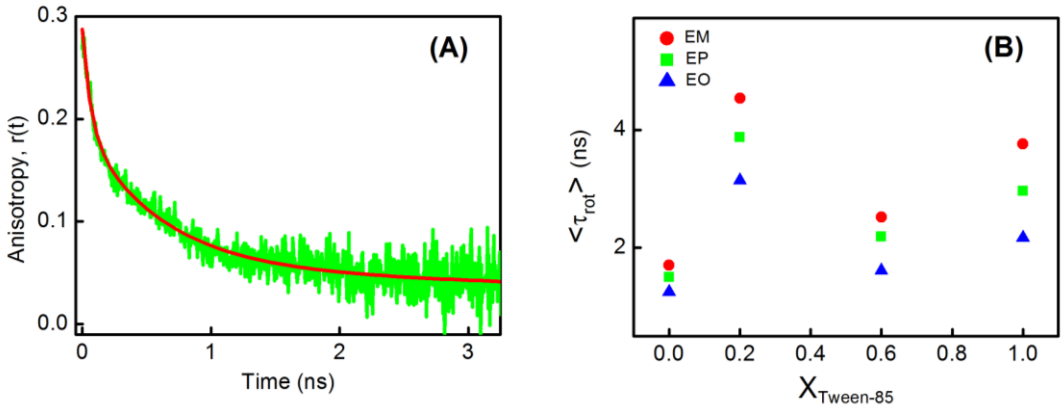


**Fig. 5.8 (A)** Representative rotational anisotropy decay of DCM in AOT/Tween-85/EM mixed reverse micellar systems at a fixed $w_0$ = 5 and at fixed $X_{Tween-85}$ = 0.6 systems. The solid lines are bi-exponential fittings. **(B)** Average rotational time constant of DCM in AOT/Tween-85/EM or EP or EO mixed reverse micellar systems at a fixed $w_0$ = 5 and as a function of $X_{Tween-85}$.

indicates progressive impose of restriction on the rotational motion of the probe as observed from previous study [69]. The imposed restriction in the Tween-85 might arise out of the strong interaction of the probe with the long POE chain of surfactant. It can also be observed from

**Table 5.6.** Anisotropy parameter of DCM probe in mixed AOT/Tween-85 RMs in different oils with varying content of Tween-85 in the mixed system ($X_{Tween-85}$) at $w_0$ =5 at 303K.

| Composition | $\tau_{r1}$ ($a_1$)ns | $\tau_{r2}$ ($a_2$)ns | $\tau_{r3}$ ($a_3$) ns | $<\tau_{rot}>$ns |
|---|---|---|---|---|
| | | **EM Oil** | | |
| $X_{T85}$ = 0.0 | 0.060(0.34) | 0.49(0.24) | 3.69(0.42) | 1.70 |
| $X_{T85}$ = 0.2 | 0.061(0.34) | 0.65 (0.33) | 13.72(0.33) | 4.53 |
| $X_{T85}$ = 0.6 | 0.065(0.33) | 0.61(0.47) | 11.70(0.18) | 2.52 |
| $X_{T85}$ = 1.0 | 0.058(0.40) | 0.72(0.32) | 12.34(0.28) | 3.76 |
| | | **EP Oil** | | |
| $X_{T85}$ = 0.0 | 0.058(0.35) | 0.29(0.18) | 3.09(0.46) | 1.50 |
| $X_{T85}$ = 0.2 | 0.061(0.36) | 0.52(0.30) | 10.90(0.34) | 3.88 |
| $X_{T85}$ = 0.6 | 0.050(0.34) | 0.41(0.28) | 5.42(0.38) | 2.18 |
| $X_{T85}$ = 1.0 | 0.056(0.35) | 0.41(0.17) | 5.97(0.48) | 2.96 |
| | | **EO Oil** | | |
| $X_{T85}$ = 0.0 | 0.056(0.35) | 0.52(0.28) | 2.94(0.37) | 1.25 |
| $X_{T85}$ = 0.2 | 0.055(0.41) | 0.49 (0.34) | 11.63(0.25) | 3.14 |
| $X_{T85}$ = 0.6 | 0.048(0.38) | 0.44(0.25) | 4.06(0.37) | 1.61 |
| $X_{T85}$ = 1.0 | 0.055(0.39) | 0.54(0.18) | 4.81(0.43) | 2.17 |

Fig. 5.7B and Table 5.6 that the rotation of the probe is eased for EO based RMs, whereas the restriction is more prominent in the EM based systems, and follows the order, EO < EP < EM. It was reported earlier that the probe DCM is highly soluble in fatty acid ester type oils (such as, IPM) [43].

So, we expect that the change in chemical architecture of these type of oils (herein, EM, EP and EO) should affect the oil/water interface. Subsequently, probe will experience the changed microenvironment in presence of these oils. The obliged restriction of DCM in EM based RMs might occur due to higher penetration of EM into the oil/water interface compared to EP and EO and as a result impose rigidity to the surfactant charged interface.

## 5.3 Conclusion

Progressive addition of Tween-85 in aqueous AOT solution favors early micellization due to preferential adsorption of the polyoxyethylene (POE) chains of Tween-85 with simultaneous increase in the hydrophobic interactions between the surfactant tails of both surfactants. Mixed compositions reveal non-ideal solution behavior and synergistic interaction between the constituent surfactants, which is supported by the negative values of interaction parameter $\beta^m$. Both micellization as well as adsorption processes show increasing trend of spontaneous micelle formation with gradual incorporation of Tween-85 in AOT micelle. Incorporation of Tween-85 in AOT micellar system produces a relatively better synergistic interaction compared to earlier reports based on mixed AOT-nonionic systems in terms of interaction parameter [28, 29].

All the RM systems exhibit a considerable synergism in the water solubilization capacity upon the addition of Tween-85 in AOT RMs and are influenced by characteristic features of the oils. The droplet size of these systems increases with the increasing content of Tween-85 ($X_{Tween\text{-}85}$) and follows the trend; EM < EP < EO, which is well corroborated with the measurement of transport property and aggregation numbers. FTIR measurement concludes that the relative abundance of the "bound" water molecules decreases at the expense of an increase in the content of "bulk-type" water molecules as $X_{Tween\text{-}85}$ increases. The differences in behavior of these oils towards the relative population of water molecules at the interfacial region (*i.e.*, trapped water) in these systems justify the different degrees of oil penetration into the surfactant aggregate. Micropolarity of the microenvironment of RMs is probed by the solvatochromic dye DCM and shows more polar environment in EM-derived RMs compared to the other two oils. Incorporation of Tween-85 in AOT RMs produces more flexible interface as the solvation dynamics of DCM becomes faster with increasing $X_{Tween\text{-}85}$. Further, the faster average solvation time for EO-based system compared to EP and EM-based systems may be due to the larger droplet sizes of the former RMs. Restriction on the rotational motion of DCM increases with increasing $X_{Tween\text{-}85}$ as revealed from time-resolved anisotropy study. Also, the

obliged restriction of DCM in EM based RMs occurs due to higher penetration of EM into the oil/water interface compared to EP and EO and consequently, imposes rigidity to the surfactant charged interface.

The present study investigates the performance of biocompatible Tween-85 in AOT based self-organized assemblies either in aqueous or in non-toxic ethyl esters of fatty acid medium. The preferential adsorption of Tween molecules in the AOT monolayer, as evidenced from the micellization study, makes the RM droplet to accommodate more water (as evident from the DLS study) which eventually increase the abundance of bulk-type water in the RMs (FTIR study) and also, manifested in the accelerated solvation dynamics (time resolved fluorescence study). The physical properties of water entrapped in mixed RMs can thus be tuned by varying the mixing stoichiometry, the inherent mechanism being rooted in the inter-surfactant interactions. This synergistic interaction of binary mixtures would pave new ways for exploration in application arena of surface science. The results obtained from this study are important for designing an effective ME system to encapsulate and stabilize bioactive components for incorporation into food, beverage, and pharmaceutical products [90].

## 5.4 References

[1] D.J. Mitchell, B.W. Ninham, Micelles, vesicles and microemulsions, Journal of the Chemical Society, Faraday Transactions 2: Molecular and Chemical Physics, 77 (1981) 601-629.
[2] M.J. Lawrence, Surfactant systems: microemulsions and vesicles as vehicles for drug delivery, European journal of drug metabolism and pharmacokinetics, 19 (1994) 257-269.
[3] J.H. Fendler, Microemulsions, micelles, and vesicles as media for membrane mimetic photochemistry, The Journal of Physical Chemistry, 84 (1980) 1485-1491.
[4] T. Goloub, R. Pugh, B. Zhmud, Micellar interactions in nonionic/ionic mixed surfactant systems, Journal of colloid and interface science, 229 (2000) 72-81.
[5] P.M. Holland, D.N. Rubingh, Mixed surfactant systems-an overview, ACS Symposium Series, Amer Chemical Soc 1155 16Th ST, NW, Washington, DC 20036 USA, 1992, pp. 2-30.
[6] X.Y. Hua, M.J. Rosen, Synergism in binary mixtures of surfactants: I. Theoretical analysis, Journal of Colloid and Interface Science, 90 (1982) 212-219.
[7] A.B.E. Attia, Z.Y. Ong, J.L. Hedrick, P.P. Lee, P.L.R. Ee, P.T. Hammond, Y.-Y. Yang, Mixed micelles self-assembled from block copolymers for drug delivery, Current Opinion in Colloid & Interface Science, 16 (2011) 182-194.
[8] C. Rupp, H. Steckel, B.W. Müller, Solubilization of poorly water-soluble drugs by mixed micelles based on hydrogenated phosphatidylcholine, International journal of pharmaceutics, 395 (2010) 272-280.
[9] Y. Mrestani, L. Behbood, A. Härtl, R.H. Neubert, Microemulsion and mixed micelle for oral administration as new drug formulations for highly hydrophilic drugs, European Journal of Pharmaceutics and Biopharmaceutics, 74 (2010) 219-222.
[10] S. Moulik, B. Paul, Structure, dynamics and transport properties of microemulsions, Advances in Colloid and Interface science, 78 (1998) 99-195.

[11] A. Kitahara, Solubilization and catalysis in reversed micelles, Advances in Colloid and Interface Science, 12 (1980) 109-140.
[12] A. Bumajdad, J. Eastoe, S. Nave, D.C. Steytler, R.K. Heenan, I. Grillo, Compositions of mixed surfactant layers in microemulsions determined by small-angle neutron scattering, Langmuir, 19 (2003) 2560-2567.
[13] Q. Li, T. Li, J. Wu, Comparative study on the structure of reverse micelles. 2. FT-IR, 1H NMR, and electrical conductance of H2O/AOT/NaDEHP/n-heptane systems, The Journal of Physical Chemistry B, 104 (2000) 9011-9016.
[14] S. Chatterjee, S. Nandi, S.C. Bhattacharya, Interface of AOT/Igepal CO720/cyclohexane/water mixed reverse micelle by spectroscopic approach, Colloids and Surfaces A: Physicochemical and Engineering Aspects, 279 (2006) 58-63.
[15] A. Shome, S. Roy, P.K. Das, Nonionic surfactants: a key to enhance the enzyme activity at cationic reverse micellar interface, Langmuir, 23 (2007) 4130-4136.
[16] M. Andersson, J.S. Pedersen, A.E. Palmqvist, Silver nanoparticle formation in microemulsions acting both as template and reducing agent, Langmuir, 21 (2005) 11387-11396.
[17] K. Maiti, I. Chakraborty, S.C. Bhattacharya, A.K. Panda, S.P. Moulik, Physicochemical studies of octadecyltrimethylammonium bromide: a critical assessment of its solution behavior with reference to formation of micelle, and microemulsion with n-butanol and n-heptane, The Journal of Physical Chemistry B, 111 (2007) 14175-14185.
[18] S. Das, I. Mukherjee, B.K. Paul, S. Ghosh, Physicochemical behaviors of cationic gemini surfactant (14-4-14) based microheterogeneous assemblies, Langmuir, 30 (2014) 12483-12493.
[19] J.H. Mondal, S. Ahmed, D. Das, Physicochemical Analysis of Mixed Micelles of a Viologen Surfactant: Extended to Water-in-Oil (w/o) Microemulsion and Cucurbit [8] uril-Assisted Vesicle Formation, Langmuir, 30 (2014) 8290-8299.
[20] F.D. Souza, B.S. Souza, D.W. Tondo, E.C. Leopoldino, H.D. Fiedler, F. Nome, Imidazolium-based zwitterionic surfactants: characterization of normal and reverse micelles and stabilization of nanoparticles, Langmuir, 31 (2015) 3587-3595.
[21] J. Bhattacharjee, G. Verma, V. Aswal, V. Patravale, P. Hassan, Microstructure, drug binding and cytotoxicity of pluronic P123–aerosol OT mixed micelles, RSC Advances, 3 (2013) 23080-23089.
[22] R.R. Gupta, S.K. Jain, M. Varshney, AOT water-in-oil microemulsions as a penetration enhancer in transdermal drug delivery of 5-fluorouracil, Colloids and Surfaces B: Biointerfaces, 41 (2005) 25-32.
[23] H. Liu, S. Li, Y. Wang, F. Han, Y. Dong, Bicontinuous water-AOT/Tween85-isopropyl myristate microemulsion: A new vehicle for transdermal delivery of cyclosporin A, Drug development and industrial pharmacy, 32 (2006) 549-557.
[24] M.D. Chavanpatil, A. Khdair, J. Panyam, Surfactant-polymer nanoparticles: a novel platform for sustained and enhanced cellular delivery of water-soluble molecules, Pharmaceutical research, 24 (2007) 803-810.
[25] R. Engel, S. Riggi, Intestinal absorption of heparin facilitated by sulfated or sulfonated surfactants, Journal of pharmaceutical sciences, 58 (1969) 706-710.
[26] A.S. Narang, D. Delmarre, D. Gao, Stable drug encapsulation in micelles and microemulsions, International journal of Pharmaceutics, 345 (2007) 9-25.
[27] R. Dong, J. Hao, Complex fluids of poly (oxyethylene) monoalkyl ether nonionic surfactants, Chemical reviews, 110 (2010) 4978-5022.
[28] R. Sharma, A. Shaheen, R.K. Mahajan, Cyclic voltammetry and viscosity measurements of aggregated assemblies of anionic surfactants with nonionic surfactants and triblock copolymers, Colloid and Polymer Science, 289 (2011) 43-51.
[29] R.K. Mahajan, D. Nandni, Micellization and phase behavior of binary mixtures of anionic and nonionic surfactants in aqueous media, Industrial & Engineering Chemistry Research, 51 (2012) 3338-3349.
[30] A. Hemavathi, H.U. Hebbar, K. Raghavarao, Mixed reverse micellar systems for extraction and purification of β-glucosidase, Separation and Purification Technology, 71 (2010) 263-268.

[31] C.F. Komives, D.E. Osborne, A.J. Russell, Characterization of a nonionic surfactant reversed micellar system for enzyme catalysis, The Journal of Physical Chemistry, 98 (1994) 369-376.
[32] Y. Hayashi, M.M.R. Talukder, J. Wu, T. Takeyama, T. Kawanishi, N. Simizu, Increased activity of Chromobacterium viscosum lipase in AOT reverse micelles in the presence of short chain methoxypolyethylene glycol, Journal of Chemical Technology and Biotechnology, 76 (2001) 844-850.
[33] Y. Yamada, R. Kuboi, I. Komasawa, Extraction of enzymes and their activities in AOT reverse micellar systems modified with nonionic surfactants, Journal of chemical engineering of Japan, 27 (1994) 404-409.
[34] P. Boonme, K. Krauel, A. Graf, T. Rades, V.B. Junyaprasert, Characterization of microemulsion structures in the pseudoternary phase diagram of isopropyl palmitate/water/Brij 97: 1-butanol, Aaps Pharmscitech, 7 (2006) E99-E104.
[35] J.F. Ontiveros, C. Pierlot, M. Catté, V. Molinier, A. Pizzino, J.-L. Salager, J.-M. Aubry, Classification of ester oils according to their Equivalent alkane carbon number (EACN) and asymmetry of fish diagrams of C 10 E 4/ester oil/water systems, Journal of colloid and interface science, 403 (2013) 67-76.
[36] X. Yanyu, L. Fang, P. Qineng, C. Hao, The influence of the structure and the composition of water/AOT-Tween 85/IPM microemulsion system on transdermal delivery of 5-fluorouracil, Drug development and industrial pharmacy, 38 (2012) 1521-1529.
[37] S.C. Chuo, S.H. Mohd-Setapar, S.N. Mohamad-Aziz, V.M. Starov, A new method of extraction of amoxicillin using mixed reverse micelles, Colloids and Surfaces A: Physicochemical and Engineering Aspects, 460 (2014) 137-144.
[38] H. Liu, Y. Wang, Y. Lang, H. Yao, Y. Dong, S. Li, Bicontinuous Cyclosporin a loaded Water-AOT/Tween 85-isopropylmyristate microemulsion: Structural characterization and dermal pharmacokinetics in vivo, Journal of pharmaceutical sciences, 98 (2009) 1167-1176.
[39] M. Meyer, J. Mialocq, Ground state and singlet excited state of laser dye DCM: Dipole moments and solvent induced spectral shifts, Optics communications, 64 (1987) 264-268.
[40] S.K. Pal, D. Mandal, D. Sukul, K. Bhattacharyya, Solvation dynamics of 4-(dicyanomethylene)-2-methyl-6-(p-dimethylaminostyryl)-4H-pyran (DCM) in a microemulsion, Chemical physics letters, 312 (1999) 178-184.
[41] C.A. Munson, G.A. Baker, S.N. Baker, F.V. Bright, Effects of subzero temperatures on fluorescent probes sequestered within aerosol-OT reverse micelles, Langmuir, 20 (2004) 1551-1557.
[42] R. Saha, P.K. Verma, R.K. Mitra, S.K. Pal, Structural and dynamical characterization of unilamellar AOT vesicles in aqueous solutions and their efficacy as potential drug delivery vehicle, Colloids and Surfaces B: Biointerfaces, 88 (2011) 345-353.
[43] R. Saha, S. Rakshit, R.K. Mitra, S.K. Pal, Microstructure, morphology, and ultrafast dynamics of a novel edible microemulsion, Langmuir, 28 (2012) 8309-8317.
[44] R.K. Mahajan, R. Sharma, Analysis of interfacial and micellar behavior of sodium dioctyl sulphosuccinate salt (AOT) with zwitterionic surfactants in aqueous media, Journal of colloid and interface science, 363 (2011) 275-283.
[45] A. Chakraborty, S.K. Saha, S. Chakraborty, Effect of size of tetraalkylammonium counterions on the temperature dependent micellization of AOT in aqueous medium, Colloid and Polymer Science, 286 (2008) 927-934.
[46] I. Capek, S. Janíčková, P. Capek, J. Kováčik, P. Koštial, Interaction studies of nonionic emulsifiers and carboxymethylstarch and polymerization of vinyl acetate, Chemical Papers, 59 (2005) 48-54.
[47] J.H. Clint, Micellization of mixed nonionic surface active agents, Journal of the Chemical Society, Faraday Transactions 1: Physical Chemistry in Condensed Phases, 71 (1975) 1327-1334.
[48] D.N. Rubingh, Mixed micelle solutions, Solution chemistry of surfactants, Springer1979, pp. 337-354.
[49] G.B. Ray, I. Chakraborty, S. Ghosh, S. Moulik, R. Palepu, Self-aggregation of alkyltrimethylammonium bromides (C10-, C12-, C14-, and C16TAB) and their binary mixtures in

aqueous medium: a critical and comprehensive assessment of interfacial behavior and bulk properties with reference to two types of micelle formation, Langmuir, 21 (2005) 10958-10967.
[50] Q. Zhou, M.J. Rosen, Molecular interactions of surfactants in mixed monolayers at the air/aqueous solution interface and in mixed micelles in aqueous media: the regular solution approach, Langmuir, 19 (2003) 4555-4562.
[51] R. Wang, Y. Li, Micellar and Interfacial Behavior in Mixtures of Dodecyldiethoxylamine Oxide with Ionic Surfactants, Journal of Chemical & Engineering Data, 58 (2013) 2240-2247.
[52] K. Manna, C.-H. Chang, A.K. Panda, Physicochemical studies on the catanionics of alkyltrimethylammonium bromides and bile salts in aqueous media, Colloids and Surfaces A: Physicochemical and Engineering Aspects, 415 (2012) 10-21.
[53] D.A.S. J.F. Scamehorn, J.H. Harwell,, Encyclopedia of Surface and Colloid Science, Marcel Dekker, New York,, DOI (2004) pp. 1458–1469.
[54] J.M. Rosen, Surfactants and Interfacial Phenomena, Wiley-Interscience, New York, DOI (2004).
[55] W.H. Ansari, N. Fatma, M. Panda, Solubilization of polycyclic aromatic hydrocarbons by novel biodegradable cationic gemini surfactant ethane-1, 2-diyl bis (N, N-dimethyl-N-hexadecylammoniumacetoxy) dichloride and its binary mixtures with conventional surfactants, Soft Matter, 9 (2013) 1478-1487.
[56] K.-u. Din, M.S. Sheikh, A.A. Dar, Analysis of mixed micellar and interfacial behavior of cationic gemini hexanediyl-1, 6-bis (dimethylcetylammonium bromide) with conventional ionic and nonionic surfactants in aqueous medium, The Journal of Physical Chemistry B, 114 (2010) 6023-6032.
[57] R.K. Mahajan, S. Mahajan, A. Bhadani, S. Singh, Physicochemical studies of pyridinium gemini surfactants with promethazine hydrochloride in aqueous solution, Physical Chemistry Chemical Physics, 14 (2012) 887-898.
[58] S. Wang, T. Yin, W. Shen, Comparative investigations on mixing behaviors of cationic gemini surfactant with surface active ionic liquid in water and in ethylammonium nitrate, Industrial & Engineering Chemistry Research, 53 (2014) 18202-18208.
[59] M.J. Rosen, A.W. Cohen, M. Dahanayake, X.Y. Hua, Relationship of structure to properties in surfactants. 10. Surface and thermodynamic properties of 2-dodecyloxypoly (ethenoxyethanol) s, C12H25 (OC2H4) xOH, in aqueous solution, The Journal of Physical Chemistry, 86 (1982) 541-545.
[60] S. Ghosh, A. Das Burman, G.C. De, A.R. Das, Interfacial and self-aggregation of binary mixtures of anionic and nonionic amphiphiles in aqueous medium, The Journal of Physical Chemistry B, 115 (2011) 11098-11112.
[61] R. Sanan, R. Kaur, R.K. Mahajan, Micellar transitions in catanionic ionic liquid–ibuprofen aqueous mixtures; effects of composition and dilution, RSC Advances, 4 (2014) 64877-64889.
[62] D. Liu, J. Ma, H. Cheng, Z. Zhao, Solubilization behavior of mixed reverse micelles: effect of surfactant component, electrolyte concentration and solvent, Colloids and Surfaces A: Physicochemical and Engineering Aspects, 143 (1998) 59-68.
[63] R. Leung, D.O. Shah, Solubilization and phase equilibria of water-in-oil microemulsions: II. Effects of alcohols, oils, and salinity on single-chain surfactant systems, Journal of colloid and interface science, 120 (1987) 330-344.
[64] D. Evans, D. Mitchell, B. Ninham, Oil, water, and surfactant: properties and conjectured structure of simple microemulsions, The Journal of Physical Chemistry, 90 (1986) 2817-2825.
[65] M.J. Hou, D. Shah, Effects of the molecular structure of the interface and continuous phase on solubilization of water in water/oil microemulsions, Langmuir, 3 (1987) 1086-1096.
[66] P.D. Huibers, D.O. Shah, Evidence for synergism in nonionic surfactant mixtures: enhancement of solubilization in water-in-oil microemulsions, Langmuir, 13 (1997) 5762-5765.
[67] Q. Li, T. Li, J. Wu, Water solubilization capacity and conductance behaviors of AOT and NaDEHP systems in the presence of additives, Colloids and Surfaces A: Physicochemical and Engineering Aspects, 197 (2002) 101-109.

[68] B.K. Paul, R.K. Mitra, Water solubilization capacity of mixed reverse micelles: effect of surfactant component, the nature of the oil, and electrolyte concentration, Journal of colloid and interface science, 288 (2005) 261-279.
[69] A. Das, R.K. Mitra, Does the optimum hydrophilic lipophilic balance condition affect the physical properties of mixed reverse micelles? A spectroscopic investigation, The Journal of Physical Chemistry B, 118 (2014) 5488-5498.
[70] A. Das, A. Patra, R.K. Mitra, Do the physical properties of water in mixed reverse micelles follow a synergistic effect: a spectroscopic investigation, The Journal of Physical Chemistry B, 117 (2013) 3593-3602.
[71] D. Liu, J. Ma, H. Cheng, Z. Zhao, Investigation on the conductivity and microstructure of AOT/non-ionic surfactants/water/n-heptane mixed reverse micelles, Colloids and Surfaces A: Physicochemical and Engineering Aspects, 135 (1998) 157-164.
[72] X. Zhang, Y. Chen, J. Liu, C. Zhao, H. Zhang, Investigation on the structure of water/AOT/IPM/alcohols reverse micelles by conductivity, dynamic light scattering, and small angle X-ray scattering, J. Phys. Chem. B, 116 (2012) 3723-3734.
[73] J.N. Israelachvili, D.J. Mitchell, B.W. Ninham, Theory of self-assembly of hydrocarbon amphiphiles into micelles and bilayers, Journal of the Chemical Society, Faraday Transactions 2: Molecular and Chemical Physics, 72 (1976) 1525-1568.
[74] D.F. Evans, B. Ninham, Molecular forces in the self-organization of amphiphiles, The Journal of Physical Chemistry, 90 (1986) 226-234.
[75] L.M. Nazário, T.A. Hatton, J.P. Crespo, Nonionic cosurfactants in AOT reversed micelles: effect on percolation, size, and solubilization site, Langmuir, 12 (1996) 6326-6335.
[76] J.-L. Lemyre, S. Lamarre, A. Beaupré, A.M. Ritcey, A new approach for the characterization of reverse micellar systems by dynamic light scattering, Langmuir, 26 (2010) 10524-10531.
[77] K.M. S. P. Moulik, On the Versatile Surfactant Aerosol-OT (AOT): Its Physicochemical and Surface Chemical Behaviours and Uses, Proc. Ind. National Sci. Acad. Rev., Article No. 3 (1996) 215-232.
[78] H. Preu, A. Zradba, S. Rast, W. Kunz, E.H. Hardy, M.D. Zeidler, Small angle neutron scattering of D 2 O–Brij 35 and D 2 O–alcohol–Brij 35 solutions and their modelling using the Percus–Yevick integral equation, Physical Chemistry Chemical Physics, 1 (1999) 3321-3329.
[79] A. Das, A. Parta, R.K. Mitra, Modulation of anionic reverse micellar interface with non-ionic surfactants can regulate enzyme activity within the micellar waterpool, Colloid and Polymer Science, 294 (2016) 715-726.
[80] T.K. Jain, M. Varshney, A. Maitra, Structural studies of aerosol OT reverse micellar aggregates by FT-IR spectroscopy, The Journal of Physical Chemistry, 93 (1989) 7409-7416.
[81] Q. Zhong, D. Steinhurst, E. Carpenter, J. Owrutsky, Fourier transform infrared spectroscopy of azide ion in reverse micelles, Langmuir, 18 (2002) 7401-7408.
[82] J.-B. Brubach, A. Mermet, A. Filabozzi, A. Gerschel, D. Lairez, M. Krafft, P. Roy, Dependence of water dynamics upon confinement size, The Journal of Physical Chemistry B, 105 (2001) 430-435.
[83] N. Zhou, Q. Li, J. Wu, J. Chen, S. Weng, G. Xu, Spectroscopic characterization of solubilized water in reversed micelles and microemulsions: sodium bis (2-ethylhexyl) sulfosuccinate and sodium bis (2-ethylhexyl) phosphate in n-heptane, Langmuir, 17 (2001) 4505-4509.
[84] K. Kundu, S. Bardhan, S. Banerjee, G. Chakraborty, S.K. Saha, B.K. Paul, Influence of chemical architecture of oils and ionic liquid on the physicochemical and thermodynamic properties and microenvironment of anionic surfactant based microemulsion, Colloids and Surfaces A: Physicochemical and Engineering Aspects, 469 (2015) 117-131.
[85] C. González-Blanco, L.J. Rodríguez, M.M. Velázquez, Effect of the solvent on the water properties of water/oil microemulsions, Journal of colloid and interface science, 211 (1999) 380-386.
[86] A. Koti, M. Krishna, N. Periasamy, Time-resolved area-normalized emission spectroscopy (TRANES): a novel method for confirming emission from two excited states, The Journal of Physical Chemistry A, 105 (2001) 1767-1771.

[87] M.D. Fayer, N.E. Levinger, Analysis of water in confined geometries and at interfaces, Annual Review of Analytical Chemistry, 3 (2010) 89-107.
[88] R.K. Mitra, S.S. Sinha, P.K. Verma, S.K. Pal, Modulation of dynamics and reactivity of water in reverse micelles of mixed surfactants, The Journal of Physical Chemistry B, 112 (2008) 12946-12953.
[89] R. Pramanik, S. Sarkar, C. Ghatak, V.G. Rao, P. Setua, N. Sarkar, Microemulsions with surfactant TX100, cyclohexane, and an ionic liquid investigated by conductance, DLS, FTIR measurements, and study of solvent and rotational relaxation within this microemulsion, The Journal of Physical Chemistry B, 114 (2010) 7579-7586.
[90] S. Roohinejad, I. Oey, J. Wen, S.J. Lee, D.W. Everett, D.J. Burritt, Formulation of oil-in-water β-carotene microemulsions: effect of oil type and fatty acid chain length, Food chemistry, 174 (2015) 270-278.

# Chapter 6: Formulation and Structure of Mixed Biocompatible Microemulsion System

## 6.1 Introduction

Microemulsions are isotropic, fluid, transparent, thermodynamically stable dispersion of oil and water, stabilized by surfactant(s)[1, 2]. The structure of ME can be idealized as a set of interfaces dividing polar and nonpolar domains. Depending on the composition of the system, the microstructure of an ME may exist as water-in-oil (w/o) droplets, oil-in-water (o/w) droplets, or a bicontinuous structure. Over the last few decades MEs have attracted more interest as potential drug delivery systems[3-5]. Part of this interest appears as a consequence of their transparency, ease of preparation, nanometric size and long-term stability. These properties as well as their ability for incorporating drugs of different lipophilicity are some of the reasons for which MEs have seriously been considered for pharmaceutical purposes. However, the limitations on the use of MEs in pharmaceutical and cosmetic fields arise greatly from the need for all the constituting components to be biologically and pharmaceutically acceptable, particularly the surfactants and cosurfactants. The selection of components for MEs suitable for cosmetic and pharmaceutical use is one of the most important factors to fulfil the requirements of a good delivery system. One of the most preferred biocompatible ME is based on lecithin (L), which is a nontoxic surfactant as recognized by safe (GRAS) status[6]. Being highly lipophilic lecithin tends to form nematic liquid crystalline phases in presence of oil and water[5]. Biocompatible lecithin based organogels have been found to be clear and viscoelsatic, and are used for pharmaceutical applications[7]. Phase behaviour, structure and pharmaceutical applications of lecithin/short chain alcohol based ME systems have also been investigated in details[8-16]. Low toxic formulation have been reported using linker molecules[17-19]. Many of these formulations however, possess high viscosity, which refrains these formulations from specific pharmaceutics applications. Moreover, the short-chain alcohols used in the ME systems are prone to affect cell membrane[20]. It thus stands important to formulate low toxic low viscous ME systems containing lecithin and cosurfactant. A potential replacement of toxic short-chain alkanols is buytl lactate (BL) which is a well-known pharmaceutical flavouring agent[21] and has been used to formulate MEs[22-24].

Mixtures of surfactants have often been found to be advantageous over the use of single surfactants, since they can extract properties superior than the individual ones. Blending of two

non-ionic surfactants [25] or ionic and non-ionic surfactants[26, 27] can provide better solubilization capacity and affect the phase behavior relative to the individual ones. Blending of surfactants can tune the hydrophilic-lipophilic balance (HLB) of the constituting surfactants in order to optimize the solubilization capacity. Earlier our group has reported the phase behavior as well as other physical properties of a series of mixed ME systems [28-31]. Herein we report the detailed phase behavior and structural aspects of a mixed surfactant ME system composed of lecithin and Triton X-100. TX100 is a biocompatible[32] and one of the most widely used nonionic surfactants for lysing cells to extract protein and other cellular organelles or to permeabilize the living cell membrane for transfection[33, 34]. We chose isopropyl myristate (IPM) as the oil phase as it has widely been used in biocompatible formulations[14, 15, 23]. The principle objective of this work is to establish the enrichment of solubilization behavior of this mixed system as a lipophilic surfactant lecithin (HLB ~ 4) is mixed with a hydrophilic surfactant TX-100 (HLB ~ 13.5) to tune the optimum HLB of the mixed system using BL as the cosurfactant. Phase diagrams for the single and mixed surfactant systems have been constructed in order to compare the solubilization behavior of these systems. The fluidity of these ME systems have been estimated using viscosity measurements. The network structure of water in the oil-rich region is determined by monitoring the O-H stretching frequency modes by FTIR spectroscopy.

## 6.2 Results and Discussions

***Phase Study:*** Figure 6.1(a) shows the pseudo-ternary phase diagrams of the system composed of L/BL/IPM/water, TX-100/BL/IPM/water and L+TX-100(1:1, w/w)/BL/IPM/water at room temperature. We denote these systems as L, T and LT respectively. The surfactant(s): BL ratio is kept fixed at 1:2 (w/w). In the figure, only single phase ME region has been demarcated. As can be observed from the figure, the system L offers a very thin single phase region along the amphiphile/oil axis. The system T offers a somewhat larger single phase region compared to L, expanding in the surfactant/water axis also. The mixed (LT) system offers even better single phase region compared to the individual (L and T) systems, especially along the surfactant/oil axis. The detailed phase diagrams of L and LT are shown in figure 6.1b.

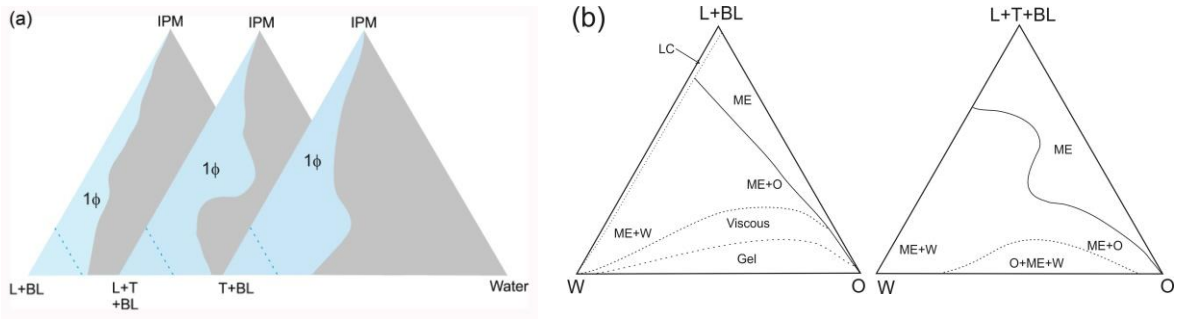


**Figure 6.1.** (a) Pseudo-ternary phase diagrams of Lecithin (L)/TX-100 (T)/butyl lactate (BL)/IPM/water systems. The dotted lines represent the dilution line through which samples are chosen for physical measurements. The surfactant(s):cosurfactant ratio is fixed at 1:2 (w/w). 1ϕ represents single phase ME region. (b) Detailed phase diagram of L and L+T (mixed) systems. The surfactant(s):cosurfactant ratio is fixed at 1:2 (w/w). W, O, ME and LC represents water, oil (IPM), ME and liquid-crystalline phases, respectively.

The phase behaviour of L is characteristic of the presence of various meso-phases[19]. It can be observed that there remains a considerable fraction of viscous and gel phases, specially in the oil-rich region. The mixed system, however, offers a less complicated behaviour with absence of highly viscous or gel phases; rather a three phase region appears at low amphiphile concentration. Appearance of a three-phase region signifies a perfect balance of the hydrophilic-lipopilic balance (HLB) of the mixed system[35]. This corresponds to a proper mixing of hydrophilic TX-100 and lipophilic lecithin with BL, which brings about enhanced solubilization capacity of the mixed surfactant systems and thus a larger ME region is obtained. The single phase boundary does not appreciably change in the temperature range of 10-40$^0$C (data not shown). For potential pharmaceutical application, the ME system should also be stable at various physiologically relevant environments, and to check that, we determine the phase behaviour of the LT system at pH = 2.6 and in 0.9% salt concentration. It is found that the phase behaviour of the LT system remains almost unaltered in these two conditions revealing the stability of the system in these environments. The pseudo-ternary phase triangle provides with the information on the extent of single phase region and from that one can choose suitable composition to carry out further physical investigations. Here we adopt an oil/water dilution route in which the total amphiphile concentration is kept fixed at 80% in all the three systems. This helps to extract information on the relative change of properties as the dispersed medium changes from oil rich to water rich at a fixed amphiphile concentration. We choose five such compositions, in which the oil:water (w/w) ratios are 10:1 (LT1), 2.3:1 (LT2), 1:1 (LT3), 1:2.3 (LT4) and 1:7 (LT5).

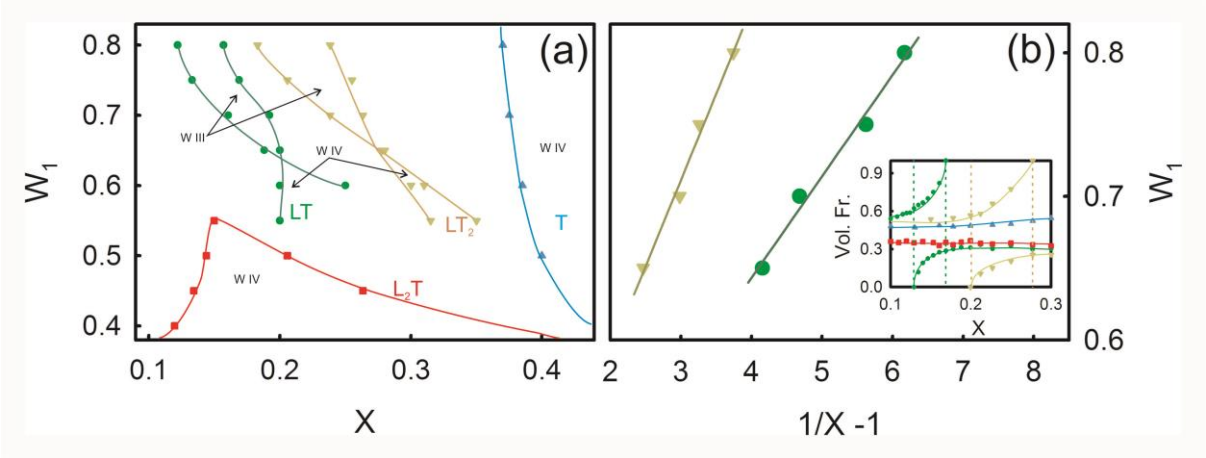


**Figure 6.2.** (a) Vertical sections through the pseudo-quaternary phase prism for lecithin/TX-100/butyl lactate/IPM/water systems at a constant water:oil ratio of 1:1 (w/w). The lecithin:TX-100 ratio has been chosen as: 2:1 ($L_2T$: red square), 1:1 (LT: green circle), 1:2 ($LT_2$: yellow inverted triangle) and 0:1 (T, blue triangle). W III and W IV stand for tri-phasic and single-phase region, respectively. (b) Butyl lactate weight fraction values ($W_1$) as a function of (1/X -1) obtained from the midpoints of the three-phase bodies in figure 6.2a. The straight lines are linear fits. The correlation of co-efficient (R-square) values obtained are 0.988 for LT and 0.987 for $LT_2$ systems, respectively. Volume fraction of the different phases of the systems $L_2T$: red square, LT: green circle, $LT_2$: yellow inverted triangle and T: blue triangle, for $W_1$=0.75 are shown in the inset. The dotted lines enclose three-phase areas.

In order to extract information on the maximum solubilization capacity we construct the so-called 'fish tail' diagrams[36]. Vertical sections bisecting the water-oil axis of the phase prism for the pseudo-four component systems are shown in figure 6.2a in which X stands for the total amphiphile weight fraction, ($X = \frac{S+BL}{O+W+S+BL}$), where O and W stands for oil and water, respectively, S stands for surfactant(s) (L or T or L+T). $W_1$ denotes the BL weight fraction in the total amphiphile, i.e., $W_1 = \frac{BL}{S+BL}$. In the figure W III and W IV represent Winsor III (three phase) and Winsor IV (single phase) systems, respectively[37]. The appearances of liquid crystal or viscous-gel phase are not shown in the figure. We choose four different compositions depending upon the L:T mixing ratios (w/w), namely, 2:1 ($L_2T$), 1:1 (LT), 1:2 ($LT_2$) and 0:1 (T). As can be observed from the figure, three phase body is observed only in case of LT and $LT_2$ systems, and not for the other two systems, wherein only single phase and biphasic bodies are identified. The L system does not produce any single-phase region within the experimental window. Optimum mixture of LT with BL gives rise to a balance ME as manifested with the appearance of a three-phase body as evidenced in LT and $LT_2$ systems. It is interesting to note that the formation of single phase domain shifts towards higher X values as the content of T increases in the mixture. We plot the volume fraction of different phases as a function of X (figure 6.2b, inset) in order to understand the composition of the dispersed phases. At high X, the formulation is found to be of W II type (i.e. w/o type ME on top and the excess water phase

at the bottom) at a fixed $W_1$ value. As the amphiphile concentration (X) decreases, the bending elasticity of the interface monolayer changes gradually and eventually it tends to bend in an opposite direction to produce W I (Winsor I) systems (o/w ME in the lower phase with excess oil in the upper one) passing through a W III or W IV body. At low $W_1$ the system is predominantly hydrophilic and the amphiphile monolayer bends itself around the oil phase in order to produce o/w droplets (W I system). With increasing BL content, the radius of curvature increases and droplet nature of the ME is converted into a bicontinuous one and a Winsor III system is formed. On further increase of BL the increasing lipophilicity of the amphiphile mixture tunes the monolayer to bend around water in order to produce w/o droplets in oil continuous medium (Winsor II system). The point at which the three-phase body meets the single-phase body corresponds to the maximum solubilization capacity of the system[35], and the corresponding amphiphile concentration is denoted by $X_b$ and that of BL is denoted by $W_{1b}$. $X_b$ indicates the minimum concentration of total amphiphile (surfactant plus cosurfactant) required for the formation of single-phase ME with equal amount of water and IPM. The lower the value of $X_b$, the higher is the solubilization capacity. For the present systems we obtain the $X_b$ and $W_{1b}$ values to be 0.2, 0.633 for LT and 0.289, 0.65 for the $LT_2$ systems, respectively. It therefore clearly indicates that the mixed systems exhibit better solubilization behaviour than the corresponding single surfactant systems.

Interfacial composition inside the three phase body can be estimated in the following manner: for a particular surfactant mixture, the three-phase region is a non-variant region as all the intensive variables (temperature, pressure and oil-water ratio) are fixed for the pseudo-four component system. The composition and structure of the ME phase along the midst curve in the three-phase body would also be fixed and would essentially be equal to that of the single-phase body at this point[35, 38]. The three-phase region consists of micro-oil and micro-water sub-domains separated by amphiphile interface[39]. The surfactant molecules are essentially adsorbed at the micro-oil–water interface and form an interfacial layer. We assume negligible monomeric solubility of the amphiphiles in the microoil-microwater domains. It can be noted here that the total phase behaviour of the pseudo-four component system can be represented by a composition tetrahedron (in which the four different components act as the vertices of the three dimensional tetrahedron) at constant temperature and pressure. In such a tetrahedron an HLB plane[40] of maximum solubilization can be drawn which essentially includes the particular three-phase tie-triangle including the ME in the middle curve of the Winsor III region. The subsequent HLB plane equation is given as,

$$W_1 = S_1^S - \frac{S_1(1-S_1^S)}{(1-S_1)}.\alpha.(\frac{1}{X} - 1) \quad (6.1)$$

where α is the weight fraction of oil in oil and water mixture (herein 0.5), $S_1^S$ represents the BL solubility in the total amphiphilic mixture (L+T+BL) at the water–oil interface inside the ME phase. $S_1$ is the monomeric solubility of BL in the micro-oil domain and is equal to the BL fraction in the excess oil phase. $S_1^S$ can be obtained as the intercept of the linear plot of (1/X − 1) against $W_1$, and $S_1$ can be calculated from the slope of the straight line. We plot 1/X as a function of $W_1$ for the LT and $LT_2$ systems and good linear fits are obtained (figure 6.2b). The calculated $S_1^S$ and $S_1$ values are 0.361 and 0.181 for the LT system, and 0.351 and 0.27 for the $LT_2$ system, respectively. It appears therefore that in LT system BL is more localized at the oil-water interface rendering its better solubilization behaviour compared to $LT_2$. The corresponding surfactant and cosurfactant concentration at the micro-interface can be obtained as[29, 41],

$$C_1 = X_b W_{1b} - \frac{\alpha(1-X_b)}{1-S_1} S_1 \quad (6.2)$$

$$C_2 = X_b(1 - W_{1b}) \quad (6.3)$$

where $C_1$ and $C_2$ are the respective weight fractions of BL and (L+T) in the system at the water–oil interface within the single ME phase at the maximum solubilization point. We calculate the $C_1$ and $C_2$ values of 0.04 and 0.075 for the LT system and 0.056 and 0.101 for the $LT_2$ system, respectively. The rationale behind the observed increase in the solubilization capacity for the 1:1 LT mixture is twofold: firstly, a decreased value of $S_1$ signifies the lower monomeric solubility of BL in the micro-oil phase which eventually increases the net solubilization capacity of the surfactant layer at the oil-water interface inside the ME, and secondly, a low value of the $C_1$+$C_2$ signifies a more efficient interface inside the ME. As a combined effect the solubilizing power per surfactant molecule itself increases as L and T is mixed in 1:1 (w/w) ratio. We also construct the three phase behaviour of the LT system in presence of 0.9% NaCl (data not shown). It has been found that the maximum solubilization limit is achieved at $X_b$=0.22 and $W_{1b}$=0.6 with the corresponding $S_1^S$ and $S_1$ values of 0.406 and 0.17 respectively. The observed marginal change in the amphiphile distribution profile is consistent with previously reported ME systems[29].

The phase study thus establishes the fact that mixing of surfactants offers enhanced solubilization capacity of the mixed surfactant systems compared to the single ones. We now investigate how the physical properties of the ME system change upon mixing L and T. In order to achieve this we choose single phase ME systems at a fixed amphiphile concentration

of 80% (w/w) and varied the water content following the dotted line shown in figure 6.1a. The choice of amphiphile concentration is to ensure that all the three systems (L, T and LT) produce single phase ME.

***Viscosity, Adiabatic Compressibility and Conductivity Study:*** Viscosity is one of the most important macroscopic properties of a ME system which specifies its applications, specially in the field of pharmacology [3, 42-44]. Figure 6.3 depicts the viscosity profile of all the studied systems. In figure 6.3a, specific viscosity is plotted against the weight fraction of water in the formulations. All the systems follow a Newtonian fluidity and offer a lower viscosity than the previously reported lecithin based ME/organogel systems[15, 16]. It is observed that the T systems are ~23% while the LT systems are ~15% less viscous than the L systems. This result identifies that mixing of surfactants effectively brings down the viscosity of the lecithin based systems. Viscosity increases as the content of water increases in all the systems. It can be noted here that IPM has a 4-5 times higher viscosity than water, yet the water rich region offers a higher viscosity than the oil rich region, which might due to the stronger interaction between the droplets, a phenomenon much consistent with the previously reported biocompatible ME systems[23, 28]. However, the observed linear trend of the viscosity profile is markedly different from the apprehended bell shaped trend in which a w/o droplet system gets converted into a o/w droplet system passing through an intermediate bi-continuous phase[28]. The viscosity results thus strongly identify the droplet character of all the chosen samples. The viscosities of all these systems are measured at different temperatures in order to probe the energetic of the viscous flow. Figure 6.3b depicts the viscosity behaviour of the mixed surfactant systems at different temperatures (20-60$^0$C). With increase in temperature, viscosity expectedly decreases. The activation enthalpy $\Delta H^*_{Vis}$ (which is equivalent to the energy of activation for viscous flow $\Delta E^*_{Vis}$) is obtained from[28]

$$\eta = \frac{Nh}{V} \exp\left(\frac{\Delta H^*_{vis}}{RT}\right) \exp\left(-\frac{\Delta S^*_{vis}}{R}\right) \qquad (6.4)$$

where $h$ is the Plank constant, $N$ is the Avogadro number, $V$ is the molar volume, and $\Delta S^*_{Vis}$ is the entropy of activation for the viscous flow; other terms have their usual significance. Assuming $\Delta S^*_{Vis}$ to be independent of temperature, a straight line plot between ln $\eta$ vs. $T^{-1}$ is expected from the slope of which $\Delta H^*_{Vis}$ can be calculated. All the studied systems produce good linear fits for ln $\eta$ vs $T^{-1}$ plot. A representative plot has been shown in figure 6.3c. The obtained $\Delta H^*_{Vis}$ values for all the systems are plotted in figure 6.3c as a function of water content. The values range in the order of 20-25 kJ mol$^{-1}$, which is in good agreement with other biocompatible ME systems[28]. The $\Delta H^*_{Vis}$ values do not follow any significant trend; for L

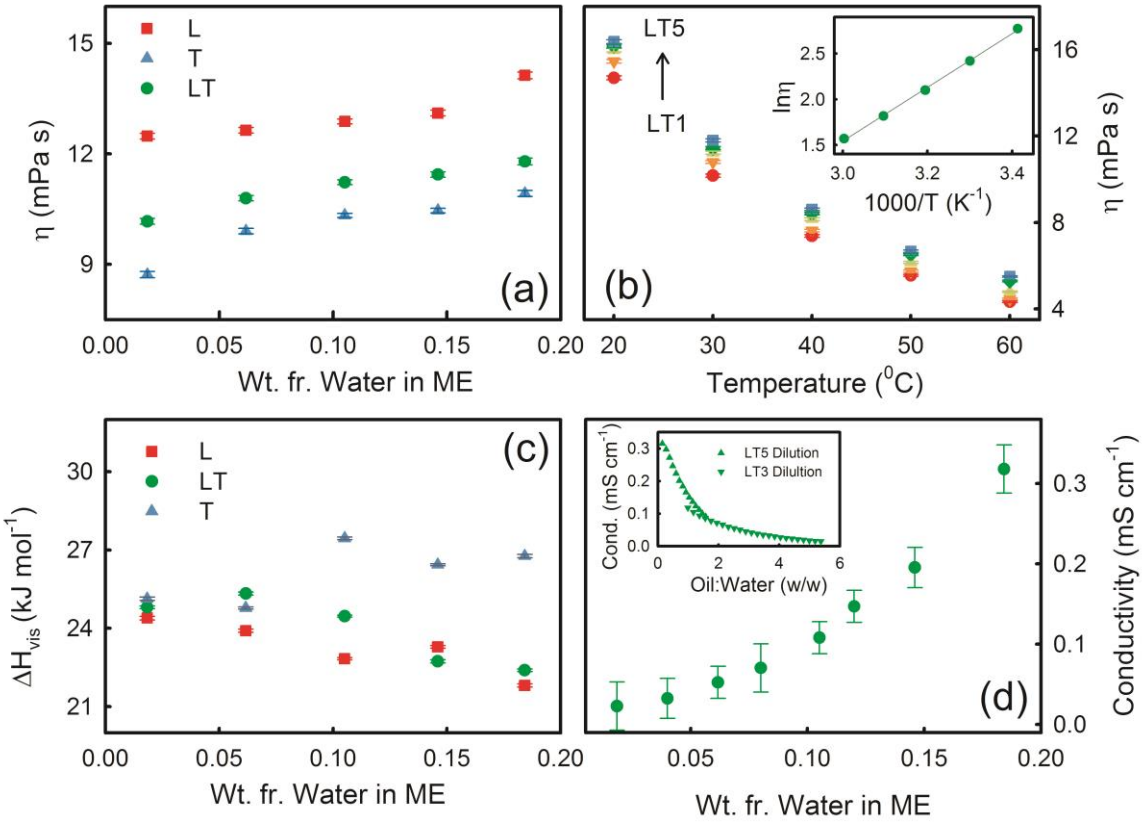


**Figure 6.3.** (a) Viscosity of three different ME systems L, LT and T as a function of water content in the ME. (b) Viscosity of LT ME system as a function of temperature. Inset: Plot of ln $\eta$ vs 1/$T$ for a representative LT ME system. The straight line corresponding to a linear fit. The correlation of co-efficient (R-square) value is 0.99. (c) The activation enthalpy ($\Delta H^*_{vis}$) of three different ME systems L, LT and T as a function of water content in the ME. (d) Conductivity of LT ME systems as a function of water concentration in ME. Inset: Conductivity as a function of oil-water weight ratio for two dilution routes.

and LT systems it suffers a marginal decrease, whereas for the TX-100 based system, it shows a slight increase beyond 10% water content. The absence of any remarkable trend in $\Delta H^*_{Vis}$ coupled with the observed linearity in specific viscosity rules out the possibility of the presence of any bicontinious phase in the chosen concentration regime. We also determine the specific viscosity of the LT systems at two terminal pH conditions of pH=2.0 and 12.0 in order to check their sustainability in drastic physiological conditions. It has been found that viscosity of the LT systems offer only marginal variation indicating their potential to be applied for specific pharmaceutical applications.

The transition of structures in ME systems can also be monitored through conductance studies, which offers detectable change as the dispersing phase changes its polarity. We measure the conductivity of the mixed system (in presence of 0.9% NaCl) as a function of water concentration and the result is depicted in figure 6.3d. It can be observed from the figure that conductivity increases expectedly with increasing water concentration and a distinct change in the slope can unambiguously be identified at 10% water content, which signifies a

sharp transition of the dispersant medium from oil continuous to water continuous. It could be noted here that 10% water content corresponds to an equal oil-water ratio and in many systems such a system offers bicontinuous phase. In a previous study with Tween-80/BL/IPM system, the conductivity profile showed two distinct changes in the slopes identifying a w/o to o/w phase through an intermediate bicontinuous phase[23]. The appearance of a single break in the slope signifies a sharp w/o to o/w droplet transition in the present study as also has been evidenced from the viscosity studies. We also measure the conductivity as a function of oil:water (w/w) ratio following oil dilution lines starting from LT3 (water:amphiphile (w/w)=0.125) and LT5 (water:amphiphile (w/w)=0.23). We observe two distinct slopes intersecting at oil:water=1 (figure 6.3d, inset) strongly corroborating our conclusion of the droplet nature of all the systems.

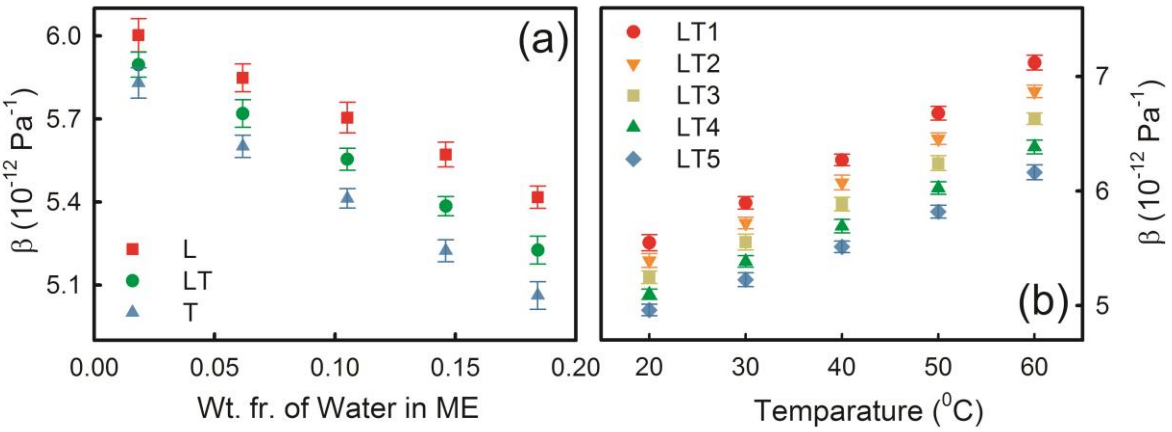


**Figure 6.4.** (a) Compressibility (β) of three different ME systems L, LT and T as a function of water content. (b) Variation of compressibility (β) of different LT systems as a function of temperature.

Figure 6.4 shows the iso-entropic compressibility β for all the studied systems. β expectedly decreases as the system becomes more water rich. The observed higher compressibility of the system at low water content is in good agreement with the viscosity behaviour of the system, which suggests the hard sphere-like character of the water globules in oil continuous medium (w/o). The temperature dependency of β also shows a linear trend (figure 6.4b), which strongly demands the absence of any intermediate structural modification other than the droplet type.

***FTIR Study:*** The equilibrium structural features of different components in self-assembled systems could efficiently be resolved using FTIR spectroscopy. Previously, lecithin based reverse micellar systems in hydrocarbon oils have been studied using FTIR spectroscopy[45-47]. While much attention has been paid on the P=O and C-H bond stretching vibrations of

lecithin molecule, studies on the structural alteration of water is rather sparse[48, 49]. It often stands necessary, specially during the application of w/o type ME as a water soluble drug carrier, to understand how the equilibrium structure of water modifies with the change in composition. In the present study we measure the MIR (Mid Infra-Red) FTIR spectra of LT1, LT2 and LT3 systems to determine the water structure inside the ME droplets. From the conductance study (figure 6.3d), LT1 and LT2 systems can safely be assumed to possess w/o type droplets while LT3 is in the onset of formation of o/w type droplets. In all these measurements we subtract the data of surfactant (or mixture of surfactants)/BL/IPM ternary systems from the hydrated quaternary systems and thus the signals essentially provide information on the water molecules present in the systems only. We focus our attention to the 3000-3800 $cm^{-1}$ frequency window as this is a fingerprint region for the symmetric and asymmetric vibrational stretch of O-H bonds in water[50]. A representative FTIR spectrum has been shown in figure 6.5a.

The FTIR spectrum of water in this frequency window can be deconvoluted into three Gaussian sub-bands peaking at ~3600, 3460 and 3330 $cm^{-1}$ regions[51]. The peak at ~3600 $cm^{-1}$ is due to the 'multimer' or 'bound type' water molecules which make bonds with the interface and thus do not produce strong hydrogen bonds with the neighbouring water molecules and have generally been realized in extreme hydrophobic environments. The second component peaking at 3460 $cm^{-1}$ involves the so-called 'intermediate' water molecules which are unable to develop fully hydrogen bonds and somewhat connected to other water molecules with distorted H-bonds. Finally, the third kind of water molecule (i.e. peaking at 3330 $cm^{-1}$) originates from the 'network' or 'bulk type' water molecules which are fully hydrogen bonded with the neighbouring water molecules and contributes its majority of share in pure water. We deconvolute the MIR spectra of all the systems into three Gaussian components keeping the peak positions fixed as those of pure water (a representative figure is shown in figure 6.5a). A free fitting often produces more accurate contributions; however, fixing the peak positions allows comparing the change in the relative weightage of each component at variable interfacial compositions. We plot the relative contribution of each curve towards the total spectra and plot it as a function weight percentage of water (figure 6.5b-d). This relative contribution is essentially proportional to the fraction of water molecules belonging to that particular stretching mode. In a previous study my Maitra et al.[48] in lecithin based reverse micellar systems the FTIR spectra had been deconvoluted into two contributions: one peaking at ~3250 $cm^{-1}$ (bound water) and the other at ~3460 $cm^{-1}$ (free water), the relative content of these

molecules had been found to be dependent on the system composition. We herein prefer a three peak fitting, which provided better fitting results compared to the two peak fittings.

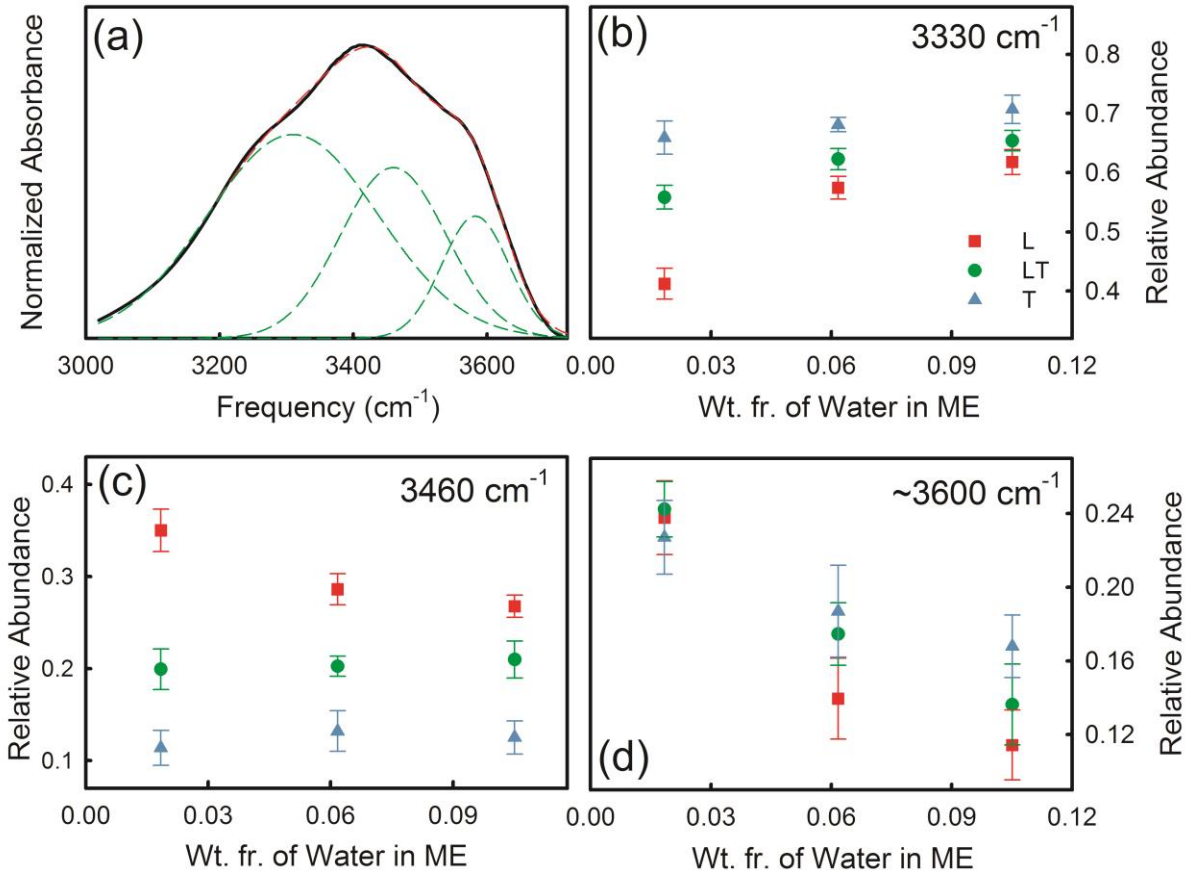


**Figure 6.5.** (a) A representative FTIR curve deconvoluted into three different contributions (green broken lines). The red broken line represents the overall fit. The relative area under curves peaking at 3330 $cm^{-1}$ (b), 3460 $cm^{-1}$ (c) and ~3600 $cm^{-1}$ (d) for the three different ME systems L, LT and T are shown as a function of water content in the ME.

It can be observed from figure 6.5d that the relative abundance of the 'multimer' water molecules decreases with increasing water content, which is due to the formation of strongly hydrogen bonded water network at elevated water concentration. The lecithin based system shows a lower abundance of the 'multimer' water molecules compared to the TX-100 based systems, with the LT systems lying in between. It is interesting to note that for the L1, T1 and LT1 systems, where the water concentration is only ~2%, the difference is very marginal, which perhaps is apprehended taking into account the tight binding nature of water molecules with the interface. The population corresponding to the 'intermediate' water (peaking at 3460 $cm^{-1}$) shows marginal variation with water content, specially for the T and LT systems, with a faint decreasing trend for the corresponding L systems (figure 6.5c). The population of

'network' water (peaking at 3330 $cm^{-1}$) increases with increasing the weight percentage of water, faintly with the LT and T systems, and considerably with the L systems (figure 6.5b). As mentioned earlier, the abundance of 'network' water is a signature of the bulk nature of the water present in the systems. In pure water this corresponds to ~70%. As observed from the figure, such abundance is eventually reached for the T based system, while for the LT system it increases from 55% (for the w/o system) to 64% (for o/w system), and for L it increases from 40% to 61%. This shows that in L based systems, the water structure is more perturbed than the corresponding T and LT systems. Interestingly L also has the lowest abundance of the 'multimer' water, confirming a high abundance of 'intermediate' water, which suggests a strong interaction between lecithin and water. Earlier studies by Carvallro et al[49]. concluded insignificant effect of water content on the FTIR spectra, whereas Maitra et al. [48] concluded that the O-H bond stretching frequency suffers significant change upon interaction with lecithin and also depends upon the nature of the oil phase. However, it should be taken into consideration that both these previous studies dealt with visco-elastic reverse micellar systems with very low water content. Our investigated systems are relatively low viscous ME containing 2-10% (w/w) water, which explains the presence of three different species of water molecules and the observed variation in their relative abundance with different interfacial compositions. We carry out the FTIR studies at two terminal pH conditions of pH=2.0 and 12.0 in order to determine whether the water structure suffer any perturbation at different pH conditions. It is evident that the relative population of various type of water is independent of the pH of the aqueous phase.

## 6.3 Conclusion

The present investigation was aimed towards the formulation of a lecithin based biocompatible low-viscous ME system. Most of the previously reported lecithin based formulations are visco-elastic gel like formulations[15, 16] and for certain specific applications, it is important to formulate low viscous systems. Lecithin being highly lipophilic is very sensitive to form gel like structures, however blending with a hydrophilic surfactant TX-100 and a lipophilic cosurfactant butyl lactate produces considerable low viscous ME systems, with a synergistic enhancement of single phase region compared to the individual surfactants. The mixed systems produce three-phase body which reveals a perfect hydrophilic-lipophilic balance and maximum solubilization limit, which is otherwise not obtained with either lecithin or TX-100. The increased solubilization capacity is due to the decrease in both $S_1$ (monomeric solubility of BL in the micro-oil domain) as well as small values of $C_1$+$C_2$ (increased effecetive colubilization

capacity of the amphiphiles). Viscosity, conductivity and adiabatic compressibility measurements provide evidences of droplet nature of the formulations at high surfactant concentrations. FTIR spectroscopic studies in the oil rich regions identifies the presence of three distinct types of water molecules present in the systems, and the relative abundance of such type of water molecules changes with composition. The measured physical propoerties of the mixed surfactant systems do not drastically differ from those obtained for the lecithin based systems and is also independent on pH and presecne of electrolytes with the additional advantage of being less viscous. Our study thus offers a biocompatible low viscous lecithin based ME system that can serve as a basis for further investigations in drug delivery and as nontoxic nanotemplates for other applications in future.

## 6.4 References


[1] B.K. Paul, S.P. Moulik, Microemulsions: an overview, Journal of Dispersion science and Technology, 18 (1997) 301-367.

[2] M. Kahlweit, Microemulsions, Science, 240 (1988) 617-621.

[3] A. Kogan, N. Garti, Microemulsions as transdermal drug delivery vehicles, Adv. Colloid Interface Sci., 123-126 (2006) 369-385.

[4] M.J. Lawrence, G.D. Rees, Microemulsion-based media as novel drug delivery systems, Adv. Drug Delivery Rev., 64 (2012) 175-193.

[5] S. Tenjarla, Microemulsions: An Overview and Pharmaceutical Applications, Crit, Rev. Ther. Drug Carrier Systems, 16 (1999) 461-521.

[6] E.J. Acosta, T. Nguyen, A. Witthayapanyanon, J.H. Harwell, D.A. David A. Sabatini, Linker-Based Bio-compatible Microemulsions, Environ. Sci. Technol., 39 (2005) 1275-1282.

[7] S. Raut, S.S. Bhadoriya, V. Uplanchiwar, V. Mishra, A. Gahane, S.K. Jain, Lecithin organogel: A unique micellar system for the delivery of bioactive agents in the treatment of skin aging, Acta Pharm. Sinica B, 2 (2012) 8-15.

[8] C. von Corswant, P.E.G. Thorén, Solubilization of Sparingly Soluble Active Compounds in Lecithin-Based Microemulsions: Influence on Phase Behavior and Microstructure, Langmuir, 15 (1999) 3710-3717.

[9] G. Wolf, E. Kleinpeter, Pulsed Field Gradient NMR Study of Anomalous Diffusion in a Lecithin-Based Microemulsion, Langmuir, 21 (2005) 6742-6752.

[10] V. Papadimitriou, T.G. Sotiroudis, A. Xenakis, Olive Oil Microemulsions: Enzymatic Activities and Structural Characteristics, Langmuir, 23 (2007) 2071-2077.

[11] E.D. Tzika, M. Christoforou, S. Pispas, M. Zervou, V. Papadimitriou, T.G. Sotiroudis, E. Leontidis, A. Xenakis, Influence of Nanoreactor Environment and Substrate Location on the Activity of Horseradish Peroxidase in Olive Oil Based Water-in-Oil Microemulsions, Langmuir, 27 (2011) 2692-2700.

[12] M. Harms, S. Mackeben, C.C. Müller-Goymann, Thermotropic transition structures in the ternary system lecithin/isopropyl myristate/water, Colloids and Surfaces A: Physicochemical and Engineering Aspects, 259 (2005) 81-87.

[13] K.C. Pestana, T.P. Formariz, C.M. Franzini, V.H.V. Sarmento, L.A. Chiavacci, M.V. Scarpa, E.S.T. Egito, A.G. Oliveira, Oil-in-water lecithin-based microemulsions as a potential delivery system for amphotericin B, Colloids and Surfaces B: Biointerfaces, 66 (2008) 253-259.

[14] M. Changez, M. Varshney, J. Chander, A.K. Dinda, Effect of the composition of lecithin/n-propanol/isopropyl myristate/water microemulsions on barrier properties of mice skin for transdermal permeation of tetracaine hydrochloride: In vitro, Colloids and Surfaces B: Biointerfaces, 50 (2006) 18-25.
[15] B. Brime, M.A. Moreno, G. Frutos, M.P. Ballesteros, P. Frutos, Amphotericin B in oil-water lecithin-based microemulsions: Formulation and toxicity evaluation, J. Pharma. Sci., 91 (2002) 1178-1185.
[16] M.A. Moreno, M.P. Ballesteros, P. Frutos, Lecithin-based oil-in-water microemulsions for parenteral use: Pseudoternary phase diagrams, characterization and toxicity studies J. Pharma. Sci., 92 (2003) 1428-1437.
[17] J.S. Yuan, M. Ansari, M. Samaan, E.J. Acosta, Linker-based lecithin microemulsions for transdermal delivery of lidocaine Int. J. Pharm., 349 (2008) 130-143.
[18] J.S. Yuan, E.J. Acosta, Extended release of lidocaine from linker-based lecithin microemulsions, Int. J. Pharm., 368 (2009) 63-71.
[19] X.-Y. Xuan, Y.-L. Cheng, E. Acosta, Lecithin-Linker Microemulsion Gelatin Gels for Extended Drug Delivery, Pharmaceutics, 4 (2012) 104-129.
[20] S.C. McKarns, C. Hansch, W.S. Caldwell, W.T. Morgan, S.K. Moore, D.J. Doolittle, Correlation between Hydrophobicity of Short-Chain Aliphatic Alcohols and Their Ability to Alter Plasma Membrane Integrity, Fundamental Applied Toxicology, 36 (1997) 62-70.
[21] R.C. Rowe, P.J. Sheskey, S.C. Owen, Handbook of Pharmaceutical Excipients, 5th ed., Pharmaceutical Press and American Pharmacists Association, London, 2006.
[22] F. Comelles, A. Pascual, Microemulsions with Butyl Lactate as Cosurfactant, J. Disp. Sci. Technol., 18 (1996) 161-175.
[23] R. Saha, S. Rakshit, R.K. Mitra, S.K. Pal, Microstructure, Morphology, and Ultrafast Dynamics of a Novel Edible Microemulsion, Langmuir, 28 (2012) 8309-8317.
[24] R.K. Mitra, B.K. Paul, Physicochemical Studies on Mixed Surfactant Microemulsion Systems III. Phase behaviours of Microemulsions derived from a Nonionic Surfactant (Brij-56) and the influence of Ionic Surfactants, Cosurfactants, Oil, Temperature and Additives, J. Surf. Sci.Technol., 19 (2003) 139-158
[25] H. Kunieda, M. Yamagata, Mixing of nonionic surfactants at water-oil interfaces in microemulsions, Langmuir, 9 (1993) 3345-3351.
[26] M. Kahlweit, B. Faulhaber, G. Busse, Microemulsions with Mixtures of Nonionic and Ionic Amphiphiles, Langmuir, 10 (1994) 2528-2532.
[27] J.A. Silas, E.W. Kaler, R.M. Hill, Effect of Didodecyldimethylammonium Bromide on the Phase Behavior of Nonionic Surfactant−Silicone Oil Microemulsions, Langmuir, 17 (2001) 4534-4539.
[28] R.K. Mitra, B.K. Paul, Physicochemical investigations of microemulsification of eucalyptus oil and water using mixed surfactants (AOT + Brij-35) and butanol, J. Colloid Interface Sci., 283 (2005) 565-577.
[29] R.K. Mitra, B.K. Paul, Effect of Temperature and Salt on the Phase Behavior of Nonionic-Ionic Microemulsions with Fish-Tail Diagram, J. Colloid Interface Science, 291 (2005) 550-559.
[30] R.K. Mitra, B.K. Paul, Physicochemical investigations of (Anionic-Nonionic) Mixed Surfactant Microemulsions in Nonaqueous Polar Solvents: I Phase Behavior, Colloid Polym. Sci., 284 (2006) 733-744.
[31] D. Nandy, R.K. Mitra, B.K. Paul, Phase Behavior of the Mixtures of Polyoxyethylene(10) stearyl ether (Brij-76), 1-butanol, isooctane and Mixed Polar Solvents: I Water and Formamide (or N, N-dimethyl formamide), J. Colloid Interface Sci., 300 (2006) 361-367.
[32] S.A. Ostroumov, Biological Effects of Surfactants, CRC Press2005.
[33] F. Gennuso, C. Fernetti, C. Tirolo, N. Testa, F. L'Episcopo, S. Caniglia, M.C. Morale, J.D. Ostrow, L. Pascolo, C. Tiribelli, B. Marchetti, Bilirubin protects astrocytes from its own toxicity by inducing up-regulation and translocation of multidrug resistance-associated protein 1 (Mrp1) Proc. Natl. Acad. Sci. USA, 101 (2004) 2470-2475.

[34] A. Rajagopal, A.C. Pant, S.M. Simon, Y. Chen, In Vivo analysis of human multidrug resistance protein (MRP1) activity using transient expression of fluorescently Tagged MRP1, Cancer Res., 62 (2002) 391-396.
[35] H. Kunieda, A. Nakano, M.A. Pes, Effect of Oil on the Solubilization in Microemulsion Systems Including Nonionic Surfactant Mixtures, Langmuir, 11 (1995) 3302-3306.
[36] M. Kahlweit, Microemulsions, Science, 240 (1988) 617-621.
[37] P.A. Winsor, Hydrotropy, solubilisation and related emulsification processes, Trans. Faraday Soc., 44 (1948) 376-398.
[38] M.A. Pes, K. Aramaki, N. Nakamura, H. Kunieda, Temperature-Insensitive Microemulsions in a Sucrose Monoalkanoate System J. Colloid Interface Sci., 178 (1996) 666-672.
[39] M.A. Pes, H. Kunieda, Surfactant distribution in mixed surfactant microemulsions, Trends Phys. Chem., 5 (1995) 75-89.
[40] H. Kunieda, K. Shinoda, Evaluation of the hydrophile-lipophile balance (HLB) of nonionic surfactants. I. Multisurfactant systems, J. Colloid Interface Sci., 107 (1985) 107-121.
[41] X. Li, K. Ueda, H. Kunieda, Solubilization and Phase Behavior of Microemulsions with Mixed Anionic−Cationic Surfactants and Hexanol, Langmuir, 15 (1999) 7973-7979.
[42] N. Garti, Microemulsions as microreactors for food applications, Curr. Opinion Colloid Interface Sci., 8 (2003) 197-211.
[43] N. Garti, A. Yaghmur, M.E. Leser, V. Clement, H.J. Watzke, Improved Oil Solubilization in Oil/Water Food Grade Microemulsions in the Presence of Polyols and Ethanol, J. Agric. Food Chem., 49 (2001) 2552-2562.
[44] N. Garti, A. Yaghmur, A. Aserin, A. Spernath, R. Elfakess, S. Ezrahi, Solubilization of active molecules in microemulsions for improved environmental protection Colloids Surf. A: Physicochemical and Engineering Aspects, 230 (2003) 183-190.
[45] Z. Shervani, T.K. Jain, A. Maitra, Nonconventional lecithin gels in hydrocarbon oils, Colloid Polym. Sci., 269 ( 1991 ) 720-726
[46] V. Arcoleo, M. Goffredi, G. La Manna, V.T. Turco Liveri, F. Aliotta, Study of lecithin reverse micelles by FT-IR spectroscopy, Prog. Colloid Polym. Sci., 105 (1997) 220-223.
[47] A. Ruggirello, V.T. Liveri, FT-IR investigation of the urea state in lecithin and sodium bis(2-ethylhexyl)phosphate reversed micelles, J. Colloid Interface Sci., 258 (2003) 123-129.
[48] A. Maitra, T.K. Jain, Z. Shervani, Interfacial water structure in lecithin-oil-water reverse micelles Colloids Surf., 47 (1990) 255-267.
[49] G. Carvallaro, G. La Manna, V.T. Liveri, F. Aliotta, M.E. Fontanella, Structural Investigation of Water/Lecithin/Cyclohexane Microemulsions by FT-IR Spectroscopy, J. Colloid Interface Sci., 176 (1995) 281-285.
[50] S.A. Corcelli, J.L. Skinner, Infrared and Raman Line Shapes of Dilute HOD in Liquid H2O and D2O from 10 to 90 °C, J. Phys. Chem. A, 109 (2005) 6154-6165.
[51] A. Das, A. Patra, R.K. Mitra, Do the Physical Properties of Water in Mixed Reverse Micelles Follow a Synergistic Effect: A Spectroscopic Investigation, J. Phys. Chem. B, 117 (2013) 3593-3602.

# Chapter 7: Modification of Anionic Interface and Its effect on Enzyme Activity

## 7.1 Introduction

Reverse micelles have emerged as a potential nano-reactor system to mimic biological environment and to host many enzyme catalyzed reactions as enzymes can be sheltered and protected from the solvents within RMs[1-3]. The water molecules inside RM waterpool offer markedly different physical behaviour compared to those of the bulk owing to their confinement and interaction with the RM surface[4]; these physical properties could systematically be tuned by altering the interface charge type, extent of hydration ($w_0 = \frac{[water]}{[surfactant]}$), addition of electrolyte etc. Enzyme kinetics rate in RM depends upon several factors like the microenvironment in the surroundings of the enzyme and the substrate, the partitioning of the substrate between the RM droplets and the external solvent, surfactant concentration, their charge type, $w_0$ etc. There has been number of previous studies where the rate of enzyme kinetics in RM has been controlled by change of hydration number ($w_0$), surfactant concentration, substrate partition, pH of the buffer solution, salt concentration, temperature, nature of surfactant etc.[5-13], however, the possible role of hydration dynamics in governing such kind of reaction has rarely been addressed[14]. Moreover, most of the earlier studies were carried out with 1,4-bis(2-ethylhexyl)sulphosuccinate (AOT), a well-studied biocompatible anionic surfactant[15-17], that has been considered as a model system for micellar enzymology in hydrocarbon oils also[18-20]. There has been only limited number of efforts to introduce another variable in terms of mixing of surfactants to regulate the reaction kinetics[5, 21]. Also the biocompatibility of the hydrocarbon oils used in the earlier studies remains a major concern for biotechnological applications. To address this issue we have investigated the water structure, dynamics and rate of an enzyme catalysis reaction in mixed RM systems composed of anionic AOT and nonionic Brij surfactant(s) of varying hydrophilicity in a biocompatible oil, isopropyl myristate (IPM)[22]. The physical properties of water entrapped in RM water pool can be varied by simply tuning the surfactant charge type as well as its hydrophilic-lipophilic balance (HLB)[23] (HLB of a surfactant is a measure the extent of its hydrophilicity or lipophilicity and can be calculated following the definition by Griffin[24]). We have initiated a systematic approach to understand the altered hydration dynamics and activity in mixed RM systems[25-27]; it has been concluded that for an anionic-

nonionic mixed RM system, the activity can be tuned linearly[25], however, such a trend is not followed in a nonionic-nonionic mixed system in which partition of the substrate, which in turn is governed by the HLB, plays a key role in determining the reaction kinetics[27]. In the present investigation our aim is twofold: (i) to form stable AOT RMs using a biocompatible oil IPM and to modulate the interfacial charge type by doping Brij(s) of different HLB into it. In addition, we also investigate the change in the water structure and dynamics inside the mixed RM waterpool; (ii) to investigate an enzyme catalysis reaction in which α-chymotrypsin (CHT) cleaves the peptide linkage of the substrate Ala–Ala–Phe–7-amido-4-methyl-coumarin (AMC) in these mixed RMs and whether mixing of surfactants can serve as a regulator of the reaction kinetics. From previous studies[5, 20, 28, 29] it has been reported that at $w_0$=10 hydration level the activity and size for accommodation of enzyme CHT is optimum, therefore we choose this hydration level for enzymatic hydrolysis. In order to modulate the interfacial stoichiometry we have used three different Brij series of different hydrophilicity, namely Brij-30/Brij-35 (having 12 carbon alkyl units); Brij-52/Brij-58 (having 16 carbon alkyl units) and Brij-92/Brij-97 (having 18 carbon alkyl units); the corresponding polyethyleneoxide (PEO) units are 4 and 23; 2 and 20; 2 and 10, while their HLB values are 9.7, 16.9, 5.0, 16.0, 4.0 and 12.0, respectively. We replace AOT with the Brij(s) in the RM interface at a constant mole fraction of Brij [$X_{Brij} = \frac{n_{Brij}}{n_{AOT}+n_{Brij}}$] of 0.1 keeping the total surfactant concentration in oil fixed at 0.2 M. The sizes of the RM droplets are determined using dynamic light scattering (DLS) technique. Water structure inside RM is obtained using mid infrared FTIR spectroscopy technique while the dynamics of the entrapped water is estimated using time resolved fluorescence spectroscopy (TRFS) with ammonium 8-anilino-1-naphthalenesulfonate (ANS) as the emitting fluorophore.

## 7.2 Results and Discussions

***Solubilization Measurements:*** Water solubilization capacity (SC) is one of the most essential criteria of an RM from its application point of view. We measure the SC of the RMs and table 7.1 depicts the maximum values ($w_{0,max}$) of AOT and mixed surfactant RM systems in IPM. AOT forms RM with $w_{0,max}$ ~ 24. SC of AOT + Brij(s) mixed systems increases initially with increasing Brij content ($X_{Brij}$) and then decreases after passing through a maximum value ($X_{Brij,max}$). The observed optimum mixing ratios are $X_{Brij\text{-}30,max}$ = 0.2, $X_{Brij\text{-}35,max}$ = 0.05, $X_{Brij\text{-}52,max}$ = 0.3, $X_{Brij\text{-}58,max}$ = 0.05, $X_{Brij\text{-}92,max}$ = 0.3 and $X_{Brij\text{-}97,max}$ = 0.05 with the corresponding $w_{0,max}$ values of 33.0, 26.0, 43.2, 29.0, 33.3 and 30.0 respectively. $w_{0,max}$ and $X_{Brij,max}$ values are dependent on the HLB of the added nonionic surfactant. It has been observed that $X_{Brij,max}$

is a function of the size and composition of the head group of the added Brij(s)[30, 31]. Brij-35 (HLB ~ 16) is more hydrophilic than Brij-30 (HLB ~ 9.7) and consequently Brij-35 produces the solubilization maximum at a lower $X_{Brij,max}$ value compared to that in Brij-30. The same trend is also obtained for the Brij-52/Brij-58 and Brij-92/Brij-97 pairs. The synergism observed in the SC of mixed RMs can be explained in terms of the inter-droplet interaction and surfactant monolayer elasticity[30, 32]. IPM moderately penetrates at the RM interface, accordingly the interface becomes rigid which eventually reduces the inter-droplet interaction and thereby limits the SC[30, 33]. The interfacial bending stress of the rigid interface is relaxed by the incorporation of Brij molecules thereby accommodating more water, the extent of fluidity being dependent on the PEO chain length of the added Brij molecules. However, the induced fluidity on its turn increases the attractive interaction between the droplets and thereby limits the SC. The optimization of these two opposing effects determines the observed $X_{Brij,max}$ and $w_{0,max}$. Since Brij-97, Brij-35 and Brij-58 have larger number of PEO units they offer lower $X_{Brij,max}$ values.

***DLS Measurements:*** We estimate the size of the RM droplets using DLS technique assuming the droplets to be spherical in nature. It is found that the distribution is essentially mono-modal with the appearance of single peak for each of the studied systems. The estimated hydrodynamic diameters of the RMs are plotted as a function of $w_0$ in figure 7.1a. The observed droplet size of 9.3 nm at $w_0$=10 of AOT/IPM system is comparable to that obtained for AOT/hydrocarbon RM systems[26, 34]. It is observed that droplet size increases almost linearly with increasing $w_0$; this trend is indicative of the fact that with increasing $w_0$ the water content per micelle increases rather than the formation of new micelles. It is interesting to note that for $w_0$=10, the size of the droplets does not change appreciably for the low HLB Brijs (Brij-52 and -92), however, for the hydrophilic Brijs the size gets moderately increased, the effect being the most prominent in Brij-35 where a twofold increase in the size is observed (figure 7.1b). We estimate the aggregation number ($N_{agg}$) of the RMs using the methodology described in the supporting information section and is plotted

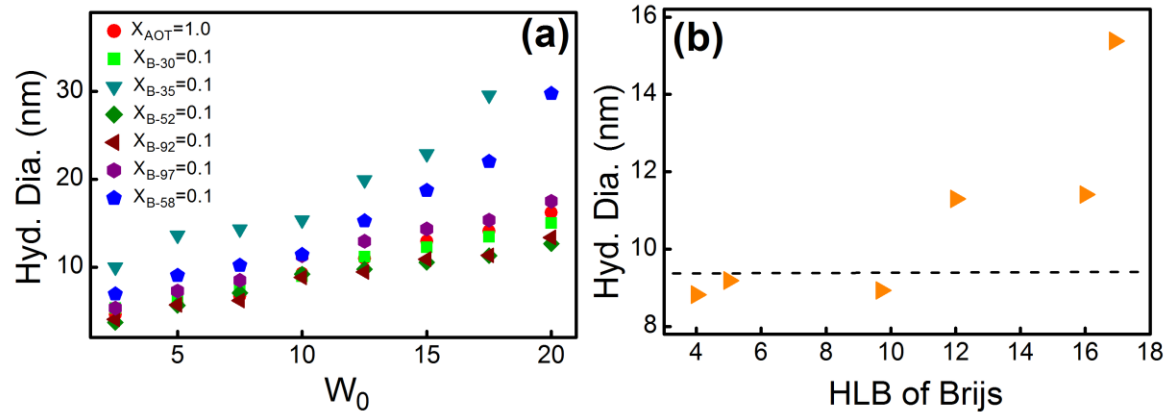


**Figure 7.1.** (a) Average hydrodynamic diameter of RMs at different water content ($w_0$). (b) The size of the mixed RM droplets at $w_0$=10 as a function of the HLB (Hydrophilic-lipophilic balance) of the added Brij. The dotted line represents the size of AOT/IPM RM.

as a function of water content ($w_0$) in figure 7.2. The aggregation number obtained for AOT RMs is in good agreement with previous studies [13]. $N_{agg}$ follows a trend comparable to that of the droplet size (figure 7.1a). It can be intuited that with the addition of Brij, the charge interaction at the interface gets reduced which eventually accommodates more surfactant molecules as has been also evidenced from the increase in the droplet size. The effect seems more prominent for high HLB number Brijs with larger PEO chains.

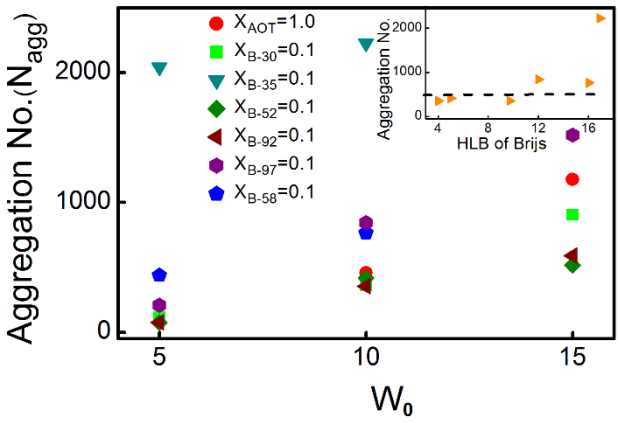


**Figure 7.2** Aggregation number of RMs at different water content ($w_0$). The inset shows the aggregation number of the mixed RMs as a function of the HLB of the added Brij. The dotted line is the aggregation number of the AOT/IPM RM system.

***FTIR Measurements:*** MIR FTIR is a potential tool to extract structural information of water encapsulated in RM nanopool[35-37]. Instead of pure water the use of HOD molecule as a probe has been shown to be advantageous, as the O–D band is decoupled from the O–H band and appears in a region (2200–2800 $cm^{-1}$) which is comparatively free from other strong

absorptions[38, 39]. The O–D stretching band reveals only the H-bonding interactions between water molecules as the intra-molecular interactions between the two OH (or OD) oscillators in $H_2O$ (or $D_2O$) molecules do not complicate the O–H (O–D) stretching band contour as observed for pure water[38]. The overall spectrum of pure water in this frequency window produces a smooth curve peaking at ~2508 $cm^{-1}$ (not shown). For RM systems, however, the curves get broadened and could be deconvoluted into three Gaussian sub-bands peaking at 2640±10, 2545±5 and 2450 $cm^{-1}$.

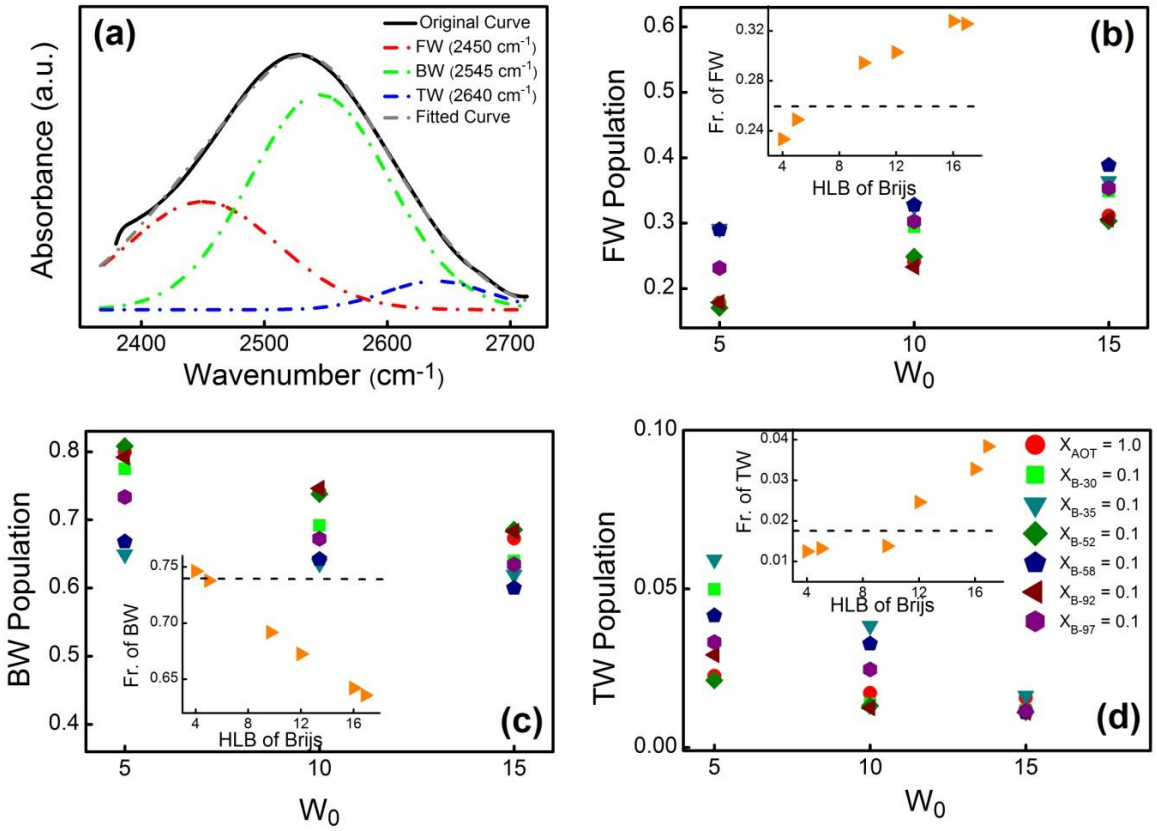


**Figure 7.3.** (a) FTIR spectrum of AOT/IPM RM system at $w_0$ = 10. The black line is the experimental curve. The spectrum is deconvoluted into three Gaussian curves peaking at 2450 $cm^{-1}$ (red), 2545 $cm^{-1}$ (green) and 2640 $cm^{-1}$(blue). The grey broken line represents the overall fit. Relative area under each deconvoluted curves as a function of $w_0$ for studied RM systems are plotted in (b-d). The insets of b-d show the corresponding relative area of the mixed RMs at $w_0$=10 as a function of the HLB of the added Brij. The dotted line of each plot is the relative area of the AOT/IPM RM system.

We deconvolute the MIR spectra of all the RM systems into these three Gaussian components and the relative area contribution of each curve are used to determine the abundance of different types of water species inside the waterpool[40]. A representative result of the deconvolution of AOT RM at $w_0$=10 is depicted in figure 7.3a. According to the 'three states model', the solubilized water in RMs can be identified as free water (FW), bound water (BW) and trapped

water (TW) molecules[40]. The FW molecules (~2450 $cm^{-1}$), occupying the cores of water pool of RMs, involve in strong hydrogen bonds with the neighbouring water molecules. The second component peaking at ~ 2545 $cm^{-1}$ involves the so-called 'bound water' (BW) which are unable to form fully developed hydrogen bonds and somewhat stuck to the surfactant head groups. The third type of water molecules absorbing in the high frequency region (~ 2640 $cm^{-1}$) are generally dispersed among the long hydrocarbon chains of surfactant molecules. We calculate the relative area contribution of each curve towards the total spectra and plot it as a function of $w_0$ (figure 7.3b-d). For understanding the effect of Brij inclusion on the entrapped water, we plot the abundance of each type of water as a function of the HLB number of the Brijs in the insets of the each corresponding plots.

We observe a high abundance of BW which is a characteristic feature of RMs [26, 41, 42]. The relative abundance of FW increases, while those of BW and TW decrease as the water content ($w_0$) increases which can be explained on the basis of increasing bulk water content in the RM droplets with increasing $w_0$ as has also been evidenced from the increase in the droplet size (figure 7.1a)[26]. Let us now consider the effect of inclusion of Brij(s) of different HLBs. It can be observed that except for the lowest HLBs (Brij-52 and -92), the water structure suffers considerable deviation from that of the AOT based RM system. The content of FW increases at the expense of a concomitant decrease in the BW content, while the content of TW is comparatively low and increases from ~2% to ~4% for HLB>10. This trend does not exactly follow the trend observed in the size distribution profile inferring that apart from the size of the droplets, the interaction of the surfactant head group with the embodied water molecules plays pivotal role in determining the physical properties of water. As Brij molecules are doped into the AOT interface, the ionic interaction is replaced by a feebler PEO-water interaction which in turn decreases the content of BW molecules and it follows a near linear dependency with the PEO content as well as the HLB of the added surfactant molecules.

***Fluorescence Measurements:*** Steady state and time resolved fluorescence are studied using ANS as the fluorophore which is a well-known probe to extract information of micro heterogeneous systems like RMs[43-47]. It is important to note that ANS is a well-known probe that can undergo twisted intramolecular charge transfer (TICT) upon photoexcitation[48] and hence its internal photophysics is not that straightforward. However, water inside RM is less polar and highly viscous compared to bulk water which minimizes the rate of non-radiative electron transfer process and thus the TICT process, if any, does not significantly affect the conclusions drawn from the fluorescence measurements[43]. Further support for such a

conclusion has also been obtained from the TRANES data (see later). ANS produces absorption maximum ($\lambda_{max}^{abs}$) (subtracted data of $\lambda_{max}^{abs}$ of dry ($w_0$~0) RM from those of the hydrated RMs) at 375 nm with a less intense shoulder at 350 nm in AOT/IPM RM at $w_0$=10 which is considerably red shifted compared to that in pure water (~350 nm) (figure 7.4a, inset). Figure 7.4b depicts the emission profile of ANS in the studied RM systems at $w_0$ = 10; ANS produces emission maximum ($\lambda_{max}^{em}$) at 515 nm in pure water and at 458 nm in dry AOT/IPM RM system ($w_0$ ~ 0). The hydrated AOT/IPM RM system at $w_0$ = 5 produces an emission peak at 470 nm which suffers a further red shift of ~4 nm at $w_0$=15 (figure 7.4a, table 7.1), the observed shift is in comparable agreement with AOT/heptane RM systems using the same probe[46, 47]. The red shift is due to the increased polarity of the waterpool since the relative population of bulk water increases at higher $w_0$ as has also been evidenced from FTIR studies (figure 7.3b). ANS, being an anionic probe, is expected to be contained in the core of the RM waterpool owing to the electrostatic repulsion with the sulfonate anionic head groups of AOT/IPM interface. At a fixed $w_0$ = 10, ANS produces an emission peak at 472 nm in AOT/IPM RM system, which suffers a red shift as Brij is added in the mixture [table 7.1, figure 7.4b (inset)]. A similar red shift has previously been reported by Liu et al.[47] when AOT/heptane interface is doped with Brijs. Decrease in the ionic character of the interface makes the ANS molecules to shift towards the interface and interacts with the polar PEO head group of Brij, the interaction being pronounced in hydrophilic Brijs and thus produces a larger red shift in the $\Delta\lambda_{max}^{em}$ (figure 7.4b, inset). In order to probe the dynamics of the encapsulated water, we study the time resolved emission spectroscopy. A representative emission decay transient of ANS at three different wavelengths in AOT/IPM RM at $w_0$=10 is shown in the inset of figure 7.4c. The decay transients of the probe in the blue end of the spectrum (410 nm) could be fitted with multiple decay components with time constants of 90 ps (64%), 1050 ps (25%) and 5200 ps (11%), whereas that in the red end (600 nm) could be fitted only by considering an added rise component of 1200 ps along with a decay component of 5900 ps. Such an observation is suggestive of the solvation of the probe[49] and we construct the corresponding time resolved emission spectra (a representative plot for AOT/IPM RM with $w_0$=10 is shown in figure 7.4c). From the TRES, we construct the corresponding solvent correlation function, C(t) following equation (2.11 in chapter 2). Some representative C(t) for the studied RM systems at $w_0$=10 are shown in figure 7.4e.

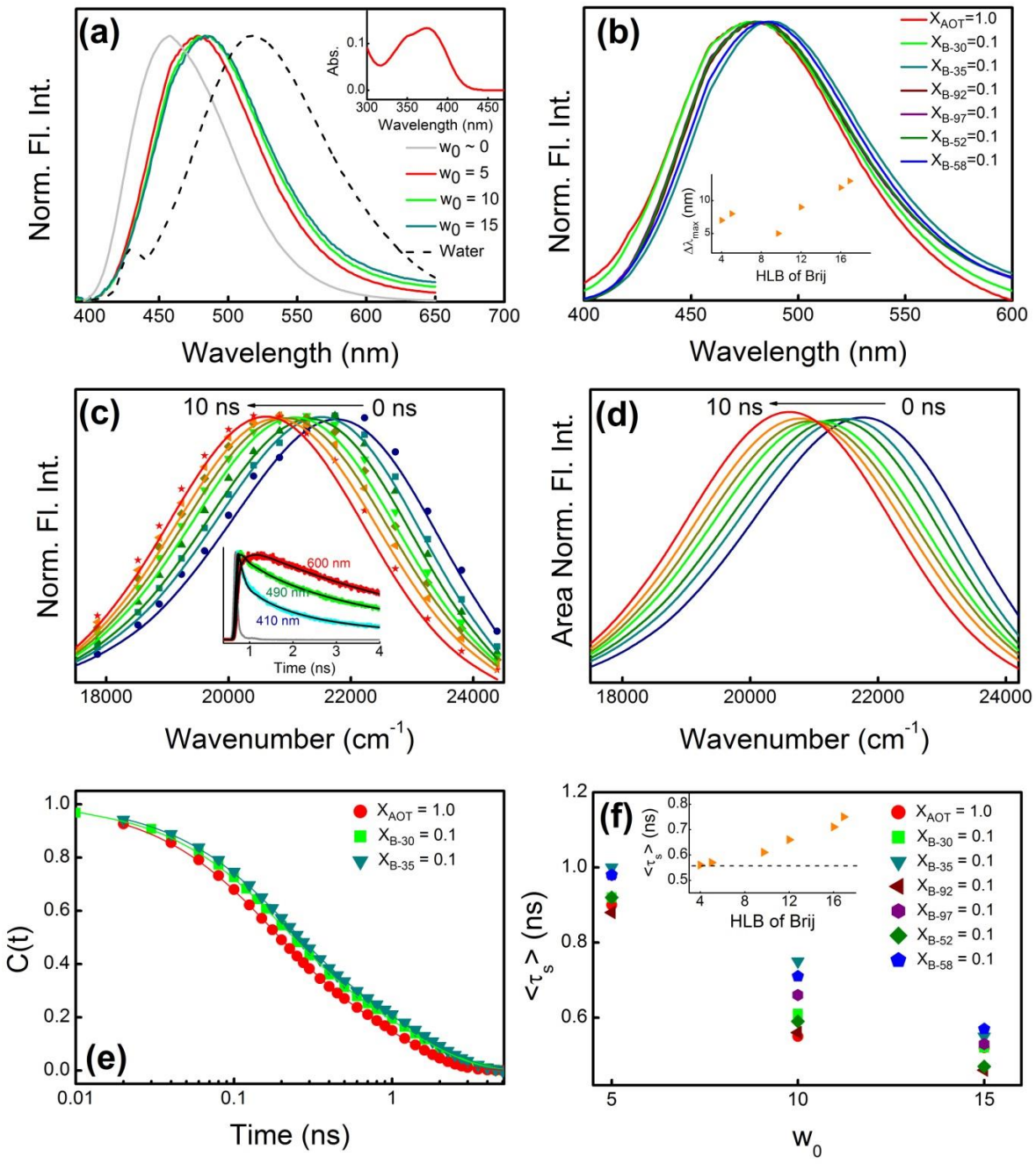


**Figure 7.3**: (a) Normalised emission spectra of ANS in AOT/IPM RM systems at different $w_0$. The inset shows the subtracted absorbance of ANS in AOT/IPM RM systems at $w_0$ = 10. (b) Normalised emission spectra of different RMs at $w_0$ =10. The inset shows $\Delta\lambda^{em}_{max}$ as a function of HLB of the added Brij. (c) Time resolved emission spectra (TRES) of ANS in AOT/IPM RM at $w_0$=10. The inset shows emission transients of ANS in AOT/IPM RM at $w_0$=10 at three different wavelengths. The solid lines are the multi-exponential fits. (d) Area normalized time resolved emission spectra (TRANES) of ANS in AOT/IPM RM at $w_0$=10. (e) Solvent correlation function, C(t) in different RMs at a fixed $w_0$ = 10. The solid lines are bi-exponential decay fits. (f) The average solvation time constant of ANS in the studied RM systems as a function of $w_0$. The inset shows the average solvation time at $w_0$=10 as a function of HLB of the added Brij while the broken line is that for AOT/IPM RM.

**Table 7.1.** Maximum solubilization capacity ($w_{0,max}$) and solvation dynamics parameters for ANS probe in AOT and different mixed RM systems at different $w_0$.

| $w_0$ | $\lambda^{em}_{max}$ (nm) | $\tau_1$ ($a_1$) (ns) | $\tau_2$ ($a_2$) (ns) | $< \tau_s >$ (ns) |
|---|---|---|---|---|
| **AOT ($w_{0,max}$ ~ 24)** | | | | |
| 5 | 470 | 0.17 (0.48) | 1.59 (0.52) | 0.90 |
| 10 | 472 | 0.19 (0.63) | 1.16 (0.37) | 0.55 |
| 15 | 474 | 0.20 (0.71) | 1.33 (0.29) | 0.52 |
| **$X_{Bj30}$ = 0.1 ($w_{0,max}$ ~ 29)** | | | | |
| 5 | 473 | 0.19 (0.48) | 1.59 (0.52) | 0.92 |
| 10 | 477 | 0.17 (0.57) | 1.20 (0.43) | 0.61 |
| 15 | 479 | 0.17 (0.68) | 1.11 (0.37) | 0.52 |
| **$X_{Bj35}$ = 0.1 ($w_{0,max}$ ~ 23)** | | | | |
| 5 | 478 | 0.21 (0.47) | 1.70 (0.53) | 1.0 |
| 10 | 485 | 0.19 (0.53) | 1.38 (0.47) | 0.75 |
| 15 | 487 | 0.16 (0.58) | 1.10 (0.42) | 0.55 |
| **$X_{Bj52}$ = 0.1 ($w_{0,max}$ ~ 29)** | | | | |
| 5 | 477 | 0.21 (0.59) | 1.95 (0.41) | 0.92 |
| 10 | 480 | 0.21 (0.69) | 1.37 (0.31) | 0.57 |
| 15 | 483 | 0.24 (0.77) | 1.24 (0.23) | 0.47 |
| **$X_{Bj58}$ = 0.1 ($w_{0,max}$ ~ 23)** | | | | |
| 5 | 478 | 0.21 (0.49) | 1.71 (0.51) | 0.98 |
| 10 | 484 | 0.19 (0.54) | 1.32 (0.46) | 0.71 |
| 15 | 486 | 0.18 (0.58) | 1.10 (0.42) | 0.57 |
| **$X_{Bj92}$ = 0.1 ($w_{0,max}$ ~ 30)** | | | | |
| 5 | 477 | 0.18 (0.48) | 1.53 (0.52) | 0.88 |
| 10 | 479 | 0.16 (0.53) | 1.02 (0.47) | 0.56 |
| 15 | 483 | 0.14 (0.58) | 0.90 (0.42) | 0.46 |
| **$X_{Bj97}$ = 0.1 ($w_{0,max}$ ~ 28)** | | | | |
| 5 | 478 | 0.18 (0.40) | 1.58 (0.60) | 0.98 |
| 10 | 481 | 0.18 (0.56) | 1.26 (0.44) | 0.66 |
| 15 | 486 | 0.16 (0.58) | 1.05 (0.42) | 0.53 |

All the C(t) curves are fitted with bi-exponential decay model and the corresponding time constants are summarized in table 7.1. We calculate the average time constant, $< \boldsymbol{\tau_{solv}} >= \sum_i \boldsymbol{a_i \tau_i}$ . In order to check whether the observed time resolved spectral shift is associated with any internal photo-physics of the probe itself we construct the time-resolved area normalized

emission spectra (TRANES)[50]; a representative plot is shown in figure 7.4d. No iso-emissive point appears in the TRANES profile indicating the absence of multiple species of the probe and affirms the fact that the probe remains as a single 'species' only. Therefore, the observed time dependent spectral shift can be attributed solely to the inhomogeneity of the microenvironment experienced by the probe. This study also excludes any possible TICT in ANS which is frequently observed in bulk solvents[48]. It is important to note that because of the limited instrument resolution of the present investigation (IRF = 80 ps) we fail to detect an ultrafast component of fluorescence signal resulting from the rotational motion of bulk like water at the waterpool which occurs in sub-ps time scale[4]. It is, however, important to note that the enzyme catalysis reaction takes place mostly at the RM interface[20] wherein the water molecules are somewhat restricted and slow, and thus, while correlating the water dynamics with the enzyme activity, one can safely ignore the contribution from the ultrafast fluorescence signals. We determine the loss in the dynamic Stokes shift using the procedure developed by Fee and Maroncelli[51] where $\nu^{p}_{em}(0)$ can be calculated by the following equation:

$$\boldsymbol{\nu^{p}_{em}(0) = \nu^{p}_{abs} - [\nu^{np}_{abs} - \nu^{np}_{em}]} \qquad (7.1)$$

where $\nu^{p}_{abs}$, $\nu^{np}_{abs}$, and $\nu^{np}_{em}$ are the absorption peak of ANS in polar solvent, absorption peak in nonpolar solvent, and emission peak in nonpolar solvent, respectively. We use AOT/IPM $w_0$~0 as the nonpolar solvent (as ANS is insoluble in IPM) with absorption and emission maxima occurring at 370 and 458 nm, respectively. Water is used as the polar solvent in which ANS produces an absorption peak at 350 nm and emission peak at 515 nm. We calculate a 33% loss in the dynamical Stokes shift for $w_0$ = 5 which then increases to 50% for $w_0$ = 10-15. At $w_0$=5, most of the water molecules solvate the interface and hence less bulk water is present resulting in an overall slower dynamics. As $w_0$ increases, more 'bulk' like water molecules surround the probe resulting in a greater loss in the dynamical stoke shift. For the mixed systems the loss is relatively small; for the hydrophobic Brijs the loss is 30-40% while for the hydrophilic Brijs the loss is further small (15-30%) at $w_0$=10. This indicates the relocation of the probe in the vicinity of the interface in the high HLB Brij systems.

We plot $<\tau_s>$ as a function of $w_0$ for all the systems in figure 7.4f. It is evident that at a fixed composition, solvation dynamics gets faster with increasing $w_0$. We discuss the observed trend in $w_0$=10 system in details as the enzyme kinetics measurements are carried out at this fixed hydration. For a better comparison we plot $<\tau_s>$ as a function of HLB number of the

added Brij in the inset of plot 4f. For the hydrophobic Brijs, the solvation dynamics is more or less comparable to that in AOT/IPM RM while for the hydrophilic Brijs it gets noticeably retarded. It is important to note here that while discussing the solvation dynamics in restricted systems one needs to consider several factors, like the size of the RM droplets (and hence the abundance of FW) and the location of the probe inside the RM. The sizes of the RMs composed of the relatively hydrophilic Brijs are bigger comparable to that of AOT RM (figure 7.1a) and so also the relative abundance of FW is higher (figure 7.3). Hence the size factor itself does not suffice to explain the observed retarded dynamics of these RMs. The observed retardation in dynamics with HLB is also in lieu of the decreasing content of BW (figure 7.3c). To explain this apparent ambiguity one has also to consider the location of the probe in the waterpool and the microenvironment it experiences including a possible solvation by the PEO chains. Addition of Brij reduces the negative charge density at the RM interface which induces a larger population of ANS to relocate themselves in the vicinity of the interface (which also receives support from the increased fluorescence signal recovery and consequently to report a retarded dynamics). The observed overall dynamics is an optimization between these two opposing factors. For the hydrophobic Brijs, the PEO chains are less in number to offer only marginal effect in the charge screening eventually resulting in a subtle change in the dynamics. For the hydrophilic Brijs, however, the charge screening is considerable to overwhelm the effect of increasing droplet size and increasing FW contribution to make the dynamics eventually retarded.

The FTIR study thus reveals an increase in the content of FW with increasing hydrophilicity of the Brij added. It could be inferred that it is the inclusion of Brij head group in the AOT interface that causes the reduced abundance of BW. Such a conclusion is also supported by the TRFS study using ANS as the fluorophore. With this background we investigate the enzyme kinetics in the mixed RM systems.

***Enzyme kinetics study:*** We study the hydrolysis of AMC catalysed by CHT [scheme 7.1], a well-known serine protease globular protein with a molar mass of 24.8 kDa and dimension of $4.0 \times 4.0 \times 5.1$ nm$^3$ [28] that selectively cleaves the peptide bond of amino acids in protein[52]. The dimension of the protein is larger than the RM water pool diameter at $w_0$=10 and thus is suitable to be solubilized in both AOT and the mixed RM systems.

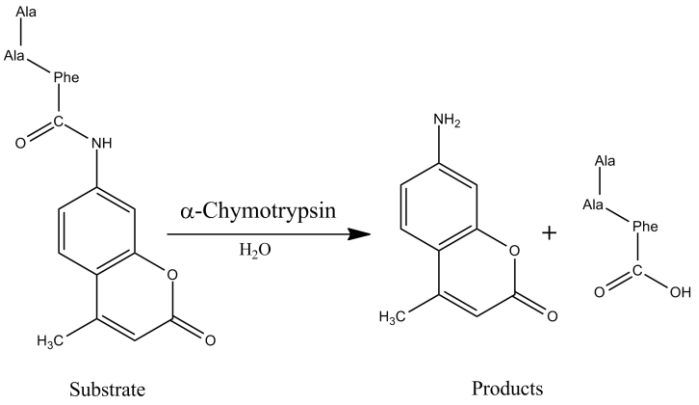


**Scheme 7.1.** The splitting of the substrate (AMC) with α-chymotrypsin.

Upon hydrolysis, the peptide sequence containing phenylalanine (Phe) is cleaved from AMC. The product 7-amino-4-methylcoumarin shows an absorption peak at 370 nm (figure 7.5a). We determine the initial reaction rate from the slope of the product absorption vs. time profile at different substrate concentrations fixing the enzyme concentration to 16 μg/ml. In a representative kinetic profile the concentration of the product (measured from the absorbance at 370 nm) as a function of time for different systems (water and RMs) with 25 μM AMC and 16 μg/ml CHT are shown in figure 7.5b. The measured initial reaction rates for all the systems are plotted as a function of the substrate concentration in figure 7.5c. The temporal changes in the product absorption in RM are found to be distinctly smaller compared to that in pure water. However, the variations in the slopes for the different RM systems at $w_0$=10 are distinguishable as observed from figure 7.5b,d. The observed rates also vary with the type of Brij added. It is clearly evident that the rate of enzyme hydrolysis for Brij-35 containing system (HLB=16.9) is distinctly small compared to that of the other mixed systems, and the difference increases with the increase in the substrate concentration. It has been reported earlier that the velocity of enzymatic reaction in RM is about two orders of magnitude slower than that in the buffer solution[20]. Keeping in mind that the global structure of CHT is not expected to change in any of the studied RM systems as the waterpool sizes are larger than the protein itself, the observed change in the kinetics is caused either by the modification of water nucleophilicity inside the mixed RMs and/or the partitioning of the substrate population in the organic and aqueous phases in the mixed RM. We observe that when Brijs with smaller HLB (Brij-52 and -92) are doped into the AOT interface the initial rate increases, whereas Brijs with higher HLB

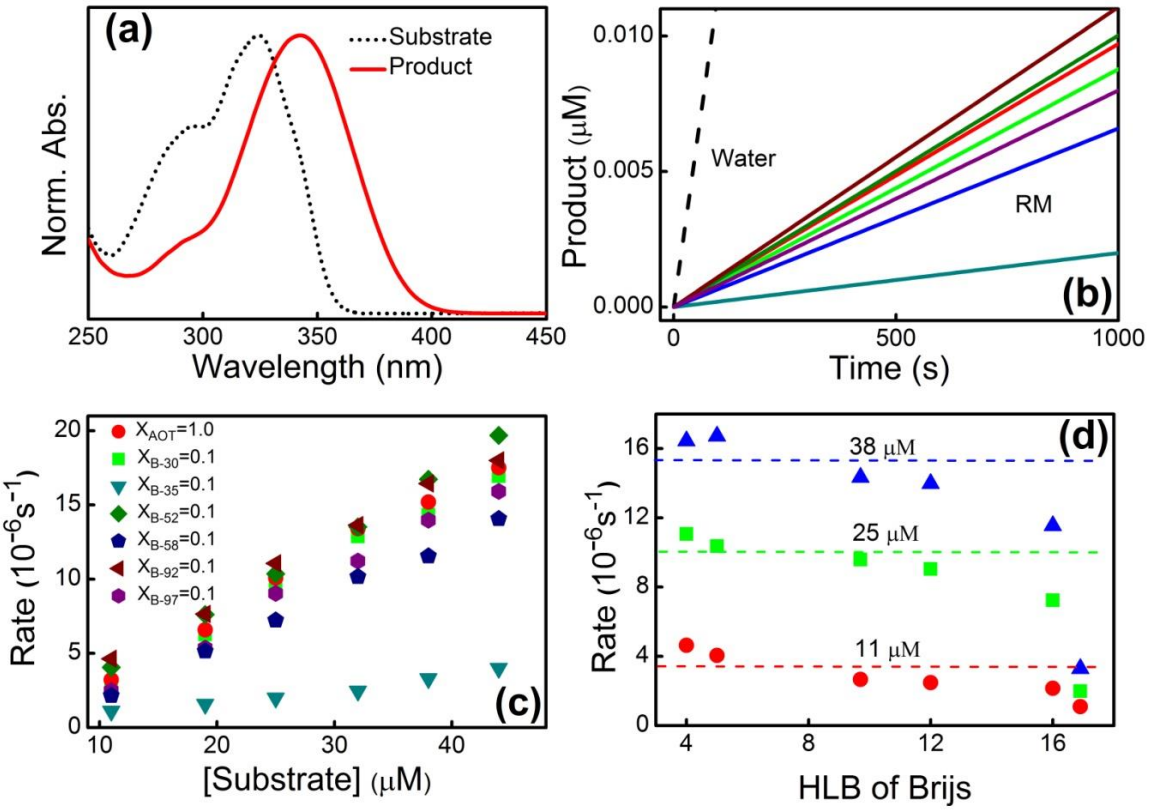


**Figure 7.5.** (a) Normalizd absorption spectra of the substrate and the product. (b) Representative kinetics plots for enzymatic hydrolysis reaction of 25μM AMC by CHT (16 μg/ml)) in different RM systems and in water. (c) Initial reaction rate in the studied RM systems as a function of the substrate (AMC) concentration. (d) Rate of reaction as a function of HLB number of the added Brijs at three different substrate concentrations of 11, 25 and 38 μM. The dotted lines are the rate obtained in AOT/IPM RM at the corresponding substrate concentration and all the kinetics measurement in RM have been carried out at fixed $w_0$=10.

decrease the rate and the decrease is drastic in Brij-35 containing system. This makes the mixed system a perfect biocompatible tool in which reactivity can be regulated and even be enhanced. The catalytic activity of CHT in RM systems is a well-studied phenomenon[19, 20, 53-55], however, less importance has been paid on the mixing of surfactant at the interface[21] as a possible regulator of the reaction[14] and also an enhancement in the activity has not been observed earlier. The peptide cleavage by CHT essentially occurs through a catalytic triad composed of Ser195, His57 and Asp102 in which water acts as a nucleophile to cleave the acyl-enzyme intermediate complex[56]. Several factors contribute to the rate of the reaction, viz. change in the polarity of the entrapped water which eventually affects the apparent $pK_a$ at the active site of the enzyme[57], or, interaction of the RM interface with the enzymes making it less mobile[18, 58], or reduced substrate inhibition[59] etc. Since AMC is sparingly soluble in hydrocarbons but soluble in the RM the catalysis reaction essentially takes place at the interface[20]. Earlier studies have confirmed that encapsulation of CHT in RM waterpool does

not significantly alter the tertiary structure of CHT[60, 61]. Thus the rate of the reaction is primarily governed by the protein-substrate interaction and the physical properties of water at the interface. The dynamic equilibrium between the BW and FW present in the restricted environments plays a key role in determining the kinetics of simple nucleophilic reactions in such systems[62, 63]. Since the reaction takes place at the interface, unlike in pure water, it is the water structure at the interface, specially the BW that eventually plays the key role in regulating the kinetics. FTIR and TRFS studies have revealed that the relative population of such 'nucleophile' water is relatively less and consequently the kinetics is slower in the AOT/hydrophilic Brij systems compared to the AOT RM itself. On the other hand, AOT/Brij-52 and -92 systems have comparable size as well as comparable abundance of BW and thus the increased rate of hydrolysis in these systems can only be explained on the basis of enzyme-substrate interaction. Perhaps the partially reduced charge of AOT by Brijs make the CHT-AMC interaction more viable compared to that in ionic AOT RM. In order to explain the highly reduced activity in Brij-35 systems, one has to consider an additional factor in the form of the size of the RM droplet which is relatively large for the AOT/Brij-35 system (figure 7.1b). The big droplet size could induce an increased rotational freedom of the encapsulated CHT[29, 64], thereby partially decreasing the approachability of the substrate to the enzyme active site. As a result the enzyme hydrolysis rate decreases severely for Brij-35 containing system relative to the other mixed systems as shown in figure 7.5d. This argument receives support from previous studies in which a bell shaped $w_0$ vs. activity profile has been reported with the maximum being observed at $w_0$=10 as this hydration level provides with the perfect size to accommodate CHT[28, 29].

## 7.3 Conclusion

Reports on the formation of stable AOT RMs using a biocompatible oil IPM is available in the literature[30, 33] however, the physical properties of the entrapped water in these RMs have not been properly known. Our study concludes that the physical properties of water are comparable to that in the RMs formed in conventional hydrocarbon oils[26, 34]. We have modified the interfacial charge type of AOT RM with the incorporation of non-ionic Brij surfactants of different HLBs into it and studied the altered structure and dynamics of entrapped water in these mixed RMs. It was observed that addition of rather low HLB Brijs offers only marginal effect on the size of the RM droplets as well as aggregation number, whereas, high

HLB Brijs induce considerable enlargement of the droplet size. FTIR studies conclude that the relative abundance of free water increases with increasing HLB with a concomitant decrease in the content of bound water. Time resolved fluorescence measurements, however, show an apparently surprising result as the dynamics get retarded with addition of high HLB Brijs, which in turn can be explained by considering the relocation of the probe near the interface as the PEO head groups of Brijs populate the interface reducing the effective charge of the AOT head group.

The second major objective was to underline the change in the activity of entrapped water upon mixing of surfactants and for that we have studied the enzymatic hydrolysis of AMC catalysed by CHT in different mixed RMs. Enzymatic activity in RMs have been reported to be dependent on various physical parameters of the RM[5-13], however, our study was aimed to open a new and easy avenue to regulate the reactivity. We found that the activity increases with the addition of low HLB Brijs while it decreases with high HLB Brijs and hence the enzyme kinetics in mixed RM system can be tuned by simply varying with HLB number of non-ionic Brij surfactant keeping the other parameters unaltered. Our study thus provides a new route to regulate and even to enhance the reaction rate in RM systems according to the purpose and could be found useful for future applications taking into consideration the non-toxicity of the components involved.

## 7.4 References

[1] M.P. Pileni, Reverse micelles as microreactors J. Phys Chem., 97 (1993) 6961-6973.
[2] M.A. Biasutti, E.B. Abuin , J.J. Silber, N.M. Correa, E.A. Lissi, Kinetics of reactions catalyzed by enzymes in solutions of surfactants, Adv. Colloid Interface Sci., 136 (2008) 1-24.
[3] P.L. Luisi, B. Steinmann-Hofmann, Activity and conformation of enzymes in reverse micellar solutions, Methods in Enzymology, 136 (1987) 188-216.
[4] N.E. Levinger, Water in confinement Science, 298 (2002) 1722-1723.
[5] S.K. Verma, K.K. Ghosh, Activity, stability and kinetic parameters for α-chymotrypsin catalysed reactions in AOT/isooctane reverse micelles with nonionic and zwitterionic mixed surfactants, J. Chem. Sci., 125 (2013) 875-882.
[6] N.W. Fadnavis, R.L. Babu, A. Deshpande, Reactivity of trypsin in reverse micelles: pH-effects on the W0 versus enzyme activity profiles, Biochimie, 80 (1998) 1025-1030.
[7] C. Will Chen, C.-W. Yeh, Kinetic model for enzymatic hydrolysis in reverse micelles, Biotechnology Letters, 20 (1998) 49-52.
[8] S. Piera-Velázquez, F. Marhuenda-Egea, E. Cadenas, The dependence of a halophilic malate dehydrogenase on ωo and surfactant concentration in reverse micelles, Journal of Molecular Catalysis B: Enzymatic, 13 (2001) 49-55.
[9] H. Hirakawa, N. Kamiya, T. Yata, T. Nagamune, Regioselective reduction of a steroid in a reversed micellar system with enzymatic NADH-regeneration, Biochemical Engineering Journal, 16 (2003) 35-40.

[10] E. Franqueville, H. Stamatis, H. Loutrari, A. Friboulet, F. Kolisis, Studies on the catalytic behaviour of a cholinesterase-like abzyme in an AOT microemulsion system, Journal of Biotechnology, 97 (2002) 177-182.
[11] A.V. Puchkaev, A.P. Vlasov, D.I. Metelitza, Stability of Glucose 6-Phosphate Dehydrogenase Complexed with Its Substrate or Cofactor in Aqueous and Micellar Environment, Applied Biochemistry and Microbiology, 38 (2002) 36-44.
[12] L.F. Aguilar, E. Abuin, E. Lissi, A Procedure for the Joint Evaluation of Substrate Partitioning and Kinetic Parameters for Reactions Catalyzed by Enzymes in Reverse Micellar Solutions: I. Hydrolysis of 2-Naphthyl Acetate Catalyzed by Lipase in Sodium 1,4-Bis(2-ethylhexyl) Sulfosuccinate (AOT)/Buffer/Heptane, Archives of Biochemistry and Biophysics, 388 (2001) 231-236.
[13] Y. Zhang, X. Huang, G. Ji, Y. Li, W. Liu, Y. Qu, Activity and kinetics studies of yeast alcohol dehydrogenase in a reverse micelle formulated from functional surfactants, cent.eur.j.chem., 7 (2009) 787-793.
[14] S. Rakshit, R. Saha, S.K. Pal, Modulation of Environmental Dynamics at the Active Site and Activity of an Enzyme under Nanoscopic Con fi nement: Subtilisin Carlsberg in Anionic AOT Reverse Micelle, J. Phys. Chem. B, 117 (2013) 11565 − 11574.
[15] J. Bhattacharjee, G. Verma, V. Aswal, V. Patravale, P. Hassan, Microstructure, drug binding and cytotoxicity of pluronic P123–aerosol OT mixed micelles, RSC Advances, 3 (2013) 23080-23089.
[16] R.R. Gupta, S.K. Jain, M. Varshney, AOT water-in-oil microemulsions as a penetration enhancer in transdermal drug delivery of 5-fluorouracil, Colloids and Surfaces B: Biointerfaces, 41 (2005) 25-32.
[17] H. Liu, S. Li, Y. Wang, F. Han, Y. Dong, Bicontinuous water-AOT/Tween85-isopropyl myristate microemulsion: A new vehicle for transdermal delivery of cyclosporin A, Drug development and industrial pharmacy, 32 (2006) 549-557.
[18] S. Barbaric, P.L. Luisi, Micellar solubilization of biopolymers in organic solvents. 5. Activity and conformation of α-chymotrypsin in isooctane-AOT reverse micelles, J. Am. Chem. Soc., 103 (1981) 4239-4244.
[19] R.D. Falcone, M.A. Biasutti, N.M. Correa, J.J. Silber, E. Lissi, E. Abuin, Effect of the Addition of a Nonaqueous Polar Solvent (Glycerol) on Enzymatic Catalysis in Reverse Micelles. Hydrolysis of 2-Naphthyl Acetate by a -Chymotrypsin, Langmuir, 20 (2004) 5732 - 5737.
[20] R. Biswas, S.K. Pal, Caging enzyme function: a-chymotrypsin in reverse micelle, Chem. Phys. Lett., 387 (2004) 221-226.
[21] K.S. Freeman, S.S. Lee, D.J. Kiserow, L.B. McGown, Increased Chymotrypsin Activity in AOT/Bile Salt Reversed Micelles, J.Colloid and Interface Science, 207 (1998) 344-348.
[22] R.C. Rowe, P.J. Sheskey, S.C. Owen, Handbook of Pharmaceutical Excipients, 5th ed., Pharmaceutical Press and American Pharmacists Association, London, 2006.
[23] H. Kunieda, K. Shinoda, Evaluation of the hydrophile-lipophile balance (HLB) of nonionic surfactants. I. Multisurfactant systems, Journal of Colloid and Interface Science, 107 (1985) 107-121.
[24] W.C. Griffin, Classification of surface-active agents by" HLB", J Soc Cosmetic Chemists, 1 (1946) 311-326.
[25] R.K. Mitra, S.S. Sinha, P.K. Verma, S.K. Pal, Modulation of Dynamics and Reactivity of Water in Reverse Micelles of Mixed Surfactants J. Phys. Chem. B, 112 (2008) 12946-12953.
[26] A. Das, A. Patra, R.K. Mitra, Do the Physical Properties of Water in Mixed Reverse Micelles Follow a Synergistic Effect: A Spectroscopic Investigation, J. Phys. Chem. B, 117 (2013) 3593-3602.
[27] A. Das, R.K. Mitra, Does the Optimum Hydrophilic Lipophilic Balance Condition Affect the Physical Properties of Mixed Reverse Micelles: A Spectroscopic Investigation, J. Phys. Chem. B 118 (2014) 5488−5498.
[28] A.L. Creagh, J.M. Prausnitz, H.W. Blanch, Structural and catalytic properties of enzymes in reverse micelles., Enzyme Microb Technol., 15 (1993) 383-392.
[29] M. Hirai, T. Takizawa, S. Yabuki, R.K. Hirai, K. Nakamura, M. Oya, K. Kobayashi, Y. Ameniya, Structure and reactivity of aerosol-OT reversed micelles containing a-chymotrypsin., J.Chem.Soc., Faraday Transactions, 91 (1995) 1081-1089.

[30] B.K. Paul, R.K. Mitra, Water solubilization capacity of mixed reverse micelles: Effect of surfactant component, the nature of the oil, and electrolyte concentration, J. Colloid Interface Sci., 288 (2005) 261-279.
[31] K. Kundu, B.K. Paul, Effect of Polyoxyethylene Type Nonionic Surfactant and Polar Lipophilic Oil on Solubilization of Mixed Surfactant Microemulsion Systems, J. Chem. Eng. Data, 58 (2013) 2668-2676.
[32] M.J. Hou, D.O. Shah, Effects of the molecular structure of the interface and continuous phase on solubilization of water in water/oil microemulsions, Langmuir, 3 (1987) 1086-1096.
[33] R.K. Mitra, B.K. Paul, Effect of NaCl and temperature on the water solubilization behavior of AOT/nonionics mixed reverse micellar systems stabilized in IPM oil, Colloids and Surfaces A, 255 (2005) 165-180.
[34] R.K. Mitra, S.S. Sinha, S.K. Pal, Temperature-Dependent Solvation Dynamics of Water in Sodium Bis(2-ethylhexyl)sulfosuccinate/Isooctane Reverse Micelles, Langmuir, 24 (2008) 49-56.
[35] A.M. Durantini, R.D. Falcone, J.J. Silber, N.M. Correa, Effect of the Constrained Environment on the Interactions between the Surfactant and Different Polar Solvents Encapsulated within AOT Reverse Micelles, ChemPhysChem, 10 (2009) 2034–2040.
[36] G. Calvaruso, A. Minore, V.T. Liveri, FT-IR Investigation of the Urea State in AOT Reversed Micelles, J. Colloid Interface Sci., 243 (2001) 227-232.
[37] E. Odella, R. Darı´o Falcone, J.J. Silber, N.M. Correa, How TOPO affects the interface of the novel mixed water/AOT:TOPO/n-heptane reverse micelles: dynamic light scattering and Fourier transform infrared spectroscopy studies, Phys. Chem. Chem. Phys., 16 (2014) 15457-15468.
[38] L.P. Novaki, N.M. Correa, J.J. Silber, O.A. El Seoud, FTIR and 1H NMR Studies of the Solubilization of Pure and Aqueous 1,2-Ethanediol in the Reverse Aggregates of Aerosol-OT, Langmuir, 16 (2000) 5573-5578.
[39] L.P. Novaki, P.A.R. Pires, O.A. El Seoud, Fourier transform-IR and 1H NMR studies on the structure of water solubilized by reverse aggregates of calcium bis(2-ethylhexyl) sulfosuccinate in organic solvents, Colloid Polym. Sci., 178 (2000) 143-149.
[40] S. Bardhan, K. Kundu, S. Das, M. Poddar, S.K. Saha, B.K. Paul, Formation, thermodynamic properties, microstructures and antimicrobial activity of mixed cationic/non-ionic surfactant microemulsions with isopropyl myristate as oil, J. Colloid Interface Sci., 430 (2014 ) 129-139.
[41] Q. Li, T. Li, J. Wu, N. Zhou, Comparative Study on the Structure of Water in Reverse Micelles Stabilized with Sodium Bis(2-ethylhexyl) Sulfosuccinate or Sodium Bis(2-ethylhexyl) Phosphate in n-Heptane, J. Colloid Interface Sci., 229 (2000) 298-302.
[42] N. Zhou, Q. Li, J. Wu, J. Chen, S. Weng, G. Xu, Spectroscopic Characterization of Solubilized Water in Reversed Micelles and Microemulsions: Sodium Bis(2-ethylhexyl) Sulfosuccinate and Sodium Bis(2-ethylhexyl) Phosphate in n-Heptane, Langmuir, 17 ( 2001) 4505-4509.
[43] J. Zhang, F.V. Bright, Nanosecond reorganization of water within the interior of reversed micelles revealed by frequency-domain fluorescence spectroscopy, J. Phys. Chem., 95 (1991) 7900-7907.
[44] S.S. Narayanan, S.S. Sinha, R. Sarkar, S.K. Pal, Validation and divergence of the activation energy barrier crossing transition at AOT/lecithin reverse micellar interface, J. Phys. Chem. B, 112 (2008) 2859.
[45] A. Patra, T.Q. Luong, R.K. Mitra, M. Havenith, Influence of Charge on the Structure and Dynamics of Water Encapsulated in Reverse Micelles, Phys. Chem. Chem. Phys., 16 (2014) 12875-12883.
[46] K.M. Glenn, R.M. Palepu, Fluorescence probing of aerosol OT based reverse micelles and microemulsions in n-alkanes (C6-C16) and quenching of Safranine-T in these systems, J. Photochem. Photobiol. A: Chem., 179 (2006) 283-288.
[47] D. Liu, J. Ma, H. Cheng, Z. Zhao, Fluorescence probing of mixed reverse micelles formed with AOT and nonionic surfactants in n-heptane, Colloids and Surfaces A: Physicochemical and Engineering Aspects, 139 (1998) 21-26.
[48] E.M. Kosower, Acc. Chem. Res., 15 (1982) 259-266.
[49] M. Maroncelli, G.R. Fleming, Picosecond solvation dynamics of coumarin 153: the importance of molecular aspects of solvation, J. Chem. Phys., 86 (1987) 6221-6238.

[50] A.S.R. Koti, M.M.G. Krishna, N. Periasamy, Time-resolved area-normalized emission spectroscopy (TRANES): A novel method for confirming emission from two excited states, J. Phys. Chem. A, 105 (2001) 1767-1771.
[51] R.S. Fee, M. Maroncelli, Estimating the time-zero spectrum in time-resolved emmsion measurements of solvation dynamics, Chemical Physics, 183 (1994) 235-247.
[52] Q. Chen, K.G. Rausch, H. Schçnherr, G.J. Vancso, α-Chymotrypsin-Catalyzed Reaction Confined in Block-Copolymer Vesicles, ChemPhysChem, 11 (2010) 3534 - 3540.
[53] E. Ruckenstein, P. Karpe, Enzymatic super- and subactivity in nonionic reverse micelles, J. Phys. Chem., 95 (1991) 4869-4882.
[54] M.L.M. Serralheiro, J.M.S. Cabral, Irreversible thermoinactivation of α-chymotrypsin in buffer and water miscible organic solvent. Comparison with a reverse micellar system, J. Mol. Cat. B: Enzymatic, 7 (1999) 191-205.
[55] R.V. Rariy, N. Bec, N.L. Klyachko, A.V. Levashov, C. Balny, Thermobarostability of α-chymotrypsin in reversed micelles of aerosol OT in octane solvated by water-glycerol mixtures, Biotechnol. Bioeng., 57 (1998) 552-556.
[56] J.M. Berg, J.L. Tymoczko, L. Stryer, Biochemistry, Sixth ed., W.H. Freeman2006.
[57] C. Grandi, R.E. Smith, P.L. Luisi, Micellar solubilization of biopolymers in organic solvents. Activity and conformation of lysozyme in isooctane reverse micelles, J. Biol. Chem., 256 (1981) 837-843.
[58] C. Laane, R. Hilhorst, C. Veeger, Design of reversed micellar media for the enzymatic synthesis of apolar compounds, Methods Enzymol., 136 (1987) 216-229.
[59] P.D.I. Fletcher, B.H. Robinson, R.B. Freedman, C. Oldfield, Activity of lipase in water-in-oil microemulsions, J. Chem. Soc., Faraday Trans. 1, 81 (1985) 2667-2679.
[60] A.V. Levashov, Y.L. Khmelnitsky, N.L. Klyachko, V.Y. Chernyak, K. Martinek, Ultracentrifugation of reversed micelles in organic solvent: New approach to determination of molecular weight and effective size of proteins, Anal. Biochem., 118 (1981) 42-46.
[61] P.D.I. Fletcher, R.B. Freedman, J. Mead, C. Oldfield, B.H. Robinson, Reactivity of α-chymotrypsin in water-in-oil microemulsions, Colloids Surf., 10 (1984) 193-203.
[62] P.K. Verma, A. Makhal, R.K. Mitra, S.K. Pal, Role of Solvation Dynamics in the Kinetics of Solvolysis Reactions in Microreactors, Phys. Chem. Chem. Phys., 11 (2009) 8467-8476.
[63] P.K. Verma, R.K. Mitra, S.K. Pal, A Molecular Picture of Diffusion Controlled Reaction: Role of Microviscosity and Hydration on Hydrolysis of Benzoyl Chloride at a Polymer Hydration Region, Langmuir, 25 (2009) 11336-11343.
[64] H. Frauenfelder, P.W. Fenimore, B.H. McMahon, Hydration, slaving and protein function, Biophys. Chem., 98 (2002) 35-48.

# Chapter 8: Summary and Future Perspective

This thesis is devoted in understanding the physicochemical properties of different types of self-assembled confined systems like micelle, reverse micelle and microemulsion composed of mixture of surfactants. Surfactant blend systems often offer more advantageous properties compared to those of the single ones. Mixture of surfactants modifies the oil-water interface which is more flexible as well as capable of uptaking more water to increase solubilization capacity. Therefore, the motivation of this thesis was to study the structure and dynamics of restricted water which mimics water in various biological processes by modifying interfaces using blend of surfactants. We investigated the role of mixed surfactant interfaces on the rate of enzyme kinetics reaction under confinement, also to understand how mixing behavior of surfactants can improve micellar properties as well as physical properties of water in RM and ME systems. Along with this it has been revealed that the mixing property of surfactant mixture varies with the charge type. The optimum HLB condition also tunes the properties of nonionic surfactant mixtures. Thus, the present thesis favors an approach to systematically address some of the above mentioned concerns which would facilitate further studies in this field of research.

In this thesis we have investigated the physical properties (structure, dynamics and activity) of water in various environments like in microemulsions and in RMs. The ultrafast dynamics of water was measured using time resolved fluorescence spectroscopy (TRFS, with a time resolution of ns to hundreds of ps) using fluorescent probe like C-500, ANS and DCM (details of these probes are given in chapter-2). The hydrogen bonded structure of water was obtained by studying the -O-H stretching band (in the mid-IR region), using FTIR, Fourier Transform Infra-Red Spectra. In order to acquire knowledge about the activity of water in restricted media we have studied the hydrolysis of benzoyl chloride and hydrolysis of protease substrates by enzyme.

Chapter 1 provides the general introduction of the micelle, RM and microemulsion (ME), its potential application in diverse areas of science, measurements of physical properties like structure and dynamics of water in these confined systems using different techniques and its advantage by using mixture of surfactants replacing single surfactant.

Chapter 2 provides the general background of spectroscopic techniques (absorption, emission and Infra-Red spectra). It includes instrumental setup of steady state and time resolved fluorescence, UV and FTIR spectroscopy. A brief description (theory and experimental methods) of solvation dynamics and fluorescence anisotropy are also provided. Moreover, it includes study of phase behavior and other various physical properties. General description about systems, surfactants, solvents, molecular probes, enzyme, substrate which are mainly used in this thesis have also been provided. Sample preparations and kinetics measurements are also discussed.

Chapter 3 to chapter 7 is based upon the experimental works that I have performed during my PhD.

In Chapter 3, we have investigated whether the mechanical properties of RM interface dictate the physical properties of entrapped water molecules in the RM waterpool. AOT/Igepal-520/Cyclohexane mixed surfactant RM system exhibits synergistic water solubilization behaviour compared to the constituent surfactants at $X_{Igepal}$=0.4. Such a phenomenon associates systematic modification of the interface curvature. DLS studies reveal linear increase in the droplet size and aggregation number of the RMs with increasing $X_{Igepal}$. FTIR study in the 3000-3800 $cm^{-1}$ region identifies that the relative population of the surface bound water molecules is higher in AOT RM compared to that in Igepal RM, and in mixed systems it also follows a linear trend with $X_{Igepal}$. Water relaxation dynamics as probed by Coumarin-500 also reveals an overall linear trend with no characteristic feature around the solubilization inflation point. Our study clearly identifies that the physical properties of water in RM is mostly governed by the interfacial stoichiometry and water content, and merely bares any dependence on the mechanical properties of the interface.

Chapter 4, is dedicated to study the structure, dynamics and activity of water molecules in RM composed of mixture of two non-ionic surfactants (Igepal 210 and Igepal 630) in cyclohexane. This mixed surfactant RM system provides a ten-fold increase in the water solubilization capacity at $X_{Ig630}$=0.3 compared to the constituent individual surfactants. Synergism in solubilization capacity in many mixed surfactant RM systems often manifests optimum HLB, inter-droplet interaction or both. The HLB could be tuned at $X_{Ig630}$~0.3 as it offers an optimum HLB value where a large fraction of surfactants are eventually partitioned at the oil-water interface. We have also investigated how the optimum HLB condition of mixed RM affects the physical properties of entrapped water molecules in the RM waterpool. DLS

studies show a bimodal distribution of droplet size in this region, whereas it is mono-modal in terminal compositions. FTIR study in the 3000-3800 $cm^{-1}$ region identifies a linear trend in which the content of 'bound' water increases at the expense of the 'network' water as the content of the hydrophilic surfactant Igepal 630 is increased in the mixture. Sub-ns relaxation dynamics of the entrapped water as revealed by the fluoroprobe coumarin 500 corroborates a similar linear trend as observed in the FTIR measurements as the rotational diffusion gets retarded with the increase of ethylene oxide chain length of Igepal. Reaction kinetics of solvolysis of benzoyl chloride reaction, however, does not offer any linear trend as it gets slower in the optimum HLB region. This non-linearity in reaction kinetics has been explained by consequence of the distribution of the substrate in the different phases.

Chapter 5 is based on the study of mixing behavior of anionic AOT and Nonionic Tween-85 mixture in aqueous system as well as reverse micellar system using fatty acid ester solvents.

In the first part we have showed how the addition of Tween-85 in aqueous AOT solution favors progressive micellization property compared to single surfactant. The observed early micellization in the mixture is due to the preferential adsorption of the polyoxyethylene (POE) chains of Tween-85 with simultaneous increase in the hydrophobic interactions between the surfactant tails of both the surfactants. Mixed compositions reveal non-ideal solution behavior and synergistic interaction between the constituent surfactants, which is supported by the negative values of the interaction parameter $\beta^m$. Both micellization as well as adsorption processes show increasing trend of spontaneous micelle formation with gradual incorporation of Tween-85 in AOT micelle. A comprehensive micellization behavior is studied at different mixed compositions ($X_{Tween\text{-}85}$) by surface tension method. Non-ideal mixing behaviors along with synergistic interaction between the constituent surfactants in the mixed micelles are evidenced. Mixed micelles illustrate favorable micellization behavior in terms of thermodynamic parameters.

In the next part we have explored the influence of mixing behavior on the properties of mixed RM composed of AOT and Tween-85 in fatty acid esters like EM, EP and EO. These mixed RMs show synergism in water solubilization capacity. Microstructures of these systems are investigated by conductance, DLS, and FTIR studies. The solvation and rotational relaxation dynamics provides the effect of $X_{Tween\text{-}85}$ as well as chemical architecture of fatty acid esters on the excited state dynamics of fluorophore DCM. Solvation dynamics is found to be faster with increase in $X_{Tween\text{-}85}$ and the average solvation time follows the order, EO < EP

< EM, which corroborates well with droplet size and abundance of bulk-like water. Anisotropy studies reveal a decrease in the rotational restriction on the probe for EO based RMs. Therefore, this work have the potential to serve as good bio-mimic models to study various processes occurring in biological molecules embedded in biomembranes.

In Chapter 6, we report the formation and characterization of a biocompatible microemulsion (ME) system composed of lecithin (L), Triton-X 100 (T) as the surfactant(s), butyl lactate (BL) as the cosurfactant, isopropyl myristate (IPM) as the oil phase and water. Detailed phase construction reveals that mixing of surfactant (L and T) produces larger single phase ME region compared to L. In the mixed surfactant systems, three phase body appears which is otherwise not obtained in the single surfactant counterparts signifying the synergistic solubilization behaviour upon mixing. The maximum solubilization capacity decreases as the content of T increases in the mixture. Viscosity, conductance and adiabatic compressibility measurements of the single-phase ME systems at a constant amphiphile concentration (80% w/w) show a linear trend with increasing water content revealing a droplet type structure of all the studied formulations. FTIR studies in the w/o region identify the presence of three distinct types of water molecules in these systems and their relative content changes with the interfacial composition as well as the total water content in the system. Our study offers a biocompatible mixed ME system in which the physical properties do not differ much from those of the lecithin based systems with the additional advantage of having higher solubilization capacity, low pH dependency and low viscosity, which renders its potential to be used for specific pharmaceutical applications.

In Chapter 7, we have studied the effect of replacing anionic surfactant AOT by nonionic surfactant(s) (Brijs) of varying HLB on the structure, dynamics and activity of water encapsulated in RMs formed in a biocompatible oil IPM. From DLS study, it has been observed that addition of rather low HLB Brijs offers only marginal effect on the size of the RM droplets as well as aggregation number, whereas, high HLB Brijs induce considerable enlargement of the droplet size. FTIR studies conclude that the relative abundance of free water increases with increasing HLB with a concomitant decrease in the content of bound water. TRFS measurements show that the dynamics get retarded with addition of high HLB Brijs due to relocation of the probe near the interface as the PEO head groups of Brijs populate the interface reducing the effective charge of the AOT head group. We spectroscopically measure the enzymatic activity of α-chymotrypsin on the substrate Ala–Ala–Phe–7-amido-4-methyl-coumarin (AMC) in these mixed RM systems. It has been found that the rate could either be

enhanced or reduced depending on the HLB of the added Brij(s). Such result could be found useful in modulating the reaction for specific applications.

## 8.1 Future Direction

Hydrogen bonded structure and sub-ns relaxation dynamics of water molecules encapsulated in the DDAB–cyclohexane (Cy)–water RM system has been measured previously[1, 2]. From these results it is concluded that phase modification has only marginal effect on the relaxation dynamics. Unlike many conventional surfactants, DDAB is insoluble in both Cy and water, and thus resides at the RM interface only[3]. The interfacial film of DDAB–Cy undergoes significant alteration upon addition of water as the microscopic phase changes from cylindrical aggregates to distinct droplets. DDAB/ Nonionic mixed surfactant system has been studied previously [4, 5]. However, complete understanding of such mixed RM system still remains unaddressed with special reference to water structure and solvation dynamics. DDAB/Igepal-520/Cy mixed RM is a good candidate to carry out such studies. Our plan is to study the physical and dynamic properties of water in this mixed RM system and compare the observations with those of anionic (AOT)/Ig-520/Cy mixed RM systems. In that case we will study the DLS, solubilization, FTIR study with 10% $D_2O$ mixture in the 2400-2800 $cm^{-1}$ and time resolved fluorescence spectroscopy.

Next, I plan to study the THz dielectric relaxation (with a time resolution of a few ps to sub-ps) of water in those mixed RM systems with hydrogen bond stretching and libration band in the far-IR region. THz spectroscopy (1 THz=$10^{12}$ Hz =$1ps^{-1}$) has emerged as an efficient tool to provide information about the solvation layers with the libration and collective hydrogen bond stretching vibration bands [6-9]. Previously Mittleman et al. have studied dielectric relaxation of water in the region (0.2-3.0 THz) inside AOT RM [10-12]. THz dielectric relaxation studies would indicate a distinct change in hydrogen bonded network when water is introduced to such mixed interface [12-14].

My next plan is to study the photoluminescence of D-luciferin in mixed surfactant RM system. D-luciferin is responsible for the bioluminescence found in Lampyridae fireflies, a family of winged insects. To understand the dynamics of excited-state proton transfer (ESPT) processes in biological water, many researchers group have studied ESPT in RMs [15-17]. The protolysis reaction of D-luciferin in the water pool of AOT RMs strongly depends on the size of the RMs [18, 19]. The intermolecular ESPT rate of D-luciferin in nanoconfined environment depends on the hydrogen bonding ability of the interface due to constrained mobility, slower

solvation and closeness of the ion pair [20]. It is important to study how ESPT rate of D-luciferin depends on interface in different mixed surfactant RM systems.

## 8.2 References


[1] A. Patra, T.Q. Luong, R.K. Mitra, M. Havenith, Solvent dynamics in a reverse micellar water-pool: a spectroscopic investigation of DDAB–cyclohexane–water systems, Physical Chemistry Chemical Physics, 15 (2013) 930-939.

[2] A. Patra, T.Q. Luong, R.K. Mitra, M. Havenith, The influence of charge on the structure and dynamics of water encapsulated in reverse micelles, Physical Chemistry Chemical Physics, 16 (2014) 12875-12883.

[3] G.G. Warr, R. Sen, D.F. Evans, J.E. Trend, Microemulsion formation and phase behavior of dialkydimethylammonium bromide surfactants, The Journal of Physical Chemistry, 92 (1988) 774-783.

[4] A. Bumajdad, J. Eastoe, Conductivity of water-in-oil microemulsions stabilized by mixed surfactants, Journal of Colloid and Interface Science, 274 (2004) 268-276.

[5] B.K. Paul, R.K. Mitra, Water solubilization capacity of mixed reverse micelles: Effect of surfactant component, the nature of the oil, and electrolyte concentration, Journal of Colloid and Interface Science, 288 (2005) 261-279.

[6] S. Ebbinghaus, S.J. Kim, M. Heyden, X. Yu, U. Heugen, M. Gruebele, D.M. Leitner, M. Havenith, An extended dynamical hydration shell around proteins, Proceedings of the National Academy of Sciences USA, 104 (2007) 20749-20752.

[7] B. Born, H. Weingärtner, E. Bründermann, M. Havenith, Solvation Dynamics of Model Peptides Probed by Terahertz Spectroscopy. Observation of the Onset of Collective Network Motions, Journal of the American Chemical Society, 131 (2009) 3752-3755.

[8] K. Meister, S. Ebbinghaus, Y. Xu, J.G. Duman, A. DeVries, M. Gruebele, D.M. Leitner, M. Havenith, Long-range protein–water dynamics in hyperactive insect antifreeze proteins, Proceedings of the National Academy of Sciences, 110 (2013) 1617-1622.

[9] M. Heyden, J. Sun, S. Funkner, G. Mathias, H. Forbert, M. Havenith, D. Marx, Dissecting the THz spectrum of liquid water from first principles via correlations in time and space Proceedings of the National Academy of Sciences USA, 107 (2010) 12068-12073.

[10] J.E. Boyd, A. Briskman, C.M. Sayes, D. Mittleman, V. Colvin, Terahertz Vibrational Modes of Inverse Micelles, The Journal of Physical Chemistry B, 106 (2002) 6346-6353.

[11] J.E. Boyd, A. Briskman, V.L. Colvin, D.M. Mittleman, Direct Observation of Terahertz Surface Modes in Nanometer-Sized Liquid Water Pools, Physical Review Letters, 87 (2001) 147401.

[12] D.M. Mittleman, M.C. Nuss, V.L. Colvin, Terahertz spectroscopy of water in inverse micelles Chemical Physics Letters, 275 (1997) 332-338.

[13] C. Ro/nne, L. Thrane, P.-O. Åstrand, A. Wallqvist, K.V. Mikkelsen, S.r.R. Keiding, Investigation of the temperature dependence of dielectric relaxation in liquid water by THz reflection spectroscopy and molecular dynamics simulation, The Journal of Chemical Physics, 107 (1997) 5319-5331.

[14] K.J. Tielrooij, D. Paparo, L. Piatkowski, H.J. Bakker, M. Bonn, Dielectric Relaxation Dynamics of Water in Model Membranes Probed by Terahertz Spectroscopy, Biophysical Journal, 97 (2009) 2484-2492.

[15] B. Cohen, D. Huppert, K.M. Solntsev, Y. Tsfadia, E. Nachliel, M. Gutman, Excited state proton transfer in reverse micelles, Journal of the American Chemical Society, 124 (2002) 7539-7547.

[16] S.-Y. Park, O.-H. Kwon, T.G. Kim, D.-J. Jang, Ground-state proton transfer of 7-hydroxyquinoline confined in biologically relevant water nanopools, The Journal of Physical Chemistry C, 113 (2009) 16110-16115.

[17] M. Sedgwick, R.L. Cole, C.D. Rithner, D.C. Crans, N.E. Levinger, Correlating proton transfer dynamics to probe location in confined environments, Journal of the American Chemical Society, 134 (2012) 11904-11907.
[18] J. Kuchlyan, D. Banik, N. Kundu, S. Ghosh, C. Banerjee, N. Sarkar, Effect of Confinement on Excited-State Proton Transfer of Firefly's Chromophore d-Luciferin in AOT Reverse Micelles, The Journal of Physical Chemistry B, 118 (2014) 3401-3408.
[19] J. Kuchlyan, D. Banik, A. Roy, N. Kundu, N. Sarkar, Excited-State Proton Transfer Dynamics of Firefly's Chromophore D-Luciferin in DMSO–Water Binary Mixture, The Journal of Physical Chemistry B, 118 (2014) 13946-13953.
[20] Y. Erez, D. Huppert, Excited-state intermolecular proton transfer of the firefly's chromophore D-luciferin, The Journal of Physical Chemistry A, 114 (2010) 8075-8082.